

University of Nottingham
UK | CHINA | MALAYSIA

Removal of Carbon Dioxide from High Pressure Natural Gas by Adsorption on Activated Carbons

A Thesis Submitted to

The University of Nottingham

By

Khalil Al Hanashi

Supervisors

Prof. Hao Liu, Prof. Colin Snape

Dr Chenggong Sun, Dr Lee Stevens

For the degree of

Doctor of Philosophy

School of Chemical and Environmental Engineering
The University of Nottingham
United Kingdom

March 2019

Abstract

The presence of carbon dioxide (CO_2) in raw natural gas is a major challenge for the natural gas industry because it decreases the heating value of the natural gas and promotes corrosion in the piping materials used for transportation. Today, the natural gas industry is dominated by the energy-intensive amine chemical absorption process to remove the CO_2, however, pressure swing adsorption process has the potential to provide a sustainable and low energy penalty alternative. This research investigated the feasibility of using activated carbons as solid adsorbents for pressure swing adsorption process to remove CO_2 from high pressure and high CO_2 natural gas.

Two sets of 14 samples of activated carbons were synthesised from two different precursors: date pits biomass and coal tar pitch. A two-step chemical activation process with potassium hydroxide (KOH) was used to convert the date pits biomass into activated carbons, and a one-step KOH chemical activation process was used to produce activated carbons from the coal tar pitch. Nitrogen adsorption based characterisation revealed that both series of activated carbons were dominated by micropores when prepared with various KOH to carbon ratios (ranging from 1 to 4) and various activation temperatures (600 to 800 ^oC). However, some mesoporosity was seen at an activation temperature of 900 ^oC.

All the samples were performance tested for CO_2 and methane (CH_4) working adsorption capacities by gravimetric measurement. These tests revealed higher CO_2 working capacities compared to that of CH_4, confirming that the activated carbons have a potential use as solid adsorbents for CO_2/CH_4 separation. The performance test conditions were based on the process conditions of a South Oman gas field (100 bar pressure, 50 ^oC temperature and 20% CO_2 content). The CO_2 uptake and the CH_4 uptake by the activated carbons were found to positively correlate with the BET surface area and micropore volume of the activated carbons. However, larger micropores in the activated carbons (>1.6 nm) were found to be less favourable for CO_2 adsorption.

The effect of water on CO_2 uptake and CH_4 uptake of the activated carbons were investigated from two aspects: as a contaminant and as CO_2 selectivity enhancement agent. A small amount of water (10% in the vapour phase) was used

to investigate water as a contaminant and showed a negative effect on both CO_2 and CH_4 adsorption capacities. A large amount of pre-adsorbed water (50%) increased the CO_2/CH_4 working capacity ratios at high pressure indicating CO_2/CH_4 selectivity enhancement but reduced CO_2 uptake capacity.

CO_2 and CH_4 adsorption isotherms were successfully measured using a high pressure volumetric analyser. The measured isotherms were best fitted with the Dual Site Langmuir (DSL) model compared to the Langmuir or Sips models. The extended DSL model was used to predict the binary mixed gas (CO_2 and CH_4) adsorption after gravimetric measurements of total adsorption were employed to select the right pair of the extended DSL equation to overcome the issue of site matching. The binary gas adsorption calculations showed favourable adsorption for CO_2 over CH_4 as CO_2 partial pressure in the mixture increased. However, the co-adsorption of CH_4 in the activated carbon also increased as CH_4 partial pressure increased which would decrease the purity of the removed CO_2 in a Pressure Swing Adsorption (PSA) process.

In conclusion, the activated carbons synthesised from low cost precursors by simple chemical activation method showed good potential for separating CO_2 from CH_4. This potential was demonstrated by CO_2/CH_4 working capacity ratios higher than one for most samples, and confirmed by DSL adsorption model of mixed gas (CO_2 and CH_4) adsorption on activated carbons. Future work could include improving the activated carbon mechanical strength, reducing CH_4 adsorption in addition to designing a PSA process to demonstrate the expected energy saving.

Acknowledgements

All praise is due to Allah Almighty for giving me the strength and the ability to complete this work. Thanks and gratitude to my supervisors. Professor Hao Liu for his supervision, guidance and support in all aspects of this work. Professor Colin Snape for providing his expertise to explore the wider aspects of this research. Dr Chenggong Sun for his valuable advice and comments. Dr Lee Stevens for his training and help with HPVA equipment and software. Dr Jingjing Liu for providing the raw coal tar pitch sample. Thanks are also due to others who supported me in the lab. Dr Xin Liu for his help and advice and Adrian Quinn for keeping the lab running despite many requests. I would like to also thank Dr Elisabeth Steer for her help with the SEM analysis and Ms Teresa Needham for her help with the XRF analysis. I am also grateful to the Government of Oman and to Petrolume Developmen Oman LLC for their financial support.

I am forever indebted to my mother, Aishah, and to my beloved late father, Khamis, for the upbringing they gave me and the opportunities they allowed me to have, including allowing me to explore and experiment freely in this world when I was young. My brothers, Ahmed and Ibrahim, should not go unmentioned; they always got my back in anything I needed while I was away from home. My sisters, Lila and Aliya, their support and prayers have always been a source of strength and inspiration to me. Thank you to my step sisters Maisa, Samyah and Eman, for their time to help my family when needed.

A heartfelt thank you to my family. My dear wife, Amal, this work would not have been possible without her love, encouragement and support, no words could express my gratitude to her for being next to me despite the hard time she encountered whilst in the UK. Little Adam, thank you for arriving in this world in the middle of my PhD. I won't forget our daily trip to the nursery that ensured I was always at my desk by 9:00 am. Azzan and Sara, thank you for just being you and for giving up the computer desk for me to work at home (sometimes).

Many thanks to all my friends in Nottingham especially the Omani community who never hesitated to support and help. Last but not least thank you to my friends Luis and Hossain for the many lunches, coffees and international politics discussions over the last four years.

Dedication

To the soul of my father and my greatest teacher, who left this world while I was pursuing my PhD.

وَيَسْـَٔلُونَكَ عَنِ ٱلرُّوحِ ۖ قُلِ ٱلرُّوحُ مِنْ أَمْرِ رَبِّى وَمَآ أُوتِيتُم مِّنَ ٱلْعِلْمِ إِلَّا قَلِيلًا

And they ask you, [O Muhammad], about the soul. Say, "The soul is of the affair of my Lord. And mankind have not been given of knowledge except a little."

The Quran , 85th verse of chapter 17

Contents

Abstract……. i

Acknowledgements iii

Dedication…. iv

Contents…… v

List of Tables xi

List of Figures xii

Chapter 1. Introduction 1

1.1 Background and Motivation 1

1.2 Aim 7

1.3 Objectives 7

1.4 Thesis Structure 8

Chapter 2. Literature review 10

2.1 Process Technologies for CO_2 Separation from Natural Gas 10

2.1.1 Absorption 11

2.1.1.1 Chemical Absorption 11

2.1.1.2 Physical Absorption 13

2.1.2 Low Temperature Phase Separation 15

2.1.3 Membrane Separation Technology 17
2.1.4 Adsorption 20
2.1.4.1 Pressure Swing Adsorption (PSA) 22
2.1.4.2 Temperature Swing Adsorption (TSA) 25
2.2 Adsorbent Materials 26
2.2.1 Zeolites 27
2.2.2 Mesoporous Silica 28
2.2.3 Activated Carbon 30
2.2.3.1 Activation Mechanism 32
2.2.3.2 Carbon Precursors 35
2.3 Adsorption Modelling 37
2.3.1 Adsorption Isotherms 37
2.3.2 Adsorption Isotherm Models 39
2.3.2.1 Single Component Gas Isotherm Models 39
2.3.2.2 Binary Component Gas Adsorption Models 41
2.3.3 Summary 43
Chapter 3. Experimental Methods 45
3.1 Preparation of Adsorbents 46
3.1.1 Activated Carbons from Date Pits 46
3.1.2 Activated Carbons from Coal Tar Pitch 49
3.2 Characterisation Techniques 50
3.2.1 Nitrogen Adsorption 50
3.2.2 Helium Pycnometry 51

3.2.3 Scanning Electron Microscopy (SEM) 52
3.2.4 Elemental Analysis (EA) 53
3.2.5 X-Ray Fluorescence (XRF) Spectrometry 54
3.3 Gas Adsorption Measurements 54
3.3.1 High Pressure Thermal Gravimetric Analysis (HP-TGA) 54
3.3.2 Atmospheric Pressure Thermal Gravimetric Analysis (TGA) 57
3.3.3 High Pressure Volumetric Adsorption (HPVA) 58
3.4 Calculation Algorithms 60
3.4.1 Buoyancy Correction of High Pressure Gravimetric Adsorption Measurement 60
3.4.2 Surface Area Determination from N_2 Adsorption Isotherms 64
3.4.3 Pore Size Distribution (PSD) from N_2 Adsorption Isotherms 66
Chapter 4. Activated Carbons Characterisation 68
4.1 Introduction 68
4.2 Date Pits Activated Carbons 68
4.2.1 Morphology 69
4.2.2 Chemical Composition 71
4.2.3 Skeletal Density 73
4.2.4 Nitrogen Adsorption Isotherms and Surface Textural Properties . 74
4.2.4.1 Surface Area 76
4.2.4.2 Pore Volume 77
4.2.4.3 Pore Size Distribution (PSD) 79
4.3 Coal Tar Pitch Activated Carbons 81

4.3.1 Morphology 81

4.3.2 Chemical Composition 82

4.3.3 Skeletal Density 83

4.3.4 Nitrogen Adsorption Isotherms and Surface Textural Properties . 84

4.3.4.1 Surface Area 87

4.3.4.2 Pore Volumes 88

4.3.4.3 Pore Size Distribution (PSD) 89

4.4 Conclusion 91

Chapter 5. CO_2 Adsorption on Activated Carbons 92

5.1 Introduction 92

5.2 CO_2 Equilibrium Adsorption Capacity 92

5.3 CO_2 Working Adsorption Capacity 103

5.4 High Pressure CO_2 Adsorption Isotherms 106

5.5 CO_2 Isosteric Heat of Adsorption 109

5.6 Water Vapour Effect on CO_2 Adsorption 111

5.7 Conclusion 114

Chapter 6. Adsorption Selectivity of CO_2 over CH_4 and the Effect of Moisture 116

6.1 Introduction 116

6.2 CH_4 Equilibrium Adsorption Capacity 117

6.3 CH_4 Working Adsorption Capacity 123

6.4 CO_2/CH_4 Working Adsorption Capacity Ratio 124

6.5 CH_4 Adsorption Isotherms 127

6.6 CH_4 Isosteric Heat of Adsorption 128

6.7 Water Vapour Effect on CH_4 Adsorption 129

6.8 Pre-adsorbed Water Effect on CO_2 and CH_4 Adsorption 130

6.9 Conclusion 137

Chapter 7. Modelling Adsorption Isotherms for Pure CO_2 and CH_4, and Calculating their Binary Mixture Adsorption 139

7.1 Introduction 139

7.2 Converting Excess Adsorption to Absolute Adsorption 140

7.3 Modelling CO_2 and CH_4 Adsorption Isotherms 143

7.3.1 Fitting Adsorption Isotherm Models 143

7.3.2 Comparison of Adsorption Isotherms Models 144

7.4 Prediction of Binary Gas Mixture Adsorption 154

7.4.1 Modelling Approach 154

7.4.2 Model Prediction Results 159

7.5 CO_2/CH_4 Selectivity Calculations 161

7.6 Conclusion 162

Chapter 8. General Conclusions and Future Work 164

8.1 Conclusions 164

8.1.1 Activated Carbons Synthesis and Characterisation 165

8.1.2 CO_2 and CH_4 Adsorption on Activated Carbons 166

8.1.3 CO_2 and CH_4 Adsorption Modelling 168

8.2 Future Work 169

8.2.1 Adsorbent Synthesis 170

8.2.2 CO_2 and CH_4 Co-adsorption..... 170

8.2.3 PSA Simulation and Economic Evaluation..... 171

References…. 172

Appendix A: CO_2 Excess and Absolute Uptake Values 186

Appendix B: CH_4 Excess and Absolute Uptake Values..... 190

Appendix C: Research Outputs 194

List of Tables

Table 1.1 Natural gas composition of various reservoirs (%) (Shimekit and Mukhtar, 2012). 2
Table 2.1 Literature examples of studies using the PSA process for CO_2 removal from natural gas. 24
Table 2.2 Literature selected high pressure zeolite equilibrium selectivity and capacity. 28
Table 2.3: Literature selection of activated carbon equilibrium capacity and selectivity for CO_2/CH_4 separation at high pressure. 32
Table 3.1 Date pits based activated carbons designation and chemical activation conditions. 48
Table 3.2 Coal tar pitch activated carbons designation and chemical activation conditions. 50
Table 3.3 CO_2 uptake measurement repeatability using HP-TGA 57
Table 4.1 Chemical composition of the raw date pits and date pits char. 71
Table 4.2 Chemical composition of the date pits based activated carbons. 72
Table 4.3 Chemical composition of the coal tar pitch activated carbons. 83
Table 6.1 Pore volume and CH_4 uptake for Pair A (DP3700, DP3900) and pair B (DP2900, DP3800) 121
Table 6.2 CO_2 and CH_4 working capacities of date pits activated carbons at 50 ^oC and the corresponding CO_2/CH_4 adsorption ratio. 125
Table 6.3 CO_2 and CH_4 working capacities of coal tar pitch activated carbons at 50 ^oC and the corresponding CO_2/CH_4 adsorption ratio. 125
Table 6.4 Relative drop in CO_2 and CH_4 uptake due to pre-adsorbed moisture from a 10% relative humidity environment 131
Table 7.1 Langmuir model parameters for CO_2 adsorption isotherms. 148
Table 7.2 Sips model parameters for CO_2 adsorption isotherms. 148
Table 7.3 DSL model parameters for CO_2 adsorption isotherms. 149
Table 7.4 Langmuir model parameters for CH_4 adsorption isotherms. 152
Table 7.5 Sips model parameters for CH_4 adsorption isotherms. 152
Table 7.6 DSL model parameters for CH_4 adsorption isotherms. 152

List of Figures

Figure 1.1 Conventional gas processing (adapted from Rufford et al. 2012). 2
Figure 1.2 Global hydrocarbon (HC) volumes with high CO_2 (15 - 80%) (Burgers et al., 2011). 3
Figure 1.3 Miscible sour gas EOR scheme in South Oman (Al-Hadhrami et al., 2014). 4
Figure 1.4 Research workflow diagram. 9
Figure 2.1: Amine absorption process (Peters et al., 2011). 12
Figure 2.2 Simplified schematic of the Selexol physical absorption process (Olajire, 2010). 14
Figure 2.3 The CFZ™ tower (Kelley et al., 2011). 16
Figure 2.4 The CryoCell® process scheme (Hart and Gnanendran, 2009). 17
Figure 2.5 Four gas diffusion mechanisms through a membrane, (a) Knudsen diffusion, (b) surface diffusion, (c) capillary condensation, and (d) molecular sieving (Ismail, Chandra Khulbe and Matsuura, 2015)..... 18
Figure 2.6 Spiral–wound membrane module (Ismail, Chandra Khulbe and Matsuura, 2015)..... 19
Figure 2.7 Skarstrom PSA cycle (Yang, 2003). 23
Figure 2.8 Schematic representation of 2-bed TSA system (Yentekakis and Goula, 2017). 25
Figure 2.9 Potassium intercalation between the carbon layers during KOH activation at temperatures above 700 ^{o}C (Romanos et al., 2012)..... 35
Figure 2.10 Raw date pits. 36
Figure 2.11 Six types of adsorption isotherms (Thommes et al., 2015)..... 38
Figure 3.1 Horizontal tube furnace used for the carbonisation and activation processes to produce activated carbons. 46
Figure 3.2 AccuPyc II1340 Pycnometer picture and simplified schematic. 51
Figure 3.3 The HP-TGA system. 55
Figure 3.4 Q500 TGA measurement chamber. 58
Figure 3.5 High Pressure Volumetric Analyser (HPVA). 59
Figure 3.6 Forces acting on a sample in the Linseis high-pressure TGA system. 61
Figure 4.1 Date pits char granules, sample DP0. 69

Figure 4.2 Date pits char (DP0) granule at higher magnification. 70
Figure 4.3 SEM image of sample DP2900 showing a complex pore network. .. 70
Figure 4.4 Skeletal density of date pits activated carbons prepared at varying activation temperatures and KOH amounts. 73
Figure 4.5 N_2 adsorption and desorption isotherms for the date pits activated carbons. 75
Figure 4.6 Variation of surface area of date pits activated carbons with varying activation temperature and KOH amount. 76
Figure 4.7 Variation of micropore volumes of date pits activated carbons with varying activation temperature and KOH amount. 77
Figure 4.8 Variation of mesopore volumes of date pits activated carbons with varying activation temperature and KOH amount. 77
Figure 4.9 PSD for date pits activated carbons calculated by NLDFT. 80
Figure 4.10 Raw coal tar pitch beads, CTP0. 81
Figure 4.11 CTP1800 (A)and CTP3800 (B) showing damage to spherical morphology due to high KOH to carbon ratio, 3:1, used for activation..... 82
Figure 4.12 Skeletal density of coal tar pitch activated carbons prepared at varying activation temperatures and with various KOH amounts. 84
Figure 4.13 N_2 adsorption and desorption isotherms for coal tar pitch activated carbons. 86
Figure 4.14 Variation of surface area of CTP activated carbons with varying activation temperature and KOH amount. 87
Figure 4.15 Variation in micropore volume of coal tar pitch activated carbons with varying activation temperature and KOH amount. 88
Figure 4.16 Variation in mesopore volume of coal tar pitch activated carbons with varying activation temperature and KOH amount. 88
Figure 4.17 PSD for coal tar pitch activated carbons calculated by NLDFT..... 90
Figure 5.1 CO_2 isothermal adsorption curves for the date pits activated carbons at 20 bar and 50 ^oC. 93
Figure 5.2 CO_2 equilibrium capacities for date pits activated carbons at 20 bar and 50 ^oC. 94
Figure 5.3 CO_2 isothermal adsorption curves for the coal tar pitch activated carbons at 20 bar and 50 ^oC. 95

Figure 5.4 CO_2 equilibrium capacities for coal tar pitch activated carbons at 20 bar and 50 ^oC. 96
Figure 5.5 BET Surface areas vs. equilibrium CO_2 uptakes by (A) date pits and (B) coal tar pitch activated carbons. 97
Figure 5.6 Total pore volume and micropore volume vs. equilibrium CO_2 uptake by (A) date pits activated carbon and (B) coal tar pitch activated carbon. . 99
Figure 5.7 Linear relationship between cumulative volumes from pores smaller than specified pore size and equilibrium CO_2 uptake for date pits activated carbons at 20 bar and 50 ^oC. 101
Figure 5.8 Linear relationship between cumulative volumes from pores smaller than specified pore size and equilibrium CO_2 uptake for coal tar pitch activated carbons at 20 bar and 50 ^oC. 102
Figure 5.9 The goodness of the linear fit per cumulative pore volume (R^2) values against their corresponding biggest pore size contributing to the cumulative pore volume. 103
Figure 5.10 CO_2 uptake of DP activated carbons at 1 bar and 20 bar with the resultant CO_2 working capacity. 104
Figure 5.11 CO_2 uptake of CTP activated carbons at 1 bar and 20 bar with the resultant CO_2 working capacity. 106
Figure 5.12 CO_2 adsorption isotherms at 25 ^oC and 50 ^oC for samples DP2900 and CTP3800. 107
Figure 5.13 Comparison of PSD for DP2900 and CTP3800. 108
Figure 5.14 Cumulative pore volume for DP2900 and CTP3800. 109
Figure 5.15 CO_2 isosteric heat of adsorption (Qst_co2) for samples DP2900 and CTP3800. 110
Figure 5.16 Controlled humidity environment set up in vacuum desiccator using saturated KOH aqueous solution. 112
Figure 5.17 Relative humidity and temperature inside the controlled humidity desiccator. 112
Figure 5.18 Dry vs 10% relative humidity CTP3800 CO_2 adsorption isotherms at 25 ^oC. 113
Figure 6.1 Equilibrium CH_4 uptake by date pits activated carbons at 80 bar and 50 ^oC. 117

Figure 6.2 Equilibrium CH_4 uptake by coal tar pitch activated carbons at 80 bar and 50 ^oC. 118
Figure 6.3 BET surface areas vs equilibrium CH_4 uptakes at 80 bar and 50 ^oC by (A) date pits and (B) coal tar pitch activated carbons. 119
Figure 6.4 Micropore volume (A) and total pore volume (B) vs CH_4 uptake at 80 bar and 50 ^oC for date pits activated carbons. 120
Figure 6.5 Cumulative pore volume and pore volume distribution (PVD), (A) DP3700 and DP3900, (B) DP2900 and DP3800. 121
Figure 6.6 CH_4 uptake at 80 bar and 50 ^oC for coal tar pitch activated carbons against (A) micropore volume and (B) total pore volume. 122
Figure 6.7 CH_4 uptake of date pits activated carbons at 1 bar and 80 bar at 50 ^oC with the resultant CH_4 working capacity. 123
Figure 6.8 CH_4 uptake of coal tar pitch activated carbons at 1 bar and 80 bar at 50 ^oC with the resultant CH_4 working capacity. 124
Figure 6.9 PSD of CTP3800 and DP3600 from NLDFT analysis. 126
Figure 6.10 CH_4 adsorption isotherms for DP2900, CTP3800 and DP3600 at 25 ^oC and 50 ^oC up to 100 bar as measured by HPVA. 127
Figure 6.11 Isosteric heat of adsorption of CH_4 when adsorbed on DP3600, DP2900 and DP3800 activated carbons. 128
Figure 6.12 CH_4 adsorption isotherm at 25 ^oC for CTP3800 and DP3600 with a dry sample (filled markers) and with 10% moisture equilibrated sample (empty markers). 130
Figure 6.13 CO_2 uptake of water loaded activated carbons at 25 ^oC, (A) CTP3800 and (B) DP3600. 132
Figure 6.14 CH_4 uptake of water loaded activated carbons at 25 ^oC, (A) CTP3800 and (B) DP3600. 135
Figure 6.15 Percentage drop in CO_2 and CH_4 uptake for wet CTP3800 with 5%, 50% and 70% pre-adsorbed water across adsorption pressure up to 100 bar. 136
Figure 7.1 Illustrative representation of excess and absolute gas uptake on a two-dimensional surface (Mason, Veenstra and Long, 2014). 141
Figure 7.2 Comparison between excess (triangles) and absolute (circles) adsorption quantities of CH_4 onto CTP3800 activated carbon at 25 ^oC.... 143

Figure 7.3 Isotherm model fitting of experimental CO_2 uptake on DP3600, DP2900 and CTP3800 at 25 and 50 ^oC. 147
Figure 7.4 Average of SSE percentages per model per temperature for CO_2 adsorption isotherms fitting to Langmuir, Sips and DSL models. 149
Figure 7.5 Isotherm model fitting of experimental CH_4 uptake on DP3600, DP2900 and CTP3800 at 25 and 50 ^oC. 151
Figure 7.6 Average of SSE percentages per model per temperature for CH_4 adsorption isotherms fitting to Langmuir, Sips and DSL models. 153
Figure 7.7 Predicted total mixed gas adsorption (q_t) from DSL_1 and DSL_2 equation pairs. Gas mix is 20% CO_2 and 80% CH_4, adsorption temperature 25 and 50 ^oC. 157
Figure 7.8 Total adsorption (q_t) experimental measurement compared to DSL_1 and DSL_2 model predictions. 158
Figure 7.9 CO_2 and CH_4 adsorbed amount from a binary gas mixture on selected activated carbon samples at varying CO_2 concentration as predicted by the extended DSL model. 160
Figure 7.10 CO_2/CH_4 selectivity calculated at 100 bar pressure and at 25 and 50^oC for DP3600, DP2900 and CTP3800 activated carbon samples. 162
Figure 8.1 CO_2 and CH_4 uptakes at 50 ^oC for DP3600 and CTP3800. 166

Chapter 1. Introduction

1.1 Background and Motivation

Global energy demand increased by 1.9% in 2017 and it is predicted that fossil fuels will continue to provide most of the global demand for energy in the short to medium term (International Energy Agency, 2018a). Natural gas is expected to achieve a steady demand growth over the next 20 years at 1.9% per year (BP P.L.C., 2015). The share that oil and coal provide to the global energy demand is expected to decrease whereas the share from natural gas and renewable energy is expected to increase (International Energy Agency, 2018b). Coping with an increase in demand for natural gas is likely to promote the production of natural gas from sour gas fields (fields with high CO_2 content) especially in places where sweet gas fields (fields with low CO_2 content) have already been exploited.

Natural gas composition varies depending on the geology, depth and type of its reservoir but this composition in most reservoirs is dominated by methane (CH_4) as shown in Table 1.1. Nearly 40% of the gas reserves around the world contain high levels of carbon dioxide making the production of natural gas from these sources not feasible due to economic constraints resulting from the high cost of gas processing required to remove the CO_2 (Total E&P, 2007). It is estimated that there are 4 trillion m^3 of net hydrocarbon gas globally in undeveloped or under-developed natural gas reservoirs containing 15-80% CO_2 (Burgers *et al.*, 2011).

Table 1.1 Natural gas composition of various reservoirs (%) (Shimekit and Mukhtar, 2012).

Component	Reservoir				
	Groningen (Netherlands)	Leaq (France)	Uch (Pakistan)	Uthmaniyah (Saudi Arabia)	Ardjuna (Indonesia)
CH_4	81.3	69	27.3	55.5	65.7
C_2H_6	2.9	3	0.7	18	8.5
C_3H_8	0.4	0.9	0.3	9.8	14.5
C_4H_{10}	0.1	0.5	0.3	4.5	5.1
C_{5+}	0.1	0.5	-	1.6	0.8
N_2	14.3	1.5	25.2	0.2	1.3
H_2S	-	15.3	-	1.5	-
CO_2	0.9	9.3	46.2	8.9	4.1

For raw natural gas to meet pipeline and Liquefied Natural Gas (LNG) quality, it must first be processed to remove non-hydrocarbon species, particularly CO_2 and H_2S. Conventional gas processing operations can be split into upstream (gas production and treating) and downstream (low temperature gas processing plant) operations. Figure 1.1 displays the main process operations in the natural gas processing and liquefaction industry.

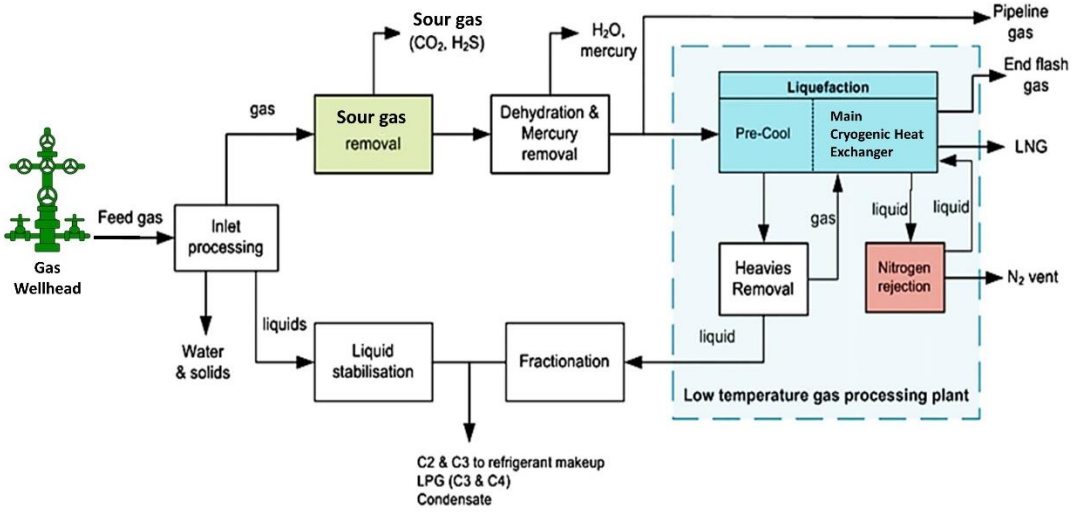


Figure 1.1 Conventional gas processing (adapted from Rufford et al. 2012).

In the upstream gas processing, the first piece of equipment is the gas wellhead. Next, there is a two-phase separation into gas and free liquid. The gas then flows through a sour gas removal unit which removes CO_2 and H_2S. Sour gas is corrosive

and requires high grade equipment; therefore it is important to position its removal upstream of the rest of the other units to reduce damage to the downstream equipment. Conventionally, the removed sour gas from the raw natural gas is incinerated. However, due to increasing environmental concerns and technology developments in Enhanced Oil Recovery (EOR) in recent years, there has been an increased utilisation of this sour gas in what is known as sour gas EOR. One example of such a project is the South Oman sour gas EOR. South Oman sour gas field is shown in a global perspective in Figure 1.2. It is one of a number of global examples of sour natural gas fields with high capacity and high CO_2 levels. It contains 17 - 27% CO_2 at 100 bar wellhead pressure and 50 ^oC gas temperature (Al-Hadhrami *et al.*, 2007).

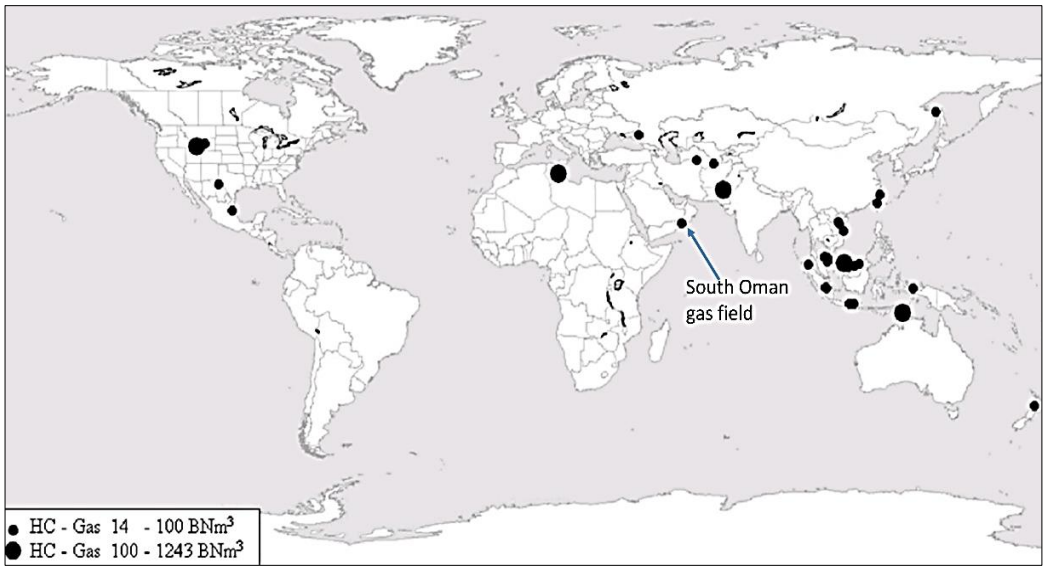


Figure 1.2 Global hydrocarbon (HC) volumes with high CO_2 (15 - 80%) (Burgers *et al.*, 2011).

An oil field located close to the South Oman sour gas field benefits from sour gas EOR. The proximity of such an oil field to a sour gas field makes the otherwise cost-prohibitive CO_2 removal by an aqueous amine process economically feasible. It was important to consider co-developing South Oman gas and oil fields in one project since the sour gas injected into the nearby oil reservoir can increase the oil

recovery factor by 40 - 50%, see Figure 1.3 illustrating the gas production, treatment and reinjection scheme in South Oman (Al-Hadhrami *et al.*, 2014). In this operation, greater focus is given to the EOR due to the higher sales value of oil compared to that of the gas. As a result, additional raw sour gas is added to the CO_2 output of the sweetening unit to provide sufficient volume for EOR reinjection. Some of the processed sour gas is exported as sweet gas and the sour gas stream is compressed to 555 bar to enable its reinjection into the subsurface formation as illustrated in Figure 1.3.

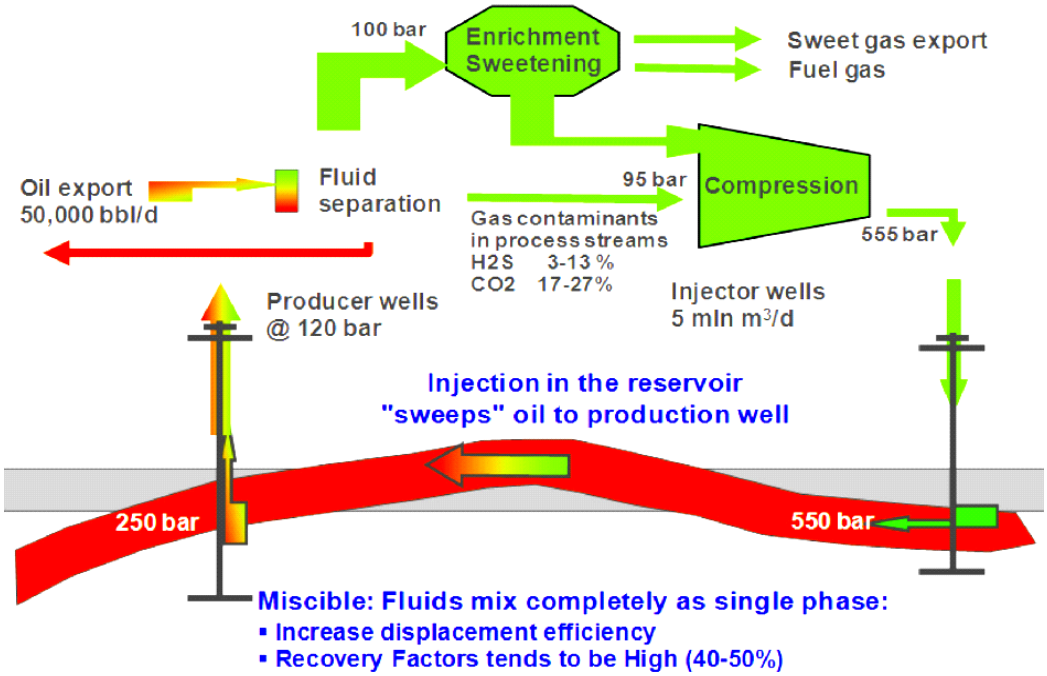


Figure 1.3 Miscible sour gas EOR scheme in South Oman (Al-Hadhrami *et al.*, 2014).

The central sour gas treating facility used in the South Oman sour gas field utilises aqueous amine absorbent process technology, which is the standard industry practice for sour gas removal when developing large-scale sour gas fields (Rufford *et al.*, 2012). The capital expenditure (CapEx) of the gas treating section can often amount to more than 50% of the total CapEx of a sour gas field (Shell Global Solutions, 2015). The energy requirement for CO_2 separation in a typical aqueous amine absorption process is 4 GJ/ton CO_2 (Rota, 2014). A recent publication puts

the cost of CO_2 removal and storage from a large natural gas project at 60 USD per ton of CO_2 for quantities more than 500 million tons of CO_2 per year (International Energy Agency, 2018). In Oman, where 22% of the total natural gas used in the country is consumed by the oil and gas industry (National centre for statistics and information, 2018), there is a need to reduce the energy intensity of the oil and gas industry itself. Economically viable development of future sour gas fields will require alternative cost-effective technologies to remove CO_2. In addition, it is important to consider smaller sour gas fields where a compact gas processing unit could enable the removal of CO_2 closer to the gas wellhead eliminating the cost of sour gas pipeline transportation and hence facilitating the development of small gas fields in a cost effective manner. There is also a need for CO_2 removal units to be of low energy demand to satisfy the increasingly stringent environmental regulations for the oil and gas industry and the limited availability of power at remote locations, such as offshore gas fields or remote desert gas fields.

High CO_2 natural gas reservoirs, such as the one in South Oman, could benefit from a gas processing system that can utilise the naturally available high pressure (100 bar) with the raw natural gas to drive the CO_2 separation process. Such processing systems would provide an attractive low energy penalty alternative to systems that need an external source of energy, e.g. aqueous amine absorption process. The Pressure Swing Adsorption (PSA) process, which utilises solid adsorbents, is an example of a low energy penalty physical adsorption gas treatment system. In addition to the low energy requirement, solid adsorbent systems do not suffer from some of the other disadvantages of aqueous amine absorption systems. For instance, low contact area between gas and liquid, amine

losses as a result of evaporation, and promoting process equipment corrosion and degradation (Yu, Huang and Tan, 2012). PSA is a promising technology used extensively in gas purification, such as nitrogen and hydrogen production, but still has limited use in natural gas CO_2 separation facilities. Developing adsorbent materials for a PSA system to achieve the desired CO_2 removal level is one of the main challenges of utilising such systems in natural gas treatment.

Low cost and high performance solid adsorbents are needed to enable the use of PSA systems for CO_2 removal from high pressure natural gas to provide a suitable rival to aqueous amine absorption systems. The ability to synthesise activated carbons from low cost precursors, such as agriculture waste or high carbon content industrial waste, makes these materials potential candidates to be used in a cost-competitive PSA system. Characteristics of the activated carbons, such as surface area and pore volume, can be modified with low cost chemical or physical processes and, unlike zeolite, activated carbons have shown more resistance to the presence of moisture as a feed contaminant and showed good cyclical stability (Sayari, Belmabkhout and Serna-Guerrero, 2011)

.

1.2 Aim

The overall aim of this research was to investigate the feasibility of using activated carbons as solid adsorbents for pressure swing adsorption process to remove CO_2 from high pressure and high CO_2 natural gas.

1.3 Objectives

The following objectives were pursued to achieve the main aim of this research:

A. Synthesising two sets of activated carbons, one from date pits (biomass) and the other from coal tar pitch using chemical activation with KOH.
B. Understanding how the synthetic conditions for the production of activated carbons influence their characteristics.
C. Examining the performance of the activated carbons for CO_2 removal from natural gas by establishing their CO_2 and CH_4 adsorption working capacities and their ratios via the measurement of CO_2 and CH_4 equilibrium adsorption capacities at atmospheric pressure and at high pressure equivalent to the CO_2 and the CH_4 partial pressure in the South Oman gas field.
D. Characterising the activated carbons to understand the relationship between their structural properties and their CO_2 uptake and CH_4 uptake.
E. Measuring CO_2 and CH_4 adsorption isotherms for selected highest performance activated carbon samples.
F. Investigating the effect of moisture on the CO_2 and the CH_4 uptake and CO_2/CH_4 selectivity for selected activated carbons using wet sample isotherm measurements.
G. Modeling the adsorption of CO_2, CH_4 and their mixture on activated carbons for natural gas sweetening at different conditions.

1.4 Thesis Structure

This thesis is structured over eight chapters. This first chapter presents the motivation for undertaking this research. It also introduces the aim and objectives of this research project. The second chapter gives a comprehensive literature review covering most common CO_2 removal technologies from natural gas with greater focus on pressure swing adsorption and associated solid adsorbents and elaborating on activated carbon adsorbents and their synthesis methods. The same chapter provides background reading on adsorption and adsorption isotherm modelling. The third chapter, is split into three main sections: the materials used in this research, their synthesis and characterisation techniques. The same chapter introduces the adsorption measurement techniques and associated algorithms that were adopted in this research. The fourth chapter presents the characteristics of the activated carbon samples, namely the morphology of the samples, their elemental composition and true density. In addition, N_2 adsorption isotherms and derived surface textural properties such as surface area, pore volume, and pore size distribution are reported. Furthermore, the activated carbon samples and their preparation conditions are related to their observed characteristics. The fifth and the sixth chapters are dedicated to CO_2 adsorption and CH_4 adsorption on the activated carbons, respectively. For each of the two gases, uptake measurements are presented and discussed in relation to the textural properties of their respective adsorbent. The same chapters also report the measured high pressure adsorption isotherms for CO_2 and CH_4 in both dry and wet conditions. Chapter seven highlights the usefulness of modelling the experimental adsorption data to assess solid adsorbents performance. The same chapter then proceeds to modelling CO_2 adsorption and CH_4 adsorption, followed by mixed gas (CO_2 and CH_4) adsorption

modelling, and finally CO_2/CH_4 selectivity calculations are presented. The final chapter, chapter eight, provides an overall conclusion and suggests some future work. Figure 1.4 illustrates the research workflow, both experimental and modelling, followed during this project.

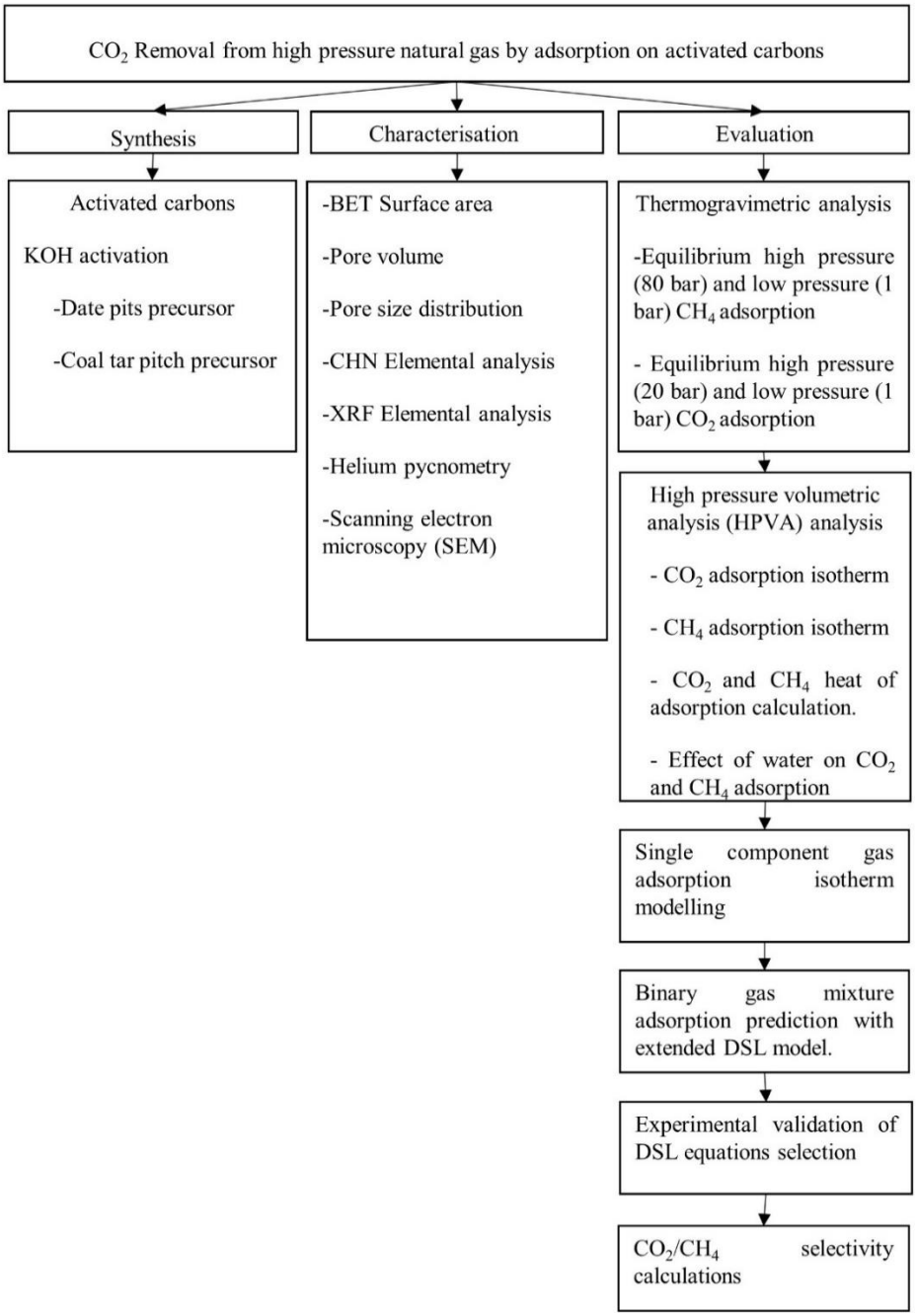


Figure 1.4 Research workflow diagram.

Chapter 2. Literature review

The existing literature related to this research was reviewed and is presented in this chapter in three sections. The first section presents an overview of the available technologies for separating CO_2 from natural gas, namely, absorption (both chemical and physical), low temperature phase separation, membrane separation technology, and adsorption process technology. The most common adsorbent materials are reviewed in section 2.2, where more focus is given to activated carbon adsorbents. The last section in this chapter explains the gas adsorption modelling techniques used to model both single and binary gas component adsorptions.

2.1 Process Technologies for CO_2 Separation from Natural Gas

In the natural gas processing industry today, the most established technology for separating CO_2 from raw natural gas is the amine chemical absorption process (Peters *et al.*, 2011). However, several other technologies have been developed with the aim of reducing one or more of the following: the process equipment footprint, the capital cost of equipment, health and environmental impact, and the energy penalty associated with CO_2 separation from raw natural gas. From the available literature, four main groups of process technologies for CO_2 separation

from raw natural gas were identified: absorption process, low temperature phase separation, membrane separation technology and adsorption process technology. Each of the four technologies has its merits and drawbacks as discussed in the following subsections.

2.1.1 Absorption

Absorption in the context of CO_2 removal from natural gas refers to the process by which CO_2 molecules are separated from the natural gas mixture by entering the bulk phase of a chemical compound to either form weakly bonded intermediate compounds (chemical absorption) or just form a mixture (physical absorption) (Rufford *et al.*, 2012). Absorption equilibria and kinetics control chemical absorption, whereas solubility and mass transfer control physical absorption (Shimekit and Mukhtar, 2012). In the next two subsections, both the chemical and physical absorption processes are briefly described and some of their merits and drawbacks are highlighted.

2.1.1.1 Chemical Absorption

The chemical absorption process using solvents, for example, amine, is one of the most established technologies for CO_2 removal in the natural gas processing industry due to its high selectivity and capacity in removing CO_2 (Olajire, 2010). Figure 2.1 shows a simplified flow sheet of an amine absorption process for CO_2 removal from a raw sour natural gas stream. The raw sour natural gas enters the absorber column from the bottom and flows upwards and countercurrently to the lean amine solutions, typically an aqueous solution containing 10 - 65% amine (Rufford *et al.*, 2012).

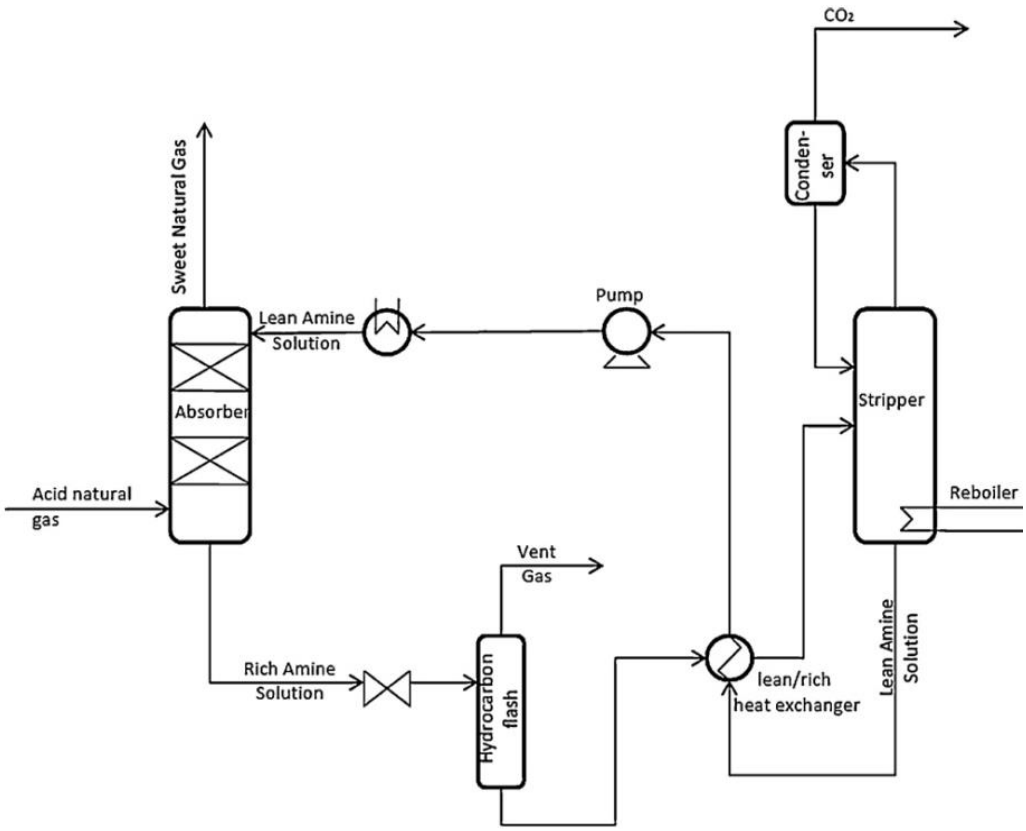


Figure 2.1: Amine absorption process (Peters *et al.*, 2011).

In the absorber column, sour gas comes into contact with the lean amine solution resulting in the CO_2 gas being absorbed by the aqueous amine. The treated gas leaves the absorber column at the top and the CO_2-rich amine solution leaves the column at the bottom and flows into the hydrocarbon flash column where any absorbed hydrocarbons are flashed to gas. The CO_2-rich amine solution is sent to the lean/rich heat exchanger where the CO_2-rich solution is heated and the CO_2-lean solution is cooled. The CO_2-rich amine solution then enters into the stripper column where it is regenerated by heating with the reboiler to evaporate the water and some of the amine. The evaporated product enters the condenser where CO_2 is liberated. The lean amine solution leaves the stripper and enters the lean/rich heat exchanger for cooling before it is pumped back to the absorber again.

The amine absorption process suffers from the high energy requirements of the regeneration and recirculation steps where energy is required to raise the temperature of the CO_2-rich amine solution to release the CO_2. Energy is also required to recirculate the lean amine back to the absorption column (Kidnay and Parrish, 2006). The energy requirement for CO_2 separation in a typical amine absorption process could be as high as 4 GJ/ton CO_2 (Rota, 2014). A high energy requirement is also indirectly associated with the amine process since the treated natural gas stream leaves the amine process saturated with water since the amine solution used is typically aqueous. This water is removed with a downstream dehydration process to meet the pipeline gas specifications which adds to the total energy requirement for processing the raw natural gas. Amine degradation and loss due to evaporation are considered some of the disadvantages of chemical absorbents (Olajire, 2010), in addition to their corrosive nature and foaming and fouling tendency (Sreedhar *et al.*, 2017).

2.1.1.2 Physical Absorption

Physical absorption depends on physical interactions between the CO_2 and a solvent to dissolve the CO_2 and create a mixture. The performance of the physical absorbent is influenced by the solubility of the CO_2, the surface area of the interface and the temperature and pressure at which the interaction occurs (Sreedhar *et al.*, 2017). Selexol, a mixture of dimethylethers of polyethylene glycol, is the physical absorbent used in what is known as the Selexol process, shown in Figure 2.2. CO_2 has higher relative solubility in Selexol compared with the rest of the natural gas components (Feng *et al.*, 2012). In the Selexol process, sour natural gas enters the absorber column and flows countercurrently to the Selexol solvent. CO_2 together with small amount of CH_4 dissolve in the Selexol to

form a CO_2-rich solution under pressure. Multi-stage flash drums are then used to drop the pressure of the CO_2-rich solution. In flash drum number one, any absorbed CH_4 is released then compressed and recycled back to the absorber column. The pressure of the solvent leaving flash drum number one is dropped in stages through the remaining two flash drums to release the absorbed CO_2 without the need for a temperature increase; hence the relatively lower energy penalty compared to the chemical absorption process. Finally, the lean Selexol solution is cooled down and recycled to the top of the absorber column.

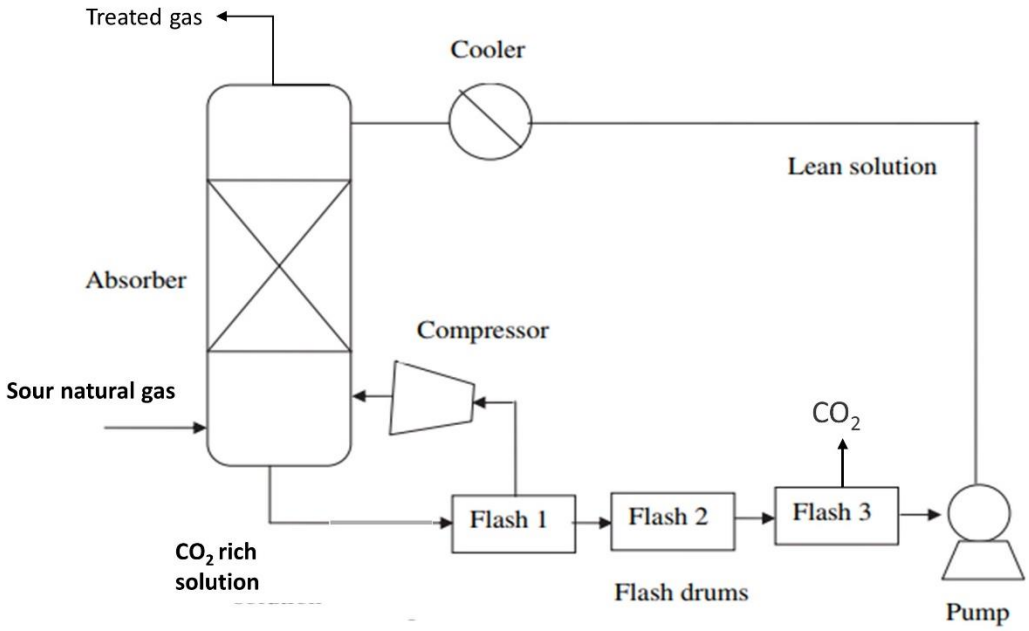


Figure 2.2 Simplified schematic of the Selexol physical absorption process (Olajire, 2010).

Ionic liquids are another example of physical absorbents where CO_2 is absorbed within the free space between the ions (Huang and Ruther, 2009). Ionic liquids, in general, are organic salts with low vapour pressure, they are non-flammable and in many cases have low toxicity (Rufford *et al.*, 2012). The low vapour pressure of the ionic liquids overcomes the disadvantage of solvent loss due to evaporation which is a known problem with amine solvents during thermal regeneration. However, high viscosity is seen as one of the drawbacks of ionic liquids that limits

its integration into industrial processes, since high viscosity increases the capital and energy cost of the pump used to circulate the ionic liquid (Park *et al.*, 2015).

Switchable solvents are a special type of ionic liquids originally discovered by Jessop *et al*. (2005). They demonstrated that a basic non polar liquid mixture can be converted into a polar ionic liquid once in contact with CO_2. This discovery paved the way for subsequent research in switchable solvents for CO_2 absorption, for example, the work of Heldebrant *et al.* (2011) in which CO_2 uptake capacity of 1.3 mol per mole of solvent was reported.

Physical absorption is govern by Henry Law, i.e. the amount of dissolved CO_2 increases linearly with increasing CO_2 partial pressure, unlike chemical absorption that is independent of CO_2 partial pressure. Therefore, physical adsorption is more suited for high pressure CO_2 removal. However, issues such as solvent handling, solvent degradation and complex solvent synthesis methods are still seen as challenges for the use of physical absorbents (Sreedhar *et al.*, 2017).

2.1.2 Low Temperature Phase Separation

Phase separation by a low temperature process, also known as cryogenic separation, of CO_2 from a natural gas mixture exploits the distinct thermodynamic properties of CO_2 compared to the properties of other light hydrocarbon components of the natural gas (mainly methane). In a typical cryogenic CO_2 separation process, the CO_2 is condensed to a liquid or in some cases solidified at a temperature and pressure where the other natural gas components remain in the mixture and in a different phase to that of the CO_2. Several process schemes exist for cryogenic CO_2 separation from natural gas such as Controlled Freeze Zone (CFZ™) and CryoCell®. In the CFZ™ process scheme the natural gas feed is

refrigerated before entering the CFZ™ tower shown in Figure 2.3. The tower is divided into three zones: CO_2 solidification region (coloured red) in the phase equilibrium (pressure-temperature-composition) envelope and two rectifying and stripping sections to handle the vapour-liquid areas above and below the CO_2 solidification region (Kelley *et al.*, 2011).

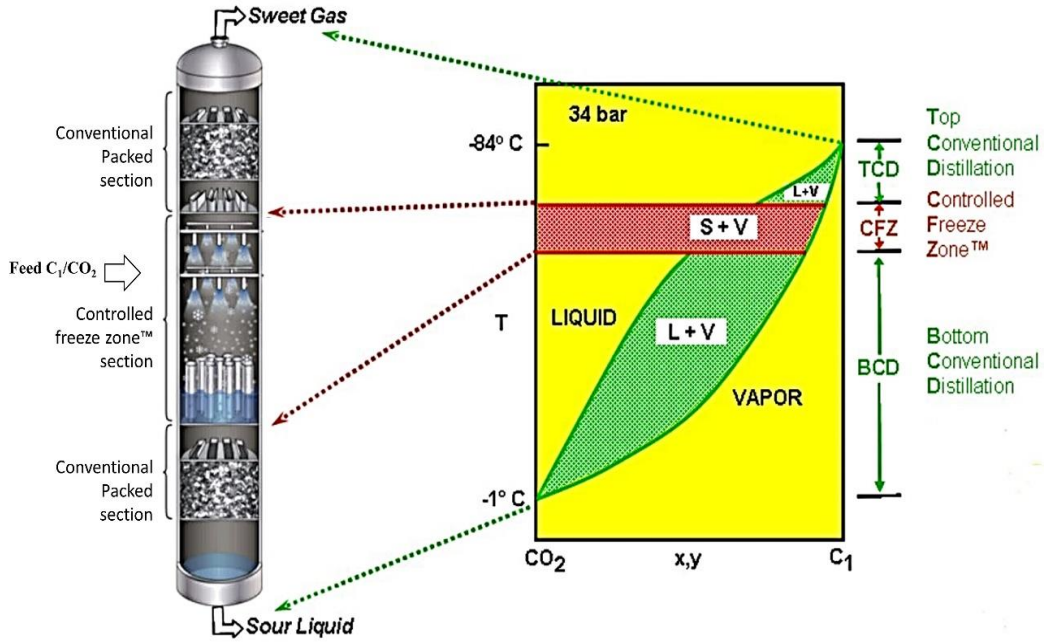


Figure 2.3 The CFZ™ tower (Kelley *et al.*, 2011).

The CryoCell® process scheme shown in Figure 2.4 is designed to allow the solidification of CO_2 by dropping the gas temperature using a chiller and a Joule-Thomson expansion system. Solid CO_2 forms inside the CryoCell® separator before it is heated to liquid CO_2 so it can be pumped out. Hydrocarbons heavier than methane in the natural gas mix are recovered as Natural Gas Liquid (NGL) upstream the chiller (Hart and Gnanendran, 2009).

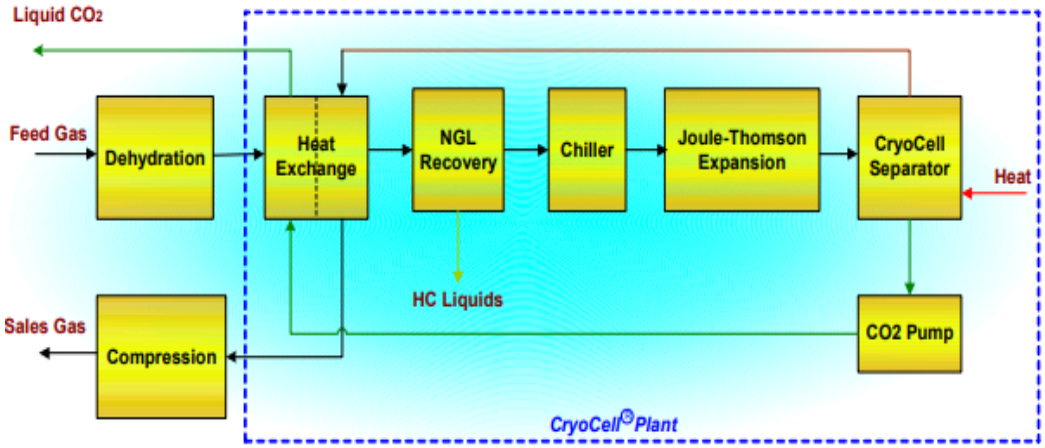


Figure 2.4 The CryoCell® process scheme (Hart and Gnanendran, 2009).

Generally, cryogenic CO_2 separation is not common in the upstream gas industry. This is in contrast to the downstream gas industry (LNG plants), because refrigeration is the main process in the LNG plant but not in the upstream gas processing industry. Furthermore, low temperature phase separation is a high energy penalty process; high-energy demand is required for refrigeration of the natural gas as seen in both the CFZ™ and CryoCell® processes. However, since the CO_2 from the cryogenic separation is in liquid form, it has the advantage of pumping the separated CO_2 underground for geological storage or EOR much easier.

2.1.3 Membrane Separation Technology

Separation of CO_2 from a natural gas mixture using membrane technology depends on the differences in the mobility of the CO_2 compared to other natural gas components when passing through the membrane, i.e. CO_2 should pass through the membrane, whilst the remaining natural gas components (mainly methane) should not. Gas separation by membranes relies on one or a combination of four different diffusion mechanisms (Ismail, Chandra Khulbe and Matsuura, 2015), as illustrated in Figure 2.5. These mechanisms are: (a) Knudsen (or free

molecule) diffusion, (b) surface diffusion, (c) capillary condensation, and (d) molecular sieving.

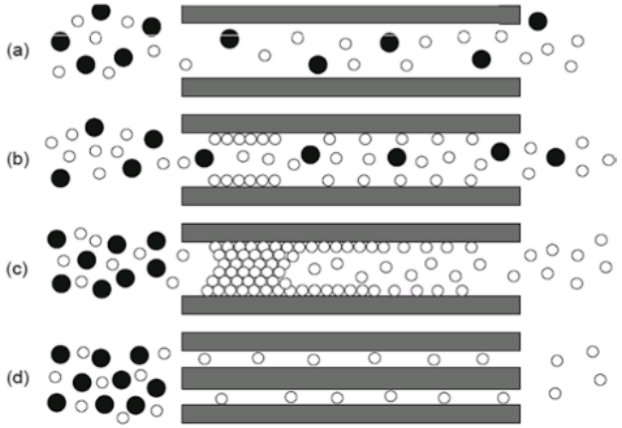


Figure 2.5 Four gas diffusion mechanisms through a membrane, (a) Knudsen diffusion, (b) surface diffusion, (c) capillary condensation, and (d) molecular sieving (Ismail, Chandra Khulbe and Matsuura, 2015).

Membranes can be divided into three main types based on their materials: polymeric, inorganic and hybrid organic/inorganic membranes (Ebner and Ritter, 2009). While polymeric membranes are the most commonly used type in the industry, there is a compromise between gas permeability and selectivity; however this has encouraged the development of mixed matrix membranes to combine the benefits of polymers and organic/inorganic fillers (Kanehashi *et al.*, 2017).

A very large membrane surface area is required to perform the separation of CO_2 at an industrial scale. Therefore, membranes are deployed in modules such as the spiral-wound membrane module shown in Figure 2.6. This also helps to reduce the footprint of the membrane.

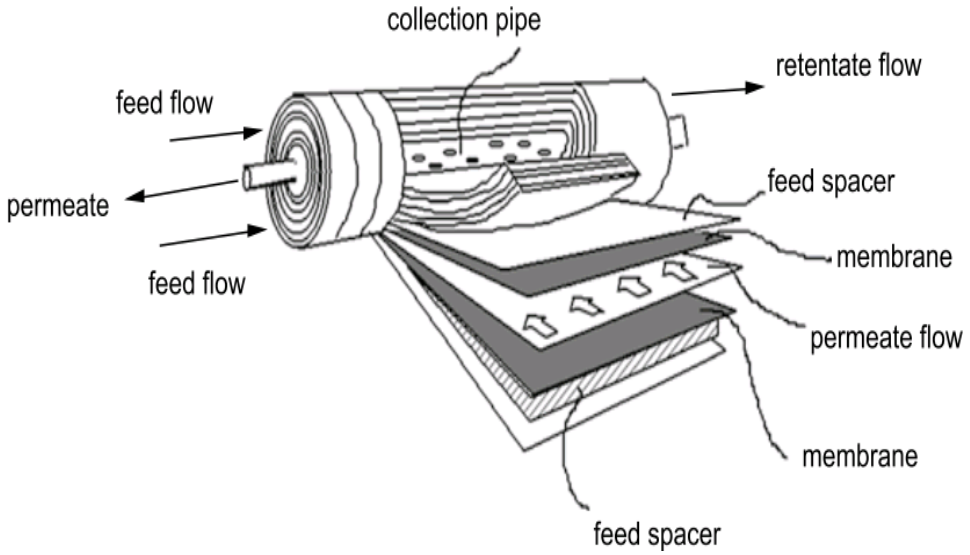


Figure 2.6 Spiral–wound membrane module (Ismail, Chandra Khulbe and Matsuura, 2015).

For the high pressure natural gas processes, the removal of CO_2 using membranes provides a simple process with a relatively small footprint and low process equipment cost (Lin and Freeman, 2005). However, high purity requirements might drive the process to a multiple membrane system where a significant pressure drop may be seen and the need for an additional compression step might arise, hence increasing the energy demand of the CO_2 removal process. In addition, high CO_2 partial pressure was reported to cause what is known as CO_2-induced plasticization on polymeric membranes where the polymer swells due to sorption of CO_2, hence accelerating the penetration of CH_4 and reducing CO_2/CH_4 selectivity (Kanehashi *et al.*, 2017). Water contamination in the natural gas stream could also cause water-induced plasticization that might result in a permanent alteration to the membrane selectivity even after drying (Yampolskii and Freeman, 2010).

2.1.4 Adsorption

Adsorption is the term used to describe the phenomenon which occurs when fluid molecules (gas molecules in this case) are attracted to a solid surface once they are in close vicinity of that surface (Grande, 2012). The adsorption of a particular gas molecule depends on the existence of a force field at the surface of the solid which acts to reduce the potential energy of that gas molecule below that of its fluid phase (Karge and Weitkamp, 2008). The number of molecules adsorbed is proportional to the increase in pressure, and due to the exothermic nature of the adsorption process is inversely proportional to the temperature (Hedin *et al.*, 2013).

The two main types of adsorption are: chemical adsorption, also known as chemisorption, and physical adsorption, also known as physisorption. The main distinction between these two types of adsorption is the type of bond formed between the adsorbed gas molecules and the solid surface. In chemisorption, the adsorption bond involves electron transfer between the adsorbed fluid molecules and the solid adsorbent surface; hence a true chemical reaction has occurred. This mechanism does not occur in physical adsorption, instead, the adsorption bond is due to weak Van der Waal forces. Furthermore, physical adsorption is associated with multilayer adsorption whereas chemical adsorption is limited to monolayer coverage (Keller and Staudt, 2005). Due to its high selectivity and low capacity, chemisorption is normally employed to remove trace impurities whereas physisorption is used for bulk separation processes due to its high capacity (Karge and Weitkamp, 2008). A third type of adsorption, a hybrid of the two main types, is called physio-chemical adsorption, as mentioned by Keller and Staudt (2005). However, since the focus of this research is the removal of bulk CO_2 rather than trace CO_2, and due to the availability of raw natural gas at high pressure which can

promote high physisorption (Keller and Staudt, 2005), only physisorption will be considered from herein.

In general, the technological advances of CO_2 separation from high pressure raw natural gas using adsorption can be grouped in two main categories:

1. The development of high performance solid adsorbent materials.
2. The development, modification and improvement in the adsorption and regeneration cyclic processes.

Both groups need to be optimised to produce a high-performance system. There are two main steps in any cyclic adsorption process. The first step is the adsorption of CO_2 under high pressure that is normally available at natural gas wellheads and this works in favour of the physical adsorption process. The second step of regeneration or desorption begins once the adsorbent is saturated with CO_2. In this step, the adsorbed CO_2 and other gases are released and the solid adsorbent can be re-used for another cycle of adsorption. Two main cyclic adsorption processes are defined depending on how the regeneration step is achieved. When the regeneration is achieved by increasing the temperature of the saturated adsorbent, the process is called Temperature Swing Adsorption (TSA). However, if the regeneration step is achieved by depressurising the saturated pressurised adsorbent, the process is known as Pressure Swing Adsorption (PSA). In comparison, PSA has a lower energy requirement since no external heat is necessary to regenerate the adsorbent. PSA is also a faster process than TSA since dropping the pressure in an adsorption bed is much quicker than increasing the bed's temperature. In the next two subsections, both PSA and TSA processes are examined within the context of CO_2 removal from high pressure natural gas.

Section 2.2 follows which outlines the adsorbent materials which can be used in these processes.

2.1.4.1 Pressure Swing Adsorption (PSA)

The PSA concept was first patented in 1932 (Wilhelm Warner F, 1932). However, it was only utilised 30 years later by Skarstrom (1960) in what is known as Skarstrom PSA cycles. The basic Skarstrom PSA cycle concept has four steps as shown in Figure 2.7. Considering only bed 1 in Figure 2.7, the basic Skarstrom PSA cycle follows these 4 steps:

1. Pressurisation. A high pressure fluid (natural gas in this case) flows to the adsorption column until the column reaches the desired pressure for the adsorption process.
2. Adsorption. The product gas (the least adsorbed) flows out of the column and, at the same time, the feed gas introduced into the column. Some of the product gas is stored in a tank to be used in step 4 as purge gas.
3. Blowdown. The pressure in the column is reduced by venting the gas until the desired desorption pressure is reached.
4. Purge. Some of the product gas is used to purge the column to remove the adsorbed molecules so that the column is ready for the next repeat cycle.

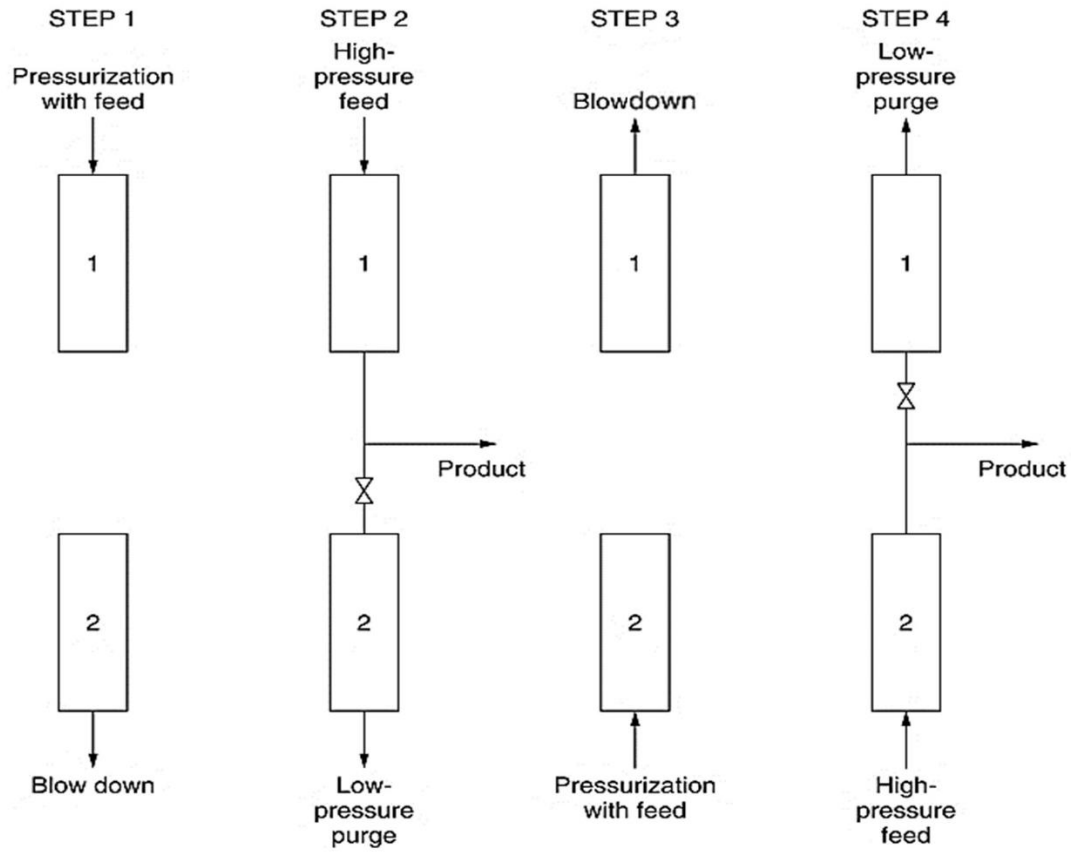


Figure 2.7 Skarstrom PSA cycle (Yang, 2003).

Using a single bed means that the separation of the gas is running as a batch process, i.e. there is no feed flow during the blowdown and purge steps. To avoid this, and to ensure a continuous process where the feed gas can be introduced to the process without interruption, a second bed can be used as shown in Figure 2.7 (Yang, 2003). While one bed is adsorbing the other bed is desorbing, therefore, keeping the feed continuous.

More beds can be added to optimise the process and achieve higher purity and higher recovery of the product. In addition to the 4 steps mentioned above, a vacuum step can be added after the purge step to maximise the removal of the adsorbate and increase the regeneration efficiency to get what is known as Vacuum Pressure Swing Adsorption (VPSA). However, the addition of a vacuum step, by using a vacuum pump, will increase the energy penalty and defy the concept of

low energy demanding PSA. Furthermore, the introduction of a vacuum pump would convert the simple PSA process, which only relies on valves switching to operate, to a more complex process. Hence, it is not desired and could be avoided if a solid adsorbent with good CO_2 capacity at high pressure and very low uptake at low pressure could be developed. Literature examples of some PSA processes for CO_2 removal are summarised in Table 2.1; their performance is measured by the CH_4 recovery and purity since it is the gas with the highest economic value.

Table 2.1 Literature examples of studies using the PSA process for CO_2 removal from natural gas.

Adsorbent	Gas mixture	Study type	PSA Type	CH_4 purity (%)	CH_4 recovery (%)	Pressure (Bar)	Ref.
Zeolite 13X and Carbon Molecular Sieve	CO_2 CH_4 N_2	Experiment	VPSA	92.5	55	1.2	(Cavenati and Grande, 2005)
Silicate	CO_2 CH_4	Simulation	PSA	100	30	1	(Delgado and Rodrigues, 2008)
Zeolite 13X	CO_2 CH_4	Simulation	PSA	99	85	4	(Santos, Grande and Rodrigues, 2011)
AC	CO_2 CH_4	Experiment	VPSA	95	65	30	(Kacem, Pellerano and Delebarre, 2015)
AC	CO_2 CH_4 C_2H_6	Simulation	PSA	91	90	70	(Grande *et al.*, 2017)

So far the only industrial application documented in the literature for the removal of CO_2 from high pressure raw natural gas by PSA is the system developed by Xebec Inc. (Grande and Blom, 2012) which was designed to treat around 6000 nm^3/h of natural gas at 20 bar and 13% CO_2. However, the unit was operated at only 3500 nm^3/h to achieve a methane recovery of 62% with a purity of 94%.

2.1.4.2 Temperature Swing Adsorption (TSA)

In the TSA process, the regeneration of the saturated solid adsorbent is achieved by increasing its temperature by purging the adsorption bed with a pre-heated gas (Yang, 1987) or by directly heating the desorption bed. While minimising the energy penalty of the CO_2 separation processing system is of paramount importance in this research, an energy intensive TSA process might be considered if it is necessary to maintain the pressure of the total system. In such a process, regenerating the saturated adsorbent occurs at high pressure, avoiding the depressurisation step of the PSA for regeneration. A simplified schematic of a TSA process used for CO_2 removal from biogas is shown in Figure 2.8.

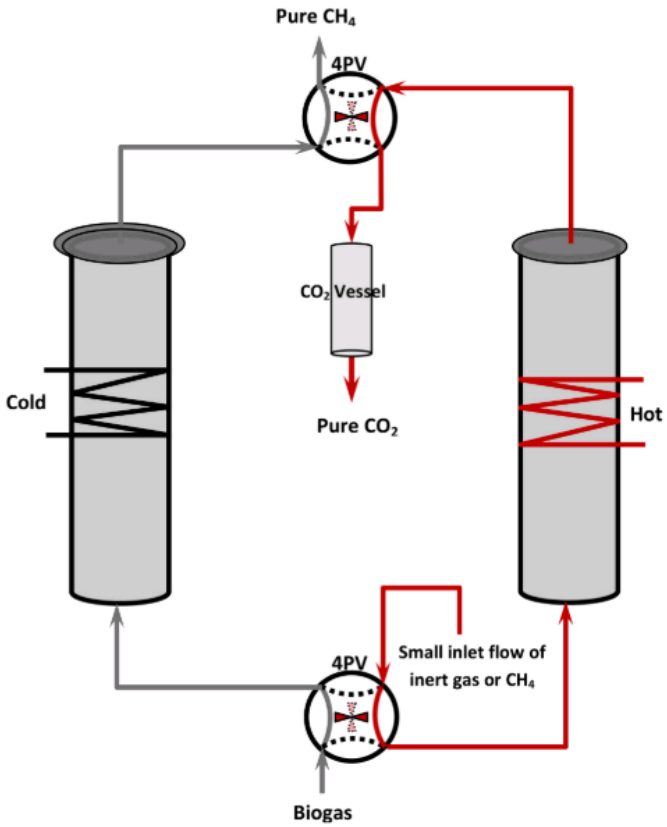


Figure 2.8 Schematic representation of 2-bed TSA system (Yentekakis and Goula, 2017).

Another disadvantage of TSA is that the cooling of the solid adsorbent before the next cycle of adsorption can occur is likely to take a long time. This would result in a need for more beds so that a continuous operation can be maintained.

2.2 Adsorbent Materials

Porous solid adsorbents can have varying pore sizes. It is useful to classify the pores according to their size into three distinct groups as per the IUPAC recommendation (Sing *et al.*, 1985) as follows:

(A) Macropores: pores with widths exceeding 50 nm.

(B) Mesopores: pores of widths between 2 nm and 50 nm.

(C) Micropores: pores with widths not exceeding 2 nm.

Adsorption performance indicators are used to report the performance of the solid adsorbents. The most common performance indicators are adsorption capacity and adsorption selectivity. Adsorption capacity is a measure of the amount of adsorbate that can be adsorbed by a unit mass of the adsorbent. Selectivity is a measure of preferential adsorption of one of two gas species (n_1 and n_2) in a gas mixture. It is defined, for one pressure, to describe the amount adsorbed and the amount left in the gas phase for one species over the other (Rouquerol *et al.*, 2014). This can be represented as

$$Selectivity\ of\ n_1\ over\ n_2 = \frac{n_{1_adsorbed}}{n_{2_adsorbed}} . \frac{n_{2_in\ gas}}{n_{1_in\ gas}} \qquad (2.1)$$

From the point of view of CO_2 adsorption using PSA in natural gas CO_2 separation, one can group the merits of any physical adsorbent into two main groups, separation performance and operation stability. Selectivity and capacity are the main indicators of separation performance. Mechanical strength and ease of

adsorbent regeneration are indicators of operation stability. Since physical adsorption is associated with multiple cycles of regeneration to maximize the use of the same adsorbent materials, mechanical strength of the adsorbent to withstand high and low pressure cycles is an important factor for selecting these materials (Yang, 1987).

Three of the most commonly used industrial solid adsorbents are zeolites, mesoporous silica and activated carbons, and they are reviews in the next subsections. Much research has been carried out on the synthesis and modifications these solid adsorbents.

2.2.1 Zeolites

Zeolites are porous crystalline aluminosilicates, with framework consisting of interlocking tetrahedrons of SiO_4 and AlO_4 linked together in various regular forms and sharing oxygen atoms (Wang *et al.*, 2011). Commercial zeolites are available in regular particle shapes (beads and pellets). A binder material (clay, alumina or a polymer) is used to bind the zeolite crystals together to reduce the pressure drop in adsorbent columns (Auerbach, Carrado and Dutta, 2003). Zeolite 13X is one of the most common commercial types of zeolites for gas purification and bulk separation including CO_2/CH_4 separation. The superiority of Zeolite 13X over four other types of zeolite (5A, 4A, WE-G 592, APG-II) in terms of adsorption capacity up to 20 bar pressure was observed in an experimental study by Siriwardane *et al.* (2005). However, compared to activated carbon, Zeolite 13X showed a lower CO_2 uptake above 1.7 bar (Siriwardane *et al.*, 2001), and a similar finding was also reported by Choi et al. (2009). In addition, an experimental study by Kacem et al. (2015) found that at higher pressures (4 - 20 bar) activated carbon outperformed zeolites in CO_2 adsorption capacity when used in the PSA process

to remove CO_2 from CH_4. The same study reported an initial drop in zeolite capacity followed by stabilisation when cycled in a PSA-like process; this drop was not seen with activated carbon. A selection of studies from the literature investigating high pressure and high temperature CO_2 separation from a methane/carbon dioxide mixture with zeolites are presented in Table 2.2.

Table 2.2 Literature selected high pressure zeolite equilibrium selectivity and capacity.

Zeolite Type	Adsorbate	Equilibrium capacity (mmol/g)	Selectivity	Pressure (bar)	Temp (°C)	Reference
13 X	CO_2	5.76	1.37	34	50	(Cavenati, Grande and Rodrigues, 2004)
	CH_4	4.2		34	50	
13 X	CO_2	5.25	-	20	30	(Siriwardane *et al.*, 2005)
	CH_4	-		-	-	
T	CO_2	2.75	2.5	20	35	(Rad, Fatemi and Mirfendereski, 2012)
	CH_4	1.1		20	35	

*Selectivity is taken as the capacity ratio of CO_2/CH_4.

2.2.2 Mesoporous Silica

The surface of pure silica is inactive and hydrophobic (Ruthven, Farooq and Knaebel, 1994). This gives silica-based materials the advantage of potentially withstanding moisture and not being poisoned by contaminants like H_2S when used for CO_2 adsorption from sour natural gas. Adsorption of pure CO_2 by MCM-41 silica was the subject of a series of investigations at high pressure (up to 45 bars) by Belmabkhout *et al.* (2009). This study showed an increasing CO_2 uptake with pressure above 30 bar where volumetric CO_2 uptake per unit surface area for MCM-41 was higher than that of activated carbon and zeolite. The MCM-41 used by Belmabkhout was mesoporous with pore diameter less than 4 nm. Adsorption at a pressure above 45 bar was not investigated. Building on the observed high

CO_2 uptake, a follow up study on binary gas separation of CO_2 and CH_4 using the same MCM-41 silica was conducted by Belmabkhout, Serna-guerrero and Sayari (2010). This study showed that MCM-41 has superior CO_2/CH_4 selectivity when compared to activated carbon (Maxsorb) and Zeolite 13X at a pressure above 10 bar and up to 45 bar. CO_2/CH_4 selectivity showed an upward trend with increasing pressure mainly above 10 bar. At ambient temperature and high pressure (above 10 bar), the physical adsorption selectivity of CO_2/CH_4 on microporous adsorbents like activated carbon was less sensitive to a pressure increase, in contrast to observations with mesoporous materials like MCM41 where selectivity increases with pressure (Belmabkhout and Sayari, 2009). However, this was not validated at pressures above 45 bar and temperature above ambient.

Another type of mesoporous silica, SBA-15, with a pore diameter of 7.7 nm was studied for high pressure adsorption of CO_2, N_2 and CH_4 (Liu *et al.*, 2007). The highest CO_2 adsorption capacity of 10 mol/g was recorded at 40 bar and at 10 bar pressure, the adsorption capacity for CO_2 was around 4.5 mol/g. Modification of SBA-15 with triethanolamine (TEA) resulted in an enhancement of CO_2 over CH_4 selectivity by seven times. SBA-15 was fully regeneration after CO_2 adsorption when purged with methane. The authors of this study suggested the potential use of SBA-15 in a PSA scheme for CO_2 removal from CH_4 and CO_2 gas mixture. However, no analysis was carried out on the resulting heat of adsorption to verify if the addition of TEA promoted chemical adsorption that might lead to a need for a TSA process for regeneration due to the strength of CO_2 binding in chemical adsorption.

2.2.3 Activated Carbon

The use of activated carbon is one of the earliest examples in using adsorbents for gas purification, with manufacturing dating back to the nineteenth century (Yang, 1987). The simplest description of activated carbon is "porosity enclosed by carbon atoms" (Marsh and Rodríguez-Reinoso, 2006) and it is this porosity that enables the activated carbon to effect separation of the gases.

Several studies have been carried out to assess the adsorption of CO_2 and CH_4 on activated carbons. Himeno *et al.* (2005) provided one of the most comprehensive comparative studies on activated carbons for CO_2 and CH_4 adsorption. They used five different types of activated carbons, four of which were commercially available and one was a specially engineered activated carbon. Temperatures ranging from 0 to 60 ^oC and pressures ranging from 0.005 to 60 bar were considered in Himeno's study using a static volumetric device. Adsorption isotherms for pure CO_2 and CH_4 gases were generated, but no binary gas mixture adsorption tests were conducted. The results showed that the amount of adsorbed CO_2 is around twice the amount of the adsorbed CH_4 on all samples, in agreement with the findings of Grande *et al.* (2013). The Maxsorb activated carbon investigated by Himeno *et al (2005)* was made from petroleum coke mixed with KOH and activated in nitrogen atmosphere. It has a surface area of 3250 m^2/g and a total pore volume of 1.79 cm^3/g and showed a CO_2 adsorption capacity of 32 mol/kg at 30 bar and 0 ^oC, the highest among the five types of activated carbons investigated. At a temperature of 50 ^oC and pressure of 47 bar, the adsorption capacity of Maxsorb dropped to 22 mol/kg. All the activated carbons used in this study were predominantly microporous. It is the view of the authors of this study that micropores contribute to the adsorption of the methane and the carbon dioxide

at room temperature (Himeno *et al.*, 2005). In addition, the adsorption capacities were found to increase with increasing BET surface area and total pore volume.

The heat released as a result of CO_2 and CH_4 adsorption (isosteric heat of adsorption) was used to provide information about the selectivity of activated carbon for CO_2 over CH_4. A more dramatic increase in isosteric heat of adsorption for certain types of activated carbon was recorded (Himeno, Komatsu and Fujita, 2005). Such an increase was correlated with increased adsorption loading of CO_2 which in turn suggested that the heat released was due to the interactions between the adsorbate molecules as well as from the adsorbent-adsorbate interactions. The difference in intermolecular interactions between CH_4 and CO_2 molecules was also cited, in the same research, as another reason for different adsorption capacities. The isosteric heat of adsorption for CO_2 increased with the increase in CO_2 uptake, which indicated that interactions between CO_2 molecules were significant in the adsorption process. In contrast, in the case of CH_4, the insignificant interaction between CH_4 molecules, due to the negligible dipole or quadrupole moments in CH_4 molecules, caused a decrease in the isosteric heat of adsorption with the increase of CH_4 uptake as adsorption sites get occupied (Mu and Walton, 2011).

In another study, using Maxsorb activated carbon for adsorption in a PSA process, it was reported that CO_2 is more selectively adsorbed than CH_4 by the activated carbon at various pressures (0.5, 2.5 and 5 bar) (Grande *et al.*, 2013). At 5 bar and 40 ^{o}C, the CH_4 loading was 8.5 mol/kg whereas the CO_2 loading was 17 mol/kg. The same study also showed a clear increase of loading of both CO_2 and CH_4 with increasing pressure.

The ability to fully regenerate the used solid adsorbent is another important factor when considering the PSA process. Activated carbon was found to be fully reversible after regeneration by pressure swing without any significant drop in its initial CO_2 capacity. However, zeolites showed an initial drop in CO_2 capacity before stabilisation when regenerated by the same pressure swing process (Kacem, Pellerano and Delebarre, 2015). Table 2.3 provides the CO_2 equilibrium capacity and selectivity figures for two common types of activated carbon used industrially.

Table 2.3: Literature selection of activated carbon equilibrium capacity and selectivity for CO_2/CH_4 separation at high pressure.

AC Type	Adsorbate	Equilibrium capacity (mmol/g)	Selectivity*	Pressure (Bar)	Temp (ºC)	Reference
Maxsorb	CO_2	12	1.8	47	40	(Grande *et al.*, 2013)
	CH_4	6.5		47	40	
Norit R1 Extra	CO_2	10.2	1.6	40	25	(Dreisbach, Staudt and Keller, 1999)
	CH_4	6.5		40	25	

*Selectivity is the taken as the capacity ratio of CO_2/CH_4.

2.2.3.1 Activation Mechanism

In the context of activated carbon synthesis, activation refers to the process by which the porosity of a carbon rich material (precursor) can be increased leading to a higher surface area and pore volume in the resulting activated carbon (Marsh and Rodríguez-Reinoso, 2006). Various methods of activation have been used to produce activated carbons from various precursors such as agricultural or industrial wastes in the attempt to produce low cost solid adsorbents. In this work, two main activation approaches are reviewed: physical activation and chemical activation. In physical activation, the precursor is activated at a very high temperature (>900 °C) in the presence of steam or CO_2 (Fu *et al.*, 2019). Steam or CO_2 are used to extract some carbon atoms from the structure of the carbon

precursor to create the porosity according to the following gasification reactions (Marsh and Rodríguez-Reinoso, 2006):

$$C + CO_2 = 2CO \quad (2.2)$$

$$C + H_2O = CO + H_2 \quad (2.3)$$

Chemical activation is achieved by either a one- or two-step process. In the one-step activation process, the carbonisation of the precursor at a high temperature in an inert atmosphere, most commonly nitrogen, is performed after the addition of a chemical activating agent such as phosphoric acid (H_3PO_4), zinc chloride ($ZnCl_2$) or potassium hydroxide (KOH). The carbonised precursor is washed afterwards by water to open up the developed porosity and to remove any excess chemicals (Marsh and Rodríguez-Reinoso, 2006). In the two-step process, the carbonisation of the selected precursor at a high temperature in an inert atmosphere to concentrate its carbon content is carried out first, followed by a chemical activation step with chemical agents. The process ends with water washing in a similar manner to the one-step approach (Fu *et al.*, 2019). Merzougui and Addoun (2008) argue that using the one-step activation approach promotes a high precursor to activated carbon yield. This is because the activating chemical is incorporated into the interior of the precursor particle so that any products from the thermal decomposition of the precursor react with the activating chemical to reduce evolution of volatile matter and inhibit any particle shrinkage. However, Fu *et al.* (2019) have shown that the two-step activation produces higher porosity activated carbons from biomass precursors with KOH as the activating agent. This might be due to the benefit of a separate carbonisation step in removing the volatile matter which maximizes the role of KOH in developing the porosity of the carbon matrix.

Adsorption of CO_2 at low pressure is influenced by the activated carbon surface chemistry, whereas at high pressure, surface area and pore volume of the activated carbon plays a bigger role in determining the CO_2 adsorption capacity (Sun *et al.*, 2013). KOH activation is widely used to produce high surface area and high pore volume activated carbons from various low cost carbon rich precursors such as biochar, coal, petroleum asphalt and coal tar pitch (Otowa, Tanibata and Itoh, 1993; Shao *et al.*, 2011; Wang and Kaskel, 2012; Jalilov *et al.*, 2017). The KOH activation mechanism is complex in nature and involves several reactions at different temperatures. Romanos *et al.*, (2012) described the KOH activation mechanism distinguishing between two groups of reactions, one below 700 ^oC and the other above 700 ^oC as follows:

Below 700 ^oC, KOH is dehydrated to produce potassium oxide (K_2O) and water:

$$2KOH \rightarrow K_2O + H_2O \qquad (2.4)$$

Some of the resulting water consumes some of the carbon (reaction 2.5) creating some initial porosity and producing CO which reacts with the remaining water to produce CO_2 (reaction 2.6). The CO_2 reacts with K_2O to produce K_2CO_3 as shown in reaction 2.7.

$$C + H_2O \rightarrow CO + H_2 \qquad (2.5)$$

$$CO + H_2O \rightarrow CO_2 + H_2 \qquad (2.6)$$

$$CO_2 + K_2O \rightarrow K_2CO_3 \qquad (2.7)$$

Above 700 ^oC, the porosity of the activated carbon develops further due to two new reactions (reactions 2.8 and 2.9) leading to the production of metallic potassium (2K). Potassium penetrates between the carbon layers and causes an expansion before it is leached out of the carbon in the washing step of the activation process leaving behind a high porosity activated carbon, as depicted graphically in Figure 2.9.

$$K_2O + H_2 \rightarrow 2K + H_2O \quad (2.8)$$

$$K_2O + C \rightarrow 2K + CO \quad (2.9)$$

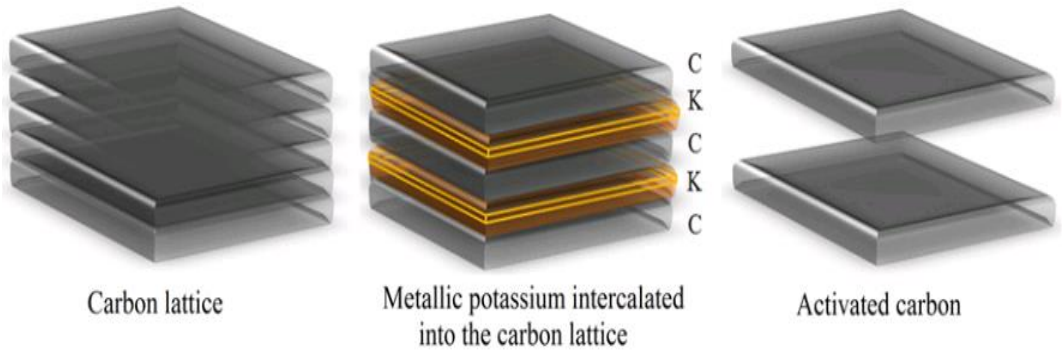


Figure 2.9 Potassium intercalation between the carbon layers during KOH activation at temperatures above 700 ^oC (Romanos *et al.*, 2012).

2.2.3.2 Carbon Precursors

Lignocellulose rich materials and coal are widely used raw materials (precursors) for the synthesis of activated carbons. Ample research exists on the preparation of activated carbons from agricultural waste such as fruit stones (Savova *et al.*, 2001; Martínez *et al.*, 2006; Olivares-Marín *et al.*, 2006) or fruit shells (Foo and Hameed, 2011; Tongpoothorn *et al.*, 2011) since they are inexpensive and easily collected as a result of fruit-based product manufacturing and packaging. An example of such agricultural waste are date pits. Date fruit is widely grown and used as a staple food in the arid and semi-arid regions of the world, for example the Middle East and North Africa, with an estimated annual global production of 7.6 million tons according to the Food and Agricultural Organization of the United Nations (2016). Date pits, also known as date stones, shown in Figure 2.10, constitute a significant proportion of the agricultural waste in the date production and packaging processes and accounts for 10 - 15% of the date fruit weight (Hossain *et al.*, 2014). Therefore, with this in mind, minimum of 760,000 tons of date pits could be produced globally on an annual basis.



Figure 2.10 Raw date pits.

Several research papers have investigated the productions of activated carbon from date pits mainly for water treatment applications, as comprehensively reviewed by Ahmed (2016). Recently, activated carbons from date pits for CO_2 capture applications has also been reported (Ogungbenro *et al.*, 2017). However, according to the literature search conducted during this project, there has been no comprehensive investigation of CO_2 adsorption on activated carbons from date pits at high pressure. Raw date pits have a carbon content of 41% which can be enriched by pyrolysis in a nitrogen atmosphere to reach up to 94.5% (Bouchelta *et al.*, 2012). Merzougui and Addoun (2008) performed chemical activation of date pits biomass with KOH and these were used to produce a microporous activated carbon with BET surface area of 1032 m^2/g. The same researchers reported that chemical activation using KOH resulted in activated carbons from date pits with a higher surface area compared to those produced using $ZnCl_2$ chemical activation.

Coal tar pitch is the second carbon precursor of interest for this research. Coal tar pitch is produced as a residue from the distillation or heat treatment of coal tar (Marsh and Rodríguez-Reinoso, 2006). It contains a complex mixture of many components, but mainly polycyclic aromatic hydrocarbons (Machnikowski *et al.*, 2002). It has been used as a precursor to produce different carbon materials including membranes for gas separation and solid adsorbents for CO_2 adsorption from flue gas (Liang, Sha and Guo, 1999). Hsu and Teng (2000) demonstrated that

chemical activation with KOH is more effective than with $ZnCl_2$ or H_3PO_4 as a higher surface area activated carbon is produced. Ganan *et al.* (2004) used chemical activation at 450 ^oC to activate coal tar pitch with KOH and then subjected the activated carbon to a physical activation process by carbonisation followed by gasification with air to enhance the porosity.

2.3 Adsorption Modelling

Gas adsorption on solid surfaces and in pore volumes is a complex phenomenon that includes mass and energy exchanges in addition to phase changes (Webb and Orr, 1997). In this section, some of the fundamental adsorption modelling techniques and assumptions are reviewed.

2.3.1 Adsorption Isotherms

Adsorption isotherm measurements show the relationship between the amount of gas adsorbed at various pressures using a known mass of solid adsorbent at a fixed temperature. It is one of the fundamental analyses to measure the gas adsorption capacity of solid adsorbents (Webb, 2003). Isothermal gas adsorption is a widely used technique for the characterisation of porous solids. Gravimetric and volumetric adsorption measurement techniques are used to establish the adsorption isotherms. According to the International Union of Pure and Applied Chemistry (IUPAC) there are six main types of adsorption isotherms depicting the relationship between the amount of gas adsorbed (y-axis) and the relative pressure (x-axis). These can be seen in Figure 2.11.

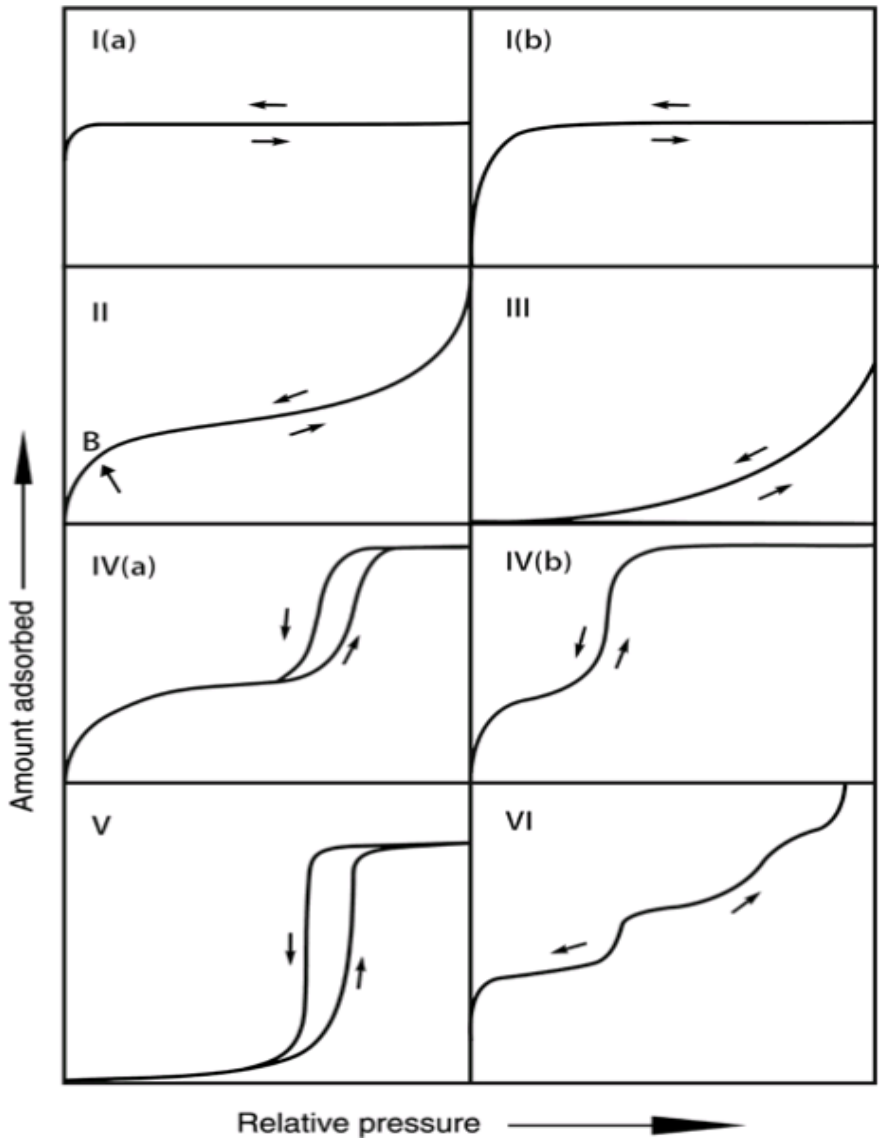


Figure 2.11 Six types of adsorption isotherms (Thommes *et al.*, 2015).

Type I isotherm is produced as a result of gas adsorption on microporous materials having pores less than 2 nm in diameter. Two subtypes of type I can be described: I(a) for adsorption on materials dominated by ultra-micropores (< 0.7 nm) and I(b) for materials containing large-micropores (> 0.7 nm). Type II isotherms are produced by physisorption on nonporous or macroporous solid adsorbents. Type III is seen in cases where the adsorptive molecules have greater attraction to one another compared with their attraction to the solid surface, common in nonporous or macroporous adsorbents subjected to fluids with high intermolecular attraction. Type IV isotherms are produced by gas adsorption on mesoporous solid

adsorbents where gas molecules can condense to a liquid-like phase giving rise to an adsorbed amount after an initial plateau stage. Two subtypes of type IV isotherm exist: IV(a) with a hysteresis loop between the adsorption and the desorption branches of the isotherm, and IV(b) without a hysteresis loop. The shape for Type V isotherms is typical for relatively weak adsorbent–adsorbate interactions at relatively low pressure followed by sharp increase in adsorbed amount at relatively high pressure and typically seen in water adsorption on hydrophobic microporous and mesoporous adsorbents. Type VI isotherms are characteristic of multilayer adsorption on a highly uniform nonporous surface (Thommes *et al.*, 2015)

2.3.2 Adsorption Isotherm Models

Isotherm models are used to predict the amount of adsorbed gas given the pressure and temperature of adsorption and based on a pre-measured adsorption isotherm for the same gas. In addition to their use in adsorption prediction, isotherm models also provide an insight into the nature of the adsorption process and whether it is physical or chemical, homogeneous or heterogeneous, monolayer or multilayer (Abdul Kareem *et al.*, 2018). Moreover, parameters for pure gas adsorption isotherm models can be used to predict the adsorption of binary gas mixtures. In the following section, common isotherm models for single and binary gas adsorptions are presented.

2.3.2.1 Single Component Gas Isotherm Models

The Langmuir isotherm model (Langmuir, 1918) is a popular two-parameter model for gas-solid adsorption. It is based on three fundamental assumptions (Ruthven, 1984):

1. The adsorption takes place at well-defined adsorption sites.
2. All the adsorption sites are energetically identical (homogenous) and each site has the capacity for one adsorbate molecule only.
3. There are no interactions between adsorbed molecules.

Mathematically, the Langmuir model expresses how much of a pure gas component (i) is adsorbed on a solid adsorbent according to equation 2.10.

$$q_i = \frac{q_s bP}{1+bP} \tag{2.10}$$

Where q_i is the amount of gas i adsorbed, P is the pressure, q_s is the adsorption saturation capacity and b is the affinity constant. However, adsorption on activated carbons is thought to be a heterogeneous process since activated carbons have a complex pore network and surface structures (Garcia *et al.*, 2013). Such a challenge to the energetically homogeneous adsorption sites assumption made by Langmuir led to the development of heterogeneous adsorption models such as the Dual Site Langmuir and the Sips models.

Dual Site Langmuir (DSL) isotherm model was aimed at addressing the heterogeneity in the adsorption process by enhancing the Langmuir model to assume that gas molecules can adsorb on two energetically different adsorption sites as opposed to the energetically similar sites of the Langmuir model. The DSL isotherm model is represented mathematically by equation 2.11 (Myers and Prausnitz, 1965).

$$q_i = \frac{q_{s1} b_1 P}{1+b_1 P} + \frac{q_{s2} b_1 P}{1+b_2 P} \tag{2.11}$$

Where q_{s1} is the saturation capacity of adsorption site 1, and q_{s2} is the saturation capacity of adsorption site 2. In addition, there are now two affinity constants, one for each adsorption site, *b1* for site one and b_2 for site 2.

The Sips isotherm model**,** also known as the Langmuir-Freundlich isotherm model, is a three parameters empirical equation that was successfully used to model hydrocarbon adsorption isotherm data on an activated carbon (Ahmadpour, Wang and Do, 1998). The mathematical form of the Sips isotherm is given by equation 2.12 (Garcia *et al.*, 2013).

$$q_i = \frac{q_s(bP)^{\frac{1}{n}}}{1+(bP)^{\frac{1}{n}}} \qquad (2.12)$$

The Sips model addresses the adsorption heterogeneity issue by introducing a heterogeneity power parameter, *n*, to accommodate the argument that the adsorption process is a heterogeneous process. However, it does not specify the source of the heterogeneity; i.e. the heterogeneity could be due to adsorbant-adsorbate interaction, adsorbate-adsorbate interaction or a combination of both (Garcia *et al.*, 2013). If the heterogeneity parameter *n* is equal to 1, then the Sips model equation reduces to the Langmuir model equation.

2.3.2.2 Binary Component Gas Adsorption Models

While unary gas isotherm measurements can be achieved with volumetric or gravimetric gas adsorption equipment, the measurement of the adsorption of a binary gas mixture requires co-adsorption or breakthrough experiments, which are normally challenging and time consuming, hence multicomponent gas adsorption isotherm models gained popularity to predict the adsorption of gas mixtures (Hu *et al.*, 2018). Accurate adsorption models describing the adsorption of a unary gas can be used to predict binary component gas adsorptions by extending the unary

gas adsorption isotherm model to a multi-component gas adsorption model (Yi *et al.*, 2013; Vieira *et al.*, 2018).

All the three single gas adsorption models presented earlier in section 2.3.2.1 have an extended form which can be used to predict the adsorption of a binary gas mixture. The extended Langmuir isotherm model for a binary adsorption system of a gas mixture of two components, i and j, was described by Ruthven, (1984) according to equations 2.13 and 2.14.

$$q_i = \frac{q_{si} b_i P\, y_i}{1 + b_i P\, y_i + b_j P\, y_j} \qquad (2.13)$$

$$q_j = \frac{q_{sj} b_j P\, y_j}{1 + b_j P\, y_j + b_i P\, y_i} \qquad (2.14)$$

Where y_i represents the fraction of gas component *i* and y_j represents the fraction of the gas component *j* in the mixture.

Ruthven (1984) points out that to guarantee the thermodynamic consistency of the extended Langmuir isotherm model, $q_{s,i}$ should be equal to $q_{s,j}$. However, this is not always true since different gases could have different saturated adsorption capacities for the same solid adsorbent. Therefore, Ruthven advocates the use of the extended Langmuir isotherm model as an analytical model rather than a physical model and argues that it should be used with caution since it might not fit adsorption data at varying pressures with the same accuracy.

The extended DSL isotherm model could be arrived at by following the same approach used to arrive at the extended Langmuir model for a gas mixture of two components (i and j) and written as shown in equations 2.15and 2.16.

$$q_i = \frac{q_{s1,i} b_{1,i} P\, y_i}{1 + b_{1,i} P\, y_i + b_{1,j} P\, y_j} + \frac{q_{s2,i} b_{2,i} P\, y_i}{1 + b_{2i} P\, y_i + b_{2j} P\, y_j} \quad (2.15)$$

$$q_i = \frac{q_{s1,i} b_{1,i} P\, y_i}{1 + b_{1,i} P\, y_i + b_{1,j} P\, y_j} + \frac{q_{s2,i} b_{2,i} P\, y_i}{1 + b_{2i} P\, y_i + b_{2j} P\, y_j} \quad (2.16)$$

The extended Sips adsorption isotherm model was described by Ruthven (1984) as thermodynamically not consistent but could provide a good correlation to many binary gas adsorption systems. It can be used to aid the process system design and takes the form given by 2.17 and 2.18.

$$q_i = \frac{q_{s,i} (b_i P\, y_i)^{\frac{1}{n_i}}}{1 + (b_i P\, y_i)^{\frac{1}{n_i}} + (b_j P\, y_j)^{\frac{1}{n_j}}} \quad (2.17)$$

$$q_j = \frac{q_{s,j} (b_j P\, y_j)^{\frac{1}{n_j}}}{1 + (b_j P\, y_j)^{\frac{1}{n_j}} + (b_i P\, y_i)^{\frac{1}{n_i}}} \quad (2.18)$$

2.3.3 Summary

In summary, the literature related to the available process technologies for removing CO_2 from high pressure natural gas was reviewed. Aqueous amine processes were found to be an established technology and widely used in the industry. However, they suffer from high energy penalty and corrosive nature. Therefore, the literature review in this work focused on solid adsorption based technologies, especially those utilising activated carbons. Activated carbon can be produced from low-cost carbon-rich materials, such as biomass and coal tar pitch, using simple chemical activation process with KOH. The literature search conducted in this project revealed that date pits, a widely available biomass in the Middle East, did not receive enough attention as feedstock to produce activated

carbon for gas separation. The effect of the textural properties of activated carbons, such as surface area and pore volume, in separating CO_2 from CH_4 were acknowledged by many researches, however, the role of different pore sizes in separating CO_2 from CH_4 at high pressure was not fully understood. This research aims to address such gap by providing some explanation related to the role of pore size distribution in CO_2 separation from CH_4 at 50^oC and 100 bar pressure.

Chapter 3. Experimental Methods

In the third chapter of this thesis, materials, experimental methods, and the calculations used in this research are presented. The chapter is divided into four main sections:

1. **Preparation of Adsorbents.** The preparation of two sets of activated carbon adsorbents synthesised from two different precursors, date pits and coal tar pitch, are described.
2. **Characterisation Techniques.** The experimental techniques used to characterise the activated carbon adsorbents are outlined.
3. **Gas Adsorption Measurement.** Three gas adsorption measurement apparatus setups used to measure CO_2 and CH_4 adsorption on the activated carbons are introduced.
4. **Calculation Algorithms.** These are used to calculate the textural properties of the activated carbons from the raw measurement of nitrogen gas adsorption. Calculations used to process the raw high pressure gravimetric gas adsorption measurements are also described.

3.1 Preparation of Adsorbents

The preparation of two sets of activated carbon adsorbents from two precursors, date pits and coal tar pitch, are described in the following two subsections.

3.1.1 Activated Carbons from Date Pits

The production of activated carbons from date pits in this research followed a two-step activation procedure: the carbonisation of raw date pits to produce char followed by chemical activation with KOH. To start with, raw date pits of "Khalas" type, native to Oman, were collected and washed with deionised water several times to remove any fruit remains and foreign materials, then they were dried in an air circulating oven at 120 ^{o}C for 24 hours to remove any moisture. The dried and clean date pits were placed in a ceramic boat and placed inside the quartz tube of a horizontal furnace, Figure 3.1, ready for the carbonisation step.

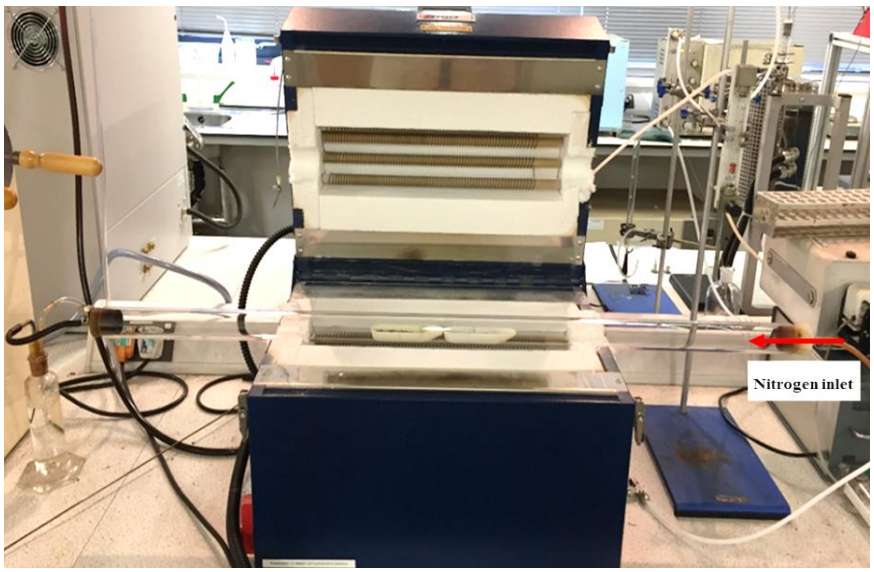


Figure 3.1 Horizontal tube furnace used for the carbonisation and activation processes to produce activated carbons.

Before switching on the heater of the horizontal tube furnace, the quartz tube was purged with nitrogen for 15 minutes to eliminate any air inside it. Carbonisation was carried out under a flowing nitrogen atmosphere under the following

conditions: nitrogen flow of 1 L/min, temperature of 450 ^{o}C, heating rate of 5 ^{o}C/min and carbonisation time of 4 hours. A carbonisation temperature of 450 ^{o}C was selected since the TGA curve of most lignocellulose materials plateaus at 450 ^{o}C (El-Hendawy, 2009). Coincidentally, this same temperature was also found to be the optimum temperature for the production of wood biochar intended for activated carbon synthesis for CO_2 capture at high pressure according to the work of Li *et al.* (2016). In addition, Girgis & El-Hendawy (2002) demonstrated, using a TGA study, that raw date pits exhibit only one large wave of weight loss between 200 ^{o}C and 450 ^{o}C indicating the removal of most of the gases and tars, once 450 ^{o}C has been reached. Once the carbonisation process had finished, the produced date char was left to cool down inside the quartz tube under a nitrogen atmosphere. The date char was then manually crushed and sieved to 0.5-1.0 mm granules. The char granules were labelled as DP0 and stored in airtight glass tubes ready for the chemical activation step.

The second step for the production of activated carbons from date pits was the chemical activation of the date char with KOH. Samples of date char (2 g) were weighed out as well as the corresponding weights of KOH pellets to obtain the desired KOH to date char mass ratios of 1:1, 2:1, 3:1 and 4:1. The KOH solid pellets were diluted with 10 mL of deionised water in a 50 mL beaker before adding the date char to the solution and manually stirring it. The beaker containing the mixture was then covered with aluminium foil and left for 24 hours at room temperature to ensure complete soaking of the date char with the KOH solution. The mixture was then transferred to a circulating air oven and dried at 105 ^{o}C for 24 hours until dry. The dry solid mixture of char and KOH was placed inside a ceramic boat and activated inside the same horizontal tube furnace used for the

carbonisation for 1 hour under flowing nitrogen of 1 L/min. The KOH/char mixture was activated at four different temperatures (600, 700, 800 and 900 ^{o}C) using a temperature ramp rate of 5 ^{o}C per minute. Each activated sample was left to cool down to room temperature under nitrogen flow then collected in a beaker to be washed with hot deionised water. Washing with hot deionised water was done several times manually to remove the potassium species and open up the created pores. Washing was stopped when the waste water had a pH of 7, measured by pH test strip. Each washed activated carbon sample was dried in an oven at 120 ^{o}C for 24 hours before being stored in an air tight glass vial. The activated carbon samples were designated, DPXY, where X is the KOH to char mass ratio and Y indicates the chemical activation temperature as seen in Table 3.1.

Table 3.1 Date pits based activated carbons designation and chemical activation conditions.

Number	Sample ID	KOH/DP0 mass ratio	Activation Temp. (^{o}C)
1	DP0	-	-
2	DP1600	1	600
3	DP1700	1	700
4	DP1800	1	800
5	DP2600	2	600
6	DP2700	2	700
7	DP2800	2	800
8	DP2900	2	900
9	DP3600	3	600
10	DP3700	3	700
11	DP3800	3	800
12	DP3900	3	900
13	DP4600	4	600
14	DP4700	4	700
15	DP4800	4	800

3.1.2 Activated Carbons from Coal Tar Pitch

Raw coal tar pitch beads of diameter 1.0 -1.5 mm were kindly provided by the Low Carbon Energy and Resources Technologies research group at the University of Nottingham. The pitch beads were prepared via an emulsion method where a blended pitch was stirred in a polyvinyl alcohol solution and heated in a sealed autoclave to 145 ^{o}C for 30 min. The pitch was then washed in deionised water, then dried in a vacuum oven, followed by 24 hours impregnation in n-heptane and then drying at 70 ^{o}C. The next step in the preparation of the coal tar pitch was to increase its stability by heating it up to 300 ^{o}C under air in a horizontal tube furnace. The stabilised pitch beads were then carbonised at a temperature of 900 ^{o}C for 30 minutes under a nitrogen flow of 1 L/min to finally yield what was labelled as raw coal tar pitch, CTP0.

Similar to the activation of the date pits char, the raw coal tar pitch beads were chemically activated by KOH under the same activation conditions by following the same procedure described in section 3.1.1 to produce a second set of activated carbons from a coal tar pitch precursor. The coal tar pitch activated carbon samples were labelled using a designation system similar to that used to label the date pits activated carbons as shown in Table 3.2.

Table 3.2 Coal tar pitch activated carbons designation and chemical activation conditions.

Number	Sample	KOH/CTP0 mass ratio	Activation Temp. (°C)
1	CTP0	-	-
2	CTP1600	1	600
3	CTP1700	1	700
4	CTP1800	1	800
5	CTP2600	2	600
6	CTP2700	2	700
7	CTP2800	2	800
8	CTP2900	2	900
9	CTP3600	3	600
10	CTP3700	3	700
11	CTP3800	3	800
12	CTP3900	3	900
13	CTP4600	4	600
14	CTP4700	4	700
15	CTP4800	4	800

3.2 Characterisation Techniques

The produced activated carbon samples were characterised using the following characterisation techniques: nitrogen adsorption, helium pycnometry, scanning electron microscopy and elemental analysis. Brief descriptions of the working principles and background science for each of these techniques are given in the following sections.

3.2.1 Nitrogen Adsorption

The textural properties such as surface area, pore volume and pore size distribution of the prepared activated carbon samples were calculated from nitrogen adsorption isotherms that were measured using a Micromeritics ASAP2420 Instrument. The

Micromeritics ASAP2420 used a discontinuous volumetric adsorption method by which a known volume of nitrogen was dosed in a sample tube and the pressure was monitored until equilibrium had been reached. The change in the pressure was correlated to the adsorbed volume of the gas. Nitrogen adsorption isotherms were measured by increasing the adsorption relative pressure (P/P_o) from 0.001 up to the saturation pressure of nitrogen at -196 ^oC (P/P_o of 1). The measurement temperature was maintained using a liquid nitrogen bath. Samples were degassed at 120 ^oC for 16 hours under vacuum before the measurement. The surface area was calculated using the BET method from N_2 adsorption isotherm data. The total pore volumes of the samples were calculated from the amount of nitrogen adsorbed at a relative pressure (P/P_o) of 0.99. Pore size distributions of the activated carbon samples were calculated using the Non Linear Density Functional Theory (NLDFT) model. All calculations were performed by MicroActive version 3.0 software which was supplied with the Micromeritics ASAP2420 Instrument.

3.2.2 Helium Pycnometry

An AccuPyc II1340 helium pycnometer from Micromeritics, shown in Figure 3.2, was used to measure the skeletal density of the activated carbons. The skeletal density was needed for the buoyancy correction in gravimetric adsorption measurements and the for free space calculation in volumetric adsorption measurements. AccuPyc II1340 is an automatic gas displacement pycnometer.

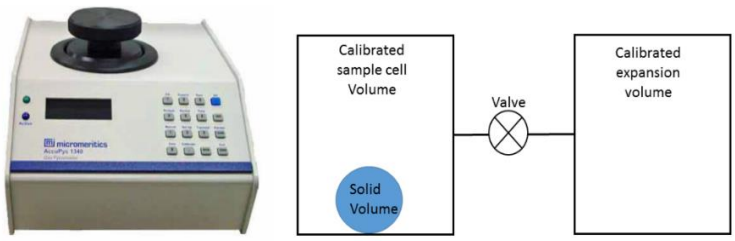


Figure 3.2 AccuPyc II1340 Pycnometer picture and simplified schematic.

The AccuPyc II1340 working principle relies on determining the skeletal volume of the activated carbon sample by measuring the pressure change of helium within two calibrated chambers. Using the ideal gas law and the dry sample weight the skeletal density can be then calculated. Helium was assumed to act as a probe gas and occupy all the pores leaving only the skeletal volume of the activated carbons unoccupied. Activated carbon samples were dried for 24 hours at 120 ^{o}C in an air circulating oven before the test to remove any moisture and any adsorbed gases. The measurement cell volume was calibrated using a standard volume made of stainless steel. The pressure transducers within the AccuPyc II 1340 were zeroed before each measurement. The skeletal density measurement sequence was started by placing an activated carbon sample of known weight in the volume-calibrated sample cell. After purging the sample cell with helium 20 times, the sample cell was sealed and pressurised to 1.35 bar and the pressure was recorded. The expansion cell was kept at atmospheric pressure, and the pressure and temperature were automatically recorded. The valve between the two cells was then opened to allow the helium to flow into the expansion cell and once equilibrium had been reached, the equilibrium pressure was recorded. The ideal gas equation, PV=nRT, was used to carry out mass balance before and after the expansion to calculate the solid volume of the sample. With the knowledge of the sample mass, the skeletal density of the carbon sample was calculated. All the calculations were done automatically using the AccuPyc II1340 software.

3.2.3 Scanning Electron Microscopy (SEM)

The morphological changes and the development of the porosity in selected activated carbon samples were examined using JEOL 6490LV Scanning Electron

Microscope (SEM). The samples were prepared for the analysis by fixing them to conductive carbon tabs on top of SEM-unique sample holders.

SEM allows the observation of the surface structure of the activated carbon at nanometre to micrometre scale. It works by exposing the activated carbon sample under examination to a finely focused beam of electrons. The interactions between the sample under investigation and the electrons produce multiple singles such as, secondary electrons, backscattered electrons and other photons of different energies. These signals can be used to construct a fine image of the surface characteristics of the sample.

3.2.4 Elemental Analysis (EA)

The LECO CHN 628 Elemental Analysis (EA) system was used to measure the carbon, hydrogen and nitrogen content of the activated carbon samples. During the elemental analysis, the activated carbon sample was exposed to a flow of oxygen at 950 ^{o}C resulting in the combustion of the sample. CO_2, H_2O, and NO_x gases were evolved and NO_x was further reduced to N_2. After combustion, the evolved gases were passed through the detector where an infrared system detected the H_2O and CO_2 and a thermal conductivity cell was used to detect N_2. Sample preparation for the analysis involved wrapping approximately 50 mg of each of the activated carbons samples in tin foil then loading it onto the automatic sample holder of the analyser. A standard calibration powder material with a known carbon, hydrogen and nitrogen content was used to check the accuracy of the analyser before and after the analysis to ensure good working order of the instrument and to check that there were no drifts during the analysis.

3.2.5 X-Ray Fluorescence (XRF) Spectrometry

An Epsilon 3XL benchtop energy dispersive XRF spectrometer system was used to measure the presence of any potassium species in the prepared activated carbon samples. In theory, energy dispersive XRF spectrometry relies on irradiating the activated carbon sample with X-rays from an X-ray tube. The elements present in the sample will subsequently emit fluorescent X-ray radiation with distinct energies and wavelengths, and as a result, the elements can be identified since each element corresponds to a specific wavelength.. The intensity of the energy levels emitted is measured to determine the concentration of each of the identified elements (Brouwer, 2003).

3.3 Gas Adsorption Measurements

The measurements of CO_2 and CH_4 adsorption on the activated carbons were conducted using two different instruments: a gravimetric measurement-based instrument designed to measure gas uptake at fixed pressure and temperature under flowing conditions, and a volumetric measurement-based instrument designed to automatically measure gas uptake isotherms at different pressures. These are both described in the following subsections.

3.3.1 High Pressure Thermal Gravimetric Analysis (HP-TGA)

A Linseis® HP-TGA measurement system, Figure 3.3, was used to measure both single and mixed gas CO_2 uptakes and CH_4 uptakes by the different activated carbons under high pressure. The measurement system consists of three main units: a gas dosing and mixing unit with pressure and flow control capabilities; a

microbalance; and a temperature control unit utilising a water chiller and electric furnace around the sample cell to control the sample and the adsorptive gas temperature. The HP-TGA was equipped with a vacuum pump to evacuate the atmosphere inside the measurement chamber. The adsorption measurement was operated under a continuous flow mode, i.e. the adsorptive gas was continuously flowing into the chamber and the pressure was controlled by a back pressure control valve that vents the excess gas to maintain the pressure set point. The temperature of the sample, the analysis pressure, the gas flow rates and the weight change signals were automatically recorded by a computer system that allowed data visualisation and processing. The gas flow rate and the analysis pressure were set and controlled by a dedicated Programmable Logic Controller (PLC) within the system. The core of the measurement system was the microbalance that operates under controlled pressure and temperature.

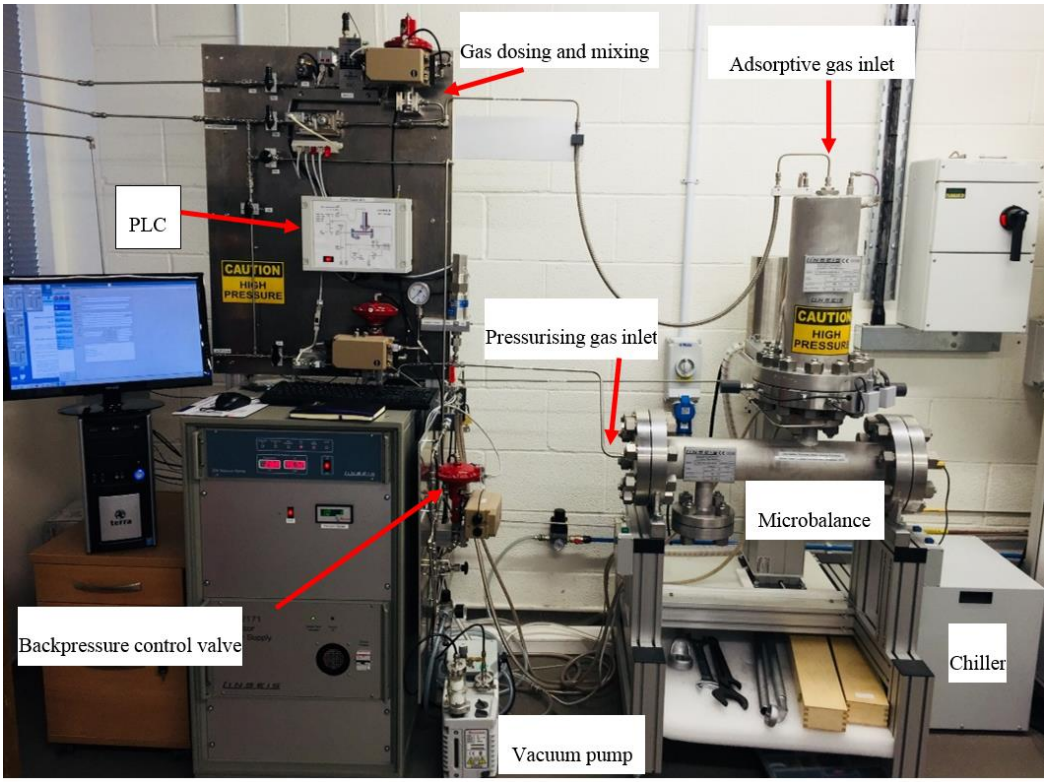


Figure 3.3 The HP-TGA system.

A typical HP-TGA gas uptake measurement run is as follows. An activated carbon sample was weighed (around 200-300 mg) using a laboratory scale before loading it into an alumina crucible which sits at the top of the microbalance. The sample was degassed inside the HP-TGA overnight then dried at 120 ^{o}C under a helium flow before it was cooled down. The dry sample weight was recorded and then the temperature was adjusted to the required adsorption temperature of 50 ^{o}C. The change in sample weight during the degassing and the drying process was recorded and subtracted from the original sample weight to give the dry sample weight. Once the temperature was stabilised at the required analysis temperature, the microbalance chamber was pressurised with helium up to the required pressure, the measurement signals were allowed to stabilise before dosing in the adsorptive gas (CO_2 or CH_4). The adsorptive gas dosing and the weight change measurement recording by the computer were stopped once the activated carbon uptake of the adsorptive gas reached equilibrium. In order to correct the measured gravimetric gas uptake for the drag force resulting from the gas movement and the buoyancy forces during a pressurised dynamic gravimetric measurement, a blank measurement run without any activated carbon sample was conducted for each uptake measurement run using the same adsorptive gas under the same pressure and temperature settings of the gas uptake measurement run. The blank measurement weight change curve was subtracted from the gas uptake measurement weight change curve.

The repeatability of the gas uptake measurement by the HP-TGA was tested by repeating the CO_2 uptake measurement for two samples (DP2900 and DP3600) at 20 bar and 50 ^{o}C, the results are shown in Table 3.3.

Table 3.3 CO_2 uptake measurement repeatability using HP-TGA

Sample	Uptake (mmol/g)	Difference (mmol/g)	Difference %
DP2900	10.24	0.056	0.55%
DP2900 (repeat)	10.30		
DP3600	7.59	0.003	0.04%
DP3600 (repeat)	7.59		

3.3.2 Atmospheric Pressure Thermal Gravimetric Analysis (TGA)

CO_2 uptake and CH_4 uptake by the synthesised activated carbons were also measured at atmospheric pressure and 50 ^oC to investigate the working capacity of the activated carbons. This is defined as the difference between the high pressure gas uptake and the low pressure uptake mimicking the adsorption step (high pressure) and desorption or regeneration step (low pressure) in the PSA process. The Q500 TGA from TA Instruments was used to conduct the atmospheric pressure CO_2 uptake and CH_4 uptake tests. At the heart of the Q500 TGA is a vertical thermo-balance housed in a temperature compensated and controlled environment where the sample-pan was hanging down from the thermos-balance arm. Figure 3.4 shows the measurement chamber in the Q500 TGA. To prepare the activated carbon samples for gas uptake measurement, they were dried under flowing nitrogen at 120 ^oC inside the Q500TGA to remove moisture and any adsorbed gases before dropping the temperature to 50 ^oC then dosing in the adsorptive gas of CO_2 or CH_4.

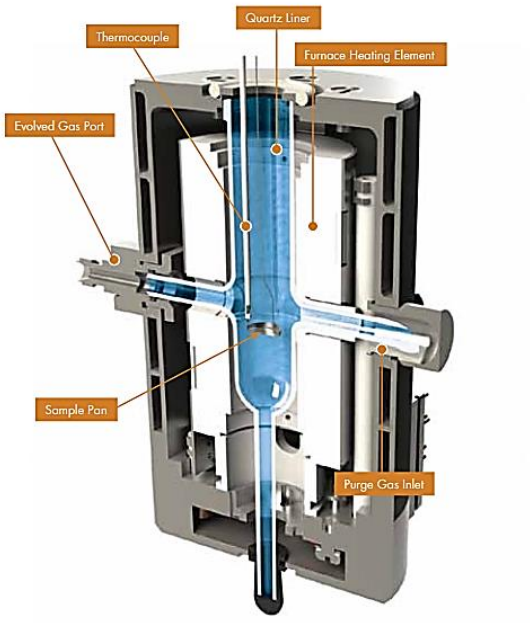


Figure 3.4 Q500 TGA measurement chamber.

3.3.3 High Pressure Volumetric Adsorption (HPVA)

The HPVA apparatus from Particulate Systems (Figure 3.5) was used to obtain high pressure adsorption isotherms for single component gases, CO_2 or CH_4. The HPVA used was based on a volumetric measurement technique that works by introducing a known volume of adsorptive gas from a volume-calibrated manifold into a temperature-controlled chamber containing the activated carbon sample. The HPVA was equipped with pressure transducers in both the manifold and the sample cell to monitor the pressure change, and when the sample reached equilibrium with the adsorptive gas, the pressure was recorded automatically by the system.

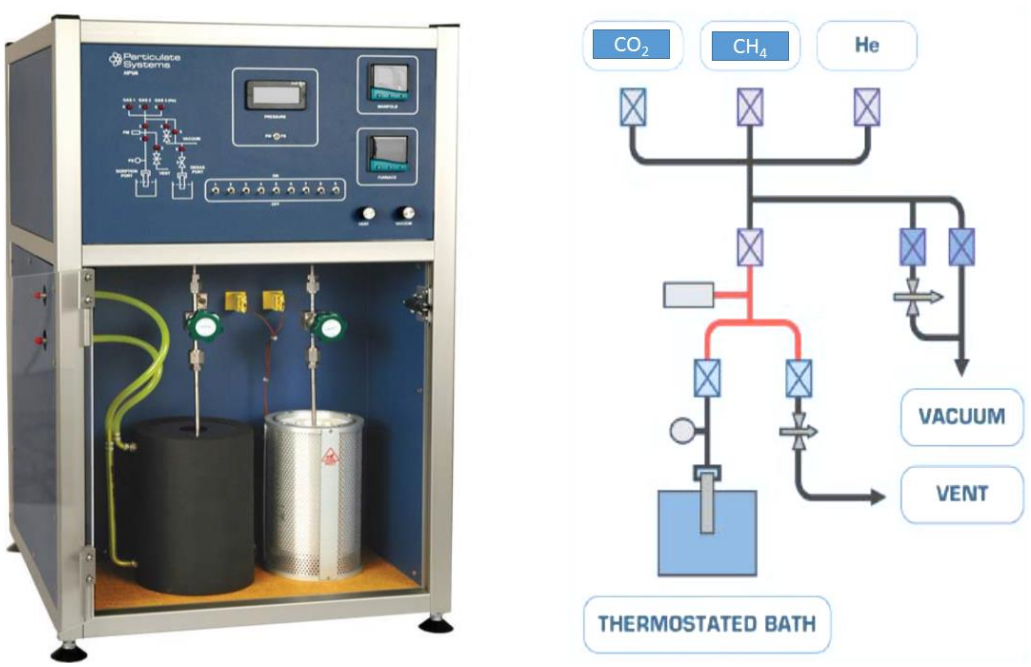


Figure 3.5 High Pressure Volumetric Analyser (HPVA).

This process was repeated at several pre-defined pressure points until maximum pressure was reached. The difference in pressure between the two gas volumes, dosed volume and sample chamber volume, allowed the calculation of the adsorbed gas volume.

A typical adsorption isotherm measurement with the HPVA was as follows. An activated carbon sample (around 400 mg) was loaded into the HPVA cylindrical stainless steel sample cell. The sample was then degassed, together with its sample holder assembly, at 120 ^{o}C for 24 hours in a separate degassing rig then moved to the analysis port of the HPVA rig for isothermal adsorption analysis. During the analysis, the temperature of the sample was controlled using a circulating ethylene glycol bath. The adsorption of CO_2 was measured at 25 ^{o}C and 50 ^{o}C, at up to 40 bar. The adsorption of CH_4 was measured at the same two temperatures mentioned above but up to pressures of 100 bar. After each adsorption analysis, the sample was dried under vacuum for 24 hours at 120 ^{o}C and the dry weight of the sample determined.

A blank measurement run was conducted for each isothermal adsorption experimental condition using empty sample cell and the same adsorptive gas (CO_2 or CH_4) at pressure and temperature similar to that of the adsorption analysis to account for any adsorption on the inner walls of the HPVA system. The adsorbed volume on the blank cell was subtracted from the volume of CO_2 or CH_4 recorded during the adsorption measurement on the activated carbons. The non-ideal gas equation was employed automatically by the HPVA computer system to calculate the adsorbed volume of the blank cell and the activated carbon sample. The compressibility factors needed for the gas volume calculations for CO_2 and CH_4 were obtained using REFPRO software employing the NIST standard reference database number 23 version 8.0 integrated within the HPVA software.

3.4 Calculation Algorithms

In the following subsections, the calculations used to correct the high pressure gravimetric measurements for the buoyancy effect are presented, and it is shown how the excess adsorption quantities from the measured adsorption values are arrived at. The algorithms used to interpret the measured nitrogen adsorption isotherms to characterise the activated carbon samples are also described.

3.4.1 Buoyancy Correction of High Pressure Gravimetric Adsorption Measurement

In gravimetric measurement under high pressure, the buoyancy force could distort the observed weight increase due to the adsorbed gas on the activated carbon samples. The buoyancy force can be explained by the Archimedes principle since the sample and its holding crucible are immersed in a dense fluid, i.e. high pressure adsorptive gas. To address the buoyancy force in the context of the HP-TGA,

consider the change in sample weight recorded by the HP-TGA microbalance as the result of the net forces acting on the sample under investigation. A simplified visual representation of such forces in the case of the Linseis HP-TGA system is shown in Figure 3.6.

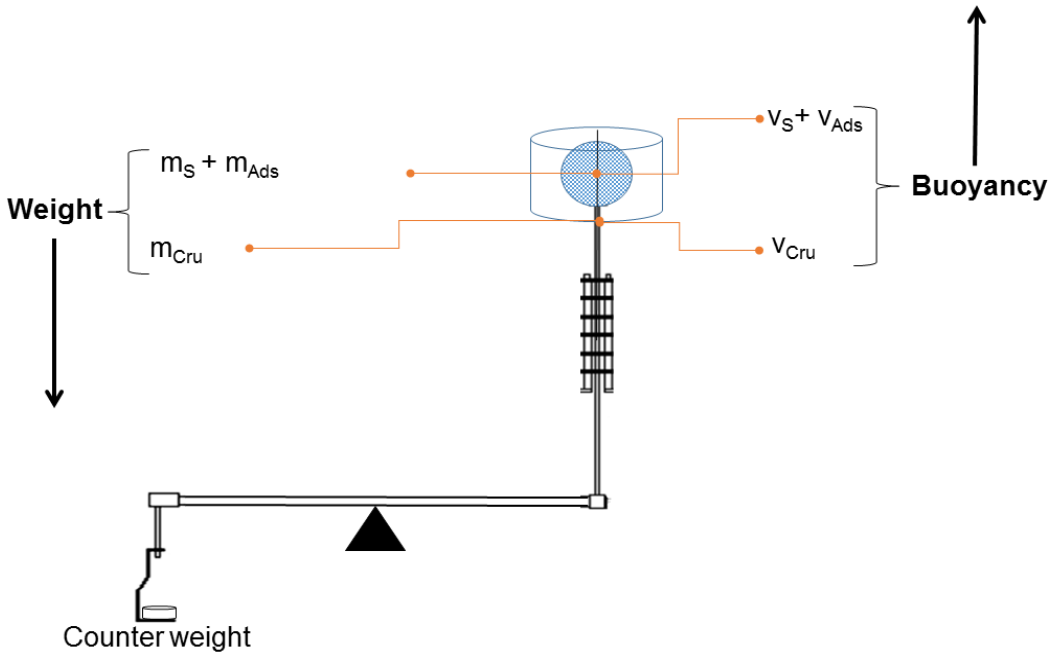


Figure 3.6 Forces acting on a sample in the Linseis high-pressure TGA system.

The weight change recorded by the microbalance during the adsorption measurement is attributed to the difference between two opposite acting forces: a downward force associated with sample weight, crucible weight and adsorbed gas weight on one side and an upward force of the buoyancy due to the volume of the crucible, the volume of the adsorbed gas and the skeletal volume of the solid sample on the other side. Within the context of the HP-TGA, weight is defined as mass multiplied by the acceleration of gravity and buoyancy as volume multiplied by the fluid density (in which the volume was immersed in) multiplied by the acceleration of gravity. During the gas adsorption measurement, it is the mass-change due to the adsorbed gas that is required to be measured. Hence, the

observed weight change should be corrected for any buoyancy from volumes within the measurement system. Therefore, the balances of forces in Figure 3.6 could be expressed mathematically by equation 3.1 , adapted from Brandani *et al.* (2016)

$$\Delta m.g = (m_S + m_{Ads} + m_{Cru}).g - (V_S + V_{Ads} + V_{Cru})\rho_{bulk}.g \quad \text{Equation 3.1}$$

Where, Δm is the apparent mass change observed as read from the microbalance. The subscripts S, Ads, and Cru refer to the sample, the adsorbed gas phase and the crucible, respectively, and g is the acceleration due to gravity, m is mass, V is volume and ρ_{bulk} is the density of the bulk gas.

Rearranging equation 3.1 after dividing both sides of the equation by the gravity acceleration constant (g) gives:

$$m_{ads} = (\Delta m - m_s) - (m_{cru} - V_{cru}.\rho_{bulk}) + V_s.\rho_{bulk} + V_{ads}.\rho_{bulk} \quad \text{Equation 3.2}$$

m_{ads} in Equation 3.2 is known as the *absolute adsorption*.

The Linsies STA–HP equipment used in this research has an automatic zeroing function at the beginning of the adsorption tests, i.e. it subtracts the weight of the adsorbent sample and sets m_s to zero in Equation 3.2. Therefore, the first term between brackets on the right hand side of Equation 3.2, $(\Delta m - m_s)$, reduces to the observed weight change (Δm) recorded directly from the microbalance reading during the adsorption test.

The second term in Equation 3.2,$(m_{cru} - V_{cru}.\rho_{bulk})$, describes the effect of the mass and the buoyancy of the crucible when under pressurised test conditions and was measured by blank tests, i.e. tests with the empty crucible under the same

conditions as the adsorption test. The blank test also established the measurement system baseline and was used to correct the effect of drag on the sample holder, assuming that difference in the drag force between an empty and full sample holder are negligible (Brandani, Mangano and Sarkisov, 2016). The measurement system force balance during a blank test can also be described by Equation 3.1 and since there is no sample loaded in the system (sample volume and mass are zero) and assuming no adsorption occurs on the empty alumina crucible (adsorbed volume and mass are zero), equation 3.1 reduces to:

$$\Delta m_{blank} = m_{cru} - v_{cru}.\rho_{bulk} \qquad \textit{Equation 3.3}$$

Equation 3.3 shows that the observed mass change during the blank test is the result of the crucible mass minus its buoyancy due to its volume. Subtracting equation 3.3 from equation 3.2, in other words, subtracting the blank run from adsorption measurements, corrects the measured adsorption mass for the buoyancy due to the volume of the crucible only. The corrected mass here is known as the *net adsorption* (Brandani, Mangano and Sarkisov, 2016), equation 3.4.

$$m_{Ads_net} = (\Delta m - m_S) - (m_{Cru} - v_{Cru}.\rho_{bulk}) \qquad \textit{Equation 3.4}$$

The third term in equation 3.2, $V_s.\rho_{bulk}$, represents the buoyancy effect due to the skeletal volume of the activated carbon samples. The skeletal volume (V_S) of the activated carbons, i.e. without the pores, was calculated from the dry sample weight and the skeletal density which was measured by a helium pycnometer. The density of the bulk gas surrounding the sample, ρ_{bulk}, is given in the NIST standard data set of gas properties. Correcting the measurement for the buoyancy effect due to the skeletal volume gives us the *excess adsorption*, equation 3.5

$$m_{Ads_exc} = (\Delta m - m_S) - (m_{Cru} - v_{Cru}.\rho_{bulk}) + V_s.\rho_{bulk} \qquad \textit{Equation 3.5}$$

The last term in equation 3.2, $V_{ads} \cdot \rho_{bulk}$, represents the buoyancy due to the adsorbed phase volume where the adsorbed phase volume was assumed to be equal to the micro pore volume (Almaz S. Jalilov *et al.*, 2017). Correcting the observed mass change for this buoyancy give us the absolute adsorption quantity. For this work, excess adsorption is reported experimentally since it is the value that can be measured directly (Cavenati, Grande and Rodrigues, 2004). Excess adsorption was used in this work to screen the adsorbents and assess their performance. However, in chapter 7, where adsorption isotherm modelling and mixed gas adsorption modelling is investigated, excess adsorption quantities were converted to absolute adsorption quantities to allow the use of adsorption models that were based on absolute adsorption.

3.4.2 Surface Area Determination from N_2 Adsorption Isotherms

Gas adsorption measurements are common practice for the characterisation of porous solids (Rouquerolt *et al.*, 1994). Nitrogen adsorption of microporous activated carbons was used to characterise all the activated carbon samples investigated in this study. N_2 isotherms, showing the adsorbed amount of N_2 in mmol/g against the N_2 relative pressure (P/P_o), were produced by a Micromeritics ASAP2420 instrument. The BET theory (Brunauer, Emmet and Teller, 1938) was used to calculate the BET surface area (S_{BET}).

The BET theory is based on three assumptions:

a) One molecule of adsorbate per adsorption site.
b) No adsorbate-adsorbate interaction is possible.

c) Condensation rate of gas molecules into the already adsorbed layer is equal to the evaporation rate from that same layer.

In the BET theory, the adsorbed gas amount V_a at pressure P is related to the adsorption relative pressure, P/P_o, saturation pressure P_o and the amount of adsorbed gas in a monolayer of adsorption V_m and a constant C according to equation 3.6:

$$V_a = \frac{V_m C P}{(P_o - P)[1+(C-1)\frac{P}{P_o}]} \qquad \textit{Equation 3.6}$$

The linear form of equation 3.6 can be written as:

$$\frac{P}{V_{a(P-P_o)}} = \frac{1}{V_m C} + \frac{C-1}{V_m C}\left(\frac{P}{P_o}\right) \qquad \textit{Equation 3.7}$$

MicroActive Version 3.0 software from the Micromeritics Instrument Corporation, USA was used to process the measured N_2 adsorption data by plotting $\frac{P}{V_{a(P-P_o)}}$ against $\left(\frac{P}{P_o}\right)$ across the relative pressure range of 0.05 to 0.30 as suggested by Webb & Orr (1997). However, this relative pressure range was used only as a starting point in this research, a narrower relative pressure range was finally used to ensure better linearity of the BET plot whilst maintaining the two criteria suggested by Rouquerol *et al*. (2007) and recommended by the IUPAC technical report by Thommes *et al*. (2015) which are:

a. The constant (C) must always be a positive value. i.e. a negative intercept is outside the linear range of the BET equation
b. The range of data used for the analyses should be only where the term V_a $(1-P/P_o)$ is always increasing with P/P_o.

The plot gave a straight line with intercept, $n = \frac{1}{V_m C}$, and slope, $sl = \frac{C-1}{V_m C}$.

The amount adsorbed in a monolayer (V_m) was calculated from the slope and intercept as

$$V_m = \frac{1}{sl+in} \qquad \textit{Equation 3.8}$$

Finally, the BET surface area (S_{BET}) was calculated according to equation 3.9 below

$$S_{BET} = \frac{V_m N A_{CS}}{M\,W} \qquad \textit{Equation 3.9}$$

Where N is Avogadro's number, A_{CS} is the cross sectional area of molecular N_2, M is the molecular weight of N_2 and W is the sample weight.

3.4.3 Pore Size Distribution (PSD) from N_2 Adsorption Isotherms

During the synthesis of activated carbons, pores of different sizes developed as a result of the physical or chemical activation mechanisms involved. The Pore Size Distribution (PSD) analysis is important to track the development of different pore sizes with the various activation mechanisms. Density Function Theory (DFT) is one of the modern methods for PSD analysis. Based on statistical mechanical methods and computational methods, DFT is able to address the difference in the density between the confined liquid-like adsorptive fluid in the pores and the corresponding bulk liquid (Lowell *et al.*, 2004). However, the interactions between the walls of the pores and the confined fluid were not considered by the DFT (Rouquerol *et al.*, 2014). The Non Linear Density Functional Theory (NLDFT) was developed to include the near pore wall interactions in addition to the fluid-fluid interaction and able to predict an equilibrium density profile across the pore

width. In the NLDFT approach to determine the PSD a set of theoretical model isotherms are calculated using methods of statistical mechanics in which equilibrium density profiles of the adsorbed fluid in the model pores are integrated. This set of isotherms constitutes the NLDFT model database and is called a kernel, which can be thought of as a theoretical reference for the adsorption system and used to calculate pore size distributions (International Organisation for Standardisation, 2007).

NLDFT is a widely accepted method for the determination of PSD of microporous and mesoporous materials and recommended by ISO-15901-3 standard for the analysis of micropores by gas adsorption which provides further details on the governing equations and the computational implementation of the NLDFT. In this work, the NLDFT model was used for the calculations of PSD using the MicroActive® Version 3.0 software from the Micromeritics Instrument Corporation, USA. The NLDFT model used assumed slit-shaped pores for N_2 adsorption on activated carbons.

Chapter 4. Activated Carbons Characterisation

4.1 Introduction

Two sets of activated carbons from two different precursors, date pit biomass and coal tar pitch beads, were synthesised following the KOH chemical activation method described in chapter three section 3.1. This chapter presents the characteristics of the synthesised activated carbons and their relationship to the activation conditions. These characteristics include general morphology as observed under Scanning Electron Microscopy (SEM), chemical composition, and skeletal density. Furthermore, textural characteristics derived from nitrogen adsorption analysis, including BET surface areas, pore volume and pore size distribution of the samples are also presented and related to the temperature and amount of KOH used in the synthesis of the activated carbons.

4.2 Date Pits Activated Carbons

Although date pits are widely available from agricultural waste in the Middle East, they have not received much attention as a source of feedstock for activated carbons for CO_2 capture at high pressure. Date pits char was chosen to be

investigated in this research as an example of a sustainable source to produce activated carbons for natural gas treatment.

A total of 14 activated carbons from date pits were characterised. The date pits char sample that was used as a precursor for the production of the date pits activated carbons was also characterised for comparison.

4.2.1 Morphology

Date pits char (DP0) together with selected date pits activated carbon samples were observed under SEM to confirm the morphological changes due to the activation process. Figure 4.1 shows the morphology of the date pits char granules produced from the pyrolysis of raw date pits under nitrogen flow for 4 hours at 450 ^{o}C.

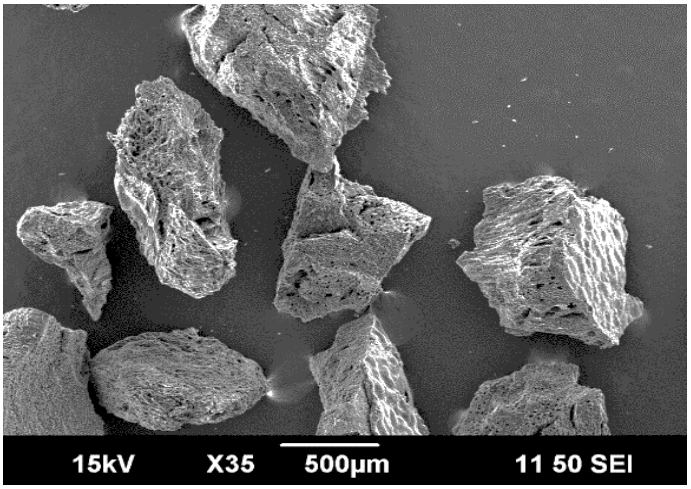


Figure 4.1 Date pits char granules, sample DP0.

The irregular shape and approximate size of 0.5-1 mm of the date pits char granules can be seen in Figure 4.1. A high magnification revealed that a single particle of the date pits char was composed of thin sheets or layers, as well as some large pores and cracks, as seen in Figure 4.2. The large pores and cracks could have developed as a result of the biomass gasification and the release of volatiles

in the char production process (Ahmadpour and Do, 1997; Lua and Yang, 2004). It is possible that such large pores and cracks could allow better KOH penetration during the wet impregnation stage of the char in the aqueous KOH solution as part of the chemical activation process.

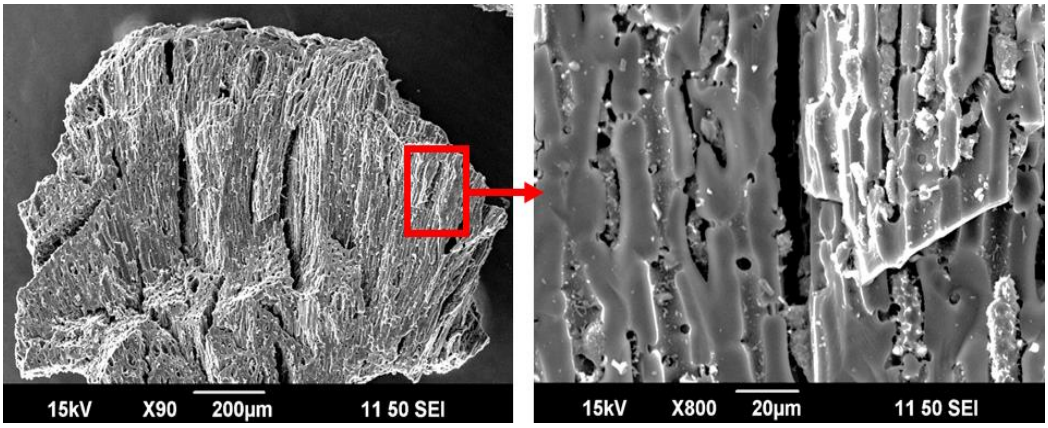


Figure 4.2 Date pits char (DP0) granule at higher magnification.

To visualise the effect of the chemical activation on the date pits char morphology, sample DP2900 was analysed using SEM. The observation revealed a complex network of pores resulting from the KOH chemical activation as shown in Figure 4.3. Large pores hosting smaller pores inside them were a common feature in this sample and could be considered advantageous for promoting gas transport to the inner micropores.

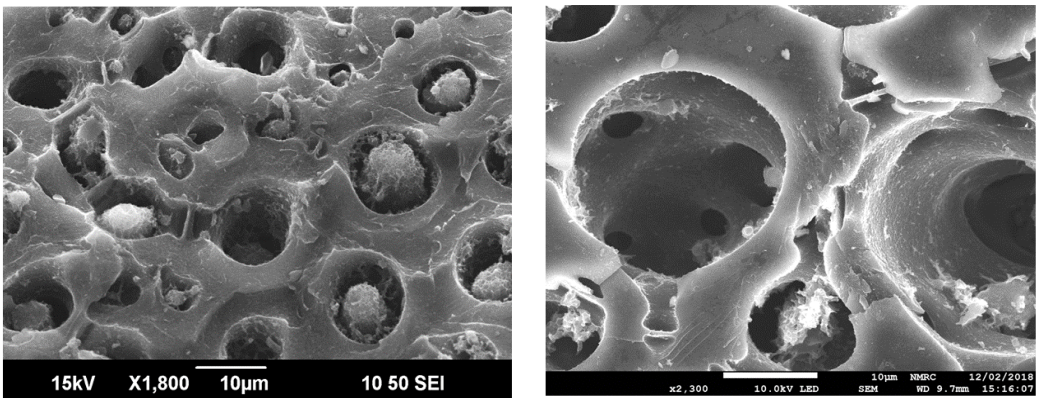


Figure 4.3 SEM image of sample DP2900 showing a complex pore network.

4.2.2 Chemical Composition

The chemical composition of the raw date pits and the date pits char (DP0) were analysed for carbon, hydrogen and nitrogen content using a LECO® elemental analyser and the results can be seen in Table 4.1. The same samples were also analysed using an XRF analyser to determine the content of potassium. It was necessary to quantify the potassium content in the date char before activation with KOH since potassium has been reported as having the highest content amongst other minerals in the raw date pits (Besbes *et al.*, 2004).

Table 4.1 Chemical composition of the raw date pits and date pits char.

Sample	C%	H%	N%	K%
Raw date pits	43.99	7.13	5.65	1.44
Date pits char (DP0)	81.07	3.37	2.27	5.35

The carbon content of the char was found to be 81.07%, a significant increase from the 43.99% carbon content of the raw date pits as a result of the carbonisation at 450 ^{o}C. In contrast, both hydrogen and nitrogen content dropped and this change is attributed to the carbonisation of the date pits biomass under nitrogen flow, where pyrolysis of cellulose or lignin releases most of the volatile matter and non-carbon elements, such as hydrogen, nitrogen and oxygen, in the form of gases and tars (Rodríguez-Reinoso and Molina-Sabio, 1992). The removal of the aforementioned non-carbon elements from the total mass of the raw date pits during pyrolysis resulted in increasing the relative concentration of the carbon content in the char.

Following the KOH activation process of the date char, as described in chapter 3 section 3.1.1, each of the activated carbon samples were analysed for their

chemical composition. The chemical compositions with activation temperature and KOH amount used are presented in Table 4.2

Table 4.2 Chemical composition of the date pits based activated carbons.

Sample ID	Temp ^{o}C	KOH:DP0 mass ratio	C%	H%	N%	K%*
DP0	450	-	81.07	3.37	2.27	5.35
DP1600	600	1:1	66.99	2.53	1.17	15.65
DP1700	700	1:1	71.18	1.84	0.92	11.74
DP1800	800	1:1	77.12	1.45	0.62	9.79
DP2600	600	2:1	70.92	1.52	1.10	12.44
DP2700	700	2:1	76.71	1.17	1.18	12.96
DP2800	800	2:1	77.24	1.01	0.942	14.50
DP2900	900	2:1	88.50	0.42	0.90	4.70
DP3600	600	3:1	64.55	3.67	0.45	13.97
DP3700	700	3:1	59.33	3.67	0.31	12.88
DP3800	800	3:1	78.44	1.50	0.92	13.52
DP3900	900	3:1	79.28	1.24	0.70	7.01
DP4600	600	4:1	55.78	3.50	0.31	12.52
DP4700	700	4:1	75.72	3.69	0.47	10.76
DP4800	800	4:1	81.28	1.85	0.47	7.23

Generally, the carbon content increased with the increase in activation temperature from 600 to 900 ^{o}C across different KOH to date pits char mass ratios in most samples. Such an increase in the carbon percentage could be attributed to the further decomposition of lignin during the activation (Bouchelta *et al.*, 2012). However, the drop in the carbon percentage of most of the activated carbons compared to that of the parent char could be due to two factors: the additional potassium in the activated carbon, up to 15% from 5.35% in the char, as a result of possible potassium intercalation deep into the carbon matrix (Liu *et al.*, 2015) , and the consumption of the carbon by KOH in the activation reactions. In general, the hydrogen content showed a decreasing trend with increasing activation temperature while nitrogen content was around 1% or less for all samples across different KOH to DP0 mass ratios. Increasing the activation temperature to 900 ^{o}C

in two samples, DP2900 and DP3900, resulted in significantly lower potassium remaining in the activated carbon sample after the water wash indicating that most of the KOH was consumed in the activation reactions at higher temperatures (900 ^{o}C).

4.2.3 Skeletal Density

The skeletal density, also known as true density, is defined as the density of the solid part of the adsorbent, excluding pores and voids (Rouquerol *et al.*, 2014). The skeletal densities of the date pits activated carbons were measured using a helium pycnometer. Overall, the measured skeletal densities increased with increasing activation temperature as seen in Figure 4.4, signifying a more organised carbon structure (Lozano-Castelló *et al.*, 2002).

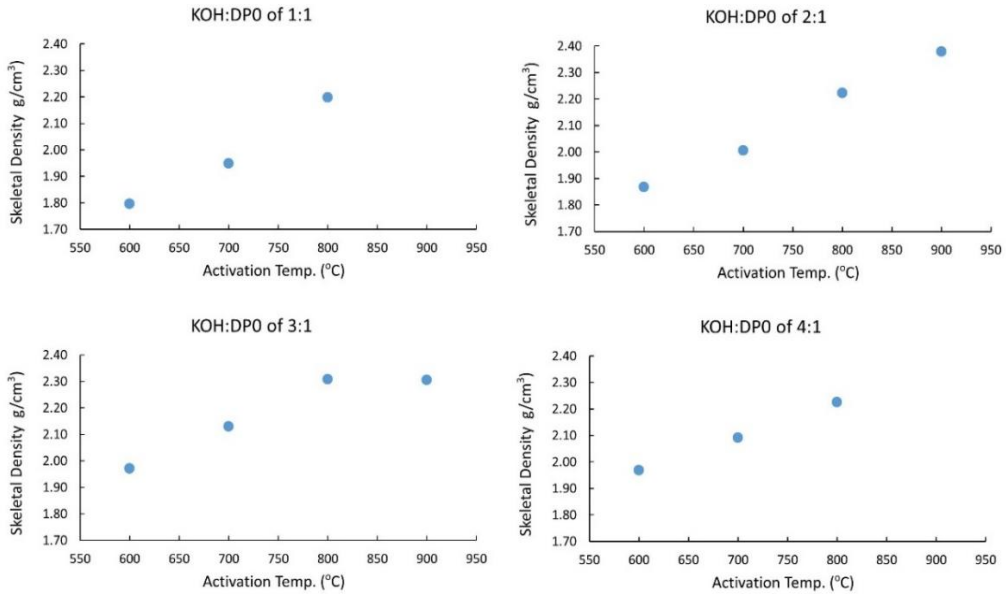


Figure 4.4 Skeletal density of date pits activated carbons prepared at varying activation temperatures and KOH amounts.

The observed increase could be attributed to the increase in the oxidisation reaction promoted by KOH that led to releasing gaseous products from the date pits char hence increasing the skeletal density (Ahmadpour and Do, 1997). A similar trend of increasing skeletal density with increasing activation temperature

for biomass based activated carbons was reported by Gurten *et al.* (2012) and Lua & Yang (2004) in two separate studies. It is worth mentioning that the date pits char sample (DP0) which was the precursor for all the date pits based activated carbons had a skeletal density of 1.45 g/cm³ which is lower than any of the activated carbon samples produced from it.

4.2.4 Nitrogen Adsorption Isotherms and Surface Textural Properties

Nitrogen (N_2) adsorption and desorption isotherms were measured at -196 ^oC for all the date pits based activated carbons, and the results are presented in Figure 4.5, where filled data points are for adsorption measurements and empty data points represent the desorption measurements. All the measured isotherms, except for DP2900, DP3800 and DP3900, were type I(a) according to IUPAC classification (Thommes *et al.*, 2015), indicating a highly microporous activated carbon with a steep uptake of N_2 at low pressure with plateaus starting at relative pressure (p/p_o) of 0.1 or lower, as seen in Figure 4.5. However, samples DP2900, DP3800 and DP3900 were classified as type I(B) showing a wider knee indicating the presence of wide micropores and some mesoporosity (Rouquerol *et al.*, 2014).

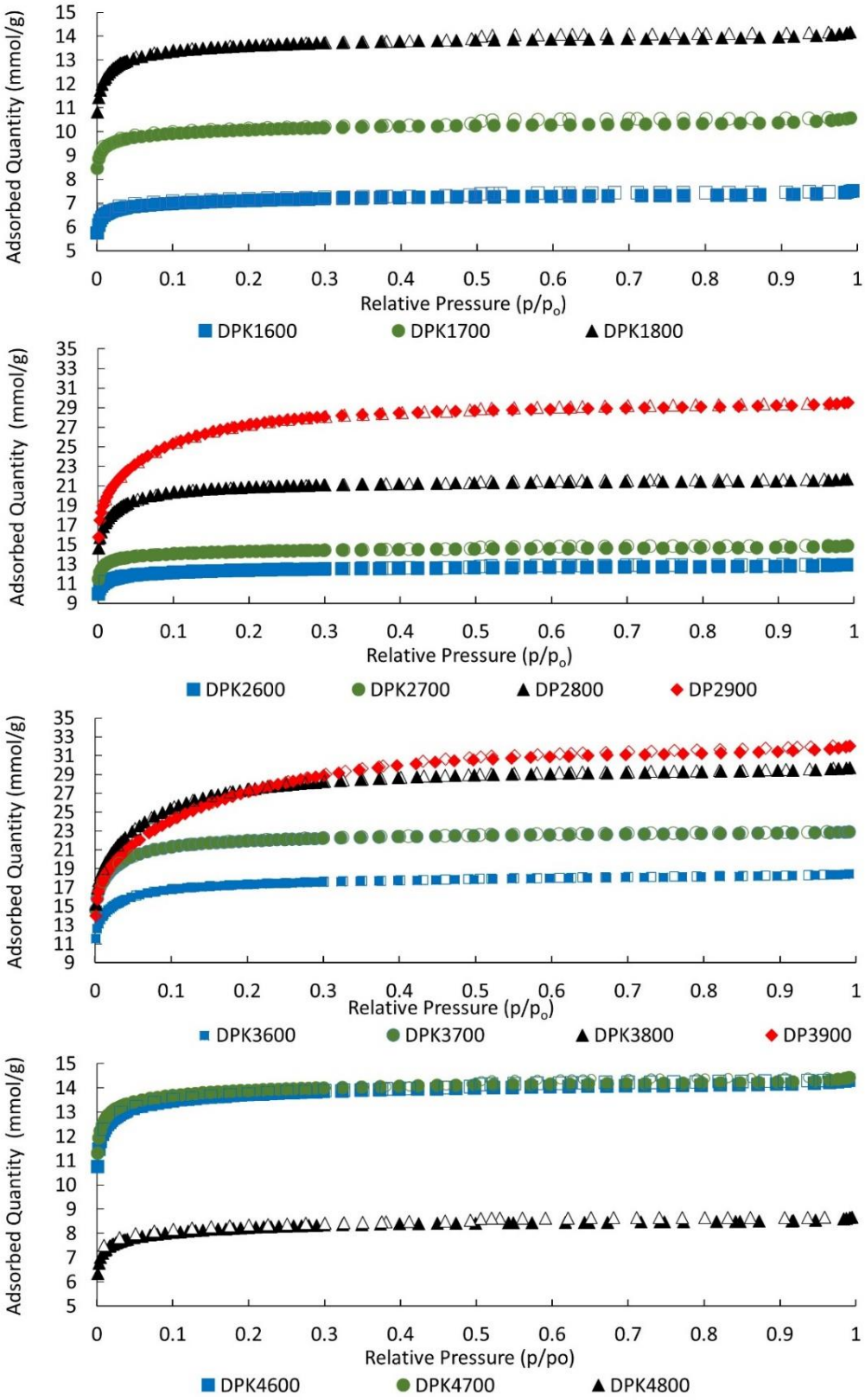


Figure 4.5 N_2 adsorption and desorption isotherms for the date pits activated carbons.

4.2.4.1 Surface Area

The surface area of each of the date pits activated carbon samples was calculated from the measured N_2 isotherm using the BET theory. Figure 4.6 shows the change in BET surface area (S_{BET}) with increasing degree of activation.

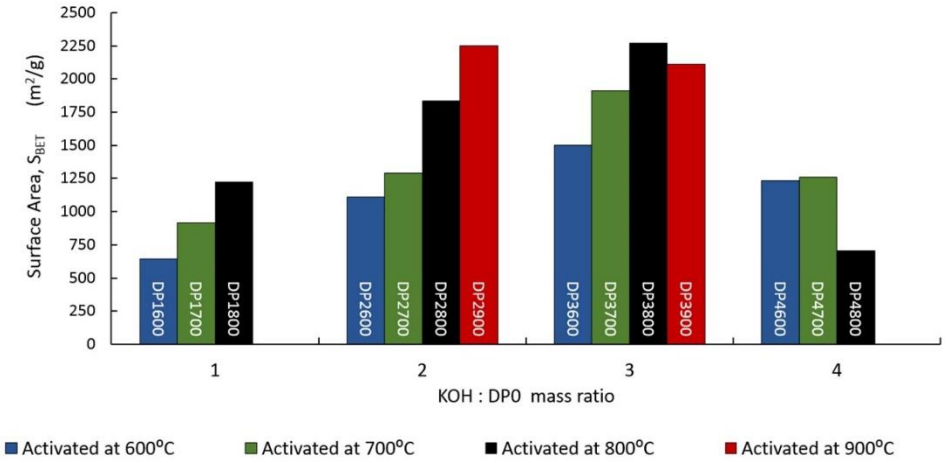


Figure 4.6 Variation of surface area of date pits activated carbons with varying activation temperature and KOH amount.

Generally, increasing the degree of activation by either increasing the activation temperature or the amount of KOH resulted in an increase in the surface area of the activated carbons. However, this trend reached a peak at sample DP3800, after which the surface area showed a drop at sample DP3900. A sharp drop in the S_{BET} was seen for all the samples activated using the 4:1 KOH to DP0 mass ratio. For sample DP3900, the drop in the surface area could be associated with higher carbon burn-off at 900 ^oC leading to the destruction or the widening of some of the micropores to produce mesopores hence reducing the surface area. Possible destruction of pore structure, due to excessive consumption of carbons in the activation reactions, could be responsible for the surface area reduction in all the samples activated with the high KOH to DP0 mass ratio of 4.

4.2.4.2 Pore Volume

Using the Non Linear Density Functional Theory (NLDFT) model, the cumulative pore volumes arising from different pore sizes for each of the date pits activated carbons were calculated then separated into micropore volumes and mesopore volumes. The values for the micropor volumes shown in Figure 4.7 represent the cumulative pore volumes arising from pores with a width of 2.0 nm or less, whereas the mesopore volumes shown in Figure 4.8 are the volumes arising from pores with width between 2.0 and 50.0 nm for each sample.

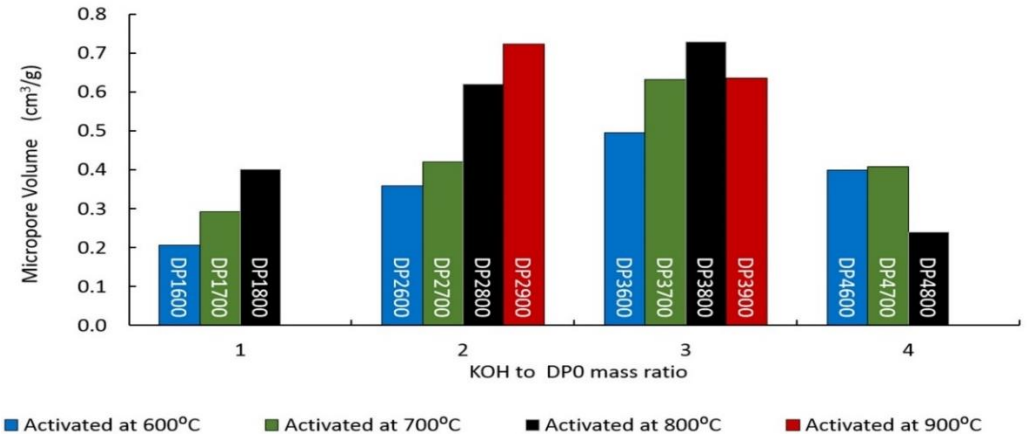


Figure 4.7 Variation of micropore volumes of date pits activated carbons with varying activation temperature and KOH amount.

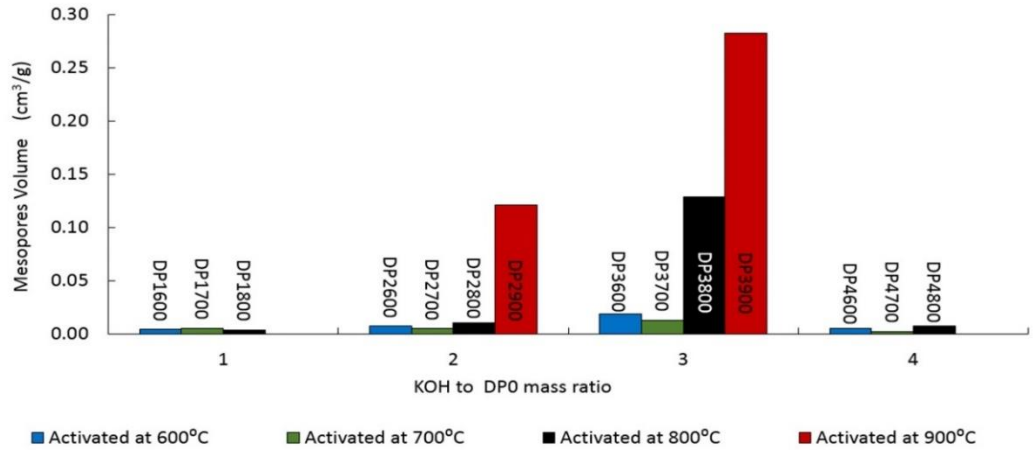


Figure 4.8 Variation of mesopore volumes of date pits activated carbons with varying activation temperature and KOH amount.

Examining the pore volumes in Figure 4.7 and Figure 4.8, it can be seen that most of the date pits activated carbons were highly microporous, with the exception of three samples which showed significant mesoporous volumes (DP2900, DP3900 and DP3800). Generally, the development of porosity with the increasing activation degree can be described as follows:

A. Micropore volume increased with increasing degree of activation by either higher activation temperature or the KOH amount. A maximum value of 0.73 cm^3/g for sample DP3800 was recorded, followed by a slight drop for DP3900, and then a drastic drop in the micropore volume for all the samples activated with KOH to DP0 mass ratio of 4.

B. The change in mesopore volume was insignificant compared to the change in micropore volume for all samples except for three samples, DP2900, DP3800 and DP3900.

C. Increasing the activation temperature from 800 to 900 ^oC increased the volume of the mesopores from 0.13 cm^3/g for sample DP3800 to a maximum of 0.28 cm^3/g for sample DP3900.

D. Samples activated with the highest and the lowest KOH to DP0 mass ratio, i.e. ratios of 1 and 4, showed the lowest mesopore volumes across all activation temperatures from 600 to 800 ^oC.

The above observations highlight the usefulness of the KOH in generating highly microporous activated carbons from date pits char with low to moderate activation degree. However, further increasing the activation degree generated mesoporosity, which was more prominent at 900 ^oC and KOH to DP0 mass ratio of 3. The development of mesoporosity could be as a result of widening large micropores

into mesopores. This was supported by the two samples activated at 900 ^{o}C where an increase in the volume of mesopores was associated with a drop in the micropore volume. A similar observation was reported by Lua & Yang (2004) in their study to activate pistachio nutshells with KOH. They reported that activation at 900 ^{o}C resulted in the development of mesoporosity due to pore widening. In addition, at 900 ^{o}C the walls of adjacent micropores could burn off leading to the creation of a mesopore as a result of opening up of two or more micropores together, as cited by the same authors above. The excessive amount of KOH to char mass ratio of 4 in this case, resulted in a detrimental effect in terms of porosity development by substantially reducing the pore volume of the activated carbon. Such pore volume reduction might be due to possible pore wall destruction due to over consumption of carbons during the activation reactions as a result of the high amount of KOH.

4.2.4.3 Pore Size Distribution (PSD)

The Non Linear Density Functional Theory (NLDFT) model integrated within the MicroActive® software assumed slit-shaped pores for N_2 adsorption on activated carbon and was used to generate the PSD curves of the date pits activated carbons as seen in Figure 4.9. Some common characteristics could be seen from the PSD of all the date pits activated carbons with the exception of the samples activated with KOH to char ratio of 4, DP4600, DP4700 and DP4800. Generally, a trend of widening pore distribution moving from small to large micropores then mesopores was observed as the degree of activation was increased by increasing the activation temperature for the same KOH:DP0 mass ratio or by increasing the KOH:DP0 mass ratio for the same activation temperature or both. However, samples activated with KOH to char ratio of 4 showed a very narrow and similar PSD

across all the three temperatures. Again, this is in line with the drop in the microporosity and the BET surface area observed when a higher KOH amount was used for activation as a result of possible destruction of the pores wall structure.

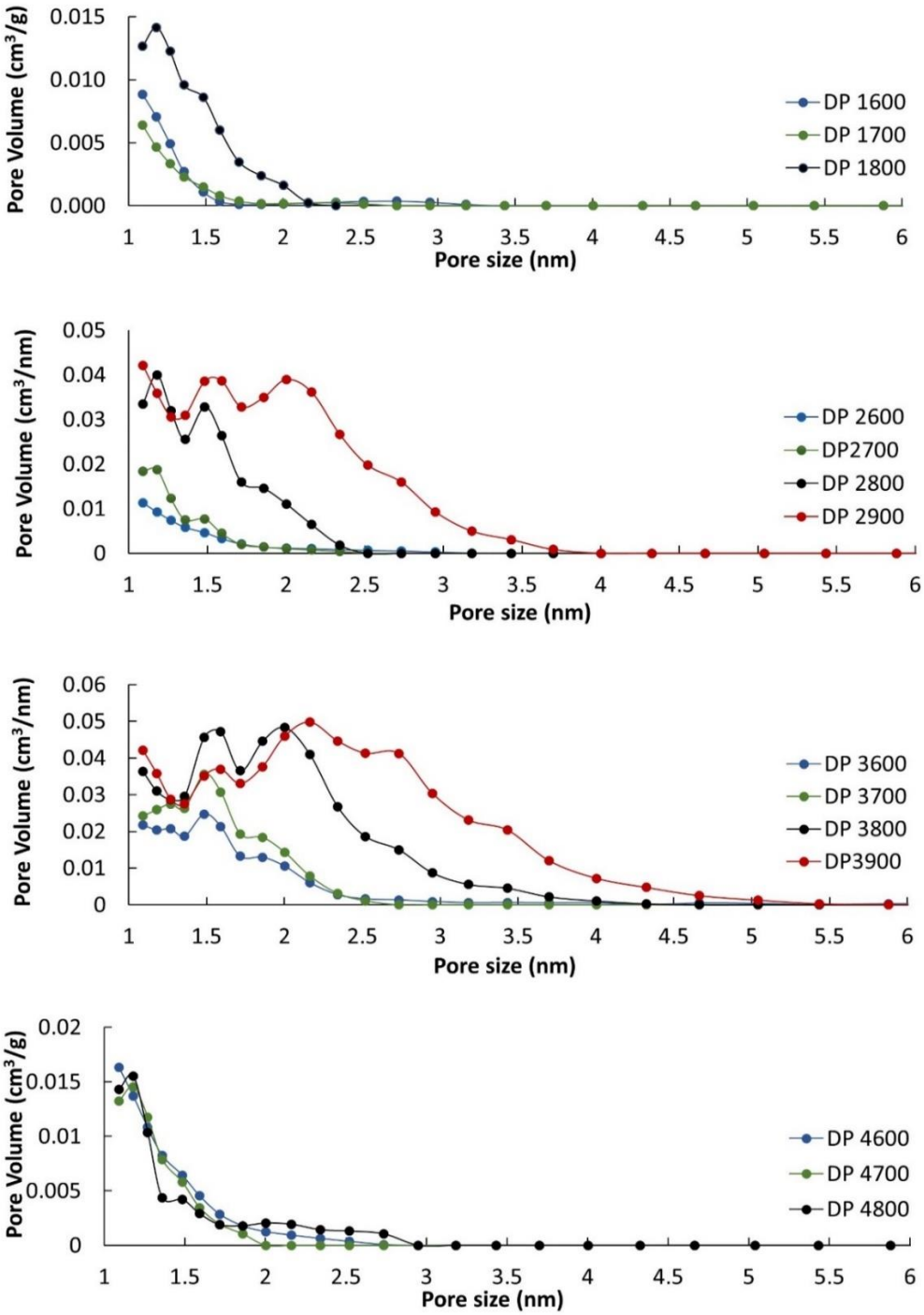


Figure 4.9 PSD for date pits activated carbons calculated by NLDFT.

4.3 Coal Tar Pitch Activated Carbons

Spherical coal tar pitch beads were activated by KOH following the method described in chapter three, section 3.1.2. These beads were chosen for the synthesis of activated carbons due to their high bulk density (1 g/cm^3) which is favourable since high density activated carbons can reduce the PSA column dimensions resulting in a reduction in process equipment cost. A total of 14 coal tar pitch activated carbon samples were synthesised using KOH chemical activation with various KOH concentrations and activation temperatures.

4.3.1 Morphology

Observation of the raw coal tar pitch precursor beads (CTP0) and some of the selected coal tar pitch activated carbons under SEM was carried out in a similar manner to the observation of the date pits samples. Figure 4.10 shows the general morphology of CTP0 beads of about 0.5 – 1.0 mm in diameter with no apparent large pores or surface cracks, unlike the date pits char.

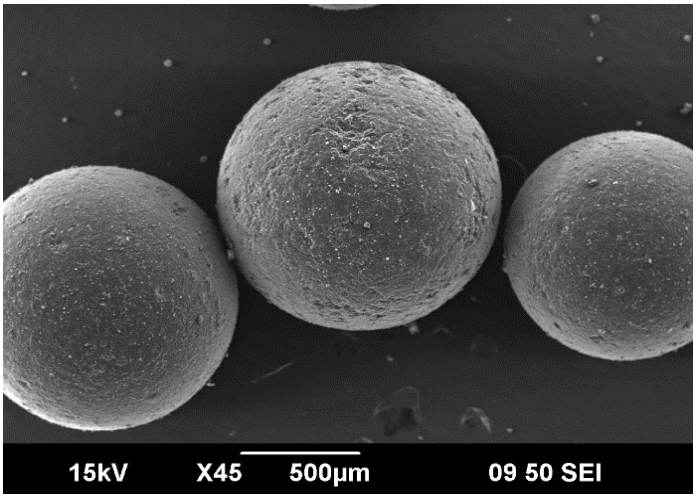


Figure 4.10 Raw coal tar pitch beads, CTP0.

The morphological changes of the coal tar pitch beads due to increased activation degree was observed under SEM using two samples, CTP1800 (Figure 4.11 A)

representing a mild activation and CTP3800 (Figure 4.11B) representing a high activation degree as the KOH to carbon ratio was increased from 1 to 3. Damage to the spherical morphology due to the high KOH to carbon ratio can be seen in part B of Figure 4.11 whereas the mild activation to produce CTP1800 resulted in some surface cracks in the beads as seen in part A of the same figure.

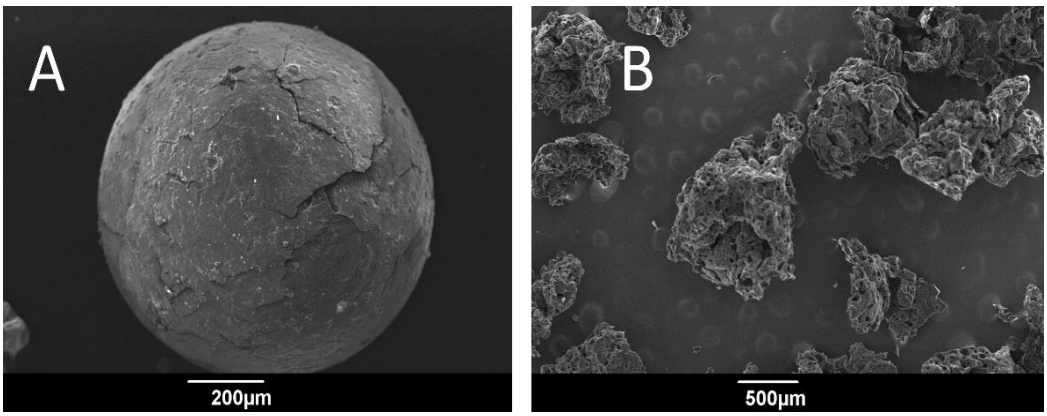


Figure 4.11 CTP1800 (A)and CTP3800 (B) showing damage to spherical morphology due to high KOH to carbon ratio, 3:1, used for activation.

4.3.2 Chemical Composition

The chemical compositions of all the 14 coal tar pitch activated carbons in addition to that of the parent coal tar pitch beads were analysed and the results are presented in Table 4.3. Generally, as the activation temperature increased for each KOH:DP0 mass ratio, an upward trend was observed in the carbon percentage content. The consumption of the carbon in the KOH activation reactions was one of the reasons for the drop in the carbon content of most samples from the initial carbon content of 83.62% in CTP0 beads as shown in Table 4.3. Such a downward trend could also be attributed to the addition of potassium, either intercalated within the carbon structure or remaining on the surface of the carbon after the activation with KOH despite extensive water washing step with hot deionised water. Liu *et al.* (2017) activated coal tar pitch using a KOH to coal tar pitch mass ratio of 0.5:1, synthesis

temperature of 700 ^{o}C and followed a similar washing procedure with deionised water. They reported that potassium intercalation was responsible for up to 6% of the potassium content in the resulting activated carbon. Higher percentage of potassium in activated carbons reported in this study compared to that of Liu *et al* (2017) could be attributed to the higher KOH to coal tar pitch mass ratio (1-4) used in this study.

Table 4.3 Chemical composition of the coal tar pitch activated carbons.

Sample ID	Temp ^{o}C	KOH:DP0 mass ratio	C%	H%	N%	K%
CTP0	-	-	83.62	2.8	1.08	0.00
CTP1600	600	1	67.13	2.19	0.72	17.38
CTP1700	700	1	75.89	1.36	0.82	13.76
CTP1800	800	1	80.47	1.32	0.63	9.77
CTP2600	600	2	62.11	2.95	0.38	13.22
CTP2700	700	2	60.88	3.45	0.23	8.96
CTP2800	800	2	67.84	2.39	0.44	15.19
CTP2900	900	2	86.78	0.7	0.99	9.13
CTP3600	600	3	60.42	3.28	0.3	11.01
CTP3700	700	3	66.07	2.78	0.4	10.35
CTP3800	800	3	63.16	2.84	0.39	10.09
CTP3900	900	3	80.83	1.09	0.92	10.20
CTP4600	600	4	58.17	3.5	0.27	10.36
CTP4700	700	4	66.09	2.76	0.33	10.19
CTP4800	800	4	79.03	1.58	0.59	6.95

4.3.3 Skeletal Density

The skeletal densities of the coal tar pitch activated carbons were measured using a helium pycnometer and plotted against the activation temperature used for each set of KOH:CTP0 mass ratios, as seen in Figure 4.12.

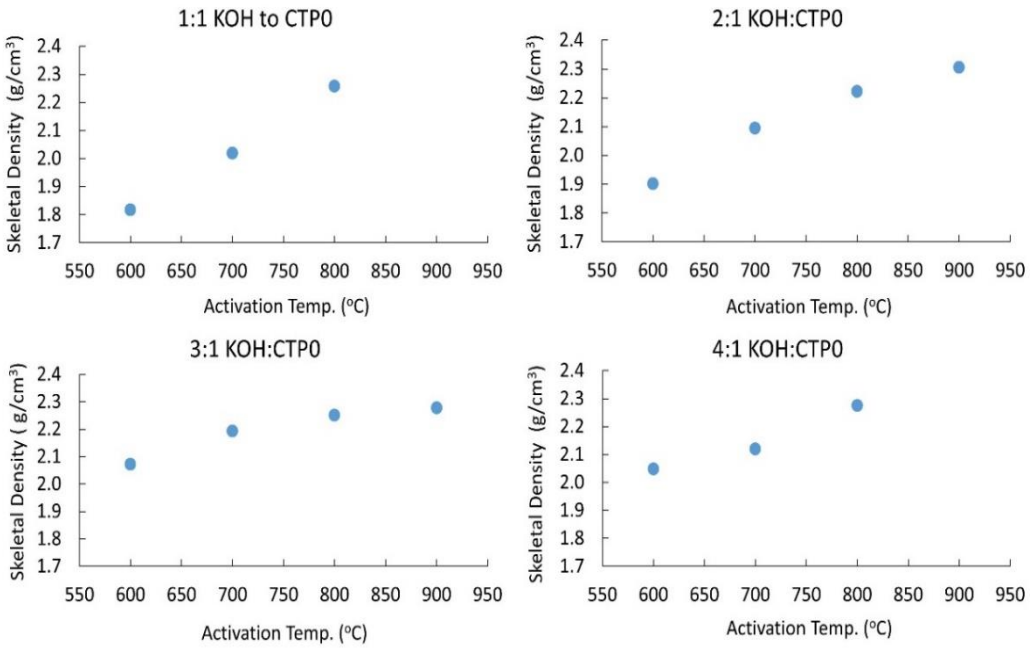


Figure 4.12 Skeletal density of coal tar pitch activated carbons prepared at varying activation temperatures and with various KOH amounts.

Overall, the increase in the skeletal densities was directly proportional to the increase in the activation temperature used to prepare the activated carbons. The highest measured skeletal density across all activation conditions was 2.31 g/cm^3 for CTP2900. The observed increase in the skeletal density trend with increasing activation degree could be associated with the removal of volatiles from the coal tar pitch at higher temperatures; this was further supported by the observed decreasing trend in hydrogen content of the coal tar pitch activated carbons with increasing activation temperatures for a fixed KOH amount as shown previously in Table 4.3.

4.3.4 Nitrogen Adsorption Isotherms and Surface Textural Properties

N_2 adsorption and desorption isotherms were measured at -196 °C for all the coal tar pitch activated carbons. The results are presented in Figure 4.13, where the filled data point are for adsorption measurements and empty data point represent

the desorption measurements. All the measured isotherms, except for samples CTP2900 and CTP3900, were type I(A) according to the IUPAC classification, showing a sharp increase in the adsorbed N_2 at low relative pressure and reaching equilibrium at relative pressure (p/p_o) of 0.1. Sample CTP2900 isotherm was type I(B) indicating the presence of large micropores. Sample CTP3900 also showed a small hysteresis loop indicating the presence of some mesopores. On increasing the activation temperature for each KOH:CTP0 mass ratio, a wider isotherm knee can be observed signifying the development of a wider micropore distribution. The total amount of adsorbed nitrogen increased with increasing activation degree, with the exception of samples activated with a KOH to CTP0 mass ratio of 4 which demonstrated a lower N_2 adsorption.

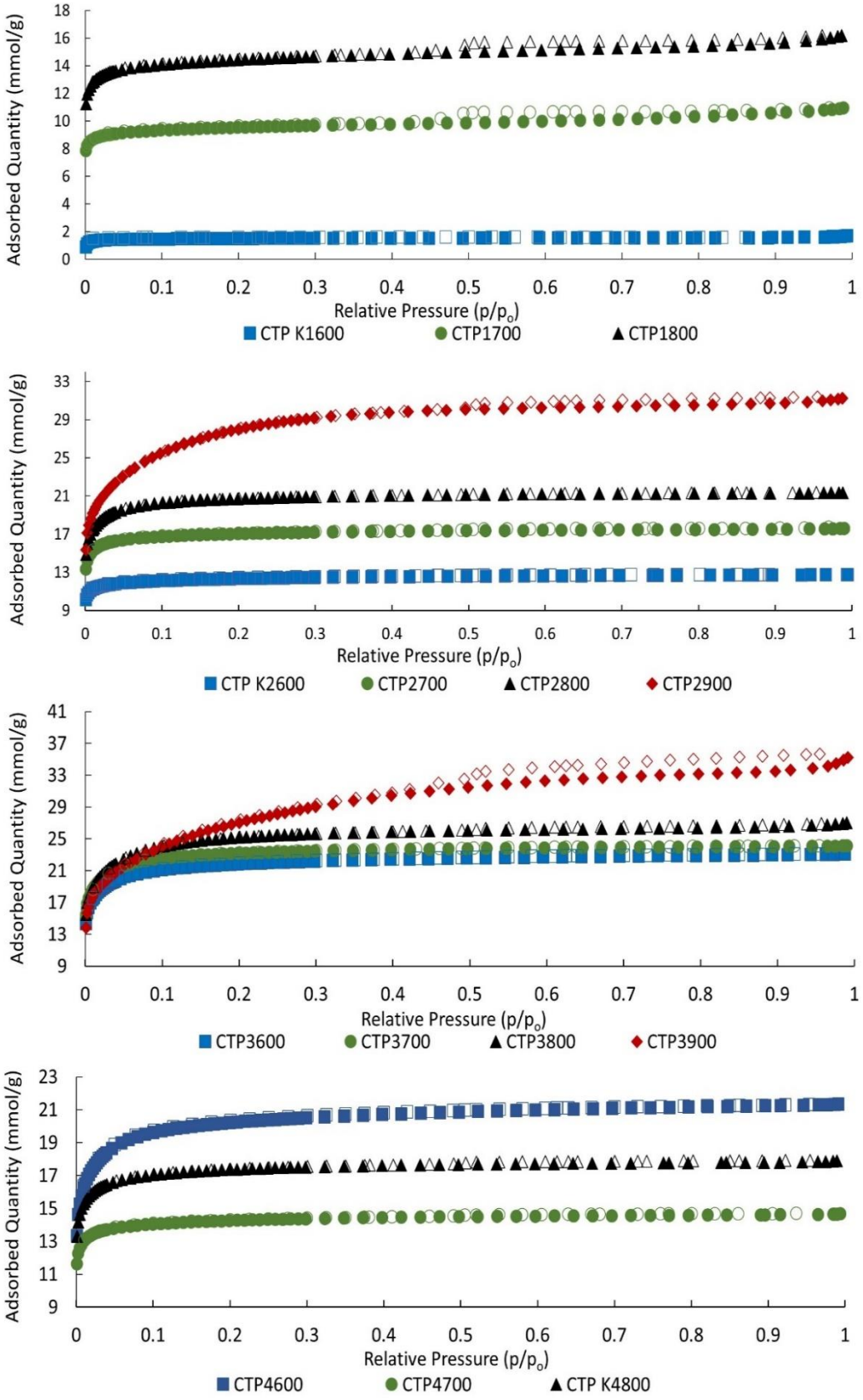


Figure 4.13 N_2 adsorption and desorption isotherms for coal tar pitch activated carbons.

4.3.4.1 Surface Area

The BET surface areas (S_{BET}) of all the synthesised coal tar pitch activated carbons were calculated from the N_2 isotherms reported in section 4.3.4. Figure 4.14 illustrates the generally positive correlation between surface area and activation degree, with a peak surface area of 2278 m^2/g for sample DP2900. However, a detrimental effect of very high activation degree on the surface area was evident in two groups of sample, the first group included all samples activated by KOH to CTP0 mass ratio of 4, and the second group included the two samples activated at 900 ^oC. For the first group, the excessive amount of KOH resulted in the total transformation of CTP0 beads into a fine powder and possibly caused the destruction of the pore wall structure due to excessive amount of KOH used. For the second group, the activation at 900 ^oC led to the development of mesopores through micropore widening causing a reduction in the microporosity, further discussed in section 4.3.4.2, which resulted in the reduced surface area for sample CTP3900 compared to sample CTP2900.

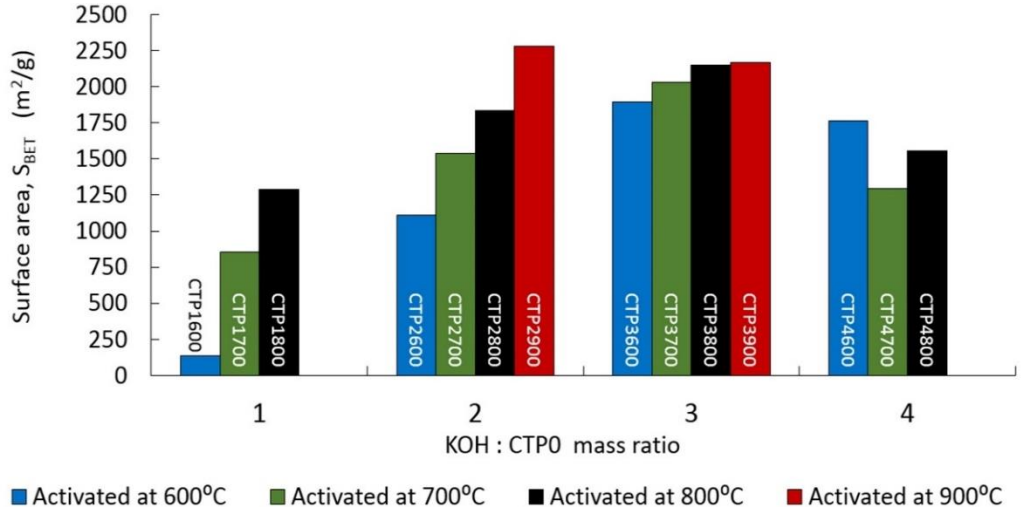


Figure 4.14 Variation of surface area of CTP activated carbons with varying activation temperature and KOH amount.

4.3.4.2 Pore Volumes

The change in the porosity of the coal tar pitch activated carbons across the increasing activation degree was investigated by measuring the changes in volume of the micropores and mesopores in all samples, as shown in Figure 4.15 and Figure 4.16.

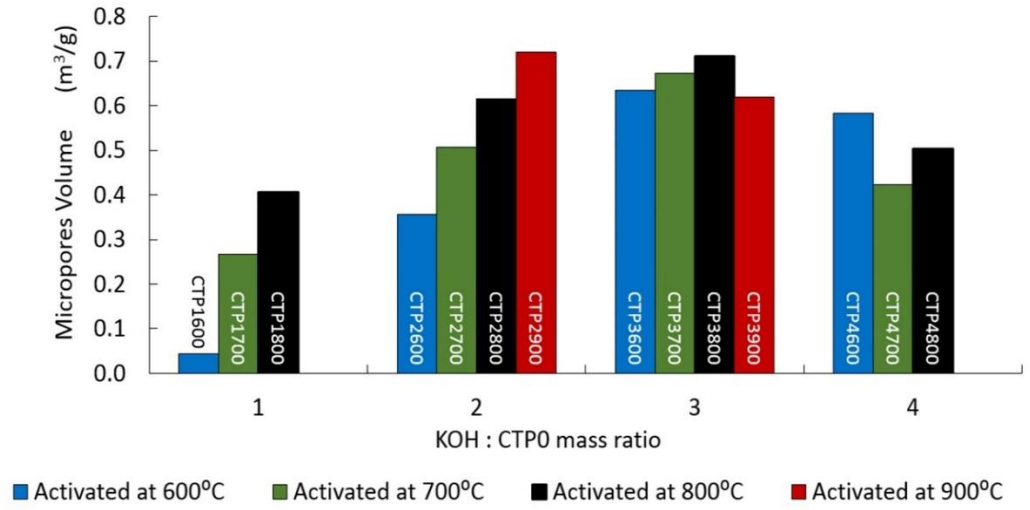


Figure 4.15 Variation in micropore volume of coal tar pitch activated carbons with varying activation temperature and KOH amount.

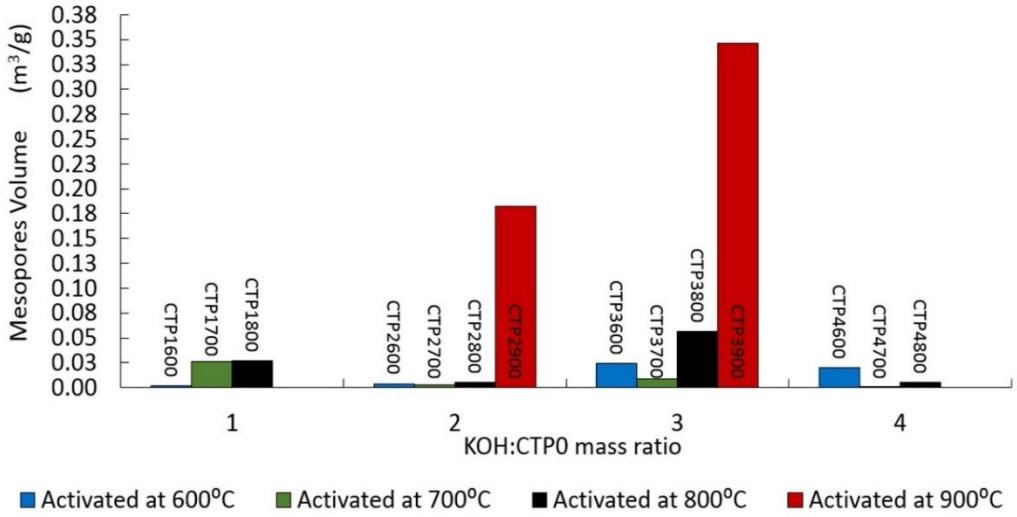


Figure 4.16 Variation in mesopore volume of coal tar pitch activated carbons with varying activation temperature and KOH amount.

The increase in the micropore volume with increasing activation degree, up to sample CTP3800, can be seen in Figure 4.15, after which a drop in micropore

volume as the activation degree is further increased is noticeable. The change in mesopore volumes was insignificant for all samples, less than 0.06 cm^3/g, except for that of the two samples activated at 900 ^oC. For these two samples, as KOH:CTP0 mass ratio was increased from 2 to 3, the mesopore volume markedly increased together with a drop in micropore volume. This simultaneous increase and decrease in volume of the two pore types is similar to that reported for the date pits activated carbons in section 4.2.4.2. Part of the observed mesoporosity here might have also resulted from the carbon burn off at 900 ^oC where a wall separating two micropores could be destroyed to form a mesopore (Hayashi *et al.*, 2000).

4.3.4.3 Pore Size Distribution (PSD)

PSD plots for coal tar pitch activated carbons were generated using MicroActive® software using the NLDFT model for N_2 adsorption on activated carbon that assumed slit-shaped pores. The PSD curves depicted in Figure 4.17 show a trend of widening pore size distribution on increasing activation degree. Except for the samples activated at 900 ^oC that showed peaks in the mesoporous range, all the other samples showed peaks in the microporous range only. The narrowing of the PSD together with low pore volumes for set D, activated with KOH to CTP0 mass ratio of 4, might be due to pore structure destruction as a result of an enhanced carbon-KOH reaction due to the excessive amount of KOH used. It would be expected that wider mesopores would continue to develop with increasing activation degree but this was not seen, suggesting that pore walls became very thin as a result of the pore widening effect then collapsed due to further carbon-KOH reactions. Similar behaviour was observed for the date pits activated carbons. A relatively wide PSD in the micropore range for samples activated at

800 ºC and 900 ºC was observed in comparison to those activated at 600 ºC and 700 ºC. This could be due to the additional activation reaction above 700 ºC by which the K_2O, that was produced as a result of the initial dehydration of the KOH below 700 ºC, reduced to metallic potassium promoted by carbon. The metallic potassium is known to be mobile at such high temperatures and can intercalate between the carbon layers to widen them, as described by Otowa *et al.* (1993)

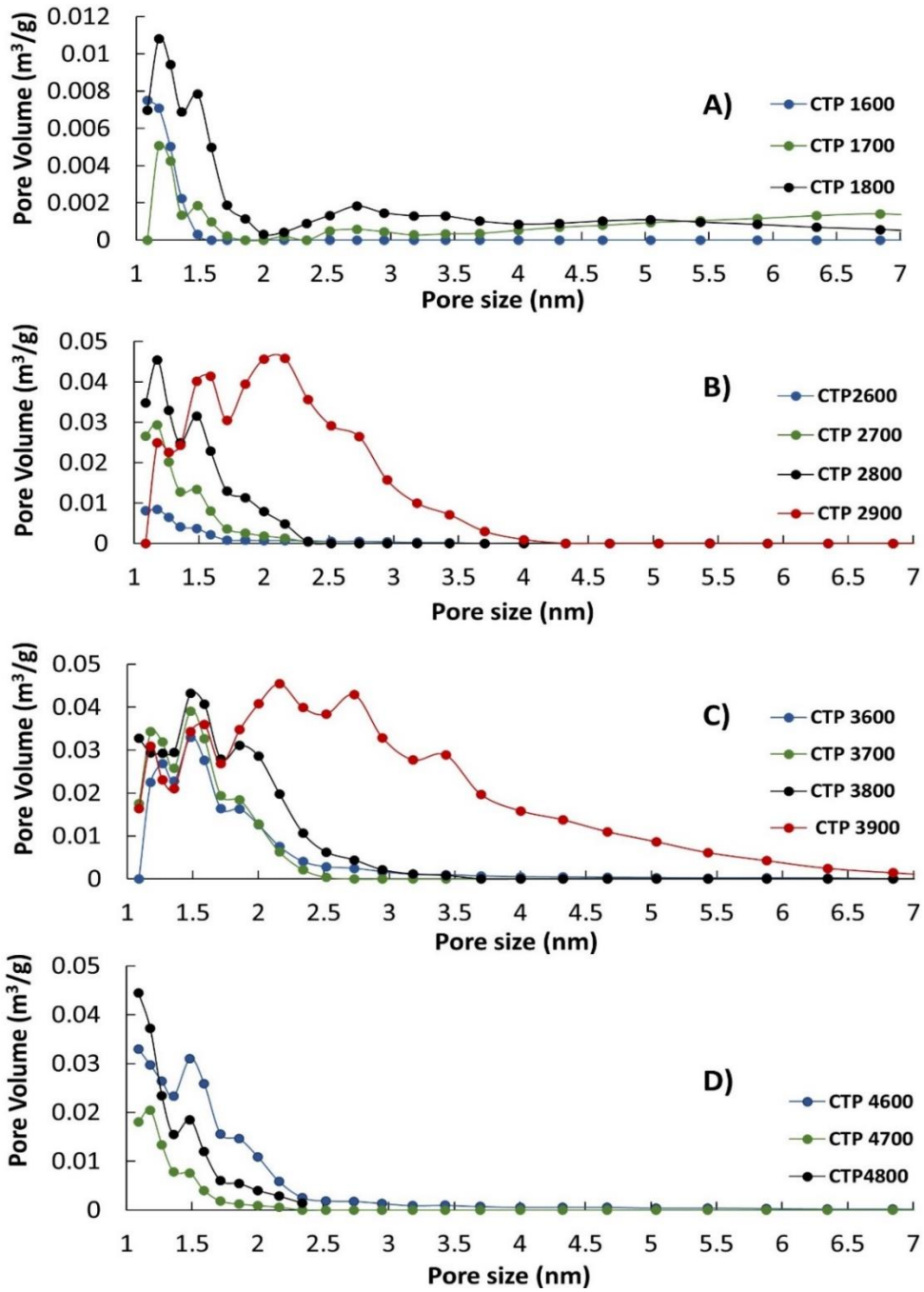


Figure 4.17 PSD for coal tar pitch activated carbons calculated by NLDFT

4.4 Conclusion

In conclusion, the two sets of activated carbons that were synthesised from date pits biomass and coal tar pitch by chemical activation with KOH were found to be highly microporous. Samples activated at 900 ºC also showed the development of mesopores.

The highest surface areas achieved were 2269 m^2/g and 2278 m^2/g for samples DP3800 and CTP2900 respectively. The slightly higher surface area for coal tar pitch activated carbons could be due to the higher carbon content in the coal tar pitch precursor (83.62%) compared to the date pits char precursor (81.07%).

The degree of activation, controlled by KOH to precursor mass ratio and activation temperature, was found to have a positive correlation with the development of the surface area and the microporosity of the activated carbons. However, there was a peak degree of activation after which an increase in the activation intensity was detrimental to the development of surface area and microporosity and led to either the development of significant mesoporosity at 900 ºC, or to the reduction of microporosity and surface area due to a possible pore wall structure destruction as was the case when a KOH to carbon precursor mass ratio of 4 was used.

Chapter 5. CO_2 Adsorption on Activated Carbons

5.1 Introduction

This chapter presents the CO_2 adsorption performance of the activated carbons that were synthesised and characterised as described in the previous two chapters. The CO_2 adsorption performance was assessed by several CO_2 uptake measurements including: equilibrium adsorption capacity, working adsorption capacity and adsorption isotherms. In addition, CO_2 isosteric heat of adsorption was measured for the high performing samples. The effect of water vapour, as a contaminant in the natural gas stream, on the CO_2 adsorption was also evaluated.

5.2 CO_2 Equilibrium Adsorption Capacity

CO_2 equilibrium adsorption capacities of the date pits and the coal tar pitch activated carbons were measured using a Linsies® HP-TGA system. The measurement was dynamic in its nature, that is the adsorptive CO_2 gas was kept flowing throughout the measurement. This approach was taken as it provided some resemblance to the PSA process operation in contrast to a static adsorption measurement approach where the gas flow is stopped to achieve equilibrium. The pressure and temperature of the adsorption measurement were selected based on the average operating conditions of the South Oman gas field which are 100 bar natural gas mixture pressure, 50 ^oC temperature and 20% CO_2 content. Therefore,

CO_2 adsorption on the activated carbons was measured at 20 bar mimicking the partial pressure of the CO_2 in the natural gas mixture.

The measured isothermal CO_2 adsorption curves for the date pits activated carbons are presented in Figure 5.1 and are grouped into four subsets based on the KOH/DP0 mass ratio used for the production of each set of the activated carbons.

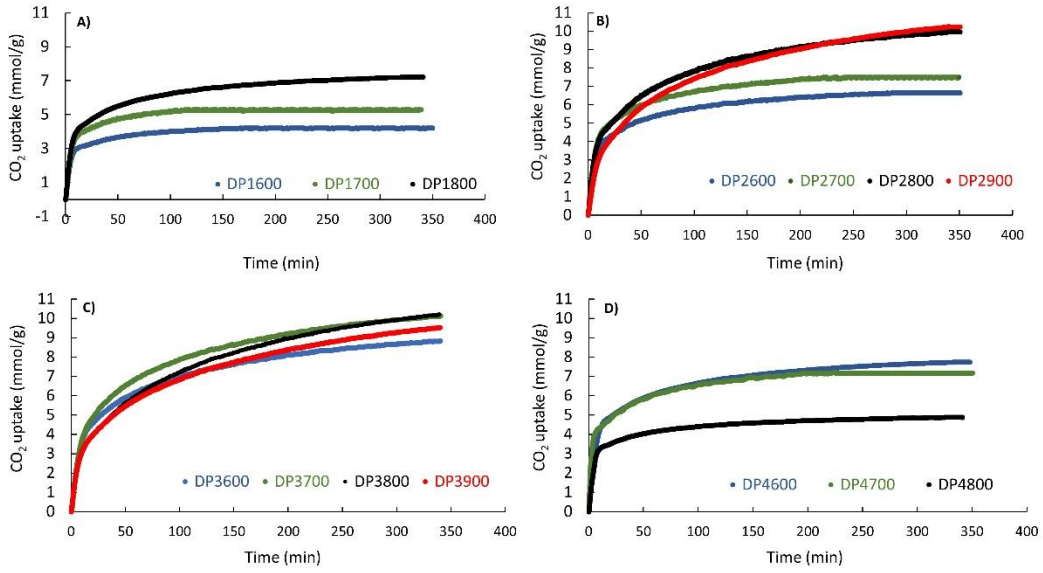


Figure 5.1 CO_2 isothermal adsorption curves for the date pits activated carbons at 20 bar and 50 ^oC.

Generally, CO_2 uptake showed a steep rise at the beginning of the measurement for samples activated with DP0/KOH mass ratio of 1 and 4 (subsets A and D in Figure 5.1). However, samples activated with KOH/DP0 mass ratio of 2 and 3 (subsets B and C in Figure 5.1) showed wider knees in their CO_2 uptake before reaching equilibrium, and achieved higher equilibrium uptake capacities compared to samples in subsets A and D. Samples in subset D showed a decrease in uptake as the activation temperature was increased from 600 to 800 ^oC, in contrast to the behaviour of the other samples that were activated using the same temperature range but with a lower KOH amount.

Figure 5.2 shows the equilibrium CO_2 uptake in mmol/g for the date pits activated carbons. The equilibrium uptake capacities of all 14 samples are organised in four subsets based on the activation temperature used. The KOH to date pit char (DP0) ratio varies across each subset as indicated by the sample ID across the x-axis.

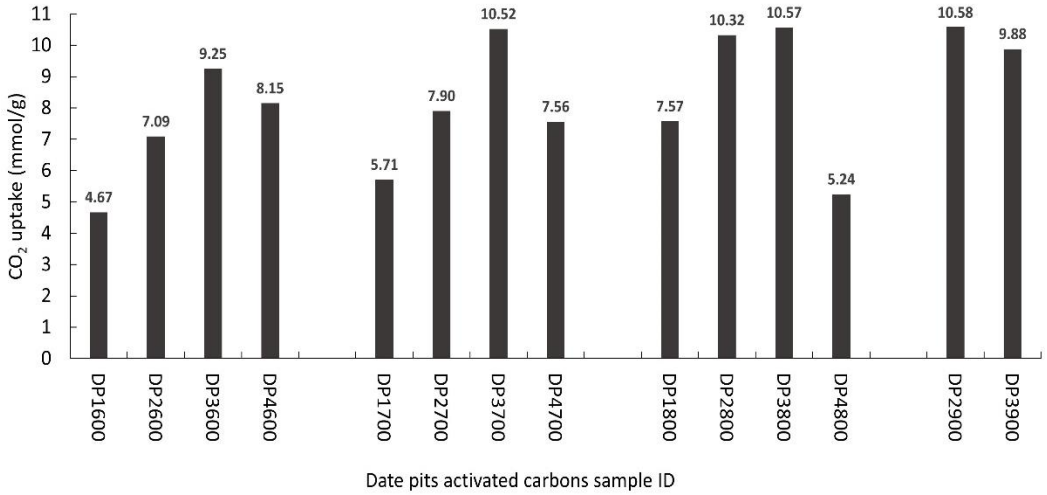


Figure 5.2 CO_2 equilibrium capacities for date pits activated carbons at 20 bar and 50 ^oC.

For the date pits activated carbon series, the highest CO_2 uptake was 10.58 mmol/g for sample DP2900, similar uptake was also achieved by sample DP3800. The equilibrium CO_2 uptake showed an upward trend with increasing KOH to DP0 ratio from 1 to 3 for the temperatures 600, 700 and 800 ^{o}C. Further increasing the KOH to DP0 ratio to 4 (samples DP4600, DP4700 and DP4800) resulted in a drop in the CO_2 uptake across all three temperatures, all such samples were found to have lower surface areas and micropore volumes as explained in the previous chapter. Furthermore, at 900 ^{o}C, increasing the KOH to DP0 mass ratio from 2 (DP2900) to 3 (DP3900) did not increase the CO_2 uptake. Sample DP3900 was shown in the previous chapter to have developed an increase in its mesopore volume at the expense of the micropore volume when compared to DP2900.

Therefore, the role of mespore volume in CO_2 uptake appears to be limited under the examined conditions.

CO_2 isothermal adsorption curves for coal tar pitch activated carbons were also measured by HP-TGA following the same approach, and are presented in four subsets (A,B,C and D) in Figure 5.3 based on the KOH/CTP0 mass ratio used during the production of each activated carbons set.

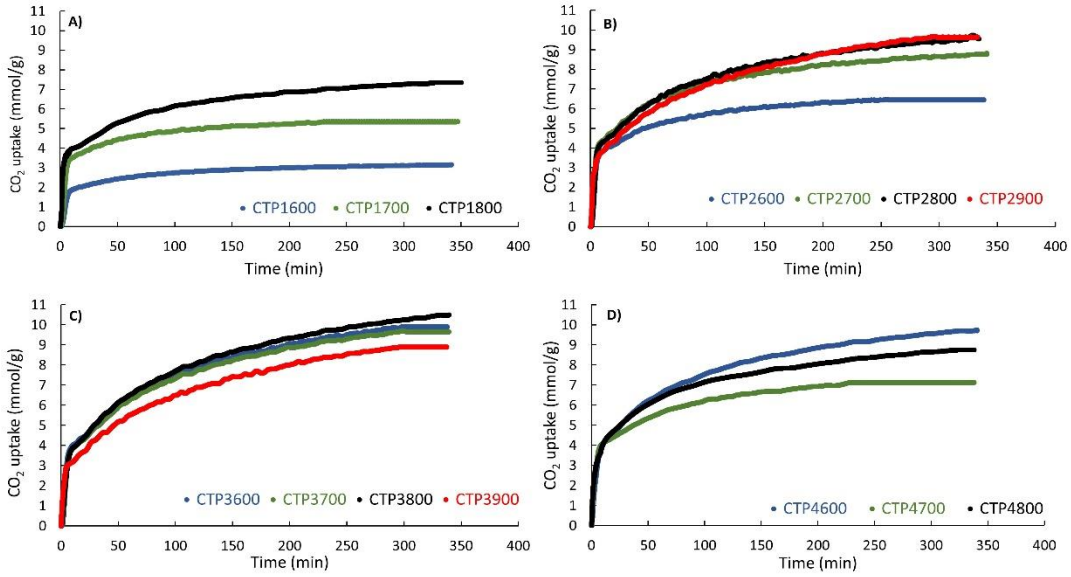


Figure 5.3 CO_2 isothermal adsorption curves for the coal tar pitch activated carbons at 20 bar and 50 ^oC.

The initial sharp increase in CO_2 uptake was seen in all isotherms in Figure 5.3 since all the samples were highly microporous. The shape of the plots of subset D isotherms, with exception of CTP3900, showed similar behaviour to each other compared to the rest of the subsets. This indicates fairly similar degree of activation with a KOH/CTP0 mass ratio of 3 across all the used activation temperatures (600 - 900 ^oC).

The equilibrium CO_2 capacities of coal tar pitch activated carbons are shown in Figure 5.4 and arranged into four subsets based on the activation temperature, 600,

700, 800 and 900 ºC. The KOH amount used to activate each sample varies within each subset as indicated by each sample ID.

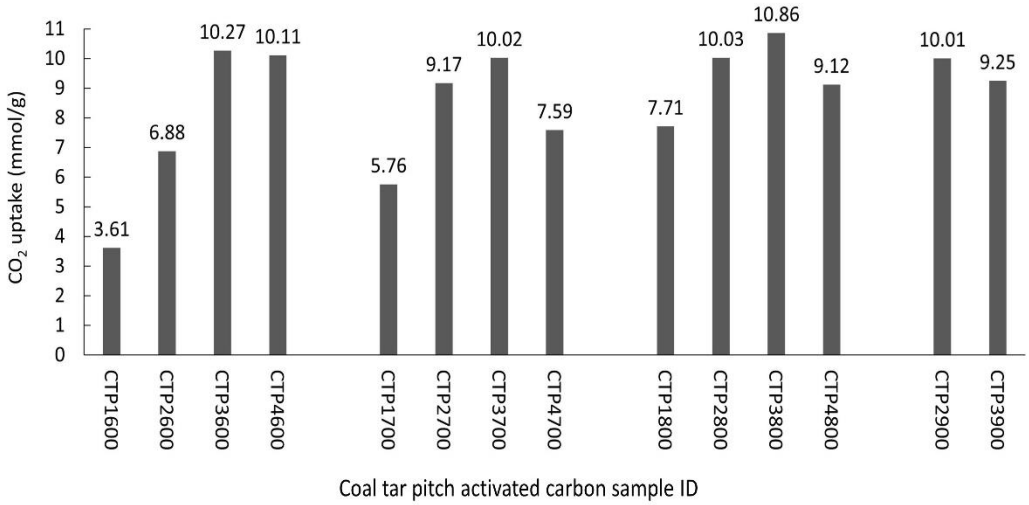


Figure 5.4 CO_2 equilibrium capacities for coal tar pitch activated carbons at 20 bar and 50 ºC.

Except for the two samples in the subset activated at 900 ºC, the equilibrium CO_2 uptake showed a similar trend across the rest of the subsets. The CO_2 uptake showed a positive correlation with increasing KOH to CTP0 mass ratio from 1 to 3 then dropped for samples activated with KOH to CTP0 mass ratio of 4. Sample CTP3800 achieved the highest CO_2 uptake of 10.86 mmol/g across the whole set. At 900 ºC, the equilibrium CO_2 uptake did not seem to benefit from the increase in the KOH to CTP0 ratio from 2 to 3 due to the mesopores volume development at the expense of micropore volume similar to the case of the date pits activated carbons.

To explore the relationship between the BET surface area and the CO_2 uptake, equilibrium CO_2 uptake values were plotted against the BET surface areas for all the samples from both date pits and coal tar pitch activated carbons as shown in Figure 5.5.

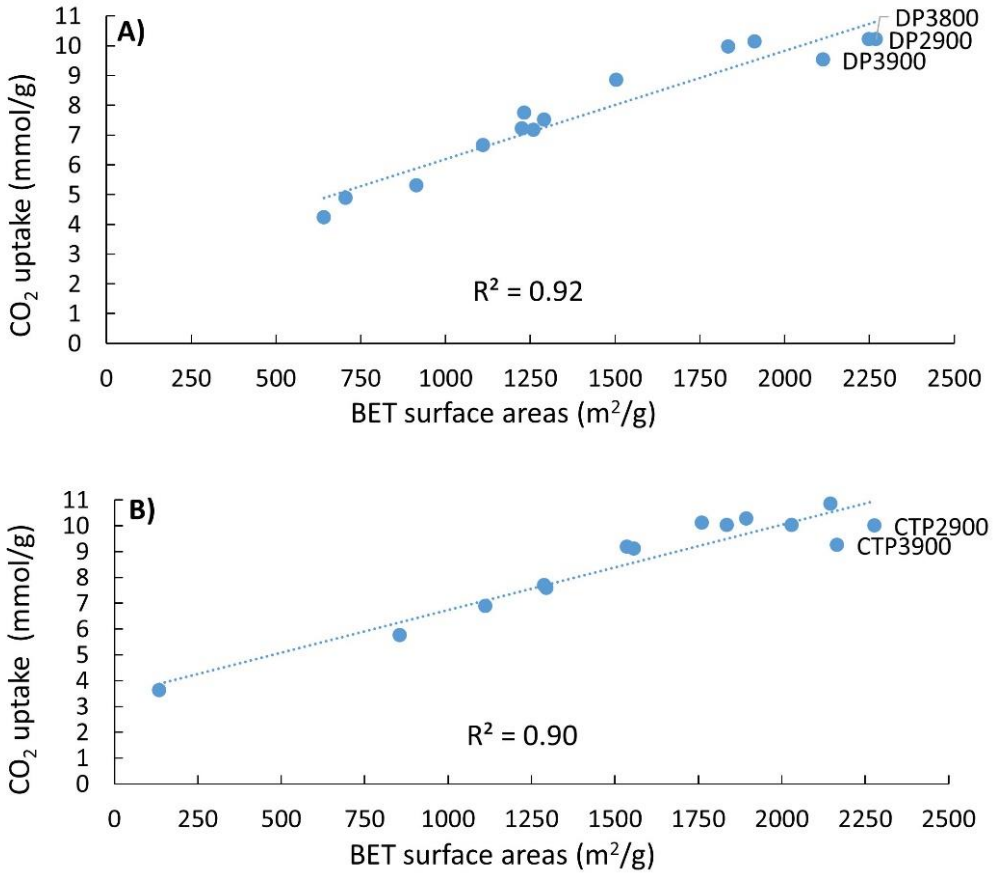


Figure 5.5 BET Surface areas vs. equilibrium CO_2 uptakes by (A) date pits and (B) coal tar pitch activated carbons.

The increase in the CO_2 uptake capacities at 50 ^oC and 20 bar was found to be directly proportional to the increase in the BET surface areas of the activated carbons. A linear line was fitted to the data and the values of R^2, indicating the goodness of fit, were 0.92 and 0.90 for date pits and coal tar pitch activated carbons respectively. This indicates a good fit and therefore a good linear correlation between the CO_2 uptake and the BET surface area. This result is in line with the findings of Drage *et al.* (2009) who tested 12 different types of activated carbons and showed a positive correlation between BET surface area and equilibrium CO_2 uptake at 41 bar. Another study conducted by Sun *et al.* (2013) on CO_2 adsorption at 40 bar on activated carbons prepared from phenolic resin also revealed a positive correlation between the BET surface area and the CO_2 adsorption at high

pressures. However, the values of R^2 reported in this current work are higher than the values reported by Drage and by Sun, 0.86 and 0.83 respectively. Such high R^2 values suggest a highly linear correlation between the CO_2 uptake at 20 bar and 50 ^oC and the BET surface area of the activated carbons synthesised from date pits and coal tar pitch with KOH in this work. Some interesting observations from Figure 5.5 are the few data points that showed a negative correlation between surface area and CO_2 uptake, i.e. samples DP2900, DP3800 DP3900 in Figure 5.5A and samples CTP2900 and CTP3900 in Figure 5.5B that showed an increase in surface area but not in CO_2 uptake. A common characteristic shared by all five of these samples is the presence of mesopores as described in chapter 4 section 4.2.4.2 and section 4.3.4.2. Therefore, for the activated carbon samples in this work, the surface area arising from mesopores does not appear to contribute significantly to the CO_2 uptake at 20 bar and 50 ^oC.

The role of the total pore volume and micropore volume in CO_2 uptake at 20 bar and 50 ^oC was investigated by plotting the total pore volume together with micropore volume against the equilibrium CO_2 uptake for both series of the activated carbons, as seen in Figure 5.6.

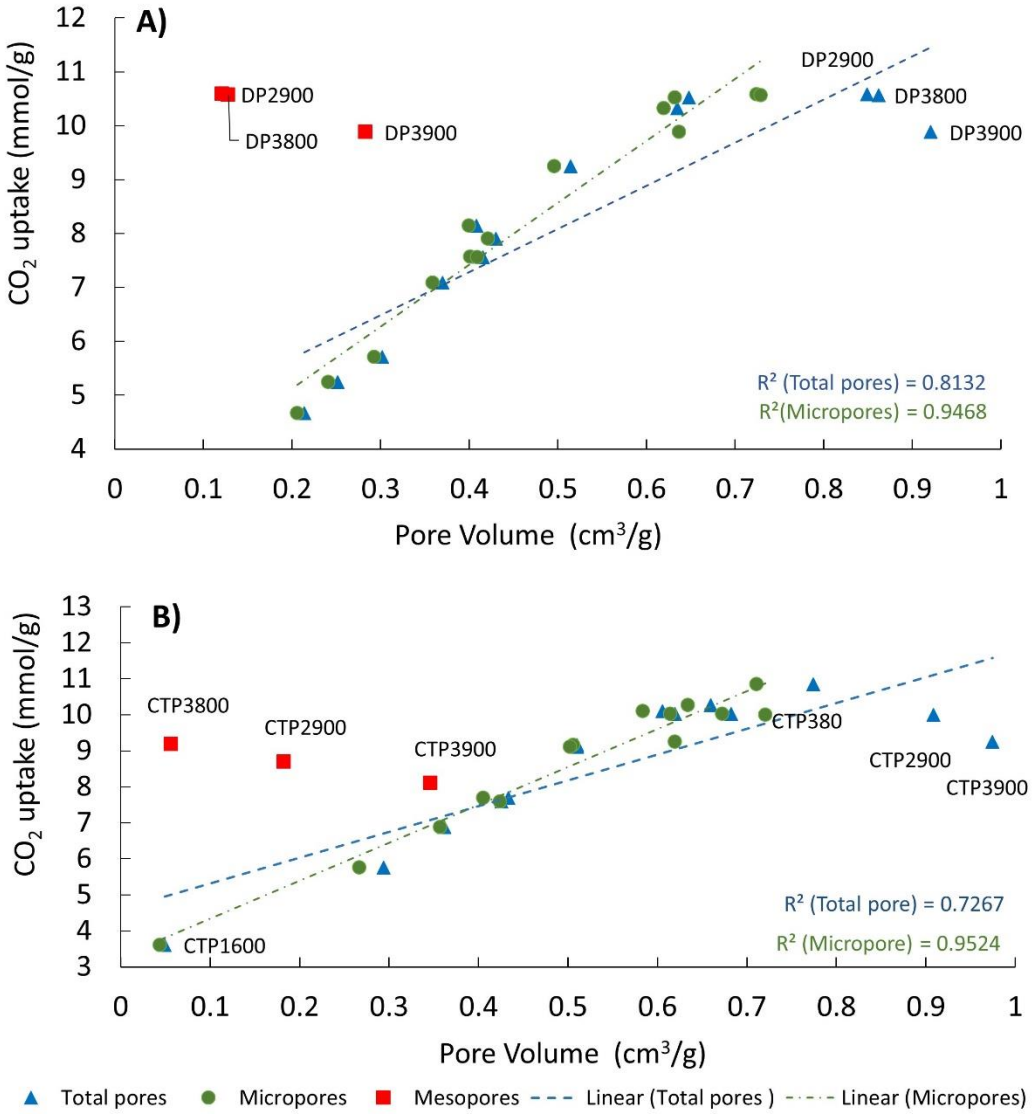


Figure 5.6 Total pore volume and micropore volume vs. equilibrium CO_2 uptake by (A) date pits activated carbon and (B) coal tar pitch activated carbon.

The equilibrium CO_2 uptake shows a positive linear correlation with the micropore volume for both types of activated carbons supported by the good linear fit for their relationship with values of R^2 of 0.9468 and 0.9524 for date pits and coal tar pitch activated carbons respectively. In comparison, the linear fit of the relationship between the total pore volume and the equilibrium CO_2 uptake showed a weaker linear correlation, owing to smaller R^2 values of 0.8132 and 0.7267 for date pits and coal tar pitch respectively. In addition, it was observed that although there was an increase in total pore volume for samples DP2900 and

DP3800, as seen in Figure 5.6A, there was no further increase in the equilibrium CO_2 uptake. Furthermore, sample DP3900 showed a drop in CO_2 uptake despite having the highest total pore volume amongst all the date pits activated carbons set. Similarly, CTP2900 and CTP3900, seen in Figure 5.6B, showed a drop in CO_2 uptake with increasing total pore volume. All the samples mentioned above have developed mesopores in addition to their micropores. This supports the previously stated argument that CO_2 uptake at 20 bar and 50 ^oC is mainly promoted by the increase in micropores and their associated surface area. The additional surface area and pore volume arising from mesopores seems to have limited contribution to the CO_2 uptake at the examined conditions.

Some of the samples showed interesting relationships between the equilibrium CO_2 uptake and micropore volume. For example, two samples showing almost the same CO_2 uptake but markedly different micropore volume are: sample DP3700 (10.52 mmol/g uptake and 0.6321 cm^3/g micropore volume) and sample DP3800 (10.57 mmol/g uptake and 0.7287 cm^3/g micropore volume). Another two samples showed almost the same micropore volume but different CO_2 uptake CTP2800 (0.6146 cm^3/g micropore volume and 10.03 mmol/g uptake) and sample CTP3900 (0.6196 cm^3/g micropore volume and 9.25 mmol/g uptake). With such observations, the PSD of these specific samples were used to examine the effect of various pore volumes given by different pores within the micropore size range. This was done by fitting a linear line (using Excel software) to the relationship between CO_2 uptake and nine different cumulative pore volumes arising from pores smaller than 1.09, 1.18,1.27,1.36, 1.48, 1.59, 1.72, 1.86 and 2.00 nm across all the date pits and coal tar pitch activated carbons as shown in Figure 5.7 and Figure 5.8.

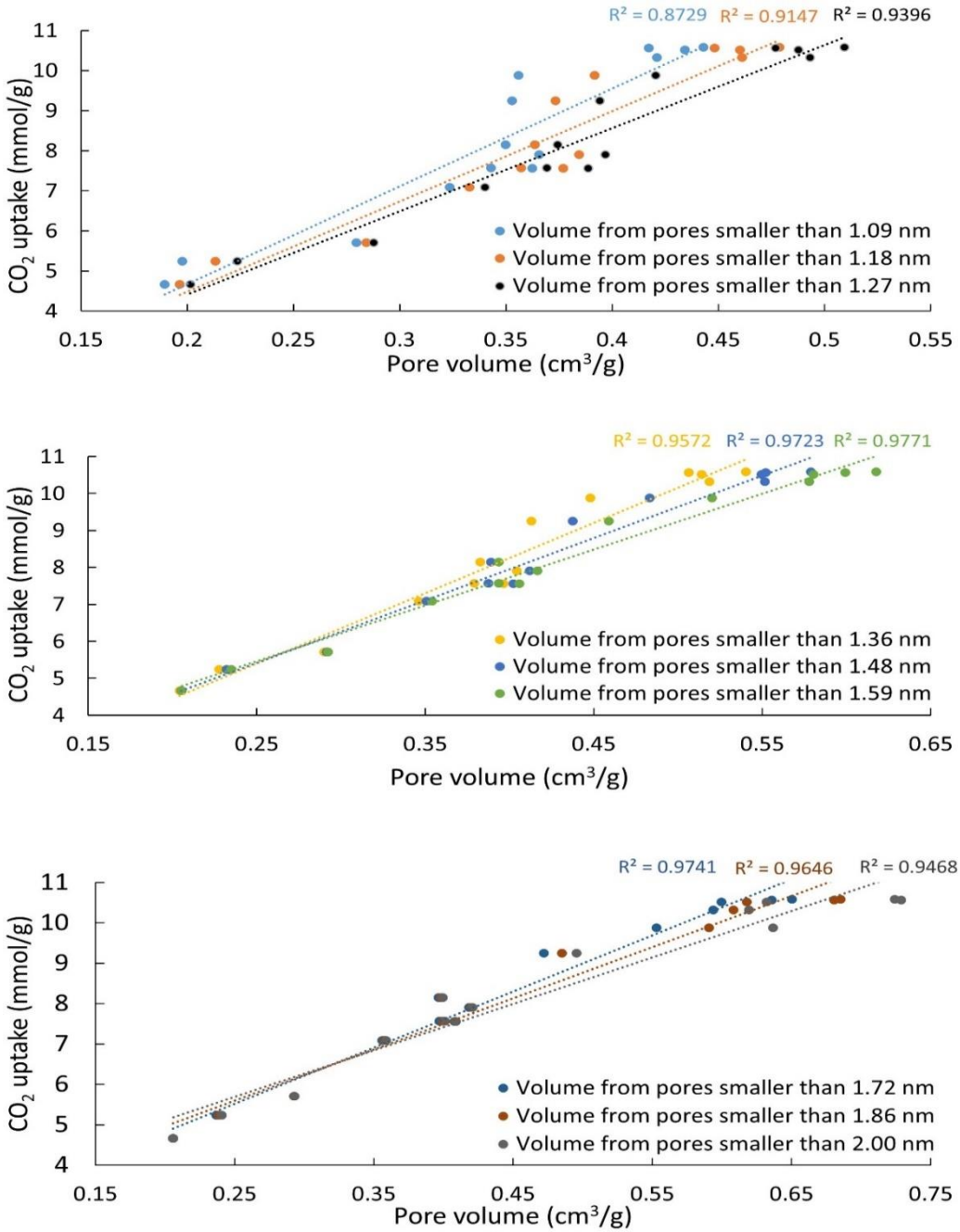


Figure 5.7 Linear relationship between cumulative volumes from pores smaller than specified pore size and equilibrium CO_2 uptake for date pits activated carbons at 20 bar and 50 °C.

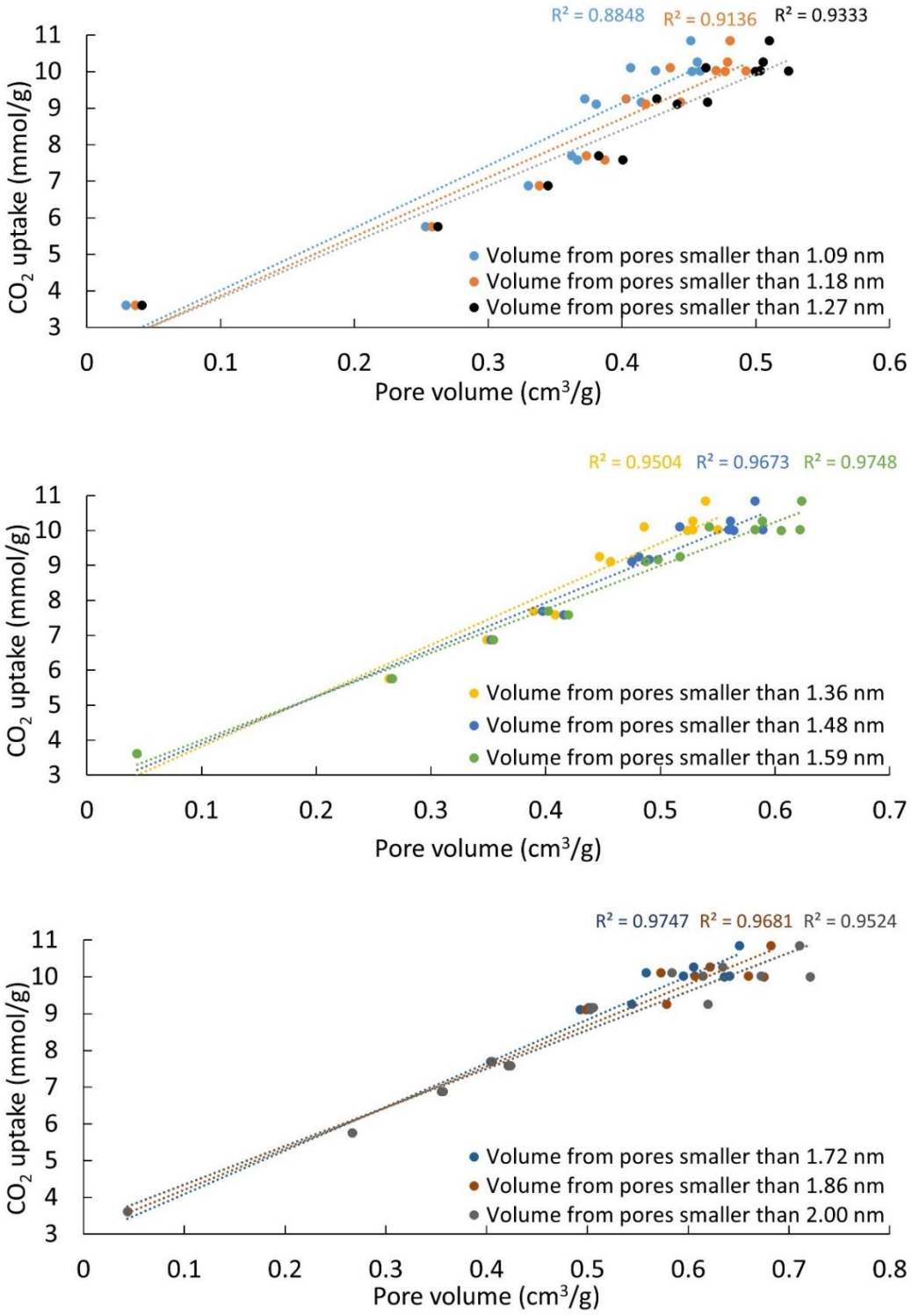


Figure 5.8 Linear relationship between cumulative volumes from pores smaller than specified pore size and equilibrium CO_2 uptake for coal tar pitch activated carbons at 20 bar and 50 °C.

The goodness of the linear fit, indicated by R^2, per cumulative pore volume in both Figure 5.7 and Figure 5.8 was used to assess the relative degree of usefulness of the additional volumes contributed by micropores having width between 1.09 nm

and 2.00 nm. Figure 5.9 shows all the values of R^2 plotted against the biggest pores included in the cumulative volume in the set of cumulative micropore volumes used in the previous analysis. Initially, the value of R^2 for both sets of activated carbons increased as additional volumes were included in the cumulative micropore volume indicating a positive correlation between CO_2 adsorption and the increase in micropore volume, i.e. "useful micropore volume". However, the value of R^2 reached a maximum after the addition of pore volume from pores of size 1.6 nm, then any additional volume from bigger pores resulted in lower R^2 values, indicating a weaker correlation between such micropore volume and CO_2 uptake, i.e. "less useful micropore volume". Based on the above it can be shown that there is a direct correlation for the CO_2 adsorption not only with the micropore volume but, more specifically, with the micropore volume arising from pores smaller than 1.6 nm.

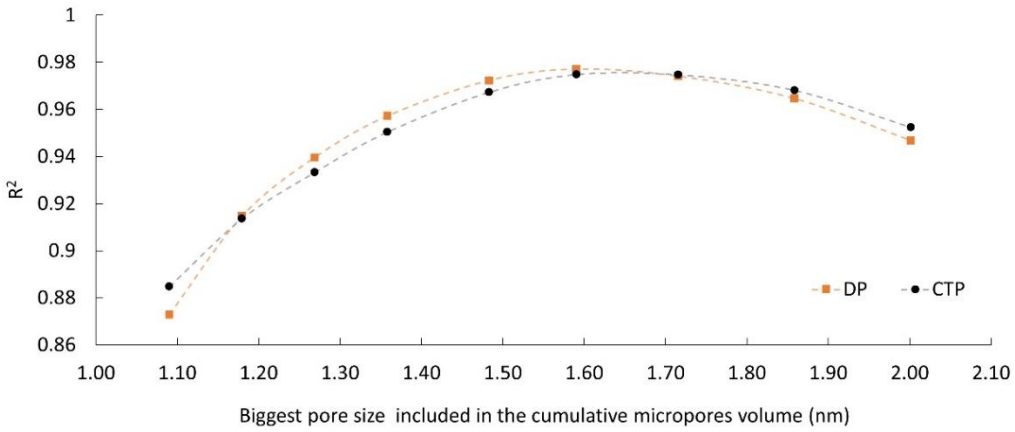


Figure 5.9 The goodness of the linear fit per cumulative pore volume (R^2) values against their corresponding biggest pore size contributing to the cumulative pore volume.

5.3 CO_2 Working Adsorption Capacity

When assessing the performance of solid adsorbents for PSA process, it is important to assess the net amount of CO_2 adsorbed as a result of an adsorption and desorption cycle which mimics the cycles in the PSA process. Therefore, it

was necessary to determine the CO_2 working adsorption capacity, in addition to the equilibrium CO_2 uptake at high pressure, of the activated carbons. Working capacity here is defined as the difference between the amount of adsorbed CO_2 at high pressure (20 bar) and the amount adsorbed at low pressure (1 bar). Therefore, high and low pressure CO_2 uptakes were measured gravimetrically and plotted in Figure 5.10 in four subsets based on the KOH to DP0 mass ratios used during the activation process.

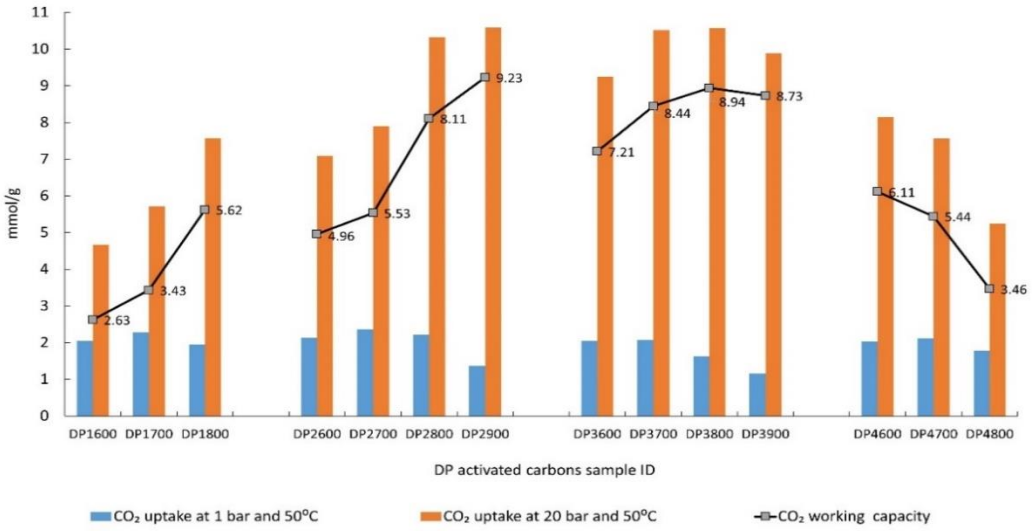


Figure 5.10 CO_2 uptake of DP activated carbons at 1 bar and 20 bar with the resultant CO_2 working capacity.

Figure 5.10 shows that the CO_2 uptake at 1 bar reached its highest value when the activation temperature of 700 ^oC was used across all four KOH to DP0 mass ratios. However, it dropped as the activation temperature increased to 800 and 900 ^oC and therefore contributed to the increase in the working capacity which was largely influenced by the rise in the adsorption at high pressure but helped by the drop in adsorption at low pressure. There was a noticeable drop in the adsorption of CO_2 at 1 bar for samples activated at 900 ^oC, namely DP2900 and DP3900. These samples share the same feature of containing micropores bigger than 1.6 nm and

some mesopores with a reduction in small micropores, as seen in the PSD discussed in chapter 4 in section 4.2.4.3. This could be considered a/n advantageous feature to achieve high CO_2 working capacity since small micropores (less than 1 nm) were highlighted in previous research as a promoting factor for the adsorption of CO_2 at atmospheric pressure (Hu *et al.*, 2009; Presser *et al.*, 2011; Wei *et al.*, 2012). However, this is not desired in this work since the aim is to reduce the adsorption of CO_2 at 1 bar so that the resulting working capacity increases. The highest CO_2 working capacity of 9.23 mmol/g was achieved by sample DP2900. Based on the observation of the CO_2 working capacities above, it is logical to say that as long as the development of wide micropores and mesopores does not reduce the effective micropore volume, it could be considered useful since it played a positive role in increasing the CO_2 working adsorption capacity by reducing the adsorption of CO_2 at low pressure.

Coal tar pitch activated carbons were also examined with respect to their CO_2 working capacities in a manner similar to that of date pits activated carbons. Figure 5.11 shows that the upward trend of the CO_2 working capacity of the coal tar pitch carbons for the first 6 samples was influenced mainly by the upward trend in the CO_2 uptake at 20 bar rather than the uptake at 1 bar which showed a slight variation across each group of carbons sharing the same KOH amount.

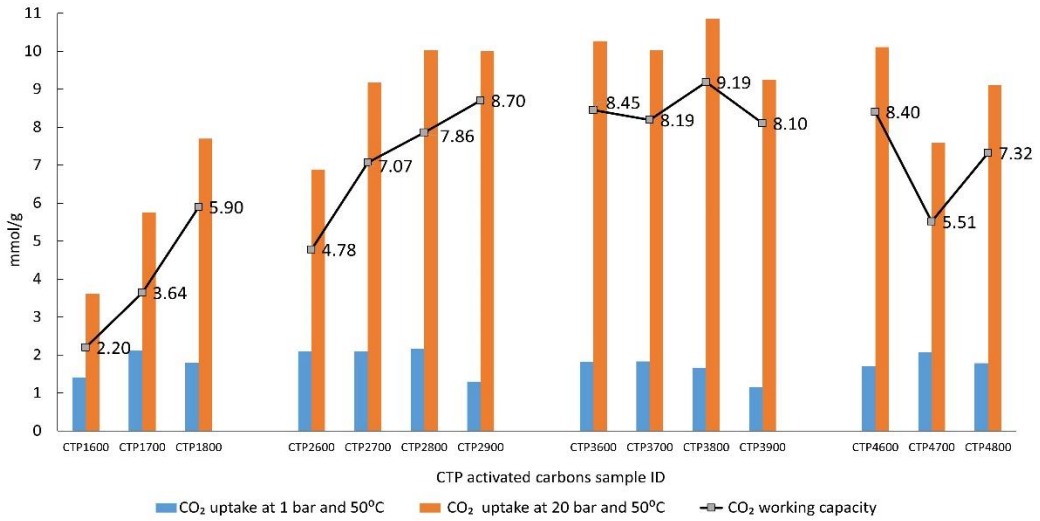


Figure 5.11 CO_2 uptake of CTP activated carbons at 1 bar and 20 bar with the resultant CO_2 working capacity.

Similar to the date pits activated carbons, coal tar pitch samples activated at 900 ^oC showed a noticeable drop in CO_2 uptake at 1 bar due to the presence of wide micropores and mesopores as highlighted by their PSD presented in chapter 4 in section 4.3.4.3, such large micropores and mesopores were not favourable for atmospheric pressure adsorption of CO_2. A similar observation with regards to reduced adsorption of CO_2 at 1 bar due to the presence of large micropores and mesopores was highlighted by Sevilla *et al.* (2018). Generally speaking, if it is possible to engineer the activated carbons to achieve high working capacity, their PSD should be shifted to larger micropores so that the adsorption at low pressure is minimised whilst maximising high pressure adsorption at the same time.

5.4 High Pressure CO_2 Adsorption Isotherms

A High Pressure Adsorption Analyser (HPVA) was used to measure CO_2 adsorption isotherms at 25 ^oC and 50 ^oC for pressures up to 40 bar for samples DP2900 and CTP3800. These two samples were selected because they demonstrated the highest CO_2 working capacity across all the activated carbons

screened in this work. Figure 5.12 shows the measured isotherms, where the dotted lines are not model fittings but rather to guide the eye.

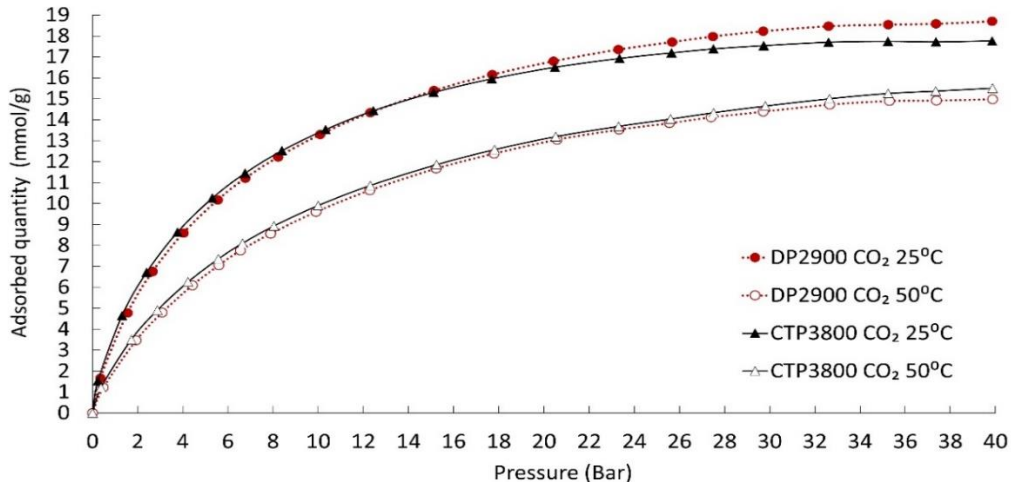


Figure 5.12 CO_2 adsorption isotherms at 25 °C and 50 °C for samples DP2900 and CTP3800.

It is clear from Figure 5.12 that the adsorbed quantities of CO_2 increased with increasing pressure (from vacuum to 40 bar) and decreased with increasing temperature (from 25 to 50 °C) for both samples. This is as expected as the adsorption process is known to be exothermic in nature (Lowell *et al.*, 2004). Despite having relatively similar micropore volumes, 0.72 cm^3/g for DP2900 and 0.71 cm^3/g for CTP3800, sample CTP3800 (solid lines) showed a slightly faster dynamic of adsorption (steeper rise) compared to DP2900 at low pressure (up to 12 bar) at both temperatures. This could be attributed to the narrower PSD for CTP3800 that was also shifted towards the smaller micropores compared to the wider PSD for DP2900 that exhibited a shift towards large micropores and some mesopores as seen in their PSD comparison in Figure 5.13 below.

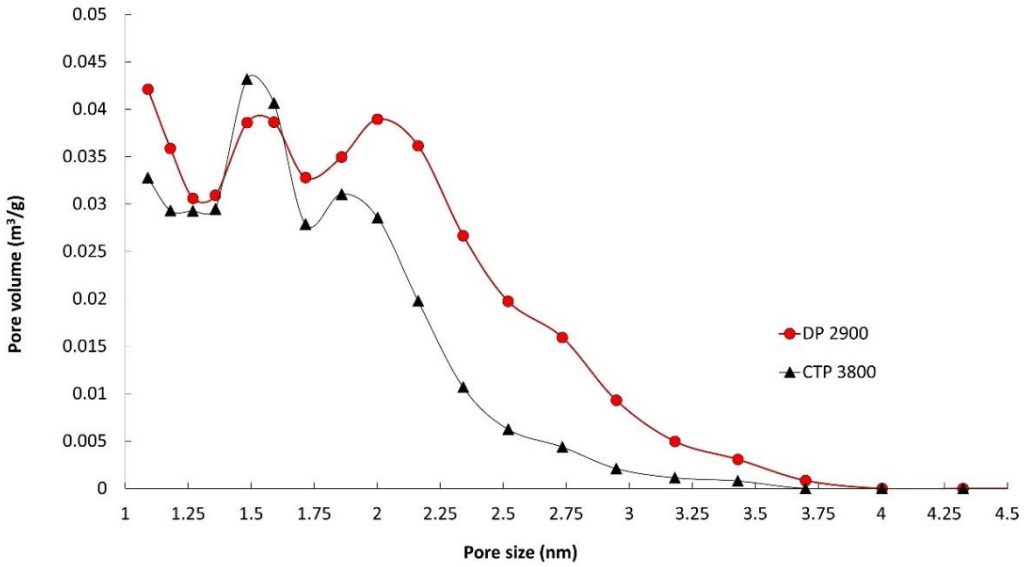


Figure 5.13 Comparison of PSD for DP2900 and CTP3800.

However, as the pressure increased above 12 bar at 25 ^{o}C, DP2900 demonstrated an increase in adsorption quantities of CO_2 in comparison with CTP3800. Such behaviour could be linked to the additional pore volume available for adsorption at high pressure contributed by the mesopores (larger than 2 nm) in DP2900, in contrast to CTP3800 which had a smaller pore volume arising from its mesopores as seen in Figure 5.14 which compares the cumulative pore volumes for both samples. This points to the role of the mesopores in adsorption of CO_2 at 25 ^{o}C where it is thought that CO_2 could condense in the mesopores giving rise to the adsorbed amount at high pressure since the CO_2 was below its critical temperature of 31.1 ^{o}C in contrast to the adsorption isotherm measuered at 50 ^{o}C where no CO_2 condensation would be expected since the temperature is higher than the critical temperature of CO_2. Therefore, the adsorbed CO_2 quantity for DP2900 did not overtake that of CTP3800 at 50 ^{o}C as the mesopore volume did not seem to enhance the adsorption of CO_2 at high pressure, above 12 bar, and high temperature, 50 ^{o}C.

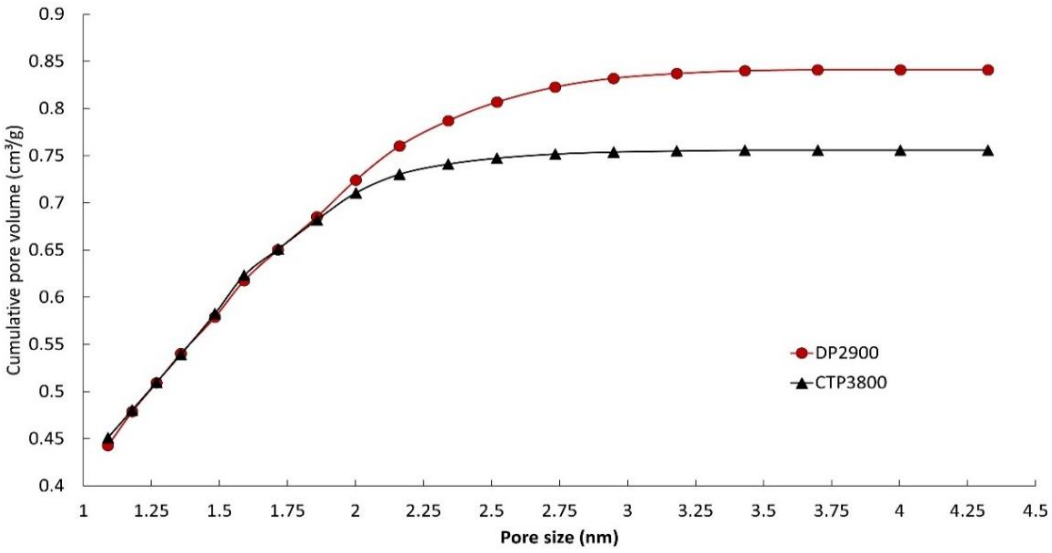


Figure 5.14 Cumulative pore volume for DP2900 and CTP3800.

5.5 CO_2 Isosteric Heat of Adsorption

Isosteric heat of adsorption (Q_{st}) provides an indication of the strength of the interaction between the adsorbate and the carbon surface (Singh and Anil Kumar, 2016). Based on the adsorbed quantities from the two isotherms measured at two different temperatures for the same activated carbon, the Clausius-Clapeyron equation, *Equation 5.1*, was used to calculate the heat of adsorption at a given specific adsorbed amount (q) (Guo, Chang and Xie, 2006).

$$Q_{st} = -R\left(\frac{\partial \ln P}{\partial(1/T)}\right)_q \qquad \textit{Equation 5.1}$$

In this research, the Clausius-Clapeyron equation embedded in MicroActive® software was used to calculate the CO_2 isosteric heat of adsorption ($Q_{st_co_2}$) for DP2900 and CTP3800 at several adsorbed quantities shown in the x-axis of Figure 5.15. The adsorbed amount and its corresponding P and T values were sourced from the previously measured CO_2 adsorption isotherms at 25 ºC and 50 ºC for DP2900 and CTP3800.

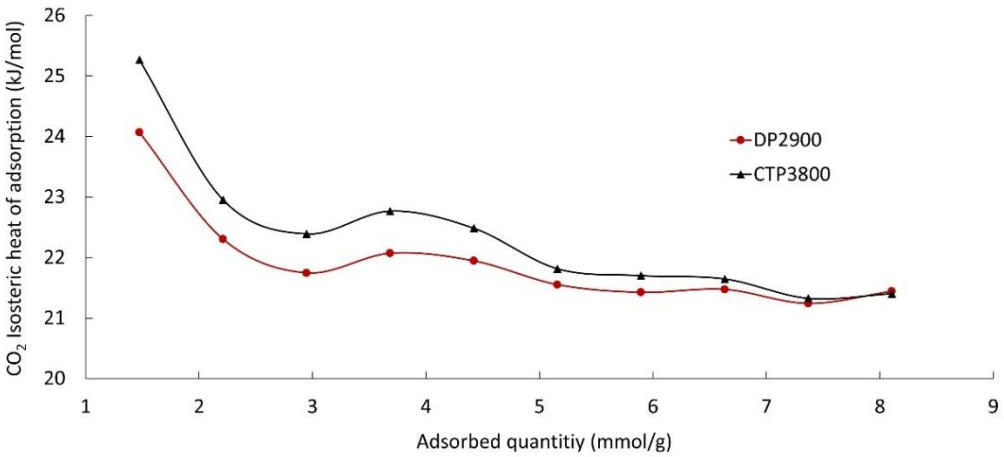


Figure 5.15 CO_2 isosteric heat of adsorption ($Q_{st_co_2}$) for samples DP2900 and CTP3800.

The trend of the calculated $Q_{st_co_2}$, as shown in Figure 5.15, reveals an initial rapid drop in $Q_{st_co_2}$ from 24 kJ/mol and 25.3 kJ/mol for samples DP2900 and CTP800 respectively with increasing CO_2 adsorbed quantities. The drop is less prominent as the adsorbed amount increases further. Singh & Anil Kumar (2016) reported a similar observation with the following explanation. Since $Q_{st_co_2}$ is associated with different forces such as Van der Waals forces or the weaker intermolecular quadrupole forces, and since at the beginning of the isotherm measurement the pores were empty, direct interactions between the gas and empty pore walls are due to the relatively stronger Van der Waals forces from the walls of the micropores, hence the initial high $Q_{st_co_2}$ values. However, as the adsorbed amount increases with increasing adsorption pressure and the micropores are filled, the relatively weaker adsorbate-adsorbate forces, such as the CO_2 quadrupole moment forces, play a dominant part, hence the drop in $Q_{st_co_2}$. The drop in $Q_{st_co_2}$ is also an indication of the heterogeneity of the adsorption surface of the activated carbon (Singh *et al.*, 2017). Furthermore, CTP3800 showed higher values of $Q_{is_co_2}$compared with DP2900 across the adsorbed amount. This observation is in line with the earlier observation of faster dynamics for sample

CTP3800 due to its narrower PSD that was also skewed towards the smaller micropores compared to that of DP2900 given that smaller micropores are expected to have higher adsorption strength to CO_2 compared with the larger micropores or mesopores and therefore higher $Q_{st_co_2}$. The range of the $Q_{st_co_2}$ estimated in this work (21.5 to 25.3 kJ/mol) is within the range of 16 to 27 kJ/mol reported by Himeno *et al.* (2005) for the heat of CO_2 adsorption for 5 different types of activated carbons. The $Q_{st_co_2}$ values estimated for DP2900 and CTP3800 were below 80 kJ/mol which indicates that the adsorption was mainly physical as opposed to chemical (Zhou *et al.*, 2012).

5.6 Water Vapour Effect on CO_2 Adsorption

Water produced with the natural gas is considered problematic for the processing and transportation of natural gas (Sui *et al.*, 2018). Conventional gas processing facilities are designed to remove this water as early as possible downstream to the gas wellhead. An alternative approach followed in some cases is to leave the water and construct the process equipment and pipeline from corrosion resistant materials and use corrosion inhibiting chemicals (Hammer *et al.*, 2000). Water vapour might also exist after the initial dehydration step of raw natural gas.

In this research, saturated KOH aqueous solution was used to create a humidity-controlled environment of 10% relative humidity at room temperature to investigate the effect of a 10% water vapour contamination in the natural gas feed stream on the CO_2 adsorption. This technique involved preparing a KOH saturated solution by dissolving 14g of KOH in 10 mL of deionised water then placing the solution in the lower section of a vacuum desiccator. The lower section of the vacuum desiccator was separated from the upper section with a metal mesh on top which the activated carbons were placed together with a relative humidity and

temperature logging device for monitoring the stability of the test environment. The described set up is shown in Figure 5.16.

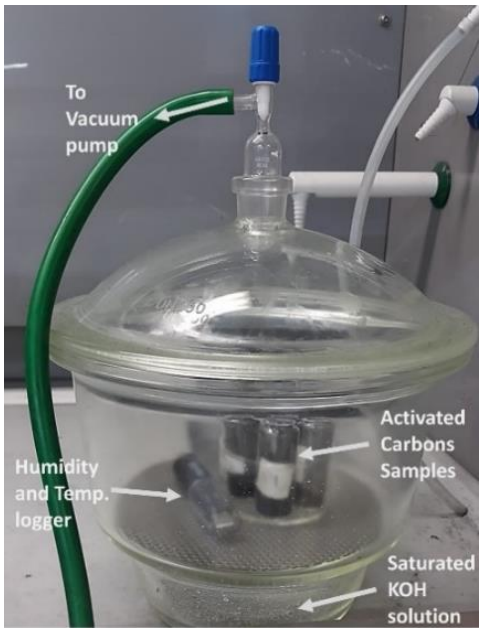


Figure 5.16 Controlled humidity environment set up in vacuum desiccator using saturated KOH aqueous solution.

Once the desiccator was tightly closed a vacuum pump was used to evacuate the atmosphere inside it for 1 hour to drop the humidity level, as seen immediately after time zero in Figure 5.17, after which the humidity increased gradually to settle at 10% relative humidity (RH).

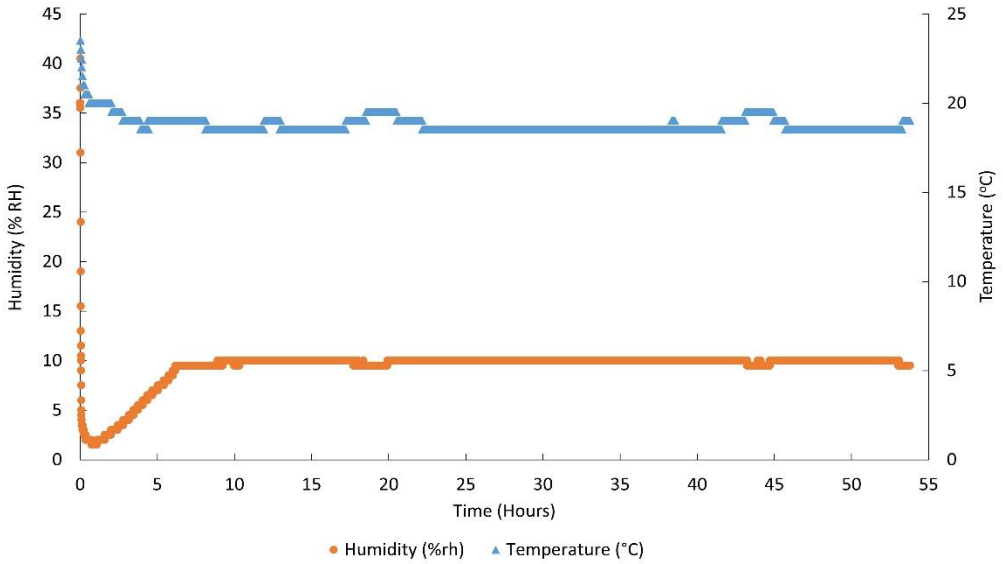


Figure 5.17 Relative humidity and temperature inside the controlled humidity desiccator.

The CTP3800 activated carbon sample was left inside the desiccator for 48 hours before moving it to the HPVA for CO_2 adsorption isothermal measurements. These measurement were later compared to the dry CO_2 isotherm measurements reported earlier in section 5.4. When operating the HPVA with the wet sample, the isotherm measurements were started at 1.5 bar then the pressure was stepped up to avoid losing the adsorbed moisture. While this experimental setup does not strictly mimic water vapour mixed with the natural gas stream, it does investigate the worst case scenario effect on CO_2 uptake due to 10% water vapour for sample CTP3800 by allowing the water vapour to adsorb without any competition from other components in the natural gas stream. The 10% relative humidity CO_2 isotherm was measured at 25 ^oC. Figure 5.18 depicts both the dry and the 10% relative humidity CO_2 adsorption isotherms for CTP3800 together with their difference expressed relative to the dry isotherm values.

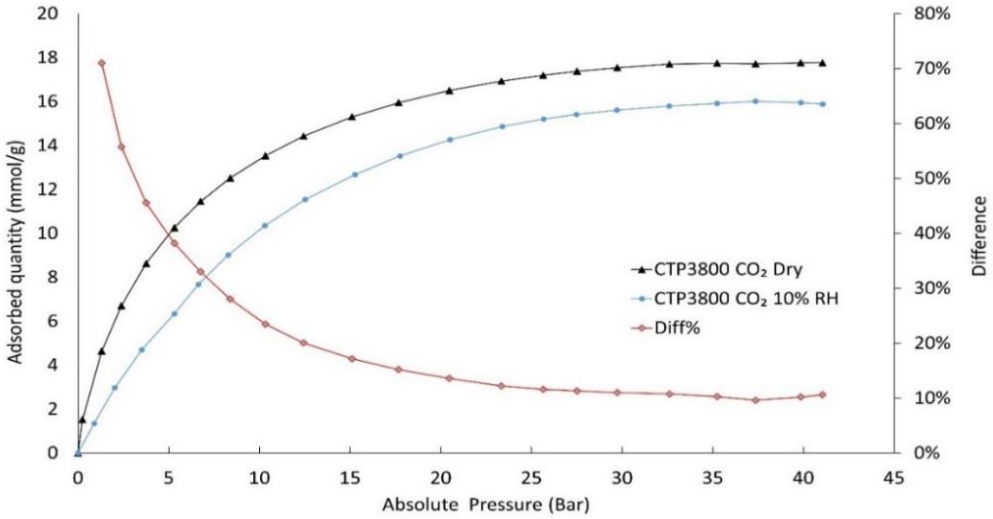


Figure 5.18 Dry vs 10% relative humidity CTP3800 CO_2 adsorption isotherms at 25 ^oC.

From Figure 5.18, we can see that the dry sample achieved high uptake of CO_2 across the full pressure range. However, the percentage difference between the dry and the 10% relative humidity isotherms was not constant across the adsorption

pressure range. Initially, the difference was as high as 72% but reduced to around 10% at high pressure.

As far as CO_2 adsorption is concerned, water has a dipole moment of 1.8546 D while CO_2 has no dipole (Lide, 2004). Therefore, water was expected to preferentially adsorb over CO_2. However, keeping in mind the application of using activated carbons in a PSA process to remove CO_2 from natural gas at high pressure, the negative effect of the 10% water vapour on CO_2 adsorption was more pronounced at low pressure, resulting in a 72% drop in CO_2 adsorption, which might be detrimental to the initial dynamics of the adsorption in PSA systems. Having said that, the same amount of water had a much lower negative impact (10% drop) on the maximum CO_2 uptake capacity of the activated carbons at high pressure as seen in Figure 5.18.

5.7 Conclusion

In conclusion, the HP-TGA was used to screen the synthesised activated carbons in this work by measuring their CO_2 isotherms at 20 bar and 50 ^oC to acquire their equilibrium CO_2 uptake capacities. The measurement was conducted at the partial pressure of CO_2 in a typical natural gas mixture found in the South Oman gas field (20 bar). The equilibrium adsorption capacities at 1 bar were also measured for all activated carbons to work out the CO_2 working adsorption capacities. The CO_2 working capacities were used to screen the synthesised activated carbons. The highest measured CO_2 working capacities were 9.23 mmol/g and 9.19 mmol/g for DP2900 and CTP3800 activated carbon respectively.

Micropore volumes and BET surface areas were found to have a highly linear correlation with the equilibrium adsorption capacities of CO_2 at 20 bar and 50 ^oC.

Cumulative pore volume, from pores smaller than 1.6 nm, was found to have the highest correlation with CO_2 uptake. Mesopore volume played a role in promoting slightly higher CO_2 adsorption capacities at high pressure and 25 ^oC but played a limited role at 50 ^oC as revealed by the HPVA adsorption isotherm measurements. Isosteric heat of adsorption values for samples DP2900 and CTP3800 were calculated using the Clausius-Clapeyron and found to decrease with increasing adsorption quantities. The calculated CO_2 isosteric heat of adsorption for CTP3800 (25.3 kJ/mol) was slightly higher than that of DP2900 (24 kJ/mol).

The influence of the presence of the activated carbons in an environment containing 10% moisture on the CO_2 adsorption of CTP3800 was investigated using wet HPVA tests. When compared with dry sample, the wet sample HPVA tests revealed that the moisture reduced the CO_2 adsorption capacity of the CTP3800 activated carbon. The moisture was found to cause more reduction to the CO_2 adsorption at low pressure (below 20 bar) compared to the reduction in total CO_2 uptake capacity of CTP3800 at high pressure (20 - 40 bar).

Chapter 6. Adsorption Selectivity of CO_2 over CH_4 and the Effect of Moisture

6.1 Introduction

Since methane is usually the main component of natural gas, any comprehensive assessment of adsorbents for the application of CO_2 removal from natural gas also needs to consider the adsorption of methane in addition to that of CO_2. While a high CO_2 uptake capacity is a desired feature for an optimum activated carbon adsorbent for the application of this research, CH_4 uptake is not. Therefore, this Chapter assesses the adsorption of CH_4 by the two sets of synthesised activated carbons, namely date pits and coal tar pitch. CH_4 equilibrium and working adsorption capacities were used to screen all the activated carbons and to understand the relationship between the textural properties of the activated carbons and the CH_4 uptake. Based on their merits of having a high CO_2/CH_4 adsorption ratio and/or high CO_2 capacity, three samples were selected for high pressure CH_4 adsorption isotherms measurements up to 100 bar and at 25 and 50 ^oC in the HPVA. The measured isotherms were used to calculate the CH_4 isosteric heat of adsorption based on the Clausius–Clapeyron equation. Finally, the effect of pre-

adsorbed water on the CO_2 over CH_4 adsorption selectivity was investigated using the HPVA to measure the adsorption of both gases onto wet activated carbons.

6.2 CH_4 Equilibrium Adsorption Capacity

A High Pressure Thermal Gravimetric Analyser (HP-TGA) was used to measure CH_4 equilibrium adsorption capacities for 14 date pits activated carbons and 14 coal tar pitch activated carbons. The adsorption measurement pressure was set to 80 bar equal to the partial pressure of CH_4 in South Oman gas field that contains 80% CH_4 at 100 bar and 50 ^oC. Figure 6.1 shows all the measured CH_4 equilibrium uptakes grouped into four subsets based on the activation temperatures (600, 700, 800 and 900 ^oC) used to produce the activated carbons; the KOH amount used to activate each sample expressed as KOH to date pits char (PD0) mass ratio varies between 1 and 4 within each subset as indicated by the first digit in each sample ID.

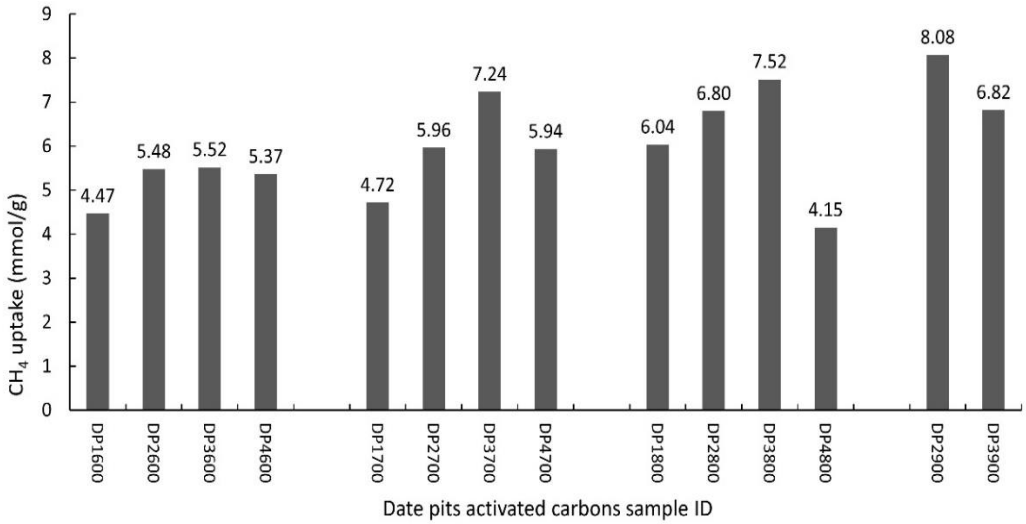


Figure 6.1 Equilibrium CH_4 uptake by date pits activated carbons at 80 bar and 50 ^oC.

The CH_4 uptake was found to increase with increasing activation degree by either increasing the activation temperature or the KOH amount used to produce the activated carbon or both but with the two exceptions:

1. Samples activated with KOH to DP0 mass ratio of 4, i.e. samples DP4600, DP4700 and DP4800, showed a drop in CH_4 uptake relative to the previous sample along the sequence of increasing activation degree.
2. Sample DP3900 showed a drop from both previous samples in the sequence of increasing activation degree, i.e. DP2900 and DP3800.

Likewise, all activated carbons synthesised from coal tar pitch were also screened by testing their equilibrium CH_4 uptake at 80 bar and 50 ^oC under the same HP-TGA operating conditions used to screen the date pits activated carbons. Figure 6.2 presents the measured equilibrium CH_4 uptake capacities achieved by all the coal tar pitch activated carbons grouped into four subsets similar to that of the date pits activated carbons as indicated by the sample ID.

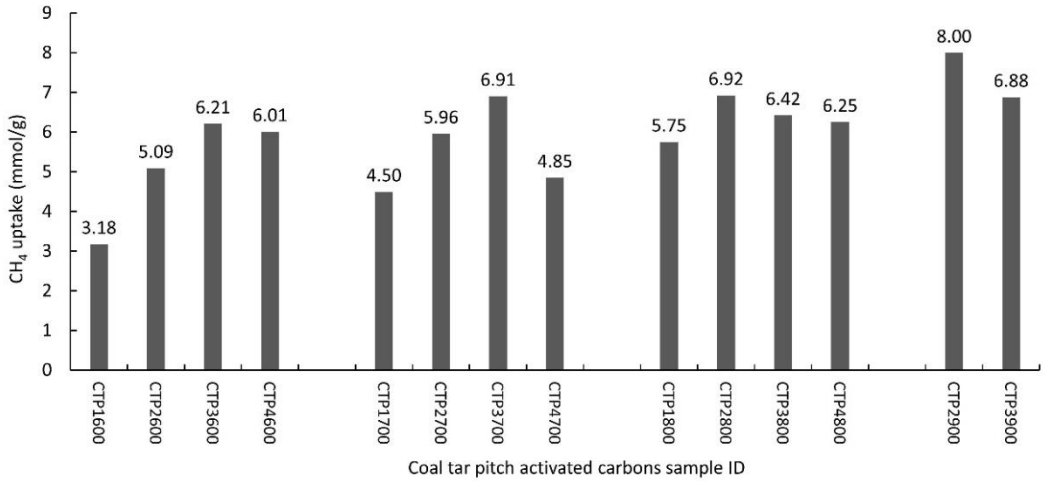


Figure 6.2 Equilibrium CH_4 uptake by coal tar pitch activated carbons at 80 bar and 50 ^oC.

Generally, for the first two subsets of the samples that were activated at 600 and 700 ^oC, the adsorbed CH_4 amount increased with increasing KOH amount used for the activation except for the samples activated with KOH to CTP0 mass ratio of 4, i.e. samples CTP4600 and CTP4700. The third subset (activated at 800 ^oC) reached a maximum CH_4 adsorbed amount of 6.92 mmol/g for sample CTP2800

then showed a decline through the remaining two samples in the set, i.e. CTP3800 and CTP4800. The highest uptake within the whole set was 8.00 mmol/g which was achieved by sample CTP2900.

To obtain further insight into the observed CH_4 adsorption trends by the activated carbons, their BET surface areas and their CH_4 uptakes were plotted against each other as seen in Figure 6.3.

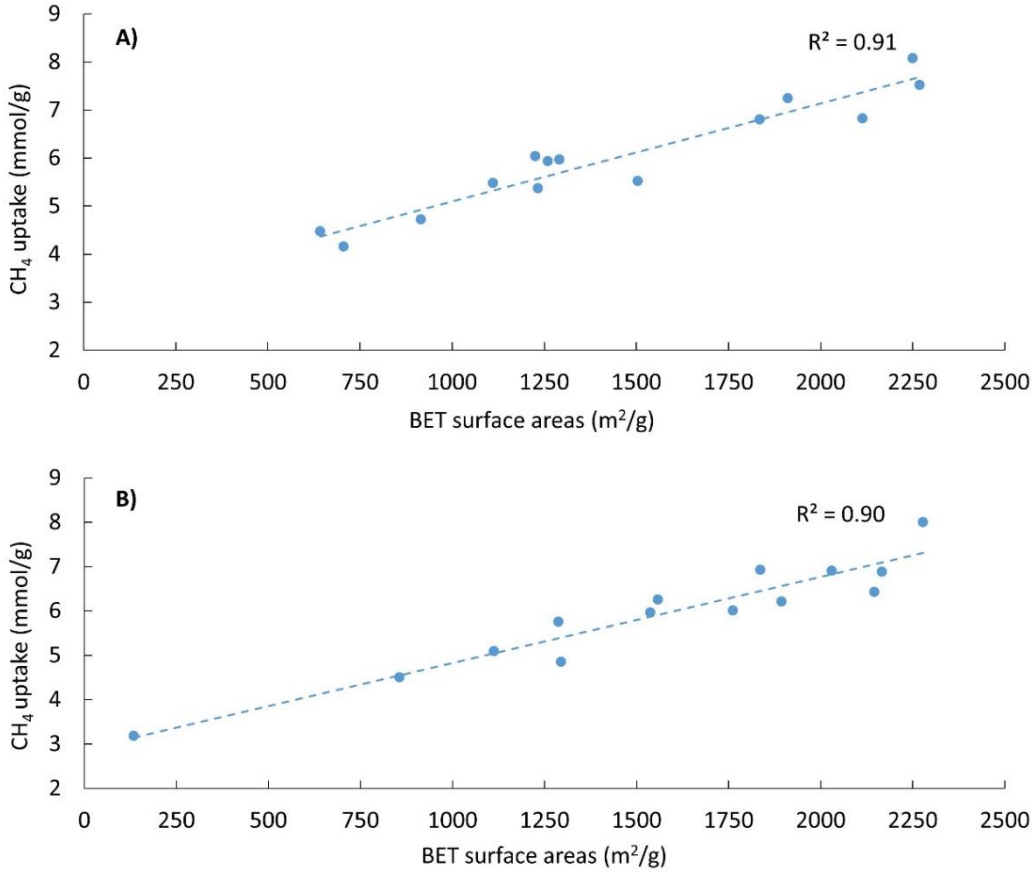


Figure 6.3 BET surface areas vs equilibrium CH_4 uptakes at 80 bar and 50 ^oC by (A) date pits and (B) coal tar pitch activated carbons.

Both sets of activated carbons presented in Figure 6.3 showed a positive linear correlation between the BET surface area and the amount of CH_4 adsorbed at 80 bar and 50 ^oC. The date pits activated carbons showed a slightly better linear

correlation with an R^2 value of 0.91 compared to the R^2 value for the coal tar pitch activated carbons of 0.90.

The total pore volumes and the micropore volumes of date pits activated carbons were plotted against the measured equilibrium CH_4 adsorption amount as shown in Figure 6.4. The CH_4 uptake at 80 bar and 50 ^oC showed a stronger linear correlation with micropore volume compared to the correlation with the total pore volume, as demonstrated by a higher R^2 value.

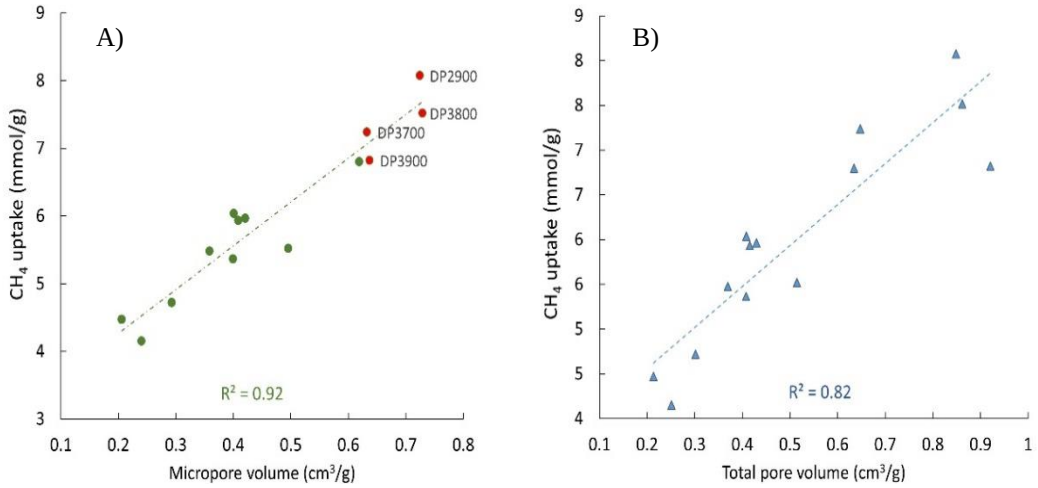


Figure 6.4 Micropore volume (A) and total pore volume (B) vs CH_4 uptake at 80 bar and 50 ^oC for date pits activated carbons.

To further probe the relationship between the micropore volume and the CH_4 uptake, two pairs of samples were selected: pair A (DP3700 and DP3900) and pair B (DP2900 and DP3800), and both pairs are marked in red in Figure 6.4 (A). In each pair, both samples showed very similar micropore volumes but distinct CH_4 uptakes as shown in Table 6.1.

Table 6.1 Pore volume and CH_4 uptake for Pair A (DP3700, DP3900) and pair B (DP2900, DP3800)

Pair	Sample ID	Micropore volume (cm^3/g)	CH_4 uptake (mmol/g)
A	DP3700	0.6322	7.24
	DP3900	0.6367	6.82
B	DP2900	0.7242	8.08
	DP3800	0.7287	7.52

To investigate the effect of various micropore sizes on CH_4 uptake, the cumulative pore volume and the Pore Volume Distribution (PVD) between 1 nm to 2 nm were plotted against the PSD for pair A and pair B as shown in Figure 6.5.

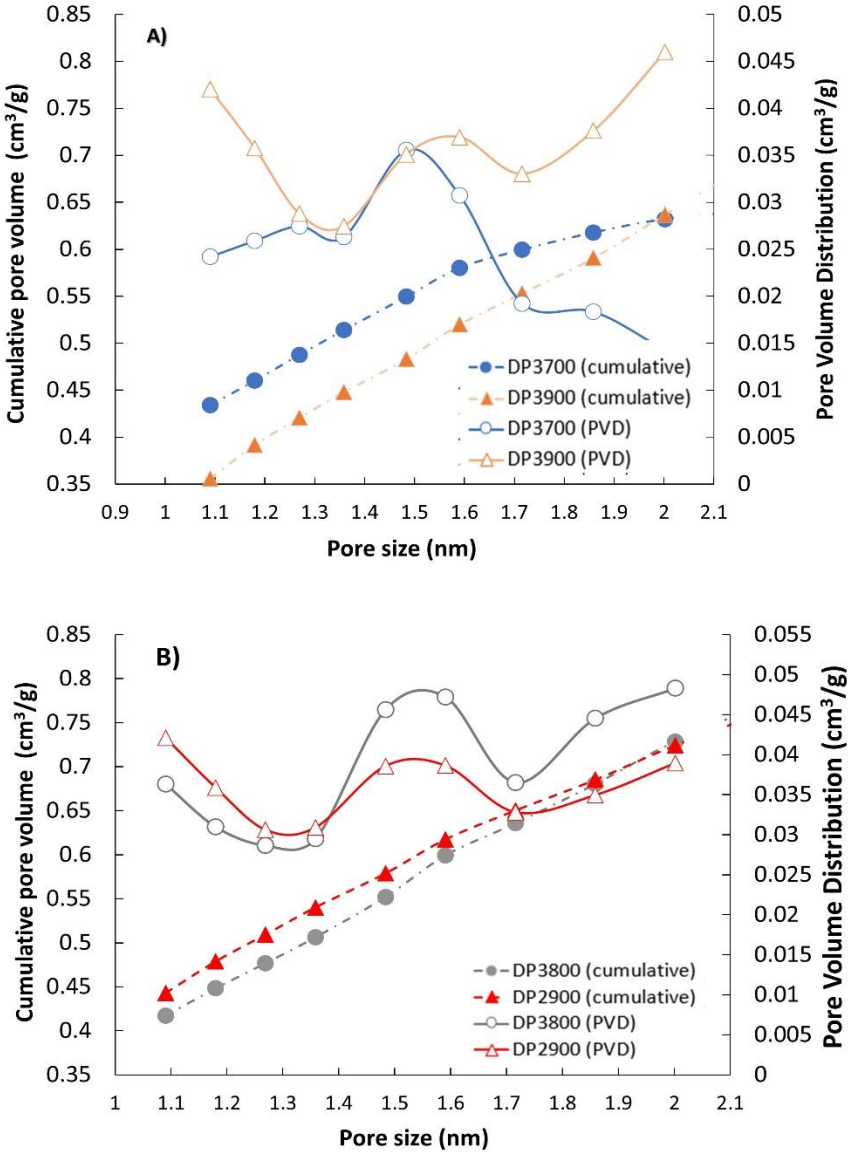


Figure 6.5 Cumulative pore volume and pore volume distribution (PVD), (A) DP3700 and DP3900, (B) DP2900 and DP3800.

A common observation from Figure 6.5 for each pair is that despite both samples in the same pair having similar micropore volumes (i.e. cumulative pore volume up to 2.0 nm), the PVD was not the same. Samples that showed higher CH_4 uptake (DP3700 and DP2900) have less volume arising from micropores bigger than 1.5 nm compared to the low CH_4 uptake samples (DP3900 and DP3800). Such observations indicate that micropores bigger than 1.5 nm are less favourable for CH_4 adsorption at 80 bar and 50 ^oC for the date pits activated carbon samples.

Coal tar pitch activated carbons were investigated for the relationship between CH_4 uptake and pore volumes in a similar manner to that of the date pits samples. Figure 6.6 illustrates the relationship between the micropore volume and the total pore volume on the one hand and CH_4 uptake on the other hand.

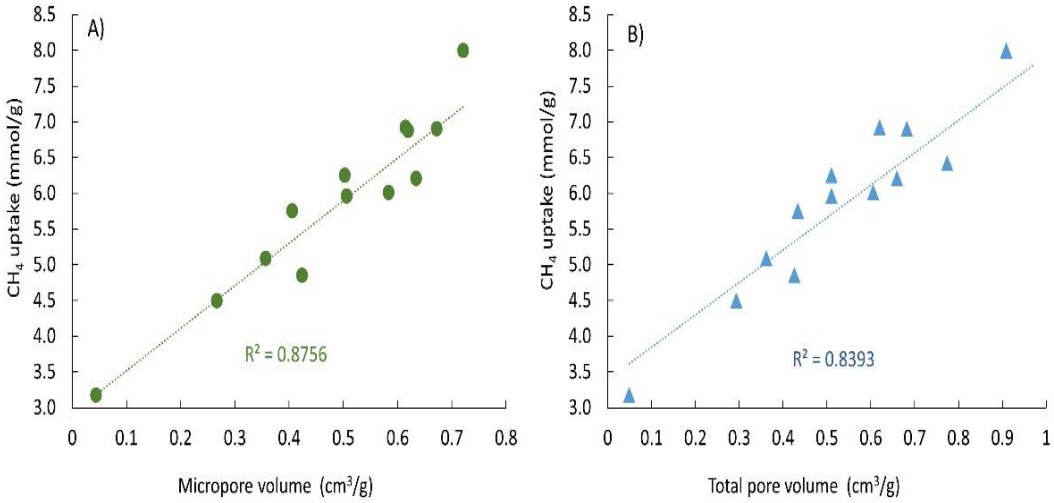


Figure 6.6 CH_4 uptake at 80 bar and 50 ^oC for coal tar pitch activated carbons against (A) micropore volume and (B) total pore volume.

CH_4 uptake by coal tar pitch activated carbons showed a better correlation with micropore volume compared to its correlation with the total pore volume signified by a higher R^2 value.

6.3 CH_4 Working Adsorption Capacity

Working capacity is defined as the difference between high and low pressure adsorbed quantities (Krishna, 2012). In this work, the low pressure was considered to be 1 bar, and the high pressure was taken as the partial pressure of the adsorbed gas in its natural gas mixture (80 bar for CH_4). The CH_4 adsorption capacities of all the activated carbons were measured at atmospheric pressure and 50 ^oC using atmospheric pressure TGA. Figure 6.7 displays the CH_4 uptake of the date pits activated carbons at the high and the low pressure with the resulting CH_4 working capacity.

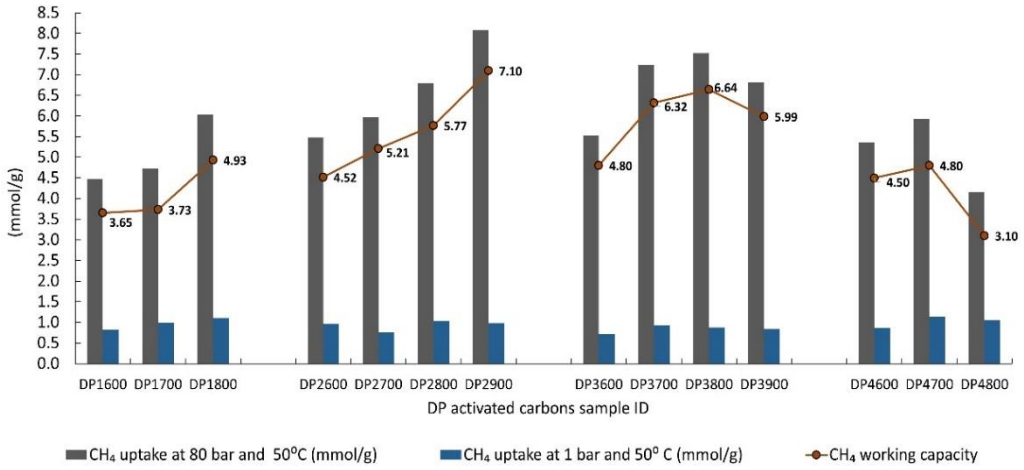


Figure 6.7 CH_4 uptake of date pits activated carbons at 1 bar and 80 bar at 50 ^oC with the resultant CH_4 working capacity.

The CH_4 working capacity in Figure 6.7 followed the trend of the high pressure CH_4 uptake and reached a maximum value of 7.10 mmol/g for sample DP2900. The CH_4 uptake at 1 bar for the date pits activated carbons was around 1 mmol/g for all the samples. The low uptake of CH_4 at 1 bar pressure and subsequently lower influence in the working capacity were also observed for coal tar pitch activated carbons depicted in Figure 6.8. The highest CH_4 working capacity was 7.15 mmol/g and was achieved by sample CTP2900.

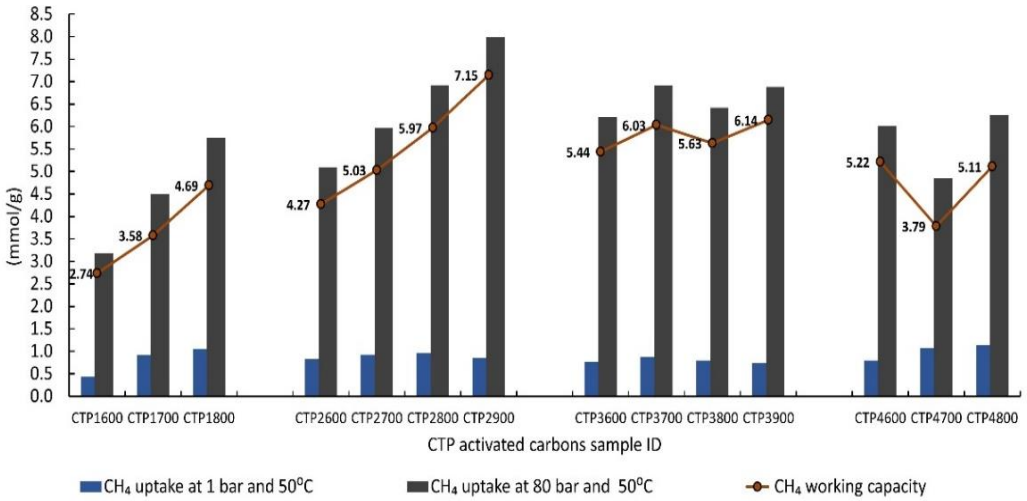


Figure 6.8 CH_4 uptake of coal tar pitch activated carbons at 1 bar and 80 bar at 50 °C with the resultant CH_4 working capacity.

6.4 CO_2/CH_4 Working Adsorption Capacity Ratio

CO_2/CH_4 working adsorption capacity ratio and the CO_2 working adsorption capacity were used as performance metrics to select the optimal candidate among all the activated carbons synthesised in this research work. Working capacity was used, as opposed to high pressure uptake capacity, to take into account adsorption (high pressure) and desorption (low pressure) capacities in line with a pressure swing in a PSA process. The working capacity ratio used here takes into account the partial pressure of CO_2 and CH_4 in the natural gas mixture and used to assess activated carbon adsorption selectivity for CO_2 over CH_4.

For date pits activated carbons, Table 6.2 lists the CO_2 and the CH_4 working capacities and their ratios from which we notice that, with the exception of the two samples activated at the lowest activation intensity (samples DP1600 and DP1700), all other samples showed a CO_2/CH_4 working capacity ratio above 1. Such observation indicates favourable CO_2 adsorption compared to that of CH_4 despite a higher adsorption pressure for CH_4 at 80 bar, four times that of CO_2.

Table 6.2 CO_2 and CH_4 working capacities of date pits activated carbons at 50 ^oC and the corresponding CO_2/CH_4 adsorption ratio.

Sample	CO_2 working capacity*	CH_4 working capacity**	CO_2/CH_4 working capacities ratio
DP1600	2.63	3.65	0.72
DP1700	3.43	3.73	0.92
DP1800	5.62	4.93	1.14
DP2600	4.96	4.52	1.10
DP2700	5.53	5.21	1.06
DP2800	8.11	5.77	1.41
DP2900	9.23	7.10	1.30
DP3600	7.21	4.80	1.50
DP3700	8.44	6.32	1.34
DP3800	8.94	6.64	1.35
DP3900	8.73	5.99	1.46
DP4600	6.11	4.50	1.36
DP4700	5.44	4.80	1.13
DP4800	3.46	3.10	1.12

*Measured at 20 bar (CO_2 partial pressure in South Oman natural gas).
**Measured at 80 bar (CH_4 partial pressure in South Oman natural gas).

Table 6.3 below shows the performance metrics for the coal tar pitch activated carbons where all samples had a CO_2/CH_4 working capacity ratio above 1, with the exception of just one sample (CTP1600).

Table 6.3 CO_2 and CH_4 working capacities of coal tar pitch activated carbons at 50 ^oC and the corresponding CO_2/CH_4 adsorption ratio.

Sample	CO_2 working capacity*	CH_4 working capacity**	CO_2/CH_4 working capacities ratio
CTP1600	3.61	3.18	0.80
CTP1700	5.76	4.50	1.02
CTP1800	7.70	5.75	1.26
CTP2600	6.88	5.09	1.12
CTP2700	9.17	5.96	1.40
CTP2800	10.03	6.92	1.32
CTP2900	10.00	8.00	1.22
CTP3600	10.27	6.21	1.55
CTP3700	10.02	6.91	1.36
CTP3800	10.85	6.42	1.63
CTP3900	9.25	6.88	1.32
CTP4600	10.11	6.01	1.61
CTP4700	7.59	4.85	1.46
CTP4800	9.11	6.25	1.43

*Measured at 20 bar (CO_2 partial pressure in South Oman natural gas).
**Measured at 80 bar (CH_4 partial pressure in South Oman natural gas).

Coal tar pitch beads produced activated carbon adsorbents which favoured the absorption of CO_2 (CO_2/CH_4 working capacity ratio greater than 1) with a relatively low activation temperature of 700 ^oC (sample CTP1700) compared with the date pits char which needed a higher activation temperature (800 ^oC) to produce an activated carbon which favoured the adsorption of CO_2 (sample DP1800). However, 25 out of the 28 samples of both date pits and coal tar pitch activated carbons showed CO_2/CH_4 adsorption ratios of more than 1. This indicates a favourable CO_2 adsorption over that of CH_4 despite the adsorption pressure being 4 times higher (80 bar) for CH_4 compared to that for CO_2 (20 bar). This demonstrates the potential of the activated carbons for CO_2/CH_4 separation. The PSD of the highest CO_2/CH_4 working capacity ratio sample from each activated carbon set (i.e. DP3600 and CTP3800) were compared as seen in Figure 6.9 to provide an insight into the role of the PSD in the separation effect.

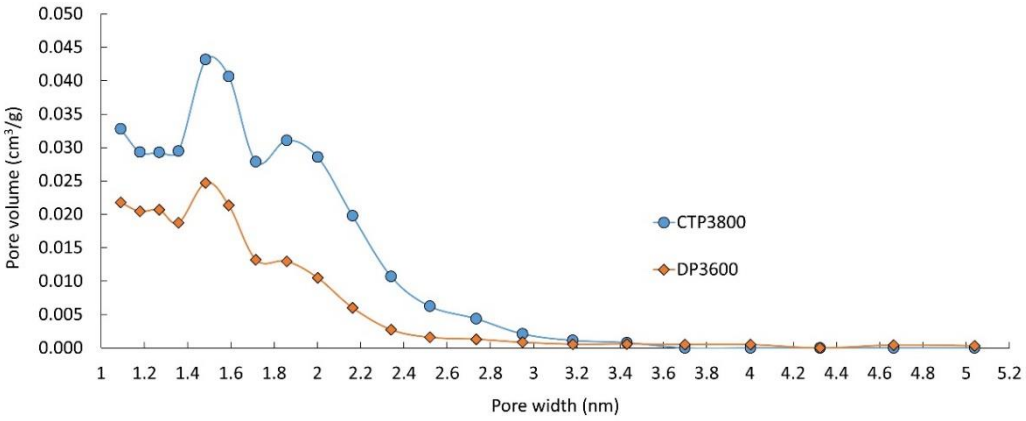


Figure 6.9 PSD of CTP3800 and DP3600 from NLDFT analysis.

Figure 6.9 shows very similar PSD curve shapes for both CTP3800 and DP3600 but shifted in the y-axis due to different pore volumes. Both PSD curves display a peak at a pore width of 1.5 nm, and the majority of the pore volume arose from micropores. This observation indicates that the PSD plays a role in the CO_2/CH_4

separation performance based on the CO_2/CH_4 working capacity ratio for the activated carbons from both date pits and coal tar pitch as studied in this work.

6.5 CH_4 Adsorption Isotherms

Three samples from both activated carbon sets were selected for further investigation by HPVA methane adsorption isotherm measurements on the basis of their high CO_2 working capacity (samples DP2900 and CTP3800) and/or the highest CO_2/CH_4 adsorption ratio (samples DP3600 and CTP3800 again). Two high pressure methane adsorption isotherms were measured for each of the three samples at up to 100 bar pressure at two different temperatures, 25 and 50 ^oC. Figure 6.10 presents the measured isotherms.

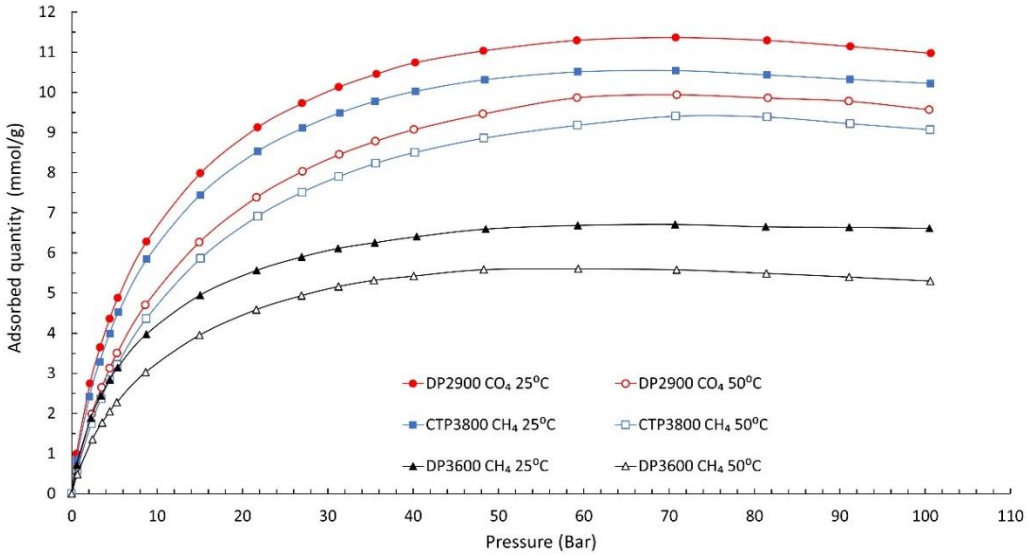


Figure 6.10 CH_4 adsorption isotherms for DP2900, CTP3800 and DP3600 at 25 ^oC and 50 ^oC up to 100 bar as measured by HPVA.

The amount of CH_4 adsorbed onto all the three samples increased with increasing pressure and decreased with increasing temperature. DP2900 showed the highest CH_4 adsorption capacity. DP3600 reached saturation at a relatively low pressure compared to the other two samples due to its relatively low micropore volume of

0.495 cm^3/g in comparison with CTP3800 and DP2900, 0.717 cm^3/g and 0.637 cm^3/g respectively.

6.6 CH_4 Isosteric Heat of Adsorption

The strength and the type of interactions between the selected activated carbons and the CH_4 were studied by calculating the isosteric heat of adsorption of CH_4 ($Q_{st_CH_4}$) using the Clausius−Clapeyron equation (Park *et al.*, 2016). The Clausius−Clapeyron equation was implemented with the aid of MicroActive® software which used the measured CH_4 isotherms for the same three samples to obtain the CH_4 adsorption values required for the calculation. Figure 6.11 shows the calculated $Q_{st_CH_4}$ values.

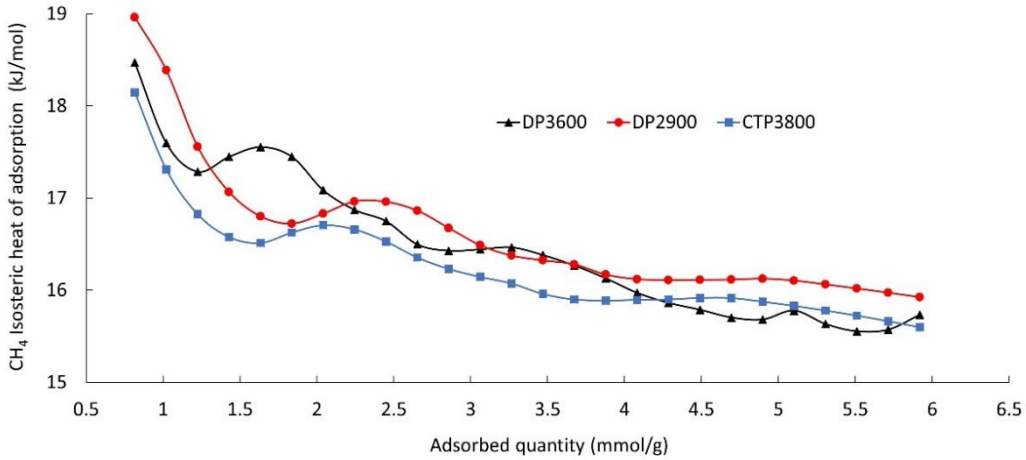


Figure 6.11 Isosteric heat of adsorption of CH_4 when adsorbed on DP3600, DP2900 and DP3800 activated carbons.

Each of the three $Q_{st_CH_4}$ trends for the three selected activated carbon samples shown in Figure 6.11 start at its highest value of 18-19 kJ/mol corresponding to the lowest adsorbed CH_4 quantity, followed by a gradual drop of the $Q_{st_CH_4}$ to around 15.5 to 16 kJ/mol. The range of the $Q_{st_CH_4}$ found in this work (19-15.5 kJ/mol) was within the range of 22-14 kJ/mol as reported by Wang *et al.* (2010) for the adsorption of CH_4 on Maxsorb II activated carbon. It is also very close to

the range reported by Grande *et al.* (2013) of 18-16 kJ/mol for CH_4 adsorption on commercial activated carbons. The same observation in regard to the drop in the value of the $Q_{st_CH_4}$ as the adsorbed CH_4 amount increased was noticed by both Wang and Grande in their separate studies. The variation of the $Q_{st_CH_4}$ with the adsorbed amount could indicate heterogeneities in the activated carbon adsorption sites. It could also be explained by a possible higher interaction strength between the CH_4 and the activated carbon at the beginning of the adsorption process due to the availability of more empty smaller pores with high adsorption potential (Singh and Anil Kumar, 2016).

6.7 Water Vapour Effect on CH_4 Adsorption

The effect of a possible water vapour contamination in the natural gas stream on the CH_4 adsorption of a dry activated carbon was investigated by first exposing CTP3800 and DP3600 activated carbons to 10% relative humidity for 48 hours using the controlled humidity setup presented in chapter 5, section 5.6 to obtain moisture-equilibrated samples. Then, CH_4 adsorption isotherms up to 100 bar on these samples were measured by HPVA and compared with the previously measured dry sample CH_4 isotherms as shown in Figure 6.12. Samples CTP3800 and DP3600 were selected as they showed the highest CO_2/CH_4 working capacity ratio for each of the activated carbon sets.

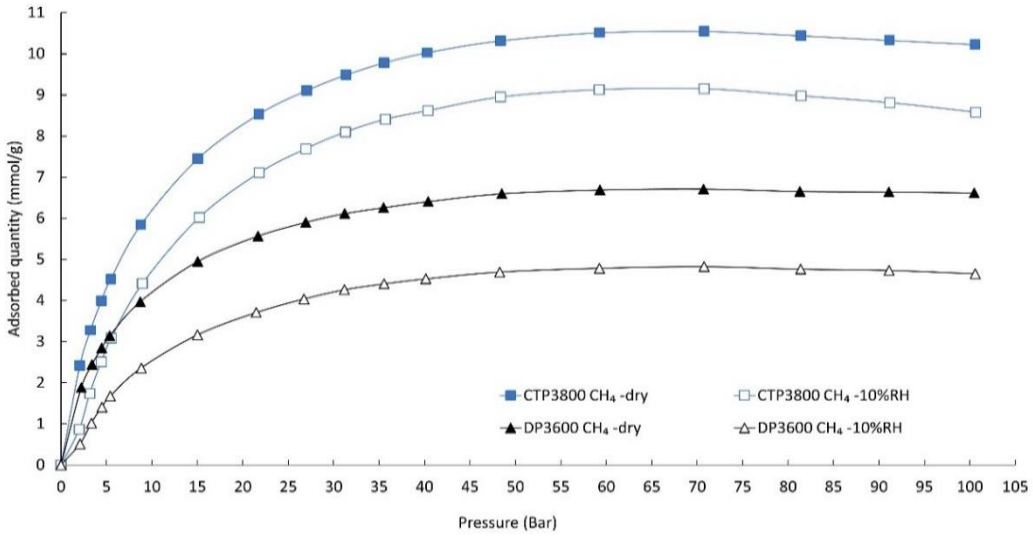


Figure 6.12 CH_4 adsorption isotherm at 25 ^oC for CTP3800 and DP3600 with a dry sample (filled markers) and with 10% moisture equilibrated sample (empty markers).

Both DP3600 and CTP3800 samples showed a drop in the amount of CH_4 adsorbed due to the presence of water in their pores. However, DP3600 showed a slightly higher drop in CH_4 adsorption relative to CTP3800; this could be due to its smaller micropore volume (0.495 cm^3/g) which was partially occupied with the pre-adsorbed water molecules leaving less free pore volume for the CH_4 molecules to adsorb, unlike CTP3800 which has a higher micropore volume (0.717 cm^3/g).

6.8 Pre-adsorbed Water Effect on CO_2 and CH_4 Adsorption

The presence of water inside the pores of the activated carbon samples due to their exposure to 10% relative humidity resulted in a drop in their CO_2 and CH_4 uptake capacities. The relative drop in CO_2 and CH_4 uptake was expressed as the percentage difference between the wet and the dry adsorption quantities relative to the dry case. The relative drop in CO_2 and CH_4 uptake, expressed as a percentage, at a pressure equal to their partial pressure in the natural gas mixture are presented in Table 6.4.

Table 6.4 Relative drop in CO_2 and CH_4 uptake due to pre-adsorbed moisture from a 10% relative humidity environment

The relative drop in uptake	DP3600	CTP3800
CO_2 at 20 Bar	27.88%	13.58%
CH_4 at 80 Bar	28.38%	31.55%

Both DP3600 and CTP3800 showed a higher drop in CH_4 uptake compared to the drop in CO_2 uptake. This will result in a positive increase for the CO_2/CH_4 uptake ratio used as an indicator for the CO_2 adsorption selectivity. Therefore, experiments were undertaken to investigate how to further enhance the CO_2/CH_4 uptake ratio of the selected activated carbons by simply introducing various amounts of water into their pore spaces before the adsorption measurement by HPVA.

Various amounts of water were introduced into the pores of each type of two activated carbon and the subsequent procedure was followed. About 0.5 gram of the activated carbon sample under investigation was put in a glass vial and dried for 24 hours at 120 ^{o}C, the dry sample weight was recorded. The dry activated carbon sample was then completely submerged in 3 mL of ultra-pure deionised water and left inside a vacuum environment for 2 hours to allow the water to penetrate to the micropores. The slurry mixture of activated carbon and water was then moved to a drying oven at 120 ^{o}C. Drying time was varied to allow partial water evaporation to achieve water to activated carbon mass ratio percentages of 5%, 50% and 70% relative to the dry activated carbon mass. The drying process involved allowing the sample to initially dry for 30 min to remove excess water then checking its weight every 1 minute until the desired water mass was reached by weighing the wet sample with a laboratory balance with an accuracy of 0.1 mg. The water loaded samples looked dry at the surface, and an ice bath was used to

cool the sample to preserve the adsorbed moisture upon its removal from the oven before conducting the HPVA tests. The HPVA tests on the wet samples were used to measure the CO_2 and the CH_4 uptake of the wet activated carbons in a similar manner to the dry sample uptake measurement.

Figure 6.13A shows the CO_2 uptake by the dry CTP3800 activated carbon sample together with its 5%, 50% and 70% water loaded samples. Figure 6.13B shows the same for DP3600 but without the 70% water loaded sample since the small pore volume of DP3600 was not able to accommodate 70% water without leaving excess water on the surface of the sample.

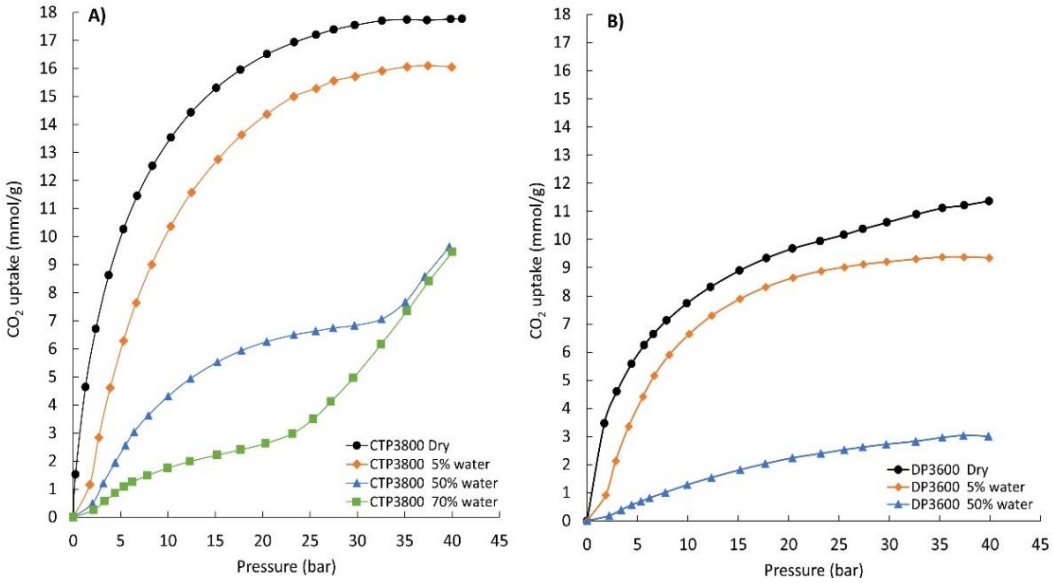


Figure 6.13 CO_2 uptake of water loaded activated carbons at 25 ^oC, (A) CTP3800 and (B) DP3600.

For the lowest amount of pre-adsorbed water (5%), the CO_2 adsorption isotherms for both CTP3800 and DP3600 showed a lower maximum uptake compared to their dry isotherm but still resembled the shape of the dry sample isotherm. This similarity could be due to the availability of sufficient empty micropores to produce the same initial steep rise in the CO_2 adsorption isotherms despite the partial occupation of some of the micropores by the pre-adsorbed water. A sharp

drop in CO_2 uptake was observed for the two samples with a higher amount of pre-adsorbed water, i.e. 50% and 70%. However, only CTP3800 showed an upward inflection after what appeared to be a plateau in CO_2 uptake. The inflection point moved from 32 bar to a lower pressure (20 bar) as the water content increased from 50% to 70%. The upward inflection point suggests the development of CO_2 hydrate also known as clathrate as reported by several previous research groups studying the effect of water on the adsorption of CO_2 on activated carbons (Wang *et al.*, 2008; Billemont, Coasne and De Weireld, 2013). CO_2 hydrates are solid inclusion compounds comprising an open lattice of water molecules that confine the guest CO_2 gas molecules without chemical bonding (Hassanpouryouzband *et al.*, 2018). Jalilov *et al.* (2017) reported similar CO_2 adsorption inflection phenomena with wet activated carbon samples and demonstrated, with the use of in-situ vibrational spectroscopy, that the formation of CO_2 hydrates in activated carbons was possible at 25 ^{o}C and at a pressure as low as 15 bar. This supports the earlier claim of Sun *et al.* (2007) who used the comparable enthalpies of CO_2 hydrate in pure water and that in wet activated carbon to conclude that the formation of hydrate is enhanced in the micropores of the activated carbon. However, the final capacities of the CO_2 uptake in the wet samples (Figure 6.13A) are less than those of the dry samples at the same pressure. This might be attributed to the unavailability of additional empty pore volumes for the hydrate to further grow; or due to the lack of higher pressure that might be required to promote the formation of hydrate in the bigger pore sizes. Due to the pressure limitations with the HPVA when using CO_2, the adsorption pressure could not be increased to more than 40 bar to investigate if higher pressure could increase the CO_2 uptake to reach

equilibrium since none of the two wet samples reached equilibrium, unlike the dry sample.

DP3600 did not show an upward inflection with 50% pre-adsorbed water as shown in Figure 6.13B. Furthermore, the observed isotherm did not show an initial steep rise in CO_2 adsorption at low pressure, which is typically attributed to the presence of micropores, indicating that all the micropores had been totally filled with water. Indeed, converting the mass of water to volume using the density of pure water and comparing this with the available total pore volume revealed that 97% of the total pore volume was filled with water. It is fair to say that the presence of enough water in the pores of the activated carbon alone was not sufficient for the formation of CO_2 hydrate at 25 ^oC. Free pore space, for the hydrate to form, is also important. The the same water to activated carbon percentage (50%) that produced the inflection point in CTP3800 did not produce any inflection point for DP3600 sample that has lower micropores volume.

CH_4 uptake of the wet activated carbons at pressures up to 100 bar was also investigated using the same two samples (DP3600 and CTP3800). The same amount of water used for the wet CO_2 adsorption was also used for the wet CH_4 adsorption. The results are shown in Figure 6.14.

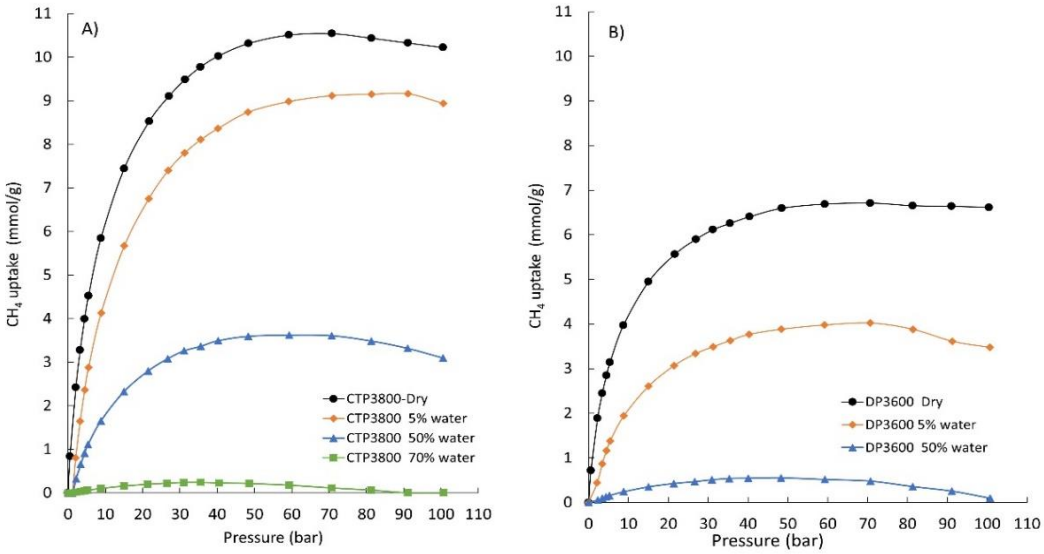


Figure 6.14 CH_4 uptake of water loaded activated carbons at 25 ^oC, (A) CTP3800 and (B) DP3600.

The CH_4 uptake of both samples, CTP3800 and DP3600, decreased with increasing amounts of water due to the occupation of the micropores with the water, leaving a smaller micropore volume in which CH_4 could adsorb onto. The use of 70% pre-adsorbed water on CTP3800 reduced the CH_4 uptake to near zero. There was no uptake inflection point observed in any of the measured wet isotherms, in contrast to the isotherms for CO_2 uptake by the same samples.

The potential benefit of the pre-adsorbed water for enhancing CO_2/CH_4 uptake ratio at high pressure could be demonstrated by examining the percentage drop of CH_4 and CO_2 adsorption in wet activated carbons relative to their dry counterparts across the measured pressure range. Sample CTP3800 was used to demonstrate such a drop due to the prominent CO_2 hydrate effect that was not seen in DP3600. The percentage drop in both CO_2 and CH_4 adsorption as a result of varying pre-adsorbed water is depicted in Figure 6.15. The same figure reveals that while the pre-adsorbed water reduced the adsorption of both gases with almost the same magnitude at low pressure (below 10 bar), the drop in CH_4 adsorption was more pronounced than that of CO_2 at high pressure. However, whilst acknowledging the

positive effect of the pre-adsorbed water in suppressing CH_4 adsorption more than CO_2, and hence enhancing the CO_2/CH_4 selectivity, the negative effect of pre-adsorbed water in reducing the CO_2 uptake capacity should not be ignored, and the trade-off between CO_2 capacity and CO_2 selectivity should be acknowledged.

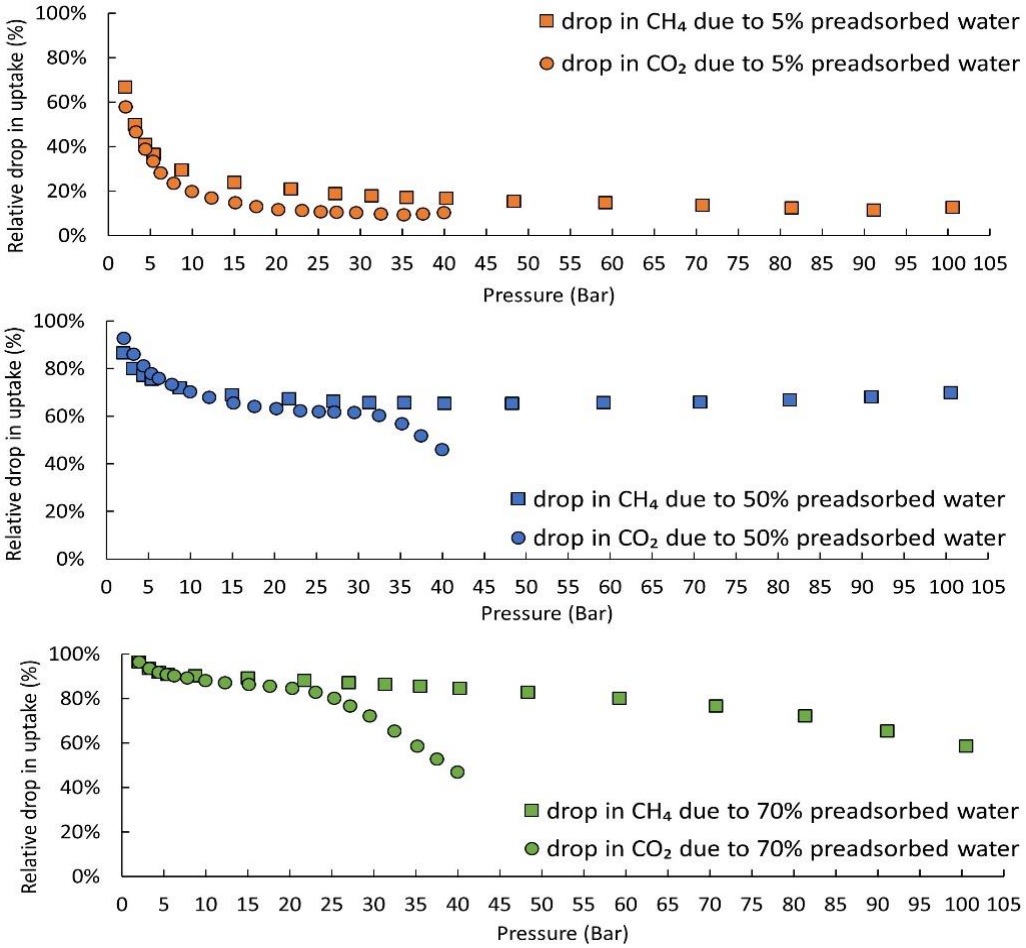


Figure 6.15 Percentage drop in CO_2 and CH_4 uptake for wet CTP3800 with 5%, 50% and 70% pre-adsorbed water across adsorption pressure up to 100 bar.

In addition to the role of CO_2 hydrate, other factors could have contributed to the difference in the adsorption between the two gases so that CO_2 achieved higher adsorption capacity on wet activated carbons. First, CO_2 is soluble in water unlike CH_4 resulting in a possible partial CO_2 uptake due to dissolved CO_2 in the water (Wang *et al.*, 2008). In addition, water-CO_2 interactions are stronger than water-CH_4 interactions so that any drop in CO_2 adsorption due to the blockage of

micropores by the pre-absorbed water might have been partially compensated for by the stronger water-CO_2 interactions, in contrast with the case for CH_4 (Billemont, Coasne and De Weireld, 2013). Furthermore, at 25 ^oC the CO_2 is subcritical, hence condensable, whereas the CH_4 is supercritical and therefore not condensable.

6.9 Conclusion

In conclusion, CH_4 adsorptions by the coal tar pitch and the date pits activated carbons were measured at high pressure (80 bar) and low pressure (1 bar) using HP-TGA. The measured capacities were used to calculate the working CH_4 capacities followed by the CO_2/CH_4 working capacity ratio. The same measured CH_4 uptakes were also used to understand the relationship between CH_4 uptake and the textural properties of the activated carbons. The highest CO_2/CH_4 working capacity ratio achieved was 1.63 by sample CTP3800 and CH_4 uptake was found to have a positive correlation with the micropore volume and the surface area of the activated carbons. However, such correlation was weaker than that for the CO_2 as found in the previous chapter owing to a smaller R^2 value for the CO_2 line correlation fit.

Methane adsorption isotherms for three selected samples were measured with HPVA up to 100 bar at 25 and 50 ^oC and used to estimate the isosteric heat of adsorption of CH_4 that was found to be less than that of CO_2 indicating weaker CH_4-carbon interactions compared to that of CO_2-carbon.

The effects of 10% water vapour and up to 70% pre-adsorbed water loading on activated carbons were investigated using wet activated carbons isotherm measurements. Generally, water was found to reduce the amount of adsorbed CO_2

and CH_4. However, the reduction of the CH_4 adsorption was more pronounced than that of the CO_2 at high pressure indicating a potential benefit of the wet activated carbon to enhance the selectivity of activated carbons towards CO_2 at high pressure but at the expense of the uptake capacity of the CO_2.

Chapter 7. Modelling Adsorption Isotherms for Pure CO_2 and CH_4, and Calculating their Binary Mixture Adsorption

7.1 Introduction

The ability of solid adsorbents to remove CO_2 from natural gas is best tested in a set up that resembles, as closely as possible, the industrial process they will eventually be used in, e.g. in a PSA process. Such a test may not always be possible due to the required time and/or expenses to set up a laboratory or industrial scale PSA testing system. Mixed gas adsorption modelling provides a versatile tool to assess the CO_2 adsorption from a gas mixture by activated carbons in the absence of a physical testing system. In this chapter, three samples, namely DP3600, DP2900 and CTP3800, underwent further investigations by adsorption modelling using simulated natural gas mixture. These samples were selected due to their high CO_2 working capacity (DP2900 and CTP3800) or high CO_2/CH_4 working capacity ratio (DP3600 and CTP3800) in comparison with the rest of the synthesised adsorbents in this work as shown in chapter 5 and chapter 6. This chapter begins by explaining the required data processing to convert the measured CO_2 and CH_4 excess adsorption quantities to absolute adsorption quantities prior to any modelling work. Next, single gas (CO_2 or CH_4) absolute adsorption isotherms are

fitted to three different adsorption models. A further section in this chapter is dedicated to investigating the use of extended single gas adsorption isotherm models to predict mixed gas adsorption quantities and the adsorbed quantity of each gas component when present in a binary mixture of CO_2 and CH_4.

7.2 Converting Excess Adsorption to Absolute Adsorption

Gas is said to be adsorbed when forces from a solid surface act on the gas molecules and result in an increased gas density relative to the normal (bulk) gas density at the same temperature and pressure (Yang, 2003). Consider the two-dimensional representation of gas molecules and a solid surface, Figure 7.1(a), that could also be extended to represent gas molecules within a pore space, Figure 7.1(b), as proposed by Mason, Veenstra and Long (2014). The dotted red line is an imaginary line known as the Gibbs dividing surface used to split the total gas volume into adsorbed and bulk volumes. Excess adsorption is defined as the additional gas molecules adsorbed in the pore volume compared with the molecules that would have been present in the same volume in the absence of pore walls, represented by the gas molecules (green circles) under the influence of the adsorption forces in Figure 7.1. Absolute adsorption equals the excess adsorption in addition to the bulk gas molecules (blue circles) that would have been present in the adsorbed region in the absence of a solid surface in Figure 7.1.

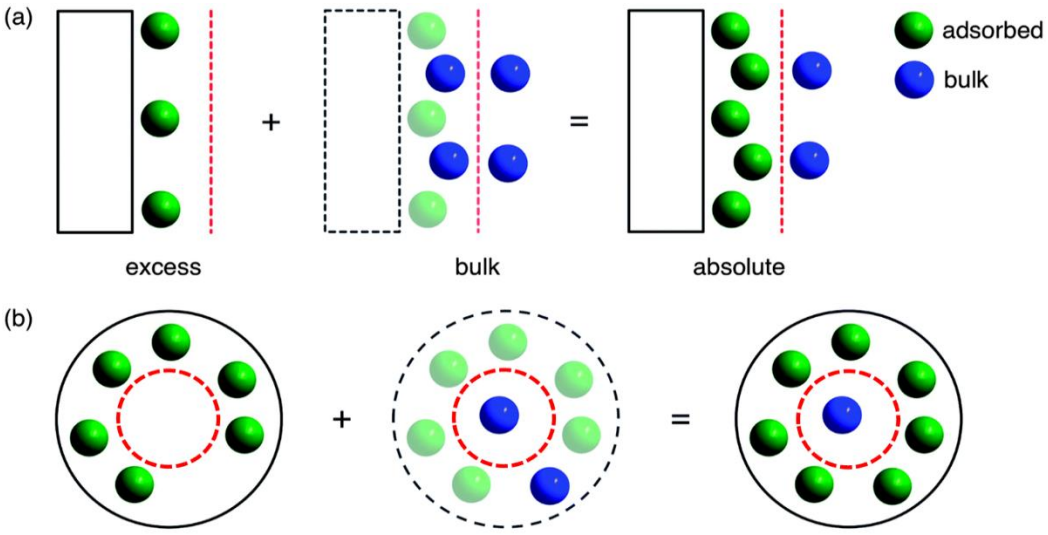


Figure 7.1 Illustrative representation of excess and absolute gas uptake on a two-dimensional surface (Mason, Veenstra and Long, 2014).

So far, all the adsorption quantities reported in this work have been an excess adsorption type since excess adsorption is the direct experimentally measured quantity reported by both gravimetric and volumetric adsorption measurement techniques (Brandani, Mangano and Sarkisov, 2016). However, excess adsorption cannot be used in the theoretical thermodynamics calculations widely used for process simulation and adsorption prediction especially for high pressure applications (Myers and Monson, 2014). Experimental gas adsorption at high pressure showed that the measured excess adsorption amount could reach a peak then starts to decrease as the adsorption pressure increases due to the increase in bulk gas density at a rate higher than the increase in adsorbed quantities. Such a peak is normally observed as the adsorbent approaches its uptake saturation point. It implies that further interpolation of such a trend to higher pressures by data modelling techniques could eventually result in negative excess adsorption, but negative adsorption has no meaning. This issue was reported in two separate research works by Myers & Monson (2002) and (2014) which led them to argue that molecular theory and simulations of adsorption should all be based on the

absolute adsorption quantities rather than the excess adsorption quantities. The absolute adsorption quantity can be estimated from the measured excess adsorption amount using the pore volume of the adsorbent and the adsorptive gas density at the measurement pressure and temperature. This estimation technique represented mathematically in equation 7.1, was used in this research to convert the measured excess adsorption of CO_2 or CH_4 to absolute adsorption values. The same technique was used by Jalilov *et al.* (2017) and Jribi *et al.* (2017).

$$q_{abs} = q_{exc} + \rho_g v_p \qquad \text{Equation 7.1}$$

A comparison between a calculated absolute adsorption isotherm and the corresponding measured excess adsorption isotherm for CH_4 in this work is shown in Figure 7.2. Tables detailing absolute and excess adsorbed quantities of CO_2 and CH_4 for the three selected activated carbons can be found in Appendix A for CO_2 and Appendix B for CH_4. From Figure 7.2 one can see that as the adsorption pressure was increased the difference between excess and absolute adsorption also increased. This difference was due to the increase in the bulk gas density with increasing pressure, hence bigger values for the term $(\rho_g v_p)$ in equation 7.1, while the additional excess adsorbed amount q_{exc} was very low as the adsorbent was nearly saturated at high pressure. The bulk gas densities used to implement Equation 7.1 in this chapter were calculated using the Peng-Robinson equation of state by using a NIST reference fluid properties software called REFPROP, version 8.

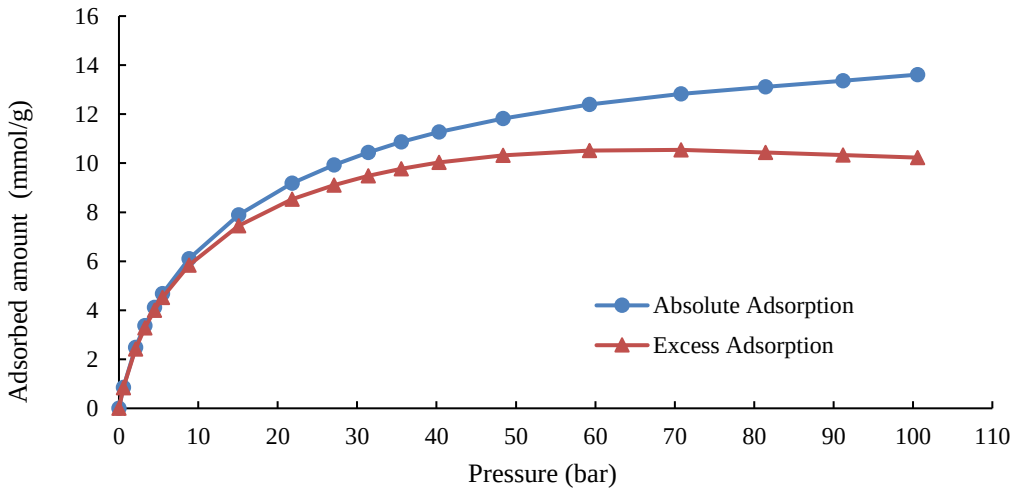


Figure 7.2 Comparison between excess (triangles) and absolute (circles) adsorption quantities of CH_4 onto CTP3800 activated carbon at 25 ^oC.

The above-described excess to absolute conversion approach was followed to convert all the measured CO_2 and CH_4 excess adsorption isotherms to absolute adsorption isotherms before proceeding to find the best model to fit the absolute adsorption quantities.

7.3 Modelling CO_2 and CH_4 Adsorption Isotherms

Isotherm models allow the prediction of adsorbed gas quantities (q_i) on a specific adsorbent at a specific pressure. It also provides the basis for predicting the binary component adsorption and selectivity calculations.

7.3.1 Fitting Adsorption Isotherm Models

All calculated CH_4 and CO_2 absolute adsorbed quantities on the three selected activated carbon samples, namely DP3600, DP2900 and CTP3800, at 25 and 50 ^oC were fitted to three different isotherm models, Langmuir, Sips and Dual Site Langmuir (DSL). For each of these models, there exists a corresponding multi-component gas model to enable modelling of binary components gas (CO_2 and CH_4) adsorption isotherms. All the isotherms were fitted to the three models named above using the Excel Solve tool. The Solve tool finds the optimum

parameters for each model by minimising an error between the experimentally derived absolute adsorption quantities (q_{exp}) and the model-predicted quantities (q_{model}). The smaller the error value, the better the model fitting. The Generalised Reduced Gradient (GRG) nonlinear option within the Excel Solve function was selected to search for the parameter of the best model fit. The Sum of Squared relative Error, SSE (%), between the measured and predicted values of each isotherm, as given by Equation 7.2 (Garcia *et al.*, 2013) , was the error function that was minimised during the search for the best model to fit the absolute adsorption isotherms.

$$SSE\ (\%) = \sqrt{\frac{\sum_1^N [\frac{q_{exp} - q_{model}}{q_{exp}}]^2}{N-1}} \ .100 \qquad \text{Equation 7.2}$$

Where N is the number of points in the isotherm.

7.3.2 Comparison of Adsorption Isotherms Models

Three adsorption isotherm models were considered in this research to fit the measured CO_2 and CH_4 adsorption isotherms. The first model was the Langmuir model (Langmuir, 1918) given by Equation 7.3. The Langmuir model is a simple two-parameter model that relates the adsorbed quantity of component i (q_i) at a pressure (P) to the adsorption saturation capacity (q_s) and an affinity constant (b).

$$q_i = \frac{q_s bP}{1+bP} \qquad \text{Equation 7.3}$$

The Langmuir model was described by Ruthven (1984) as a theoretically rigorous and thermodynamically constant model based on the assumption that all

adsorption sites are the same, i.e. it does not account for any heterogeneity in the adsorption process.

The second model used to fit the isotherms was the Sips model, given by Equation 7.4. It is a three-parameter empirical equation that was successfully used to fit hydrocarbon adsorption data on activated carbons (Ahmadpour, Wang and Do, 1998).

$$q_i = \frac{q_s (bP)^{\frac{1}{n}}}{1+(bP)^{\frac{1}{n}}} \qquad \text{Equation 7.4}$$

The third model used in this research was the Dual Site Langumir (DSL) model as represented by Equation 7.5.

$$q_i = \frac{q_{s1} b_1 P}{1+b_1 P} + \frac{q_{s2} b_1 P}{1+b_2 P} \qquad \text{Equation 7.5}$$

The DSL equation is a modification of the Langmuir equation to address the shortfalls of the Langmuir assumption that all the adsorption sites are of the same energy when the adsorption process is a heterogeneous one. The DSL model adds a second term to the well known Langmuir model equation and assumes that two energetically different adsorption sites exist, site one as a high energetic site and site two as a low energetic site (Talu, 1998; Ritter, Bhadra and Ebner, 2011).

Figure 7.3 presents all the measured CO_2 isotherms fitted with the Langmuir, Sips and DSL models. Visual inspection of the model fit lines in Figure 7.3 revealed that Sips and DSL models provided a better fit to the absolute CO_2 adsorption measurement compared to the Langmuir model that overpredicted the adsorbed CO_2 quantities at low pressure and underpredicted the adsorbed quantities at high

pressure at both temperatures (25 and 50 ºC). Caldwell *et al.* (2015) reported a similar observation when trying to fit CO_2 adsorption isotherms on activated carbons. The underprediction of CO_2 adsorption by Langmuir model at high pressure was also reported in two separate studies by Garcia *et al.* (2013) and Schell *et al.* (2012). Such poor performance could be related to the assumption of the homogenous adsorption made by Langmuir whereas the adsorption of CO_2 on the activated carbons showed some heterogeneity owing to the varying values of isosteric heat of adsorption as reported in chapter 5, section 5.5 of this work. In contrast, both the Sips and DSL models accommodate heterogeneous adsorption by including a heterogeneity term in their model equation, hence the good model fit.

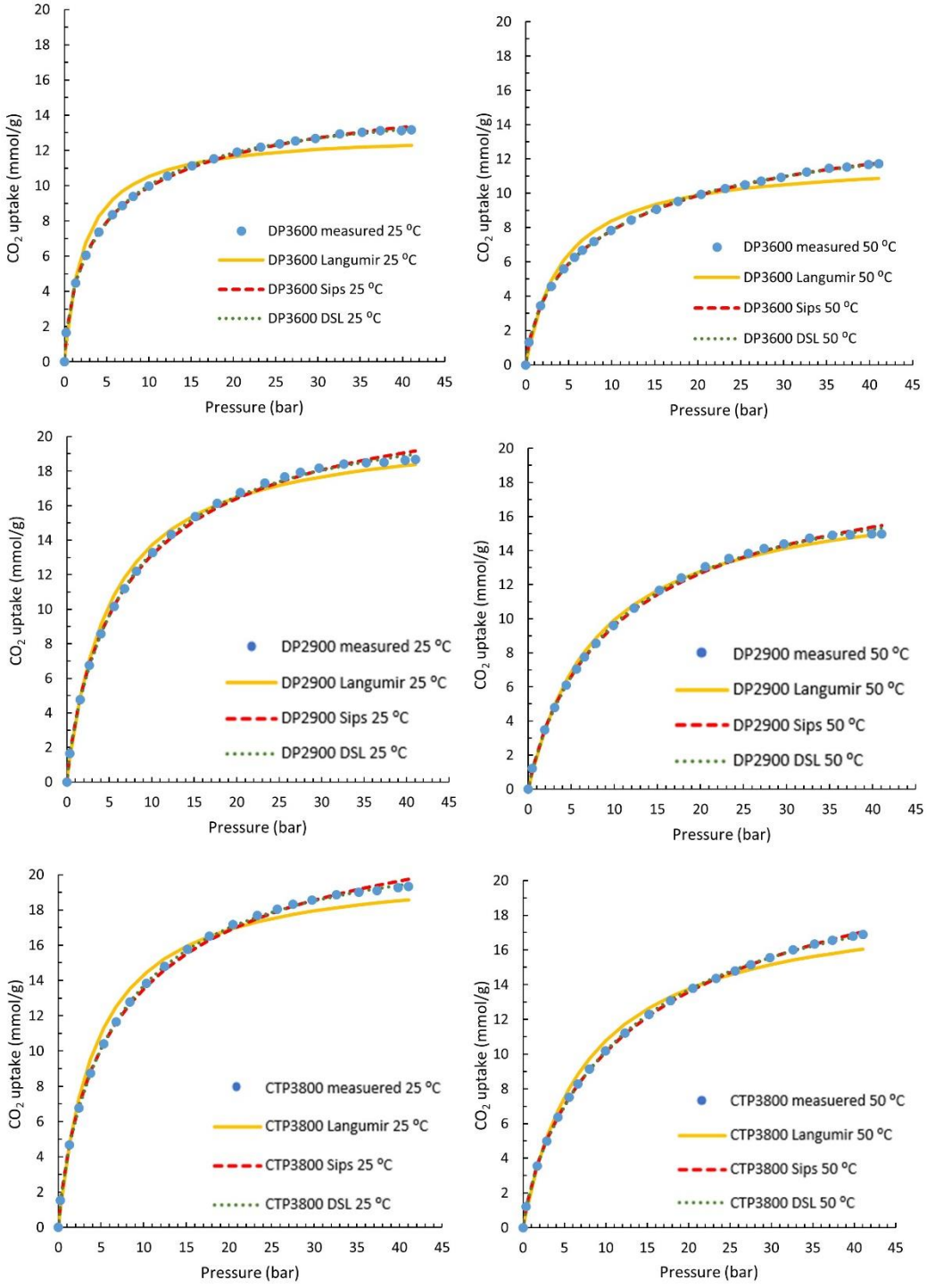


Figure 7.3 Isotherm model fitting of experimental CO_2 uptake on DP3600, DP2900 and CTP3800 at 25 and 50 °C.

The CO_2 Langmuir model parameters of all the samples are presented in Table 7.1 where the exothermic nature of the adsorption process was reflected in the decreasing value of the affinity parameter (b) as the temperature increased from

25 to 50 ºC for the same sample. The saturation capacity (q_s) also dropped as the temperature increased for the same sample in line with the exothermic nature of the adsorption process. For the Sips model parameters, listed in Table 7.2, both q_s and b were found to follow the same observation made for Langmuir with regards to the exothermic nature of the adsorption process. Furthermore, the heterogeneity parameter (n) was always above 1 for all samples indicating a degree of heterogeneity in the adsorption process. The DSL model parameters in Table 7.3 assumes site one as the high energetic site, so the saturation capacity parameter of site one (q_{s1}) for all fits was higher than the saturation capacity of site two (q_{s2}).

Table 7.1 Langmuir model parameters for CO_2 adsorption isotherms.

Sample	Temp (ºC)	q_s	b	SSE (%)
DP3600	25	13.0027	0.4254	10.14
	50	12.0021	0.2334	9.33
DP2900	25	20.6516	0.1972	5.62
	50	17.8888	0.1253	4.41
CTP3800	25	20.5464	0.2300	8.05
	50	19.0305	0.1305	7.40

Table 7.2 Sips model parameters for CO_2 adsorption isotherms.

Sample	Temp (ºC)	q_s	b	n	SSE (%)
DP3600	25	17.1434	0.1617	1.4986	0.68
	50	16.7830	0.0832	1.4399	0.27
DP2900	25	24.0671	0.1247	1.1970	1.45
	50	20.6290	0.0853	1.1432	1.54
CTP3800	25	25.6250	0.1157	1.2887	1.36
	50	25.5154	0.0590	1.2675	0.62

Table 7.3 DSL model parameters for CO_2 adsorption isotherms.

Sample	Temp (°C)	q_{s1}	b_1	q_{s2}	b_2	SSE (%)
DP3600	25	11.6520	0.1413	3.3064	3.0693	0.38
	50	11.5541	0.0826	2.8071	1.5854	0.58
DP2900	25	20.7791	0.1350	1.3899	5.4500	0.81
	50	18.4379	0.0994	0.5147	3.1593	0.90
CTP3800	25	20.6572	0.1312	2.0675	3.1652	0.39
	50	20.0725	0.0736	1.8022	1.5914	0.41

To enable a more objective comparison of the goodness of each model fitting across all samples, the average of all the SSE % values for each model on all three samples was calculated and presented per model per temperature in Figure 7.4.

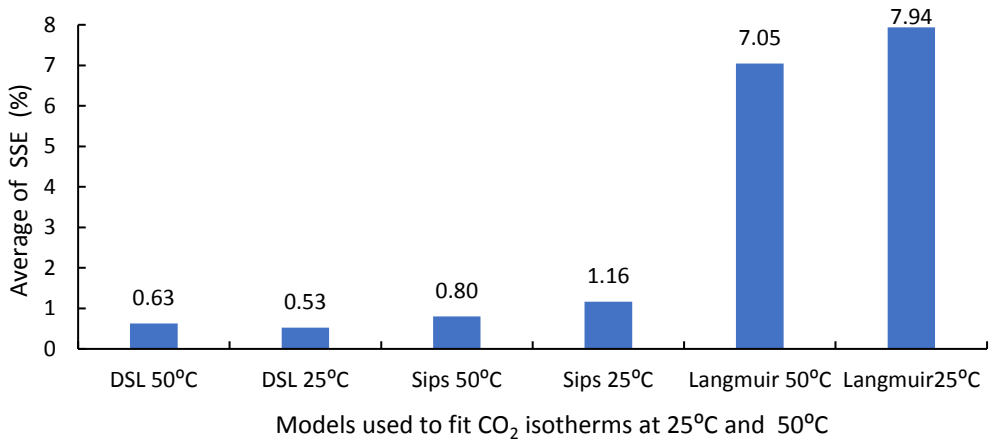


Figure 7.4 Average of SSE percentages per model per temperature for CO_2 adsorption isotherms fitting to Langmuir, Sips and DSL models.

The average of SSE percentage values from the six fittings per model on the three selected samples at both 25 and 50 °C indicated that the DSL model produced a better fit to the CO_2 adsorption data compared to the Sips model whilst the Langmuir model produced the poorest fit at both temperatures. Both DSL and Sips models fitted the experimental data well with an average error not exceeding 1.16%. From an analytical curve-fitting point of view, it could be suggested that increasing the number of model parameters from two in the case of Langmuir to

four in the case of Sips leads to a better model fitting to experimental absolute adsorption quantities. Furthermore, the good fit of both Sips and DSL could also be explained based on the assumptions made for each of the adsorption models where both these models include terms to accommodate the assumption of a heterogeneous adsorption system, unlike the Langmuir model which assumes a homogenous adsorption system. Based on these observations, it could be argued that the adsorption of CO_2 on activated carbons at high pressure as tested in this study was a heterogeneous adsorption process.

The excess CH_4 adsorption isotherm measurements for the same three samples, DP3600, DP2900 and DP3800 were presented and discussed in chapter 6. They were converted to absolute adsorption quantities before the same three adsorption models were used to fit the CH_4 data. One main difference between the CO_2 and CH_4 adsorption isotherm measurements was the maximum pressure. While the CH_4 adsorption was measured up to 100 bar, the CO_2 adsorption isotherms were only measured up to 40 bar due to experimental setup limitations with the CO_2 gas pressure of the HPVA. Figure 7.5 illustrates all CH_4 adsorption model fittings together with the experimentally measured adsorption quantities. Visual inspection of the curve fits in Figure 7.5 revealed similar observations to that of CO_2 regarding the goodness of fit of the models. The Langmuir model showed poor performance, but both the Sips and DSL models showed a good fit to the experimental CH_4 adsorption measurements. Similar to the CO_2 case, the overprediction of adsorbed quantities at low pressure and the underprediction at high pressure were the reasons for the poor performance by the Langmuir model.

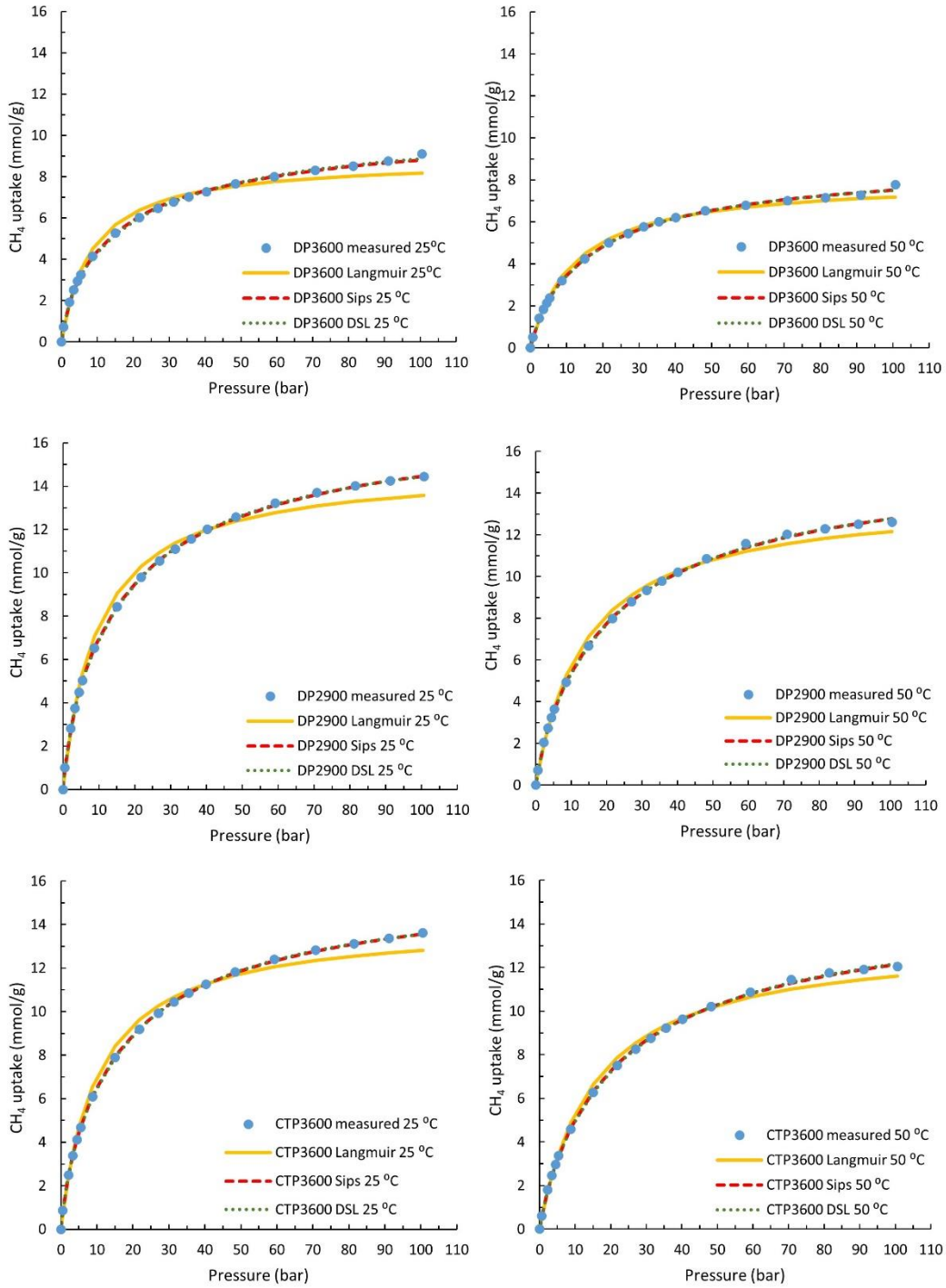


Figure 7.5 Isotherm model fitting of experimental CH_4 uptake on DP3600, DP2900 and CTP3800 at 25 and 50 °C.

The parameters for the models, as shown in Table 7.4, Table 7.5 and Table 7.6, all conformed to their meaning as follows. For the Langmuir and Sips models, the saturation capacity parameter (q_s) of all three activated carbon samples dropped as the temperature increased from 25 to 50 °C. The same was true for the affinity

parameter (b). These observations were in line with the fact that adsorption is an exothermic process and, as a result, the amount of CH_4 adsorbed on the activated carbon was expected to have an inversely proportional relationship with the temperature. For the Sips model, the heterogeneity parameter (n) was above one, indicating a heterogeneous adsorption process for CH_4 on DP3600, DP2900 and CTP3800 activated carbons.

Table 7.4 Langmuir model parameters for CH_4 adsorption isotherms.

Sample	Temp (°C)	q_s	b	SSE (%)
DP3600	25	8.8558	0.1194	7.53
	50	8.0328	0.0847	4.90
DP2900	25	14.8687	0.1037	6.71
	50	13.8725	0.0707	5.09
CTP3800	25	14.1204	0.0984	5.95
	50	13.3767	0.0656	4.61

Table 7.5 Sips model parameters for CH_4 adsorption isotherms.

Sample	Temp (°C)	q_s	b	n	SSE (%)
DP3600	25	10.8877	0.0622	1.2688	1.25
	50	9.1608	0.0573	1.1468	1.18
DP2900	25	17.7930	0.0596	1.2165	0.56
	50	16.1273	0.0461	1.1438	0.90
CTP3800	25	16.4672	0.0614	1.1795	0.57
	50	15.3499	0.0446	1.1237	0.84

Table 7.6 DSL model parameters for CH_4 adsorption isotherms.

Sample	Temp(°C)	q_s1	b1	q_s2	b2	SSE (%)
DP3600	25	7.8972	0.0387	2.6482	0.4512	0.90
	50	7.7225	0.0501	1.0886	0.4492	1.11
DP2900	25	14.0414	0.0477	2.8877	0.5175	0.35
	50	13.6860	0.0400	1.8758	0.3708	0.60
CTP3800	25	13.2675	0.0488	2.6028	0.4603	0.29
	50	13.1113	0.0373	1.8969	0.3038	0.46

To gain a holistic view into the goodness of each of the three adsorption model fittings, the average values of the SSE percentages were calculated and presented in Figure 7.6 per model per temperature. From the same figure, it could be seen that for both temperatures (25 and 50 ^{o}C) Sips and DSL models provided a good fit with less than 1% average error between the predicted and the measured CH_4 adsorption values. On the contrary, the Langmuir model prediction for the CH_4 adsorption was not as good and differed from the measured adsorption quantities by 4.87% at 50 ^{o}C and 6.73% at 25^{o}C on average. The poor performance of the Langmuir model in fitting the measured CH_4 adsorption quantities could be attributed to the assumption on which the model is based. This assumption does not account for any heterogeneity in the adsorption of CH_4, which was shown to be a heterogeneous one due to varying isosteric heat of adsorption as demonstrated in chapter 6, section 6.6 earlier in this thesis. Furthermore, Langmuir model has only two parameters to be adjusted to fit the measured adsorption quantities, which might limit its flexibility in fitting the experimental data compared to Sips (three parameters) and DSL (four parameters) models.

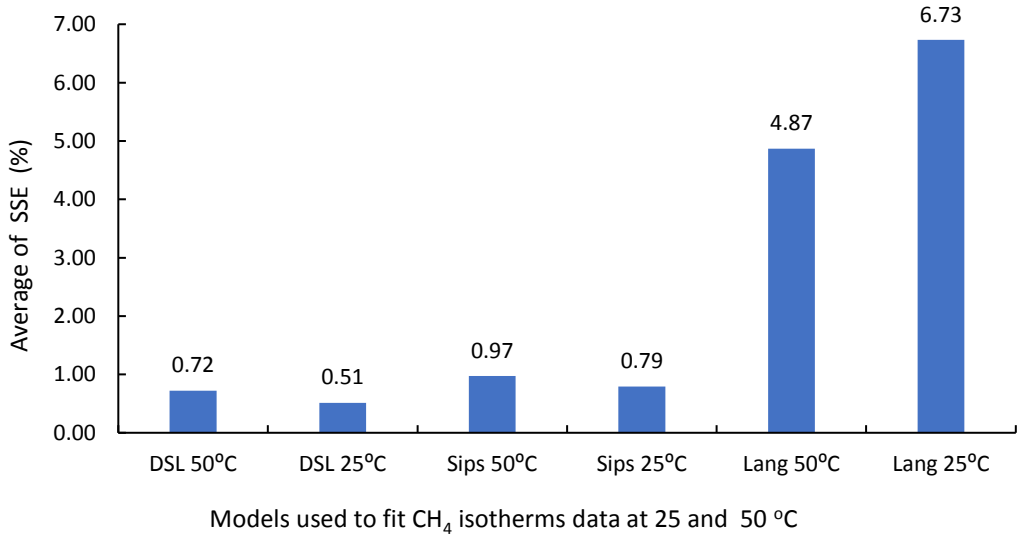


Figure 7.6 Average of SSE percentages per model per temperature for CH_4 adsorption isotherms fitting to Langmuir, Sips and DSL models.

7.4 Prediction of Binary Gas Mixture Adsorption

Accurate adsorption models describing the adsorption of a single component gas can be used to predict multicomponent gas adsorption by extending the single gas adsorption model to a multicomponent gas adsorption model (Yi *et al.*, 2013; Vieira *et al.*, 2018). In section 7.3, the superior accuracy of the DSL model over the Sips and Langmuir models in fitting the single component gas CO_2 and CH_4 experimental data was demonstrated. The DSL model can be extended to allow the prediction a binary gas mix adsorption onto activated carbons (Myers, 1983). The approach for extending DSL to predict binary gas mixture adsorption on each of the three selected activated carbons and the associated modelling results of this prediction are presented in the next sub-sections.

7.4.1 Modelling Approach

The extended DSL model was used to predict the binary (CO_2 and CH_4) mixed gas adsorption on DP3600, DP2900 and CTP3800 samples using the single gas DSL model parameters for CO_2 and CH_4, as presented in

Table 7.3 and Table 7.6. The extended DSL model to predict the adsorption of two components, i and j, from their gas mixture on a solid was first introduced by Myers (1983) and is written as

$$q_i = \frac{q_{s1,i} b_{1,i} P y_i}{1 + b_{1,i} P y_i + b_{1,j} P y_j} + \frac{q_{s2,i} b_{2,i} P y_i}{1 + b_{2i} P y_i + b_{2j} P y_j} \qquad \text{Equation 7.6}$$

As mentioned in the literature review, in chapter 2 in section 2.3.2.1, the DSL model assumes two energetically different adsorption sites. For the case of a single gas component, site one was assumed as the high energetic site, and site two as

the low energetic site. However, in a binary gas mix (CO_2 and CH_4), four gas-site interactions are possible as proposed by Ritter *et al.* (2011) which they called "energetic site matching". In other words, predicting mixed CO_2 and CH_4 gas adsorption with the DSL equation 7.6 could have four possible different representations, two for the CO_2 adsorption and two for the CH_4 adsorption. First, let us assume that both CO_2 and CH_4 molecules see the same site as their high energetic site, the DSL model is then represented by Equation 7.6A and 7.6B for CO_2 and CH_4 respectively. Note that the affinity constant, b1, is used in site one and b2 is used for site two in the DSL model equation for both q_{CO2} and q_{CH4}.

$$q_{CO2} = \frac{q_{s1,co2} b_{1,co2} Py_{co2}}{1+b_{1,co2}Py_{co2}+b_{1,ch4}Py_{ch4}} + \frac{q_{s2,co2} b_{2,co2} Py_{co2}}{1+b_{2,co2}Py_{co2}+b_{2,ch4}Py_{ch4}} \qquad \text{Equation 7.6A}$$

$$q_{CH4} = \frac{q_{s1,ch4} b_{1,ch4} Py_{ch4}}{1+b_{1,ch4}Py_{ch4}+b_{1,co2}Py_{co2}} + \frac{q_{s2,ch4} b_{2,ch4} Py_{ch4}}{1+b_{2,ch4}Py_{ch4}+b_{2,co2}Py_{co2}} \qquad \text{Equation 7.6B}$$

Alternatively, it is also possible that the site that is seen as the high energetic site by one gas is seen as the low energetic site by the other gas, the DSL model is then represented by equation 7.6C to predict q_{CO2} and equation 7.6D to predict q_{CH4}. The affinity constants b1 and b2 are used to represent the above assumption in DSL equations 7.6C and 7.6D.

$$q_{CO2} = \frac{q_{s1,co2} b_{1,co2} Py_{co2}}{1+b_{1,co2}Py_{co2}+b_{2,ch4}Py_{ch4}} + \frac{q_{s2,co2} b_{2,co2} Py_{co2}}{1+b_{2,co2}Py_{co2}+b_{1,ch4}Py_{ch4}} \qquad \text{Equation 7.6C}$$

$$q_{CH4} = \frac{q_{s1,ch4} b_{1,ch4} Py_{ch4}}{1+b_{1,ch4}Py_{ch4}+b_{2,co2}Py_{co2}} + \frac{q_{s2,ch4} b_{2,ch4} Py_{ch4}}{1+b_{2,ch4}Py_{ch4}+b_{1,co2}Py_{co2}} \qquad \text{Equation 7.6D}$$

Ritter *et al.* (2011) argued that it is not possible from the single component gas adsorption isotherm to establish which of the two pairs of the extended DSL model best describe the behaviour of the mixed gas adsorption. They suggested an

experimental validation or relying on the intuitive knowledge of the behaviour of the binary mixture of the adsorbate gas to select the right pair of equations. Experimental validation was used in this research to select one of the two pairs of equations using the following approach. Initially, both equation pairs were used to predict two possible values for each adsorbed gas (CO_2 and CH_4) at either 25 or 50 ^oC and up to 100 bar. The predicted total adsorbed amount (q_t) was calculated by adding q_{co2} and q_{ch4} from each pair of equations. The predictions resulting from Equation 7.6A and Equation 7.6B are the solid lines and labelled DSL_1 and predictions from Equation 7.6C and Equation 7.6D are the dashed lines and labelled DSL_2 in Figure 7.7.

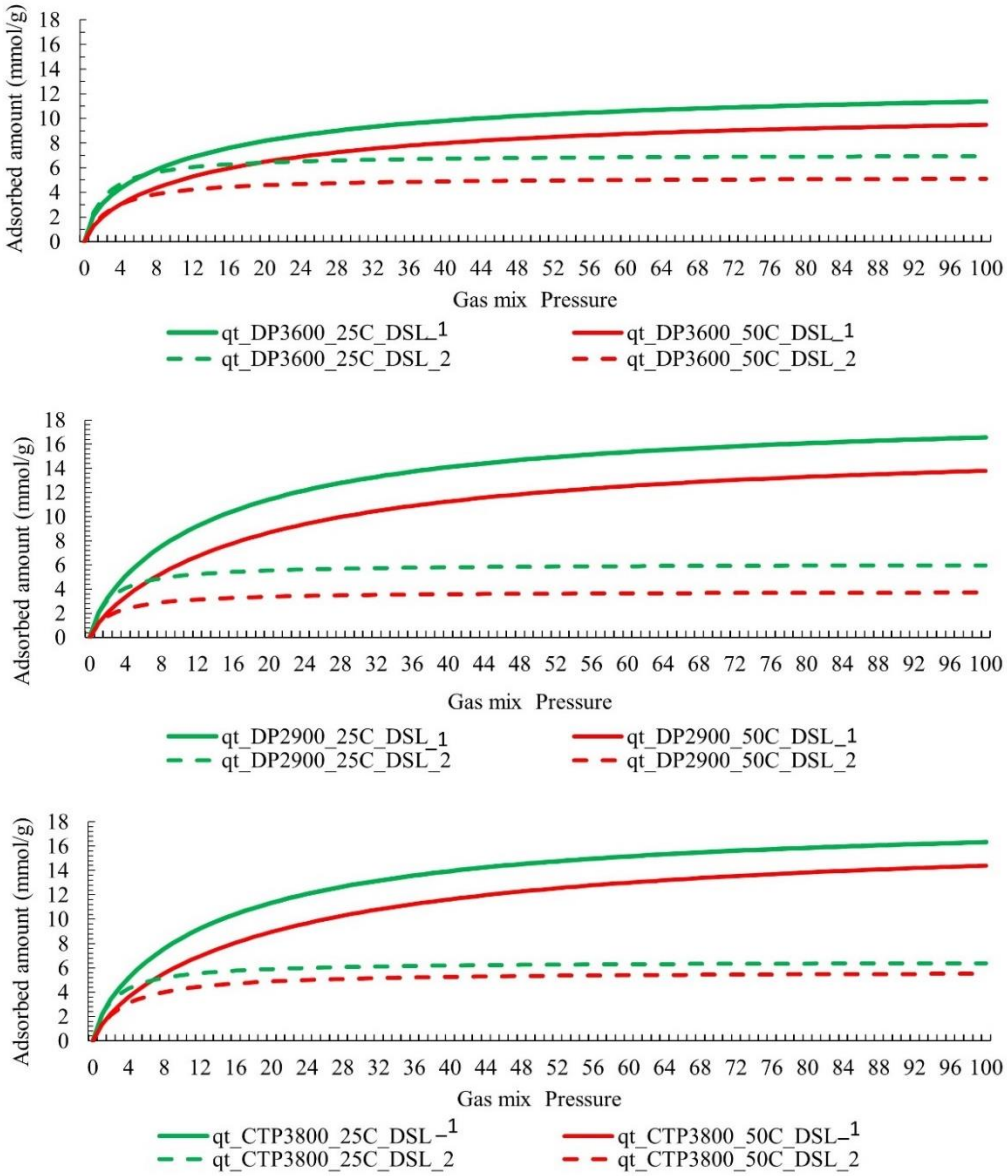


Figure 7.7 Predicted total mixed gas adsorption (q_t) from DSL_1 and DSL_2 equation pairs. Gas mix is 20% CO_2 and 80% CH_4, adsorption temperature 25 and 50 ^oC.

While the total adsorbed amount (q_t) for all samples in Figure 7.7 always decreased with increasing temperature from both sets of DSL models, the total adsorbed amount predicted by the DSL_2 equations was always lower than that predicted by the DSL_1 equations for both temperatures, 25 and 50 ^oC. The total adsorbed quantities (q_t) predicted by DSL_2 reached saturation at a lower pressure compared to DSL_1 which indicated a lower total adsorption capacity for both gases at both temperatures.

To confirm which of the two DSL equation pairs were more applicable to the adsorption system under study in this work, binary component mixed gas total adsorption experimental measurements were conducted for DP3600 and CTP3800 in the Linseis HP-TGA with a binary gas mixture of 20% CO_2 and 80% CH_4. The Linseis system was equipped with gas mixing and control capabilities with automated valves and flowmeters where the binary gas mixture was produced using the same pure CO_2 and CH_4 gases used for single component gas adsorption measurements. Helium was used to pressurise the HP-TGA before admitting the CO_2 at flow rates of 0.2 L/h and the CH_4 at a flow rate of 0.8 L/h to the gas mixing pipe arrangement that injected the gas mixture onto the activated carbon sample under investigation. Figure 7.8 compares the predicted total adsorption quantities with the measured quantities at 25 and 50 ^oC for DP3600 and CTP3800 samples.

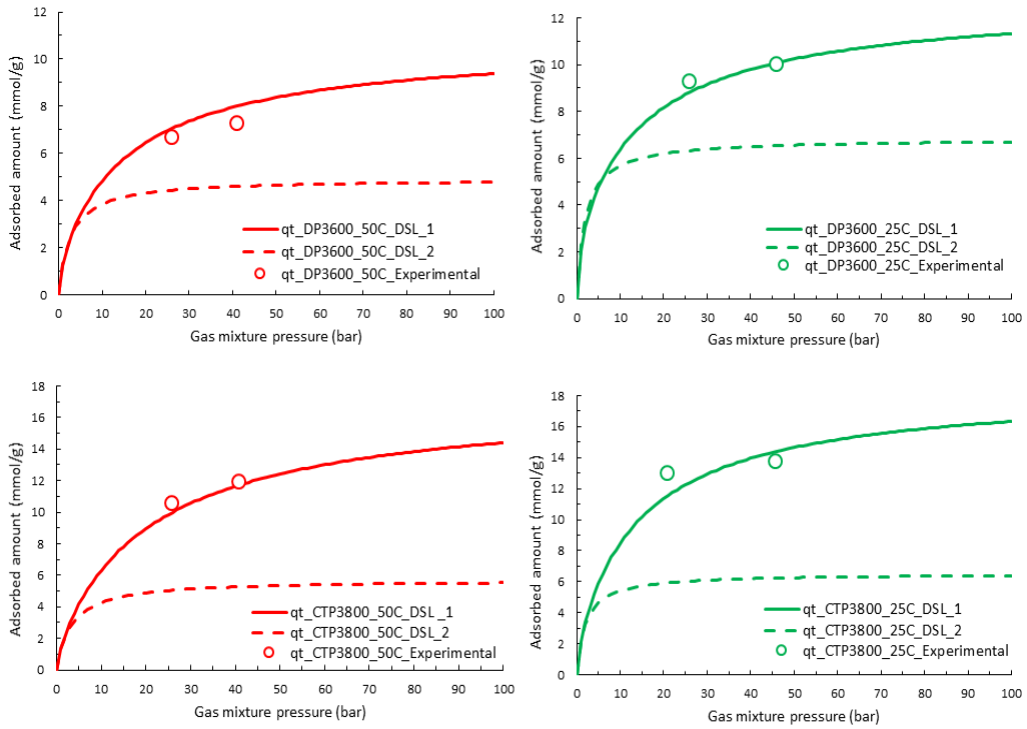


Figure 7.8 Total adsorption (q_t) experimental measurement compared to DSL_1 and DSL_2 model predictions.

From Figure 7.8, it can be seen that the measured experimental total adsorbed quantity (q_t) was closer to the values predicted by the DSL_1 pair of equations. These tests were used to conclude that both CO_2 and CH_4 see the same site as the high-energetic site as per the DSL model assumption to address the site matching issue. Therefore, the DSL_1 pair of equations was used to predict the adsorbed fraction of CO_2 and that of CH_4 from a binary component gas mixture onto the activated carbon samples selected for this study as presented in the next section.

7.4.2 Model Prediction Results

After selecting the most applicable pair of the extended DSL model equations with the aid of experimental measurements of the total adsorbed quantities (q_t), the adsorbed fraction of CO_2 (q_{CO2}) and the adsorbed fraction of CH_4, (q_{CH4}) on the selected activated carbons from their binary gas mixture were predicted. The compositions of the simulated natural gas mixture in the prediction calculations were set to 10%, 15%, 20% and 25% CO_2 balanced by CH_4. Excel software was used to calculate the predicted $q_{CO2,}$ and q_{CH4} values based on equations 7.6A and 7.6B. Figure 7.9 shows the predicted CO_2 and CH_4 adsorbed amount on the three selected activated carbons from a binary gas mixture at 25 and 50 ^oC at 100 bar.

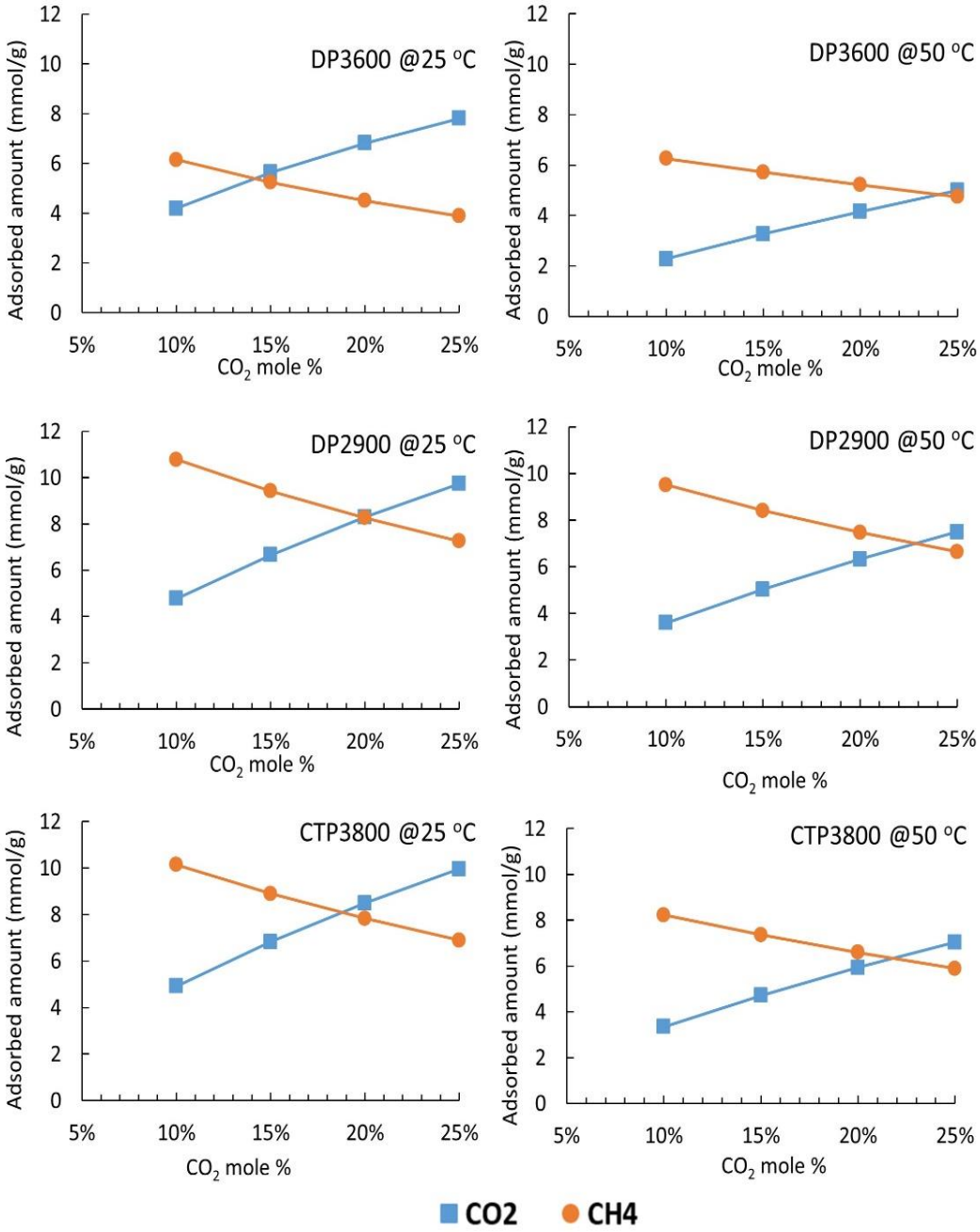


Figure 7.9 CO_2 and CH_4 adsorbed amount from a binary gas mixture on selected activated carbon samples at varying CO_2 concentration as predicted by the extended DSL model.

It can be seen from Figure 7.9 that the adsorbed amounts of CO_2 and CH_4 onto the activated carbons were proportional to the concentration of their fraction in the gas mixture. In other words, the adsorbed amount of CO_2 increased with increasing CO_2 percentage in the gas mix, and the adsorbed amount of CH_4 increased with increasing CH_4 in the gas mix. This observation indicates that the three selected activated carbon samples are more suited to the removal of CO_2 from natural gas

containing a high amount of CO_2, i.e. bulk separation. Increasing the gas mixture temperature from 25 to 50 ^oC resulted in a drop in CO_2 adsorption in all three samples. The predicted adsorbed quantities based on the equilibrium adsorption measurement and extended DSL model points to significant adsorption of CH_4 especially at low CO_2 concentration in the gas mixture which could contaminate the removed CO_2. Such contamination could be addressed by multiple purification cycles or increasing the number of adsorption beds in the PSA process to enable multiple purification cycles to reach the target CO_2 purity.

7.5 CO_2/CH_4 Selectivity Calculations

Visual examination of the adsorption isotherms for CO_2 and CH_4 gives an idea of the initial viability of using any of the assessed adsorbents for separating CO_2 from a binary CO_2-CH_4 gas mixture. However, such an examination does not provide a quantitative assessment and does not allow comparison of different adsorbents so that the best candidate for the desired separation process is selected. Selectivity calculations are used as judging criteria for adsorbent selection. Selectivity (S) is defined as the ratio of the equilibrium adsorbed quantity of CO_2 over that of CH_4 at the same pressure and temperature taking into account their ratio in the bulk gas mix, Equation 7.7 (Rege and Yang, 2001).

$$S = \frac{q_{CO_2}}{q_{CH_4}} \cdot \frac{Y_{CH_4}}{Y_{CO_2}} \qquad \text{Equation 7.7}$$

Where q_{CO2} and q_{CH4} are the absolute adsorbed amount, Y_{CO2} and Y_{CH4} are the fraction of each component in the bulk gas phase.

The absolute adsorbed quantities of CO_2 and CH_4 in a binary gas mixture were taken from the extended DSL model prediction presented earlier in section 7.4.

Figure 7.10 shows CO_2/CH_4 selectivity of DP3600, DP2900 and CTP3800 at two temperatures, 25 and 50 ^oC, and a pressure of 100 bar in a binary gas mixture of 10%, 15%, 20% and 25 % CO_2 balanced by CH_4.

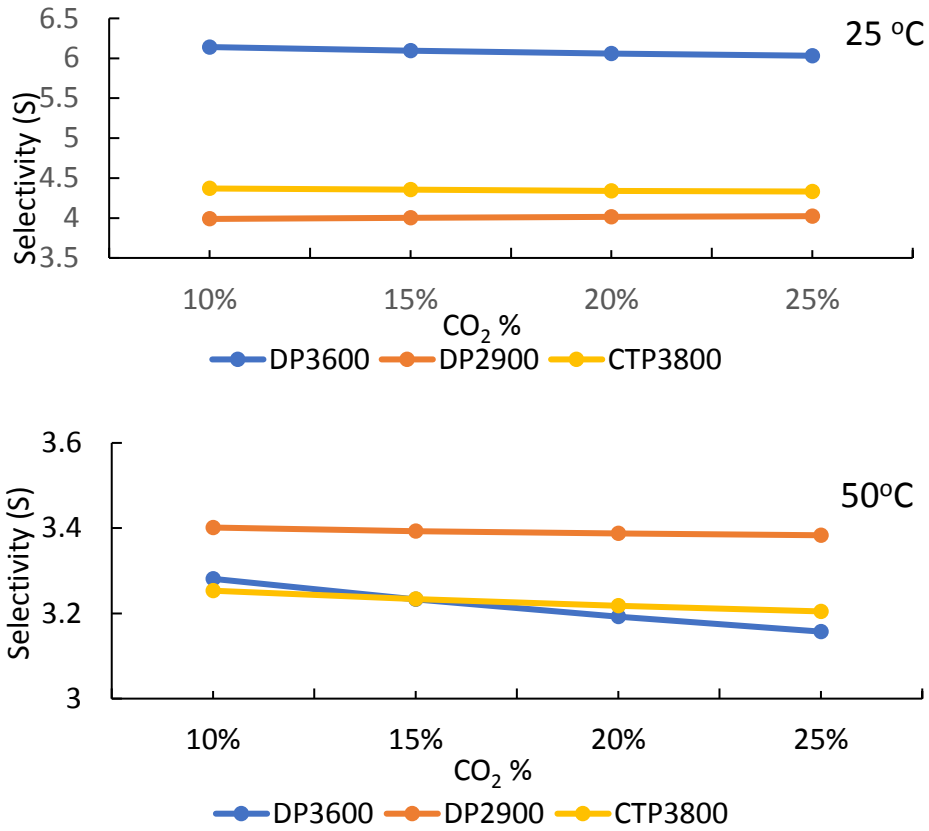


Figure 7.10 CO_2/CH_4 selectivity calculated at 100 bar pressure and at 25 and 50^oC for DP3600, DP2900 and CTP3800 activated carbon samples.

From Figure 7.10, the drop in CO_2/CH_4 selectivity for all samples due to the increase in adsorption temperature from 25 to 50 ^oC was noticeable. All samples showed a narrow spread of selectivity values between 3.2 and 3.6 at 50 ^oC, unlike their selectivity values at 25 ^oC where sample DP 3600 showed higher selectivity, around 6, compared to the selectivity of the other two samples of 4 to 4.5.

7.6 Conclusion

The measured single gas CO_2 and CH_4 excess adsorption quantities were converted to absolute adsorption quantities and were fitted to Sips and DSL adsorption models accurately, with the Sips model showing slightly better

performance. Poor fitting of the same absolute adsorption quantities to the Langmuir model was observed and could be attributed to the heterogeneity of the adsorption of CO_2 and CH_4 on activated carbons which is not accounted for by the Langmuir model, unlike both Sips and DSL models. Furthermore, a higher number of parameters in the DSL model (four parameters, compared to two in Langmuir) may have allowed for more flexibility in the model fitting and hence better model fitting of the adsorbed gas quantities.

When using the extended DSL model for predicting binary gas adsorption, a good model fit to the single gas experimental adsorption measurements was not enough to predict the mixed gas adsorption due to the site matching issue. Therefore, total mixed gas adsorption experimental measurements were needed to help select the appropriate DSL model equations that better described the adsorption of CO_2 and CH_4 from a binary mixed gas on the selected activated carbons.

CO_2/CH_4 selectivity was calculated based on the extended DSL model predicted mixed gas adsorption quantities. The highest CO_2/CH_4 selectivity at 25 ^oC was observed for sample DP3600, i.e. activation of the date pits char precursor at 600 ^oC and KOH to carbon ratio of 3. However, such activation conditions do not necessarily yield the highest CO_2 capacity. There is always a compromise between selectivity and capacity which should be carefully considered during the design of the PSA system as well as the economics of the gas separation application

.

Chapter 8. General Conclusions and Future Work

8.1 Conclusions

The overall aim of this research was to investigate the feasibility of using activated carbon as solid adsorbent for Pressure Swing Adsorption (PSA) Process to remove CO_2 from high pressure natural gas. The synthesis of various activated carbons was investigated with the aim of understanding the effect of the synthesis parameters on the produced activated carbons. The potential of these activated carbons in removing CO_2 from natural gas was assessed by measuring CO_2 uptake and CH_4 uptake by gravimetric and volumetric adsorption experiments. The measurements were conducted at pressures and temperatures equivalent to those of the South Oman gas field and assuming a PSA process. The performance of the activated carbons was linked to their textural characteristics. The effect of water on both CO_2 adsorption and CH_4 adsorption was investigated, focussing on two aspects: first, water as a contaminant in the natural gas stream and, second, water as an agent to improve the activated carbon selectivity for CO_2 over CH_4. Three different adsorption isotherm models were used to fit CO_2 and CH_4 adsorption isotherms to arrive at the optimum model to assess the mixed gas CO_2 and CH_4 adsorption behaviour on three selected activated carbon samples. The main conclusions of this work are summarised in the following three subsections

addressing: the synthesis and characterisation of the activated carbons, the performance of activated carbons in CO_2 and CH_4 adsorptions, and modelling of pure CO_2 and pure CH_4 gas adsorption in addition to their mixture on the activated carbons.

8.1.1 Activated Carbons Synthesis and Characterisation

Two precursors, coal tar pitch spherical beads and date pits biomass, were successfully used to synthesise two sets of 14 samples of activated carbon adsorbents using a simple chemical activation process with KOH. The production of the date pits activated carbons was achieved by a two-step chemical KOH activation process, the first step involved the carbonisation of the date bits biomass at 450 ^oC under nitrogen flow to produce a carbon-rich biochar that was used as a feedstock for the production of the activated carbons in a subsequent step. For the coal tar pitch, a one-step KOH chemical activation process was used to produce the activated carbons since it was already present in a carbon rich form.

The characterisation of the 28 activated carbon samples by N_2 adsorption revealed the ability of the KOH to produce highly microporous activated carbons with high surface area (2269 m^2/g and 2278 m^2/g) and high pore volume (0.73 cm^3/g and 0.72 cm^3/g) from date pits biomass and coal tar pitch respectively. The pore size distribution of the activated carbons could be influenced by either increasing the KOH amount or the temperature or both during the activation process. However, it was also found that a maximum KOH to carbon precursor mass ratio (3 for date pits and coal tar pitch carbon) exists at which point the KOH will start to become detrimental to the development of microporosity by the conversion of the micropores to mesopores when a high activation temperature (900 ^oC) was used.

Furthermore, increasing the KOH to the carbon precursor mass ratio to 4 reduced the microporosity possibly due to pore structure destruction as a result of high carbon consumption in the activation reactions due to the excessive use of KOH.

8.1.2 CO_2 and CH_4 Adsorption on Activated Carbons

All the synthesised activated carbons were tested for pure CO_2 and pure CH_4 gas equilibrium adsorption capacities using HP-TGA. The tests were carried out at a pressure equal to the partial pressure of each of the gases in the natural gas mixture of South Oman gas field (20 bar for CO_2 and 80 bar for CH_4) at 50 ^oC. The results of the tests revealed that most of the activated carbons (25 samples out of 28) showed preferential CO_2 adsorption over that of CH_4, the highest contrast between CO_2 and CH_4 adsorption was achieved by samples DP3600 and CTP3800, shown in Figure 8.1.

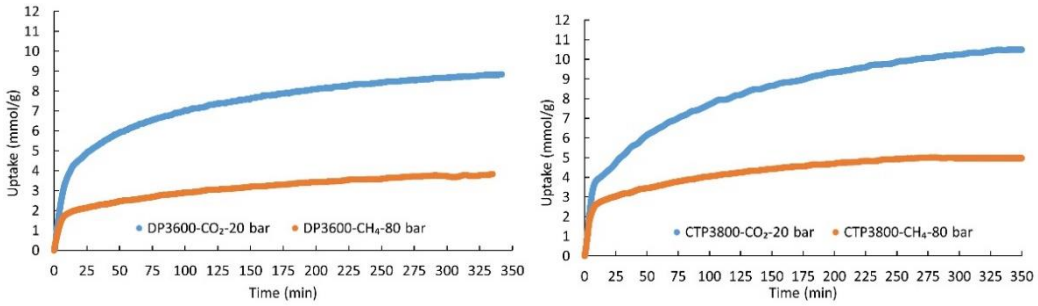


Figure 8.1 CO_2 and CH_4 uptakes at 50 ^oC for DP3600 and CTP3800.

The preference for CO_2 adsorption was also confirmed by the higher CO_2 adsorption working capacities that were calculated as the difference in uptake between 1 bar and each gas partial pressure, despite the CH_4 partial pressure of 80 bar (4 times higher than that of the CO_2). The highest calculated CO_2/CH_4 working capacity ratios for date pits and coal tar pitch activated carbons were 1.63 and 1.5 for samples DP3600 and CTP3800 respectively.

The calculated isosteric heat of adsorption was lower for CH_4 adsorption compared to that of the CO_2 on the same activated carbon sample indicating weaker interaction forces for CH_4 adsorption relative to that of the CO_2. When correlating the adsorbed CO_2 and CH_4 with different cumulative pore volumes arising from different pore sizes, both CO_2 and CH_4 were found to share an overlapping favourable micropore size range for adsorption (less than 1.6 nm for CO_2 and less than 1.5 nm for CH_4). In addition, positive correlation between the BET surface area and both CH_4 and CO_2 uptakes was also observed. While the texture properties seemed to contribute to the adsorption of both CO_2 and CH_4, the preferential adsorption of CO_2 over CH_4 at high pressure might have been influenced by the higher adsorbate-adsorbate interactions between the CO_2 molecules but not the CH_4 molecules due to the differences in their electric charge distribution. To elaborate, neither gas has a dipole moment but CO_2 does have a quadrupole moment of 4.3×10^{-26} esu cm^2 while CH_4 has none (Salehi and Anbia, 2017). This gives rise to intermolecular CO_2 interactions as an additional force for CO_2 adsorption but not for the non-polar CH_4 molecules.

Furthermore, preferential adsorption of CO_2 over CH_4 on the KOH activated carbon could have been promoted by the presence of extra framework metal (K^+) cations. The extra framework metal (K^+) cations are believed to have formed due to potassium intercalation during the chemical activation of the carbon with KOH (Liu *et al.*, 2015). This cations can form a local electric field (Liu *et al.*, 2017) which could enhance the interactions between the carbon surface and adsorbate molecules with high quadrupole moment (CO_2) compared to adsorbate molecules with no quadrupole moment (CH_4).

Due to the large fraction of methane in the natural gas mixture (80%), its co-adsorption onto the activated carbons must not be ignored from the perspective of the PSA process. This is because methane could contaminate the rejected CO_2 as it is removed from the pore space of the activated carbons in the PSA depressurisation cycle. This contamination implies that a multi-stage PSA system would be needed for applications requiring high CO_2 purity. However, for bulk CO_2 separation in sour gas EOR operations, such as the one in South Oman, the required purity of the CO_2 is not very stringent. Moreover, the removed CO_2 stream is deliberately topped up with sour gas containing CH_4 to provide sufficient volume to be injected into the reservoir for sour gas EOR as oppose to CO_2 EOR.

The effect of water, either as vapour contamination to the natural gas feed or as a pre-adsorbed selectivity enhancement agent within the activated carbons, was studied experimentally in this work. In both cases, water had the adverse effect of reducing the CO_2 and the CH_4 adsorption capacity of the activated carbons since it pre-occupies some of the micropore volume that otherwise would be available for CO_2 or CH_4 adsorption. However, the percentage drop in the CO_2 uptake due to pre-adsorbed water was lower than that of the CH_4 at high pressure due to the possible formation of CO_2 hydrate as seen in sample CTP3800. Furthermore, CO_2 solubility in water positively promoted higher CO_2 uptake in wet activated carbons relative to CH_4, suggesting that pre-adsorbed water is a potentially useful additive to enhance the CO_2/CH_4 selectivity but at the expense of lower CO_2 capacity.

8.1.3 CO_2 and CH_4 Adsorption Modelling

The conversion of the measured excess adsorption to absolute adsorption quantities was an essential step to conform the measured CO_2 and CH_4 isotherms

to the isotherm models. Pure CO_2 and pure CH_4 isotherms measured by HPVA were fitted to both Sips and Dual Site Langmuir (DSL) adsorption models quite accurately with a maximum sum of squared error of 1.5% for any single isotherm fit. In contrast, the Langmuir model overpredicted the adsorption in the low pressure region and underpredicted it in the high pressure region of both CO_2 and CH_4 isotherms, resulting in a high sum of squared errors, up to 10.14% for DP3600 CO_2 isotherm fitting. Such poor performance of the Langmuir model could be due to its lack of addressing adsorption heterogeneity and neglecting adsorbate-adsorbate interactions unlike the DSL and Sips models that both include a heterogeneity term.

Based on its slightly better fit to both single gas CO_2 and CH_4 adsorption isotherms compared to the Sips model, the extended DSL model was used for binary gas adsorption predictions to predict the adsorption and the selectivity of CO_2 over CH_4 in a mixed gas of 20% CO_2 and 80% CH_4. The issue of site matching in the extended DSL model was resolved by conducting a mixed gas adsorption measurement to select the DSL pair of equations that best described the total adsorption. At 25 ^oC the highest calculated CO_2/CH_4 selectivity was around 6 for sample DP3600, whereas as at 50 ^oC the highest selectivity achieved was 3.4 for sample DP2900.

8.2 Future Work

This study explored the opportunity provided by the use of activated carbon adsorbents for the removal of CO_2 from high pressure natural gas focusing on high CO_2 content in the natural gas. This opportunity is linked to a potential industrial application where the required purity of the removed CO_2 is not stringent (sour

gas EOR). However, the realisation of such an opportunity is still in its early stages and there are some areas of future work which could further confirm the potential of activated carbons in this application.

8.2.1 Adsorbent Synthesis

The raw coal tar pitch carbon precursor was provided in the form of spherical beads of 1.0 mm to 1.5 mm in diameter. However, achieving the highest CO_2 adsorption capacity with coal tar pitch spherical beads required a high degree of KOH activation that resulted in damaging the spherical morphology of the coal tar pitch activated carbons. Modifying the preparation process of the spherical coal tar pitch carbon beads to increase their mechanical strength is a desired feature. This could be achieved by exploring different stabilisation means including, but not limited to, the use of binders and alternative stabilisation temperatures to 300 ^{o}C.

The date pits activated carbons were produced in a granular shape which might not be favourable for the PSA system due to higher pressure drop concerns compared to a spherically-shaped adsorbent. Investigating a more favourable adsorbent shape such as spheres or cylindrical shapes will be useful in increasing the backed bed density and reducing the pressure drop in a bed packed with the date pits activated carbons. However, this might require the use of binder materials or mechanical compacting which could affect the performance of the produced activated carbons which would need further assessment.

8.2.2 CO_2 and CH_4 Co-adsorption

While the single gas CO_2 and CH_4 adsorption measurements by dynamic gravimetric and static volumetric measurement techniques showed preferential

adsorption of CO_2, the co-adsorption of both gases was only assessed by the extended DSL model in this study. The model-based assessment results showed somewhat significant adsorption of CH_4 (up to 6 mmol/g) from a natural gas mixture of 20:80 of CO_2:CH_4 composition at 100 bar and 50 ^oC. Validating such co-adsorption by an experimental fixed bed breakthrough adsorption measurement together with gas chromatography analysis will provide a more accurate and relevant assessment of the dynamic capacities for mixed gas adsorption. Such experimental work will also provide further validation of the extended DSL model before it can be used to design a cyclic PSA process for CO_2 removal from high pressure natural gas.

8.2.3 PSA Simulation and Economic Evaluation

There is a need for a detailed industrial scale PSA simulation study to assess the techno-economic feasibility of using a PSA process with activated carbons with reference to the South Oman gas field. Such a simulation study should include the potential energy saving from a PSA system in comparison to the existing amine process, in addition to the capital expenditure difference. The example of sour gas EOR in South Oman provides an opportunity for introducing a PSA system with activated carbon adsorbents for CO_2 removal from natural gas, since the purity requirements of the removed CO_2 from the sour gas is not stringent and contamination with CH_4 could be accepted to make up the required volume of sour gas for EOR operations. The same study could also be extended to assess the possibility of incorporating a novel hydration step within the PSA cycle using the produced water to manipulate the selectivity for CO_2 adsorption onto the activated carbon.

References

Abdul Kareem, F. A. *et al.* (2018) 'Adsorption of pure and predicted binary (CO2:CH4) mixtures on 13X-Zeolite: Equilibrium and kinetic properties at offshore conditions', *Microporous and Mesoporous Materials*, 267(December 2017), pp. 221–234.

Ahmadpour, A. and Do, D. D. (1997) 'The preparation of activated carbon from macadamia nutshell by chemical activation', *Carbon*, 35(12), pp. 1723–1732.

Ahmadpour, A., Wang, K. and Do, D. D. (1998) 'Comparison of models on the prediction of binary equilibrium data of activated carbons', *AIChE Journal*, 44(3).

Ahmed, M. J. (2016) 'Preparation of activated carbons from date (Phoenix dactylifera L.) palm stones and application for wastewater treatments: Review', *Process Safety and Environmental Protection*. Institution of Chemical Engineers, 102, pp. 168–182.

Al-Hadhrami, A. *et al.* (2007) 'The design of the first miscible sour gas flood project in Oman', *International Petroleum Technology Conference*, Dubai, 4–6 December, IPTC.

Al-Hadhrami, A. *et al.* (2014) 'Challenges and learning from developing deep high pressure sour reservoirs in Southern Oman by EOR MGI', in *Abu Dhabi International Petroleum Exhibition and Conference*, Abu Dhabi, 10–13 November, Society of Petroleum Engineers.

Auerbach, M., Carrado, K. A. and Dutta, P. K. (2003) *Zeolite Science and Technology*. New York, Basel: Marcel Dekker, Inc.

Belmabkhout, Y. and Sayari, A. (2009) 'Adsorption of CO_2 from dry gases on MCM-41 silica at ambient temperature and high pressure. 2: Adsorption of CO2/N2, CO2/CH4 and CO_2/H_2 binary mixtures', *Chemical Engineering Science*, 64(17), pp. 3729–3735.

Belmabkhout, Y., Serna-guerrero, R. and Sayari, A. (2010) 'MCM-41 silica : application for gas purification', *Adsorption Journal Of The International Adsorption Society*, 49(1), pp. 359–365.

Belmabkhout, Y., Serna-Guerrero, R. and Sayari, A. (2009) 'Adsorption of from dry gases on MCM-41 silica at ambient temperature and high pressure. 1: Pure CO_2 adsorption', *Chemical Engineering Science*, 64(17), pp. 3721–3728.

Besbes, S. *et al.* (2004) 'Date seeds: Chemical composition and characteristic profiles of the lipid fraction', *Food Chemistry*, 84(4), pp. 577–584.

Billemont, P., Coasne, B. and De Weireld, G. (2013) 'Adsorption of carbon dioxide, methane, and their mixtures in porous carbons: Effect of surface chemistry, water content, and pore disorder', *Langmuir*, 29(10), pp. 3328–3338.

Bouchelta, C. *et al.* (2012) 'Effects of pyrolysis conditions on the porous structure development of date pits activated carbon', *Journal of Analytical and Applied Pyrolysis*. Elsevier B.V., 94, pp. 215–222.

BP P.L.C. (2015) *Energy Outlook 2035*, available online at https://www.bankofcanada.ca/wp-content/uploads/2015/05/bp-energy-outlook-2035.pdf. , last accessed 23/3/2016.

Brandani, S., Mangano, E. and Sarkisov, L. (2016) 'Net, excess and absolute adsorption and adsorption of helium', *Adsorption*. Springer US, 22(2), pp. 1–16.

Brouwer, P. (2003) *Theory of XRF*, PANalytical BV., Almelo.

Brunauer, S., Emmet, P. H. and Teller, E. (1938) 'Adsorption of gases in multimolecular layers.', *Journal of the American chemical society*, 60, p. 309–319.

Burgers, W. F. J. *et al.* (2011) 'Worldwide development potential for sour gas', *Energy Procedia*. Elsevier, 4, pp. 2178–2184.

Caldwell, S. J. *et al.* (2015) 'Carbon dioxide separation from nitrogen/hydrogen mixtures over activated carbon beads: adsorption isotherms and breakthrough studies', *Energy & Fuels*, 29(6), pp. 3796–3807.

Cavenati, S. and Grande, C. a. (2005) ‘Layered pressure swing adsorption for methane recovery from CH_4 / CO_2 / N_2 Streams’, *Adsorption*, 11, pp. 549–554.

Cavenati, S., Grande, C. A. and Rodrigues, A. E. (2004) ‘Adsorption equilibrium of methane, carbon dioxide, and nitrogen on zeolite 13X at high pressures’, *Journal of Chemical & Engineering Data*, 49(4), pp. 1095–1101.

Choi, S., Drese, J. H. and Jones, C. W. (2009) ‘Adsorbent materials for carbon dioxide capture from large anthropogenic point sources.’, *ChemSusChem: Chemistry & Sustainability Energy & Materials*, 2(9), pp. 796–854.

Delgado, J. a. and Rodrigues, a. E. (2008) ‘Analysis of the boundary conditions for the simulation of the pressure equalization step in PSA cycles’, *Chemical Engineering Science*, 63, pp. 4452–4463.

Drage, T. C. *et al.* (2009) ‘Evaluation of activated carbon adsorbents for CO_2 capture in gasification’, *Energy & Fuels*, 23(5), pp. 2790–2796.

Dreisbach, F., Staudt, R. and Keller, J. U. (1999) ‘High pressure adsorption data of methane, nitrogen, carbon dioxide and their binary and ternary mixtures on activated carbon’, *Adsorption*, 5(3), pp. 215–227.

Ebner, A. D. and Ritter, J. A. (2009) State-of-the-art adsorption and membrane separation processes for carbon dioxide production from carbon dioxide emitting industries, *Separation Science and Technology*, 44, pp1273-1421.

El-Hendawy, A. A. (2009) ‘An insight into KOH activation mechanism via production of microporous activated carbon for heavy metal removal’, *Applied Surface Science*, 255, pp. 3723–3730.

Feng, F. *et al.* (2012) ‘Simulation and energy performance assessment of CO_2 removal from crude synthetic natural gas via physical absorption process’, *Journal of Natural Gas Chemistry*. CAS/DICP, 21(6), pp. 633–638.

Foo, K. Y. and Hameed, B. H. (2011) ‘Preparation of oil palm (Elaeis) empty fruit bunch activated carbon by microwave-assisted KOH activation for the adsorption of methylene blue’, *Desalination*, 275(1–3), pp. 302–305.

Food and Agricultural Organization of the United Nation (2016) *FAO, Statistical Databases*. Available online at: http://faostat.fao.org , last accessed: 11/9/2017.

Fu, Y. *et al.* (2019) 'Activated bio-chars derived from rice husk via one- and two-step KOH-catalyzed pyrolysis for phenol adsorption', *Science of the Total Environment*, 646, pp. 1567–1577.

Ganan, J. *et al.* (2004) 'Preparation of activated carbons from bituminous coal pitches', *Applied Surface Science*, 238, pp. 347–354.

Garcia, S. *et al.* (2013) 'Predicting mixed-gas adsorption equilibria on activated carbon for precombustion CO2 capture', *Langmuir*, 29(20), pp. 6042–6052.

Girgis, B. S. and El-Hendawy, A. N. A. (2002) 'Porosity development in activated carbons obtained from date pits under chemical activation with phosphoric acid', *Microporous and Mesoporous Materials*, 52(2), pp. 105–117.

Grande, C. a. (2012) 'Advances in pressure swing adsorption for gas separation', *ISRN Chemical Engineering*, 2012, pp. 1–13.

Grande, C. a. *et al.* (2013) 'High-pressure separation of CH_4/CO_2 using activated carbon', *Chemical Engineering Science*, 89, pp. 10–20.

Grande, C. A. *et al.* (2017) 'CO_2 capture in natural gas production by adsorption processes', *Energy Procedia*, 114, pp. 2259–2264.

Grande, C. a. and Blom, R. (2012) 'Utilization of dual - PSA technology for natural gas upgrading and integrated CO_2 capture', *Energy Procedia*, 26, pp. 2–14.

Guo, B., Chang, L. and Xie, K. (2006) 'Adsorption of carbon dioxide on activated carbon', *Journal of Natural Gas Chemistry*, 15, pp. 223–229.

Gurten, I. I. *et al.* (2012) 'Preparation and characterisation of activated carbon from waste tea using K2CO3', *Biomass and Bioenergy*, 37, pp. 73–81.

Hammer, G. *et al.* (2000) 'Natural Gas', in *Ullmann's Encyclopedia of Industrial Chemistry*. Weinheim, Germany: Wiley-VCH Verlag GmbH & Co. KGaA, pp. 709–711.

Hart, A. and Gnanendran, N. (2009) 'Cryogenic CO_2 capture in natural gas', *Energy Procedia*. Elsevier, 1, pp. 697–706.

Hassanpouryouzband, A. *et al.* (2018) 'Insights into CO2 Capture by Flue Gas Hydrate Formation: Gas Composition Evolution in Systems Containing Gas Hydrates and Gas Mixtures at Stable Pressures', *ACS Sustainable Chemistry and Engineering*. American Chemical Society, 6(5), pp. 5732–5736.

Hayashi, J. *et al.* (2000) 'Preparation of activated carbon from lignin by chemical activation', *Carbon*, 38(13), pp. 1873–1878.

Hedin, N. *et al.* (2013) 'Adsorbents for the post-combustion capture of CO_2 using rapid temperature swing or vacuum swing adsorption', *Applied Energy*, 104, pp. 418–433.

Heldebrant, D. J. *et al.* (2011) 'CO_2-binding organic liquids, An integrated acid gas capture system', *Energy Procedia*, 4, pp. 216–223.

Himeno, S., Komatsu, T. and Fujita, S. (2005) 'High-Pressure Adsorption Equilibria of Methane and Carbon Dioxide on Several Activated Carbons', *Journal of Chemical Engineering Data*, 50, pp. 369–376.

Hossain, M. Z. *et al.* (2014) 'Chemical Composition of Date-Pits and It's Potential for Developing Value-Added Product - a Review', *Polish Journal of Food and Nutrition Sciences*, 64(4), pp. 215–226.

Hsu, L. Y. and Teng, H. (2000) 'Influence of different chemical reagents on the preparation of activated carbons from bituminous coal', *Fuel processing technology*, 64(1), pp. 155–166.

Hu, X. *et al.* (2009) 'CO_2-filling capacity and selectivity of carbon nanopores: synthesis, texture, and pore-size distribution from Quenched-Solid Density Functional Theory (QSDFT)', *Journal of Physics A: Mathematical and Theoretical*, 42(36), pp. 7068–7074.

Hu, Z. *et al.* (2018) 'CO_2 capture in metal-organic framework adsorbents: an engineering perspective', *Advanced Sustainable Systems*, p. 1800080.

Huang, J. and Ruther, T. (2009) 'Why are ionic liquids attractive for CO_2 absorption? An overview', *Australian Journal of Chemistry*, 62(4), pp. 298–308.

International Energy Agency (2018a) *Market report series: energy efficiency 2O18*, available online at https://webstore.iea.org/market-report-series-energy-efficiency-2018, last accessed 2/2/2019.

International Energy Agency (2018b) *World Energy Investment 2018*, *International Energy Agency*, available online at https://www.iea.org/wei2018, last accessed 1/3/2019.

International Organisation for Standardisation (2007) *Pore size distribution and porosity of solid materials by mercury porosimetry and gas adsorption - Part 3: Analysis of micropores by gas adsorption (ISO 15901-3).*

Ismail, A. F., Chandra Khulbe, K. and Matsuura, T. (2015) *Gas Separation Membranes: Polymeric and Inorganic*, Cham, Springer International Publishing

Jalilov, A. S. *et al.* (2017) 'Increased CO_2 selectivity of asphalt-derived porous carbon through introduction of water into pore space', *Nature Energy*, 2 (December). pp932-938.

Jalilov, A. S. *et al.* (2017) 'Ultra-High Surface Area Activated Porous Asphalt for CO2 Capture through Competitive Adsorption at High Pressures', *Advanced Energy Materials*, 7(1), pp. 1–7.

Jessop, P. G. *et al.* (2005) 'Reversible nonpolar-to-polar solvent', *Nature*, 436(25), p. 1102.

Jribi, S. *et al.* (2017) 'Equilibrium and kinetics of CO_2 adsorption onto activated carbon', *International Journal of Heat and Mass Transfer*, 108, pp. 1941–1946.

Kacem, M., Pellerano, M. and Delebarre, A. (2015) 'Pressure swing adsorption for CO_2/N_2 and CO_2/CH_4 separation: Comparison between activated carbons and zeolites performances', *Fuel Processing Technology*, 138, pp. 271–283.

Kanehashi, S. *et al.* (2017) 'Can the addition of carbon nanoparticles to a polyimide membrane reduce plasticization?', *Separation and Purification*

Technology, 183, pp. 333–340.

Karge, H. G. and Weitkamp, J. (2008) *Molecular Sieves Science and Technology*. Berlin, Springer.

Keller, J. and Staudt, R. (2005) *Gas adsorption equilibria. Experimental Methods and Adsorption Isotherms*. Boston: Springer.

Kelley, B. T. *et al.* (2011) 'Controlled Freeze Zone™ for developing sour gas reserves', *Energy Procedia*, 4, pp. 824–829.

Kidnay, J. and Parrish, W. R. (2006) *Fundamentals of natural gas processing*. Boca Raton, FL. CRC Press.

Krishna, R. (2012) 'Adsorptive separation of CO_2/CH_4/CO gas mixtures at high pressures', *Microporous and Mesoporous Materials*, 156, pp. 217–223.

Langmuir, I. (1918) 'The adsorption of gases on plane surfaces of glass, mica and platinum', *Journal of the American Chemical Society*, 40(9), pp. 1361–1403.

Li, Y. *et al.* (2016) 'Biochar as a renewable source for high-performance CO_2 sorbent', *Carbon*, 107, pp. 344–351.

Liang, C., Sha, G. and Guo, S. (1999) 'Carbon membrane for gas separation derived from coal tar pitch', *Carbon*, 37(9), pp. 1391–1397.

Lide, D. R. (2004) *CRC Handbook of Chemistry and Physics*. Boca Raton, Florida: Chemical Rubber Publishing Company.

Lin, H. and Freeman, B. D. (2005) 'Materials selection guidelines for membranes that remove CO_2 from gas mixtures', *Journal of Molecular Structure*, 739, pp. 57–74.

Liu, J. *et al.* (2015) 'Spherical potassium intercalated activated carbon beads for pulverised fuel CO_2 post-combustion capture', *Carbon*, 94, pp. 243–255.

Liu, J. *et al.* (2018) 'High density and super-ultra-microporous activated carbon macrospheres with high volumetric capacity for CO_2 capture', *Advanced Sustainable Systems*, 2(2), p. 1700115.

Liu, X. *et al.* (2007) 'Adsorption and regeneration study of the mesoporous adsorbent SBA-15 adapted to the capture/separation of CO_2 and CH_4', *Chemical Engineering Science*, 62(4), pp. 1101–1110.

Liu, X. *et al.* (2017) 'Potassium and Zeolitic Structure Modified Ultra-microporous Adsorbent Materials from a Renewable Feedstock with Favorable Surface Chemistry for CO2Capture', *ACS Applied Materials and Interfaces*, 9(32), pp. 26826–26839.

Lowell, S. *et al.* (2004) *Characterization of Porous Solids and Powders: Surface Area, Pore Size and Density*. New York: Springer Science+ Business Media LLC.

Lozano-Castelló, D. *et al.* (2002) 'Influence of pore size distribution on methane storage at relatively low pressure: Preparation of activated carbon with optimum pore size', *Carbon*, 40(7), pp. 989–1002.

Lua, A. C. and Yang, T. (2004) 'Effect of activation temperature on the textural and chemical properties of potassium hydroxide activated carbon prepared from pistachio-nut shell', *Journal of Colloid and Interface Science*, 274(2), pp. 594–601.

Machnikowski, J. *et al.* (2002) 'Mesophase development in coal-tar pitch modified with various polymers', *Journal of Analytical and Applied Pyrolysis*, 65(2), pp. 147–160.

Marsh, H. and Rodríguez-Reinoso, F. (2006) *Activated Carbon, Activated Carbon*. Amsterdam: Elsevier.

Martínez, M. L. *et al.* (2006) 'Preparation and characteristics of activated carbon from olive stones and walnut shells', *Industrial Crops and Products*, 23(1), pp. 23–28.

Mason, J. A., Veenstra, M. and Long, J. R. (2014) 'Evaluating metal-organic frameworks for natural gas storage', *Chem. Sci.*, 5(1), pp. 32–51.

Merzougui, Z. and Addoun, F. (2008) 'Effect of oxidant treatment of date pit activated carbons application to the treatment of waters', *Desalination*, 222(1–3),

pp. 394–403.

Mu, B. and Walton, K. S. (2011) ‘High-Pressure Adsorption Equilibrium of CO_2 , CH_4 , and CO on an Impregnated Activated Carbon’, *Journal Chem. Eng. Data*, 56, pp. 390–397.

Myers, a. L. and Monson, P. a. (2002) ‘Adsorption in porous materials at high pressure: Theory and experiment’, *Langmuir*, 18(26), pp. 10261–10273.

Myers, a L. and Prausnitz, J. M. (1965) ‘Thermodynamics of mixed-gas adsorption’, *AIChE Journal*, 11(1), pp. 121–127.

Myers, A. L. (1983) ‘Activity Coefficients of Mixtures Adsorbed on Heterogeneous Surfaces’, *AIChE Journal*, 29(4), pp. 691–693.

Myers, A. L. and Monson, P. A. (2014) ‘Physical adsorption of gases: the case for absolute adsorption as the basis for thermodynamic analysis’, *Adsorption*, 20(4), pp. 591–622.

National centre for statistics and information (2018) *Statistical Year Book of Oman*. Muscat: National Centre for Statistics and Information.

Ogungbenro, A. E. *et al.* (2017) ‘Activated Carbon from Date Seeds for CO_2 Capture Applications’, *Energy Procedia*, 114(2017), pp. 2313–2321.

Olajire, A. A. (2010) ‘CO_2 capture and separation technologies for end-of-pipe applications – A review’, *Energy*, 35(6), pp. 2610–2628.

Olivares-Marín, M. *et al.* (2006) ‘Preparation of activated carbon from cherry stones by chemical activation with ZnCl2’, *Applied Surface Science*, 252(17), pp. 5967–5971.

Otowa, T., Tanibata, R. and Itoh, M. (1993) ‘Production and adsorption characteristics of MAXSORB: High-surface-area active carbon’, *Gas Separation and Purification*, 7(4), pp. 241–245.

Park, Y. *et al.* (2015) ‘Recent Advances in Anhydrous Solvents for CO_2 Capture: Ionic Liquids, Switchable Solvents, and Nanoparticle Organic Hybrid Materials’,

Frontiers in Energy Research, 3(October), pp. 1–14.

Park, Y. *et al.* (2016) 'Adsorption equilibria and kinetics of six pure gases on pelletized zeolite 13X up to 1.0 MPa: CO_2, CO, N_2, CH_4, Ar and H_2', *Chemical Engineering Journal*, 292, pp. 348–365.

Peters, L. *et al.* (2011) 'CO_2 removal from natural gas by employing amine absorption and membrane technology-A technical and economical analysis', *Chemical Engineering Journal*, 172(2–3), pp. 952–960.

Presser, V. *et al.* (2011) 'Effect of pore size on carbon dioxide sorption by carbide derived carbon', *Energy and Environmental Science*, 4(8), pp. 3059–3066.

Rad, M. D., Fatemi, S. and Mirfendereski, S. M. (2012) 'Development of T type zeolite for separation of CO_2 from CH_4 in adsorption processes', *Chemical Engineering Research and Design*, 90(10), pp. 1687–1695.

Rege, S. U. and Yang, R. T. (2001) 'A simple parameter for selecting an adsorbent for gas separation by pressure swing adsorption', *Preservation*, 36(15), pp. 3355–3365.

Ritter, J. A., Bhadra, S. J. and Ebner, A. D. (2011) 'On the use of the dual-process langmuir model for correlating unary equilibria and predicting mixed-gas adsorption equilibria', *Langmuir*, 27(8), pp. 4700–4712.

Rodríguez-Reinoso, F. and Molina-Sabio, M. (1992) 'Activated carbons from lignocellulosic materials by chemical and/or physical activation: an overview', *Carbon*, 30(7), pp. 1111–1118.

Romanos, J. *et al.* (2012) 'Nanospace engineering of KOH activated carbon', *Nanotechnology*, 23(1), pp. 15401–15408.

Rota, R. (2014) 'Separation process of gaseous compounds from natural gas with low exergy losses, World Intellectual Property Organization, Patent number WO 2014/128048 A1'. Italy: World Intellectual Property Organization.

Rouquerol, F. *et al.* (2014) *Adsorption by Powders and Porous Solids Principles, Methodology and Applications*. 2nd ed. Oxford: Elsevier.

Rouquerol, J., Llewellyn, P. and Rouquerol, F. (2007) 'Is the BET equation applicable to microporous adsorbents?', *Studies in Surface Science and Catalysis*, 160(1), pp. 49–56.

Rouquerolt, J. *et al.* (1994) 'Recommendations for the characterization of porous solids', *Pure & Appl. Chem.*, 66(8), pp. 1739–1758.

Rufford, T. E. *et al.* (2012) 'The removal of CO_2 and N_2 from natural gas: A review of conventional and emerging process technologies', *Journal of Petroleum Science and Engineering*, 94–95, pp. 123–154.

Ruthven, D. M. (1984) *Principles of adsorption and adsorption processes*. New York: John Wiley & Sons, Inc.

Ruthven, D. M., Farooq, S. and Knaebel, K. S. (1994) *Pressure Swing Adsorption*. New York: VCH.

Salehi, S. and Anbia, M. (2017) 'High CO_2 adsorption capacity and CO_2/CH_4 selectivity by nanocomposites of MOF-199', *Energy and Fuels*, 31(5), pp. 5376–5384.

Santos, M. P. S., Grande, C. a. and Rodrigues, A. E. (2011) 'Pressure swing adsorption for biogas upgrading. Effect of recycling streams in pressure swing adsorption design', *Industrial and Engineering Chemistry Research*, 50(2), pp. 974–985.

Savova, D. *et al.* (2001) 'Biomass conversion to carbon adsorbents and gas', *Biomass and Bioenergy*, 21(2), pp. 133–142.

Sayari, A., Belmabkhout, Y. and Serna-Guerrero, R. (2011) 'Flue gas treatment via CO2 adsorption', *Chemical Engineering Journal*, 171(3), pp. 760–774.

Schell, J. *et al.* (2012) 'Pure and binary adsorption of CO_2, H_2, and N_2 on activated carbon', *Adsorption*, 18(1), pp. 49–65.

Sevilla, M. *et al.* (2018) 'Optimization of the pore structure of biomass-based carbons in relation to their use for CO_2 capture under low- and high-pressure regimes', *ACS Applied Materials and Interfaces*, 10(2), pp. 1623–1633.

Shao, X. *et al.* (2011) 'Adsorption of CO_2, CH_4, CO_2/N_2 and CO_2/CH_4 in novel activated carbon beads: Preparation, measurements and simulation', *AIChE Journal*, 57(11), pp. 3042–3051.

Shell Global Solutions (2015) *Sour gas processing*, *Shell Global Solutions*, available online at http://s06.static-shell.com/content/dam/shell/static/globalsolutions/downloads/mediacentre/industry-commentary/sour-gas-processing.pdf. las Accessed: 27 April 2015).

Shimekit, B. and Mukhtar, H. (2012) 'Natural gas purification technologies–major advances for CO_2 separation and future directions', *Advances in Natural Gas Technology*, 9(1), pp. 235–270.

Sing, K. S. W. *et al.* (1985) 'IUPAC Recommendations, Reporting physisorption data for gas/solid systems', *Pure and Applied Chemistry*, 57(4), pp. 603–619.

Singh, G. *et al.* (2017) 'Highly efficient method for the synthesis of activated mesoporous biocarbons with extremely high surface area for high-pressure CO_2 adsorption', *ACS Applied Materials and Interfaces*, 9(35), pp. 29782–29793.

Singh, V. K. and Anil Kumar, E. (2016) 'Measurement and analysis of adsorption isotherms of CO_2 on activated carbon', *Applied Thermal Engineering*, 97(1), pp. 77–86.

Siriwardane, R. V. *et al.* (2001) 'Adsorption of CO_2 on molecular sieves and activated carbon', *Energy & Fuels*, 15(2), pp. 279–284.

Siriwardane, R. V. *et al.* (2005) 'Adsorption of CO_2 on zeolites at moderate temperatures', *Energy and Fuels*, 19(3), pp. 1153–1159.

Skarstrom, C. W. (1960) 'Method and apparatus for fractionating gas mixtures by adsorption', *U.S. patent No. US2944627A*.

Sreedhar, I. *et al.* (2017) 'Carbon capture by absorption – Path covered and ahead', *Renewable and Sustainable Energy Reviews*, 76(1), pp. 1080–1107.

Sui, P. *et al.* (2018) 'Effect of temperature and pressure on corrosion behavior of X65 carbon steel in water-saturated CO_2 transport environments mixed with H_2S',

International Journal of Greenhouse Gas Control, 73(1), pp. 60–69.

Sun, N. *et al.* (2013) 'Synthesis, characterization and evaluation of activated spherical carbon materials for CO_2 capture', *Fuel*, 113, pp. 854–862.

Sun, Y. *et al.* (2007) 'CO_2 sorption in activated carbon in the presence of water', *Chemical Physics Letters*, 437(1–3), pp. 14–16.

Talu, O. (1998) 'Needs, status, techniques and problems with binary gas adsorption experiments', *Advances in Colloid and Interface Science*, 76–77, pp. 227–269.

Thommes, M. *et al.* (2015) 'Physisorption of gases, with special reference to the evaluation of surface area and pore size distribution (IUPAC Technical Report)', *Pure and Applied Chemistry*, 87(9–10), pp. 1051–1069.

Tongpoothorn, W. *et al.* (2011) 'Preparation of activated carbon derived from Jatropha curcas fruit shell by simple thermo-chemical activation and characterization of their physico-chemical properties', *Chemical Engineering Research and Design*, 89(3), pp. 335–340.

Total E&P (2007) *Sour Gas, A History of Expertise, Group*, available online at http://www.total.com/sites/default/files/atoms/file/total-sour-gas-history-expertise, last accessed: 27/4/2015.

Vieira, R. B. *et al.* (2018) 'Polyamine-Grafted Magadiite: High CO_2 Selectivity at Capture from CO_2/N_2 and CO_2/CH_4 Mixtures', *Journal of CO_2 Utilization*, 23, pp. 29–41.

Wang, J. and Kaskel, S. (2012) 'KOH activation of carbon-based materials for energy storage', *Journal of Materials Chemistry*, 22(45), p. 23710.

Wang, Q. *et al.* (2011) 'CO_2 capture by solid adsorbents and their applications: current status and new trends', *Energy Environ. Sci.*, 4(1), pp. 42–55.

Wang, X. *et al.* (2010) 'Adsorption measurements of methane on activated carbon in the temperature range (281 to 343) K and pressures to 1.2 MPa', *Journal of Chemical and Engineering Data*, 55(8), pp. 2700–2706.

Wang, Y. *et al.* (2008) 'Comparative studies of CO_2 and CH_4 sorption on activated carbon in presence of water', *Colloids and Surfaces A: Physicochemical and Engineering Aspects*, 322(1–3), pp. 14–18.

Webb, P. . and Orr, C. (1997) *Analytical methods in fine particle technology*. Norcross, GA: Micromeritics Instrument Corporation.

Webb, P. a (2003) 'Introduction to Chemical Adsorption Analytical Techniques and their Applications to Catalysis', *MIC Technical Publications*, 13(January), pp. 1–4.

Wei, H. *et al.* (2012) 'Granular Bamboo-Derived Activated Carbon for High CO_2 Adsorption: The Dominant Role of Narrow Micropores.', *ChemSusChem*, 7(1), pp. 291–298.

Wilhelm Warner F (1932) 'Fluid treating device', *US Patent NO. 2038071 A*.

Yampolskii, Y. and Freeman, B. (2010) *Membrane Gas Separation*. Chichester, United Kingdom: Wiley.

Yang, R. (1987) *Gas Separation by Adsorption Processes*, *Gas Separation & Purification*. Stoneham, MA: Butterworth Publishers.

Yang, R. T. (2003) *Adsorbent: Fundamentals and applications*. Hoboken, New Jersey: John Wiley & Sons, Inc.

Yentekakis, I. V. and Goula, G. (2017) 'Biogas management: advanced utilization for production of renewable energy and added-value chemicals', *Frontiers in Environmental Science*, 5(7), pp. 1–18.

Yi, H. *et al.* (2013) 'Adsorption separation of CO_2, CH_4, and N_2 on microwave activated carbon', *Chemical Engineering Journal*, 215–216, pp. 635–642.

Yu, C.-H., Huang, C.-H. and Tan, C.-S. (2012) 'A Review of CO_2 capture by absorption and adsorption', *Aerosol and Air Quality Research*, 12(5), pp. 745–769.

Zhou, X. *et al.* (2012) 'Thermodynamics for the adsorption of SO_2, NO and CO_2 from flue gas on activated carbon fibre', *Chemical Engineering Journal*, 200–202(2), pp. 399–404.

Appendix A: CO_2 Excess and Absolute Uptake Values

Sample ID: DP3600- adsorbate CO_2

25°C			50°C		
Pressure (bar)	Excess adsorption (mmol/g)	Absolute adsorption (mmol/g)	Pressure (bar)	Excess adsorption (mmol/g)	Absolute adsorption (mmol/g)
0.0000	0.0000	0.0000	0.0000	0.0000	0.0000
0.2154	1.6567	1.6610	0.3431	1.3031	1.3095
1.3283	4.4394	4.4661	1.7038	3.4102	3.4420
2.5535	6.0097	6.0615	2.9554	4.5225	4.5777
4.0711	7.2804	7.3636	4.4095	5.4955	5.5783
5.7011	8.2260	8.3434	5.6670	6.1550	6.2620
6.8502	8.7385	8.8805	6.5681	6.5529	6.6774
8.1585	9.2305	9.4008	7.9118	7.0369	7.1877
10.0035	9.7726	9.9836	9.9112	7.6343	7.8248
12.2068	10.2918	10.5526	12.2735	8.2053	8.4435
15.0742	10.7914	11.1189	15.1803	8.7667	9.0650
17.7089	11.1412	11.5322	17.7270	9.1615	9.5138
20.4243	11.4406	11.8997	20.3847	9.5229	9.9331
23.2025	11.6546	12.1860	23.2122	9.7922	10.2655
25.4761	11.7905	12.3834	25.4992	9.9735	10.4992
27.3362	11.8910	12.5360	27.3609	10.1443	10.7135
29.6777	11.9773	12.6902	29.6957	10.3021	10.9274
32.5758	12.1293	12.9305	32.6608	10.5524	11.2507
35.2416	12.1460	13.0328	35.2792	10.7029	11.4678
37.3660	12.1620	13.1207	37.3560	10.7048	11.5241
39.8709	12.0850	13.1332	39.8746	10.7826	11.6698
41.0660	12.0908	13.1835	41.0446	10.8119	11.7314

Sample ID: DP2900- adsorbate CO_2

25°C			50°C		
Pressure (bar)	Excess adsorption (mmol/g)	Absolute adsorption (mmol/g)	Pressure (bar)	Excess adsorption (mmol/g)	Absolute adsorption (mmol/g)
0	0.0000	0.0000	0.0000	0.0000	0.0000
0.348553	1.6621	1.6723	0.4824	1.2162	1.2293
1.55363	4.7748	4.8206	1.9336	3.4694	3.5221
2.665611	6.7505	6.8296	3.0811	4.7928	4.8772
4.029086	8.5941	8.7144	4.4257	6.0988	6.2206
5.547637	10.1739	10.3409	5.5954	7.0567	7.2115
6.772835	11.2087	11.4140	6.5478	7.7572	7.9391
8.224133	12.2208	12.4720	7.8856	8.5616	8.7817
10.09097	13.2960	13.6076	9.9046	9.6048	9.8836
12.30348	14.3432	14.7280	12.2814	10.6333	10.9825
15.12959	15.3958	15.8770	15.2225	11.6727	12.1111
17.70264	16.1552	16.7274	17.7928	12.3878	12.9062
20.4194	16.7960	17.4677	20.5789	13.0546	13.6618
23.28983	17.3528	18.1340	23.3210	13.5316	14.2287
25.67407	17.7109	18.5870	25.5496	13.8389	14.6109
27.48649	17.9765	18.9271	27.3969	14.1205	14.9559
29.71467	18.2302	19.2758	29.7137	14.3895	15.3064
32.60421	18.4661	19.6407	32.6536	14.7273	15.7507
35.2419	18.5427	19.8417	35.2949	14.8972	16.0192
37.36365	18.5844	19.9889	37.3802	14.9224	16.1250
39.84781	18.7010	20.2355	39.8675	14.9848	16.2861
41.04439	18.7435	20.3434	41.0561	14.9802	16.3296

Sample ID: CTP3800- adsorbate CO_2					
	25°C			50°C	
Pressure (bar)	Excess adsorption (mmol/g)	Absolute adsorption (mmol/g)	Pressure (bar)	Excess adsorption (mmol/g)	Absolute adsorption (mmol/g)
0.0000	0.0000	0.0000	0.0000	0.0000	0.0000
0.2424	1.5272	1.5342	0.3758	1.2061	1.2161
1.3032	4.6399	4.6775	1.7176	3.5020	3.5479
2.3927	6.7081	6.7776	2.8676	4.9038	4.9807
3.7591	8.6276	8.7375	4.2336	6.2579	6.3722
5.3098	10.2603	10.4168	5.5824	7.3615	7.5129
6.7618	11.4527	11.6536	6.6440	8.1003	8.2813
8.3906	12.5214	12.7729	8.0315	8.9260	9.1461
10.3265	13.5328	13.8457	9.9906	9.9015	10.1775
12.4359	14.4302	14.8116	12.3055	10.8622	11.2055
15.1065	15.3027	15.7734	15.2369	11.8529	12.2834
17.6811	15.9505	16.5103	17.8133	12.5736	13.0832
20.4799	16.5062	17.1665	20.5159	13.1927	13.7867
23.3482	16.9283	17.6960	23.3025	13.6846	14.3682
25.6486	17.1943	18.0514	25.6058	14.0350	14.7946
27.5055	17.3815	18.3134	27.5129	14.3358	15.1597
29.7365	17.5403	18.5653	29.8029	14.6531	15.5564
32.6055	17.7018	18.8522	32.6438	15.0030	16.0070
35.2405	17.7409	19.0127	35.2443	15.2539	16.3533
37.3563	17.7168	19.0912	37.3465	15.3667	16.5455
39.8530	17.7604	19.2627	39.8692	15.5077	16.7845
41.0502	17.7689	19.3353	41.0510	15.5706	16.8945

Appendix B: CH_4 Excess and Absolute Uptake Values

Sample ID: DP3600-adsorbate CH_4

25°C			50°C		
Pressure (bar)	Excess adsorption (mmol/g)	Absolute adsorption (mmol/g)	Pressure (bar)	Excess adsorption (mmol/g)	Absolute adsorption (mmol/g)
0.0000	0.0000	0.0000	0.0000	0.0000	0.0000
0.5813	0.7166	0.7282	0.6685	0.4889	0.5013
2.2345	1.8868	1.9317	2.4203	1.3592	1.4042
3.4192	2.4444	2.5132	3.5610	1.7729	1.8391
4.4707	2.8477	2.9378	4.4434	2.0485	2.1312
5.3559	3.1414	3.2496	5.2502	2.2765	2.3744
8.7205	3.9718	4.1489	8.6618	3.0296	3.1918
15.0450	4.9505	5.2595	14.9660	3.9510	4.2335
21.6689	5.5656	6.0156	21.5958	4.5851	4.9962
26.9278	5.8992	6.4636	26.9145	4.9368	5.4525
31.2114	6.1143	6.7733	31.2336	5.1631	5.7649
35.5001	6.2564	7.0116	35.4078	5.3183	6.0039
40.4103	6.4050	7.2719	40.0509	5.4241	6.2038
48.4988	6.5957	7.6504	48.2638	5.5841	6.5331
59.2897	6.6871	7.9998	59.3315	5.6028	6.7837
70.6898	6.7101	8.3038	70.8675	5.5817	7.0095
81.3004	6.6516	8.5141	81.3937	5.4922	7.1491
91.0938	6.6382	8.7536	91.0733	5.4009	7.2713
100.4788	6.7342	9.0966	100.6119	5.6985	7.7809

Sample ID: DP2900-adsorbate CH_4

25°C			50°C		
Pressure (bar)	Excess adsorption (mmol/g)	Absolute adsorption (mmol/g)	Pressure (bar)	Excess adsorption (mmol/g)	Absolute adsorption (mmol/g)
0.0000	0.0000	0.0000	0.0000	0.0000	0.0000
0.5560	0.9944	1.0106	0.6477	0.6909	0.7084
2.1487	2.7417	2.8047	2.3473	1.9833	2.0469
3.3246	3.6452	3.7430	3.4984	2.6419	2.7370
4.4485	4.3547	4.4858	4.4515	3.1219	3.2430
5.4086	4.8758	5.0354	5.3028	3.5031	3.6475
8.7525	6.2747	6.5344	8.6491	4.7026	4.9391
15.0844	7.9836	8.4363	14.9402	6.2641	6.6758
21.7852	9.1232	9.7846	21.6434	7.3815	7.9830
27.0084	9.7256	10.5530	27.0433	8.0313	8.7879
31.3052	10.1315	11.0977	31.3607	8.4506	9.3327
35.7197	10.4542	11.5652	35.5842	8.7780	9.7840
40.2716	10.7381	12.0004	40.1117	9.0702	10.2103
48.2554	11.0310	12.5641	48.1985	9.4600	10.8430
59.1985	11.2938	13.2091	59.2391	9.8647	11.5858
70.7778	11.3624	13.6951	70.8992	9.9374	12.0228
81.4808	11.2912	14.0202	81.5878	9.8558	12.2808
91.2534	11.1401	14.2388	91.0637	9.7779	12.5074
100.6786	10.9720	14.4322	100.5025	9.5670	12.6026

Sample ID: CTP3800-adsorbate CH_4					
	25°C			50°C	
Pressure (bar)	Excess adsorption (mmol/g)	Absolute adsorption (mmol/g)	Pressure (bar)	Excess adsorption (mmol/g)	Absolute adsorption (mmol/g)
0.0000	0.0000	0.0000	0.0000	0.0000	0.0000
0.5379	0.8422	0.8576	0.6317	0.5909	0.6077
2.0818	2.4204	2.4803	2.2950	1.7492	1.8103
3.2513	3.2781	3.3718	3.4378	2.3648	2.4564
4.4452	3.9939	4.1223	4.4370	2.8395	2.9579
5.4768	4.5236	4.6822	5.3354	3.2190	3.3616
8.8004	5.8423	6.0986	8.7245	4.3626	4.5967
15.0470	7.4456	7.8885	15.0952	5.8633	6.2718
21.7878	8.5301	9.1791	21.7829	6.9133	7.5076
27.0661	9.1084	9.9219	26.9969	7.5115	8.2529
31.3819	9.4862	10.4365	31.2744	7.9005	8.7639
35.5468	9.7767	10.8608	35.6108	8.2324	9.2206
40.2990	10.0275	11.2667	40.1981	8.5027	9.6245
48.3735	10.3147	11.8227	48.2932	8.8589	10.2192
59.2650	10.5097	12.3908	59.2510	9.1800	10.8699
70.7750	10.5424	12.8305	70.7592	9.4059	11.4489
81.4290	10.4356	13.1106	81.4645	9.3841	11.7611
91.1666	10.3257	13.3618	91.1943	9.2211	11.9061
100.5712	10.2226	13.6124	100.6073	9.0706	12.0548

Appendix C: Research Output

Conference Poster Participation

- UK Carbon Capture and Sequestration Research Centre Programme Conference on the 11th September 2018, Sheffield.
- Energy for Life Conference 16 - 17 January 2019, Nottingham.
- UK Carbon Capture and Sequestration Research Centre Conference 16-17 April 2019, Cardiff.

Publication under preparation

- Removal of CO_2 from natural gas by adsorption on activated carbons.